

N72-28574

Unclass  
36801

EXPERIMENTAL INVESTIGATION OF THE MECHANICAL  
BEHAVIOR OF A FILLED ELASTOMER AT  
PRESSURES BELOW  $10^{-6}$  TORR

*Waiting  
for Board*

by

Gerald Lee Gregory

Thesis submitted to the Graduate Faculty of the  
Virginia Polytechnic Institute and State University  
in partial fulfillment for the degree of

DOCTOR OF PHILOSOPHY

in

MECHANICAL ENGINEERING

APPROVED:

*Henry L. Wood*  
Professor Henry L. Wood, Chairman



(NASA-TM-X-68688) EXPERIMENTAL BEHAVIOR OF  
INVESTIGATION OF THE MECHANICAL BEHAVIOR OF  
A FILLED ELASTOMER AT PRESSURES BELOW  $10^{-6}$  TORR  
THE -6TH POWER TORR Ph.D. Thesis - G.L.  
Gregory (NASA) May 1972 214 p. CSCL 11D G3/18

*J. B. Jones*  
Professor J. B. Jones

*R. K. Will*  
Associate Professor R. K. Will

*J. P. Mugler, Jr.*  
Adjunct Professor J. P. Mugler, Jr.

*J. W. Layman*  
Associate Professor J. W. Layman

May 1972

Blacksburg, Virginia

Details of illustrations in  
this document may be better  
studied on microfiche

II. TABLE OF CONTENTS

CHAPTER	PAGE
I. TITLE . . . . .	i
II. TABLE OF CONTENTS . . . . .	ii
III. LIST OF TABLES AND FIGURES . . . . .	iv
IV. LIST OF SYMBOLS . . . . .	ix
V. INTRODUCTION. . . . .	1
VI. LITERATURE REVIEW . . . . .	3
Introduction. . . . .	3
Previous Studies. . . . .	4
Description of Mechanical Behavior. . . . .	15
Summary . . . . .	50
VII. THE INVESTIGATION . . . . .	51
Test Technique and Material Selection . . . . .	51
Research Program . . . . .	52
Test Apparatus . . . . .	53
Sample Preparation. . . . .	63
Test Procedures . . . . .	67
Data Reduction. . . . .	72
Test Results. . . . .	80
VIII. ACCURACY AND ERRORS . . . . .	101
Vacuum Exposure Time. . . . .	101
Sample Loading Time . . . . .	101
Temperature . . . . .	101
Pressure. . . . .	102
Humidity. . . . .	102
Sample Cross Sectional Area . . . . .	102
Test Weight . . . . .	103
Length Strain . . . . .	103
Diameter Strain . . . . .	103
Compliance. . . . .	104
Percent Volume Change . . . . .	104
Poisson's Ratio . . . . .	105

CHAPTER	PAGE
IX. DISCUSSION OF RESULTS . . . . .	106
Introduction . . . . .	106
Observed Vacuum Behavior . . . . .	106
Analytical Correlation of Experimental Results . . . . .	128
Mechanisms of Mechanical Behavior . . . . .	139
X. SUMMARY . . . . .	147
XI. CONCLUSIONS . . . . .	149
XII. RECOMMENDATIONS . . . . .	152
XIII. ACKNOWLEDGMENTS . . . . .	153
XIV. BIBLIOGRAPHY . . . . .	154
XV. VITA . . . . .	158
XVI. APPENDICES . . . . .	159
A. Dilatational Model for a Filled Elastomer . . . . .	159
B. Arrhenius Equation for Isothermal Creep Test at Constant Stress . . . . .	165
C. Causes of Sample-to-Sample Variations . . . . .	174
D. Comparison of Data Reduction Techniques . . . . .	177
E. List of Equipment . . . . .	201

III. LIST OF FIGURES AND TABLES

FIGURE	PAGE
1. Effect of pressure on fracture stress of material A (SBR-carbon black) . . . . .	7
2. Typical stress - strain curve for TPH 3105 . . . . .	9
3. Variation of Young's modulus of TPH 3105 with storage time .	10
4. Variation of maximum stress of TPH 3105 with storage time. .	11
5. Energy required to fracture TPH 3105 . . . . .	12
6. Internal structure of filled-elastomer . . . . .	18
7. Internal structure of filled-elastomer in dewetting region .	20
8. Internal structure of filled-elastomer in filled-foam region . . . . .	22
9. Ideal strain-time response of a filled-elastomer to uniaxial constant tensile force . . . . .	23
10. Ideal creep curve illustrating location of transition points . . . . .	25
11. Strain energy technique for locating completely dewetted point . . . . .	27
12. Location of transition points from dilatational data . . .	29
13. Poisson's ratio technique for locating initiation point. . .	31
14. Basic energy diagram for Arrhenius theory . . . . .	33
15. Arrhenius plot for isothermal application of reaction rate technique. . . . .	36
16. Comparison of calculated experimental failure for cyclic loading of polyvinyl chloride propellant . . . . .	37
17. First derivative of dilatation data. . . . .	40
18. Second derivative of dilatation data . . . . .	41
19. Identification of parameters for statistical dilatational equation . . . . .	44

20.	Time-temperature superposition applied to polyethylene . . .	47
21.	Typical pressure-time history for vacuum samples . . . . .	54
22.	Photograph of test apparatus . . . . . . . . . . . . . . . . .	57
23.	Close-up photograph of creep apparatus . . . . . . . . . . . . .	58
24.	Photograph of creep apparatus with sample loaded . . . . .	60
25.	Test camera location .	62
26.	Photograph of test sample . . . . . . . . . . . . . . . . . . .	65
27.	Preconditioning storage racks . . . . . . . . . . . . . . . . .	66
28.	Storage table temperature gradient . . . . . . . . . . . . . . .	70
29.	Variation of length strain measurement for sample group tested at 51 psi in 50% r.h. air and at 83° F . . . . . . . . . . .	76
30.	Length strain results at a stress of 51 psi and at 83° F . . .	107
31.	Length strain results at a stress of 56 psi and at 83° F . . .	108
32.	Length strain results at a stress of 61 psi and at 83° F . . .	109
33.	Compliance results at 51 psi stress and 83° F . . . . . . .	111
34.	Compliance results at 56 psi stress and 83° F . . . . . . .	112
35.	Compliance results at 61 psi stress and 83° F . . . . . . .	113
36.	Poisson's ratio results at 51 psi stress and 83° F . . . . .	115
37.	Poisson's ratio results at 56 psi stress and 83° F . . . . .	116
38.	Poisson's ratio results at 61 psi stress and 83° F . . . . .	117
39.	Volume change results at 51 psi and 83° F . . . . . . . . .	120
40.	Volume change results at 56 psi and 83° F . . . . . . . . .	121
41.	Volume change results at 61 psi and 83° F . . . . . . . . .	122
42.	Failure time results at 83° F . . . . . . . . . . . . . . . .	127

43. Compliance master curve for TPH 3105 at 51 psi stress and 50% r.h. air . . . . .	133
44. Compliance master curve for TPH 3105 at 56 psi stress and 50% r.h. air . . . . .	134
45. Compliance master curve for TPH 3105 at 61 psi stress and 50% r.h. air . . . . .	135
46. Vacuum effect shift factors for TPH 3105 . . . . .	136
47. Comparison of predicted and experimental compliances . . . . .	138
48. Crosslink density of aged samples of TPH 3105 (room temperature) . . . . .	140
49. Sol content of aged samples of TPH 3105 (room temperature) . . . . .	141
50. Major outgassing constituents from TPH 3105 . . . . .	143
51. Loss modulus of TPH 3105, $10^{-5}$ torr and $77^{\circ}\text{F}$ . . . . .	146
B-1. Energy diagram for isothermal activation process in absence of external forces . . . . .	167
B-2. Energy diagram for isothermal constant stress deformation process . . . . .	169
B-3. Ratio of $\frac{N}{N_0}$ as function of loading time . . . . .	173
D-1. Length strain comparison, 51 psi stress, 50% r.h. air . . . . .	179
D-2. Length strain comparison, 51 psi stress, 51 hours vacuum . . . . .	180
D-3. Length strain comparison, 51 psi stress, 173 hours vacuum . . . . .	181
D-4. Length strain comparison, 51 psi stress, 348 hours vacuum . . . . .	182
D-5. Length strain comparison, 56 psi stress, 50% r.h. air . . . . .	183
D-6. Length strain comparison, 56 psi stress, 47 hours vacuum . . . . .	184
D-7. Length strain comparison, 56 psi stress, 170 hours vacuum . . . . .	185
D-8. Length strain comparison, 56 psi stress, 338 hours vacuum . . . . .	186

D-9. Length strain comparison, 61 psi stress, 50% r.h. air . . .	187
D-10. Length strain comparison, 61 psi stress, 46 hours vacuum . .	188
D-11. Length strain comparison, 61 psi stress, 171 hours vacuum .	189
D-12. Length strain comparison, 61 psi stress, 337 hours vacuum .	190
D-13. Diameter strain comparison, 51 psi stress, 50% r.h. air . .	191
D-14. Diameter strain comparison, 51 psi stress, 51 hours vacuum .	192
D-15. Diameter strain comparison, 51 psi stress, 173 hours vacuum.	193
D-16. Diameter strain comparison, 56 psi stress, 50% r.h. air . .	194
D-17. Diameter strain comparison, 56 psi stress, 47 hours vacuum .	195
D-18. Diameter strain comparison, 56 psi stress, 170 hours vacuum.	196
D-19. Diameter strain comparison, 56 psi stress, 338 hours vacuum.	197
D-20. Diameter strain comparison, 61 psi stress, 50% r.h. air . .	198
D-21. Diameter strain comparison, 61 psi stress, 46 hours vacuum .	199
D-22. Diameter strain comparison, 61 psi stress, 337 hours vacuum.	200

## TABLE

## PAGE

I. Vacuum effects on the fracture stress of styrene butadiene rubber (SBR) at 120°C . . . . .	6
II. Tensile properties of TPH 3105 as determined from constant strain rate testing at 2 inches per minute (Ref. 4) . . .	14
III. Parameters of importance to the dewetting process . . . . .	45
IV. Propellant batch report on TPH 3105 . . . . .	64
V. Sample group data listing . . . . .	68
VI. Failure time variations within sample groups . . . . .	75
VII. Creep measured properties of TPH 3105 . . . . .	81
VIII. Creep measured properties of TPH 3105 . . . . .	83
IX. Creep measured properties of TPH 3105 . . . . .	85
X. Creep measured properties of TPH 3105 . . . . .	87
XI. Creep measured properties of TPH 3105 . . . . .	90
XII. Creep measured properties of TPH 3105 . . . . .	91
XIII. Creep measured properties of TPH 3105 . . . . .	92
XIV. Creep measured properties of TPH 3105 . . . . .	94
XV. Creep measured properties of TPH 3105 . . . . .	96
XVI. Creep measured properties of TPH 3105 . . . . .	97
XVII. Creep measured properties of TPH 3105 . . . . .	98
XVIII. Creep measured properties of TPH 3105 . . . . .	99
XIX. Strain mean for dewetting . . . . .	125
XX. Comparison of predicted failure times to measured failure times in 50% r.h. air . . . . .	130

IV. LIST OF SYMBOLS

A	Reaction rate
$A_0$	Pre-exponential function
$\bar{A}$	Sample cross sectional area
C	Constant of integration or Arrhenius material constant
D	Diameter
$E_0$	Activation Energy
F	Force
J	Compliance
L	Length
R	Universal gas constant
S	Standard deviation
T	Temperature
V	Volume
$V_{fd}$	Volume fraction of filler dewetted
$V_{fmax}$	Total volume fraction of filler dewetted
$\Delta V$	Volume change
a	Shift factor
h	Planck's constant
k	Boltzman's constant
n	Variable of integration or sample number
t	Time
$\bar{t}$	Average time

$t_{\alpha/2, n-1}$  Student's "t" statistic

$\alpha$  Level of significance

$\epsilon$  Strain

$\bar{\epsilon}$  Average strain

$\sigma$  Stress

**Subscripts**

f Fracture state

i Time state (general)

o Initial state or reference state

T Temperature

t Indicates failure time parameter

v Vacuum

$\sigma$  Stress

1 Length direction

2 Diameter direction

## V. INTRODUCTION

With the continuation of the space program, there has been an increasing requirement to measure the engineering properties of spacecraft materials in simulated space environments. In many cases the selection of a spacecraft material is based on the performance--as determined from measurements of key engineering properties--of the material in simulated space environments. In developing criteria for the selection of spacecraft materials, much emphasis is placed on in situ testing, as well as on direct engineering property measurements, rather than inferring engineering property changes from such peripheral measurements as weight loss. Due to the large number of materials and the many anticipated mission environments that must be considered to design a spacecraft, in situ testing of spacecraft materials is fast becoming an enormous task. To better meet this task, there is a need to develop a better understanding of the nature of material-environment interactions as well as to develop test techniques which can be used in predicting environmental effects on materials.

The purpose of this thesis was to experimentally measure the effects of the vacuum of space on the mechanical behavior of a filled elastomeric spacecraft material. Special emphasis was given to the understanding of those mechanisms by which mechanical properties are changed by the vacuum environment. In addition several existing techniques, which are frequently used in the earth's environment to predict mechanical behavior, were applied to the vacuum results in order to

PRECEDING PAGE BLANK NOT FILMED

2

develop a technique which would be useful in predicting the effects of vacuum on filled elastomeric materials. The subject investigation was conducted under the auspices of the National Aeronautics and Space Administration at the Langley Research Center, Hampton, Virginia.

## VI. LITERATURE REVIEW

### Introduction

It has been shown (1-7) that the storage of filled elastomers in the vacuum environment can alter the basic engineering properties of this class of materials. Vacuum storage can improve or degrade the performance of a material depending upon the material and its application. To date the major concern of the vacuum studies on filled elastomers has been to document the magnitude and nature of these property changes. For example, references 1 and 2 show that storage of filled elastomeric heat shield materials in the vacuum environment does influence the thermal properties of these materials. Reference 3 is concerned with measurement of the mechanical behavior of various filled elastomeric systems at a vacuum of  $10^{-2}$  torr. Reference 4 deals with observation of changes in the mechanical behavior of a solid rocket propellant (a filled elastomer) as a function of vacuum storage time at  $10^{-8}$  torr. The basic processes resulting in these observed vacuum induced changes are not well understood; although, some of the above authors do discuss and suggest plausible explanations for the observed material behavior. To date, various filled elastomers have been studied in vacuum, but no one material nor property has been studied in enough depth to fully understand the vacuum interactions occurring with the materials. With the current interest in space flight and with the large number of filled elastomeric spacecraft

materials that must function in the vacuum environment, steps must be taken to understand and hence to predict the behavior of such materials in the vacuum environment.

This investigation was concerned with the mechanical behavior of filled elastomers in the vacuum environment. The approach considered was to select a typical filled elastomer, which from previous work, has been shown to be affected by vacuum, and to investigate the nature of the involved processes and how vacuum influences these processes. In addition a technique was sought whereby the vacuum behavior of the material could be predicted.

#### Previous Studies

The results of several investigations on the effects of the vacuum environment on the mechanical properties of filled elastomeric systems are discussed in the literature. These investigations vary in scope depending upon the material studied, the test technique employed, and the level of vacuum considered. However, these investigations can be generalized into two classes: (1) before and after tests and (2) in situ tests. The before and after technique is a test philosophy (5-7) in which a property measurement is made prior to vacuum, the material is then exposed to the vacuum environment, and the property is measured again after removal of the material from the vacuum environment. Vacuum changes in the material are determined by comparison of the two measurements. The in situ technique (3,4) involves

making property measurements while the material is in the vacuum environment and then comparing these measurements with those taken prior to vacuum. Evidence given in reference 4 indicates that the before and after technique is not a valid test philosophy for measuring induced vacuum changes in mechanical properties as reexposure of the material to the atmosphere can alter the value of the property being measured. It is for this reason that only the results of in situ measurements will be discussed in this section.

As part of the investigation conducted in reference 3, the mechanical properties of styrene butadiene rubber (SBR) filled with (1) carbon black and (2) silica were measured in the vacuum environment at 120° C. The technique employed was to measure, in air and in vacuum, the tensile stress required to fracture the materials. Samples 0.075 in. by 0.015 in. by 1 in. were loaded in tension in the one-inch direction from zero stress to the fracture stress. The load application rate was varied so that the samples failed approximately 30 seconds after initiation of the loading process. Table I presents the results of these measurements for a vacuum environment of 0.02 torr. For each filled material, the vacuum fracture stress is 30 to 75% higher than that stress in air. The fracture stress of the unfilled rubber was not significantly affected by the vacuum exposure. Figure 1 shows additional results from reference 3, indicating that the fracture stress of the filled materials is pressure dependent. The author of reference 3 suggests that one mechanism which may be important in the fracture of

TABLE I

VACUUM EFFECTS ON THE FRACTURE STRESS OF  
STYRENE BUTADIENE RUBBER (SBR) AT 120° C

Recipe Number*	Elastomer	Filler	Vulcanizing Agent	Strength at 760 torr, Kg/cm <sup>2</sup>	Strength at .02 torr Kg/cm <sup>2</sup>
D	SBR	Carbon Black	Dicumyl Peroxide	45 ± 5	79 ± 5
A	SBR	Carbon Black	Sulfur	72	97
C	SBR	Silca	Sulfur	88	115
B	SBR	----	Sulfur	10.6	10.9

\*See reference 3 for all ingredients.

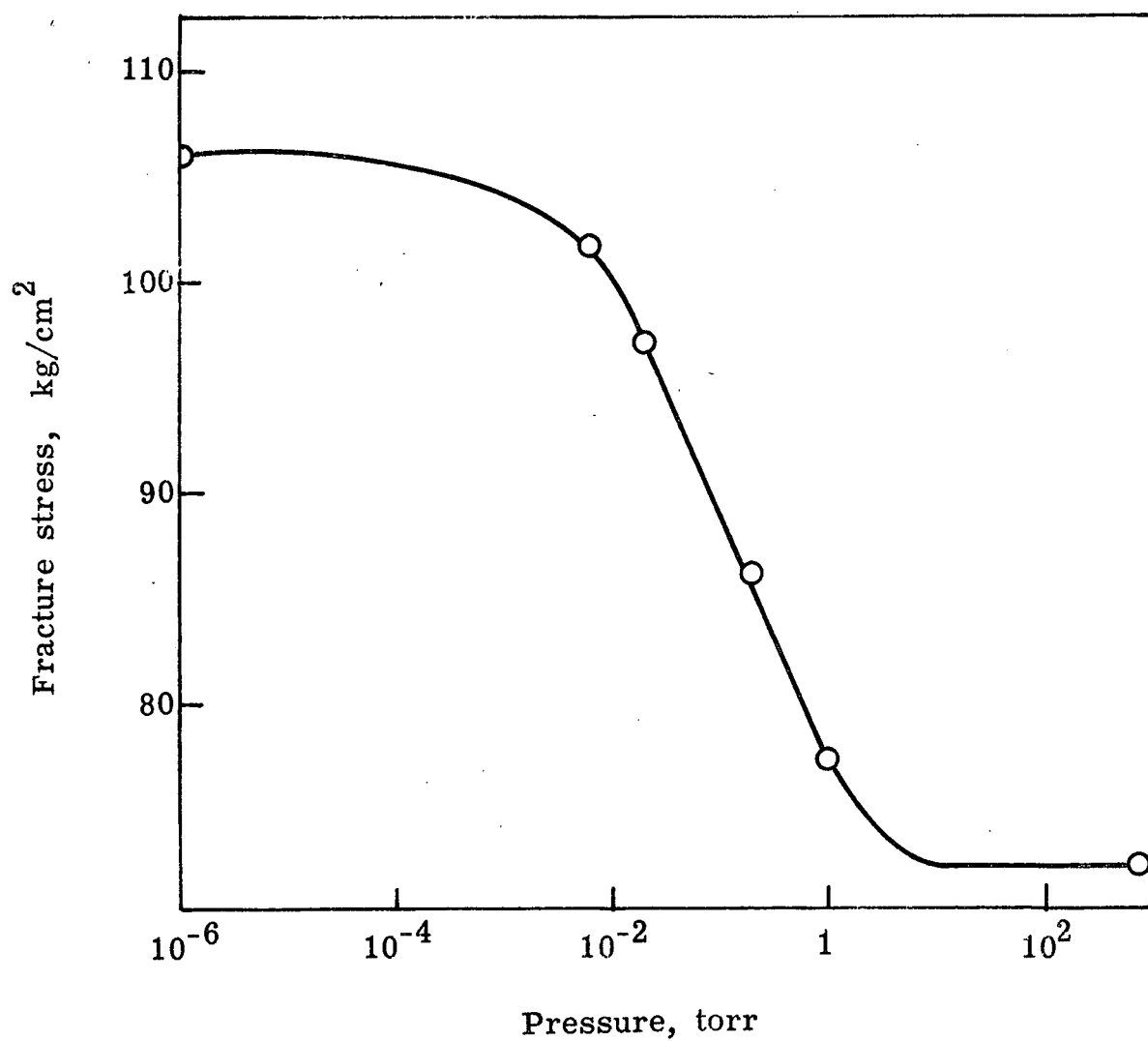


Figure 1. - Effects of pressure on fracture stress of material A  
(SBR-carbon black), 120°C.

these materials is oxidized scission of the polymer chains. In vacuum, the oxygen content of the material is reduced, retarding the chain scission process and resulting in larger fracture stresses. As pointed out by the author, the oxidized scission theory does not account for the absence of a change in the vacuum fracture stress of the unfilled rubber.

Reference 4 presents the results of an investigation to measure vacuum induced changes in the mechanical properties of a solid propellant. The propellant formulation investigated was TPH 3105 which is a composite material consisting of a polybutadiene acrylic acid (elastomer) matrix and ammonium perchlorate filler particles. The study consisted of storing and testing standard JANAF (8) tensile specimens *in situ* in a vacuum environment of  $10^{-8}$  torr. Samples were stored in vacuum for as long as 32 days, with samples being tensile tested at various intervals during the storage period. The test conducted was a uniaxial constant strain-rate loading at 2 inches/minute and was performed in accordance with standard propellant testing requirements (8). Stress-strain curves of the type shown in Figure 2 were obtained. The author defines three parameters which are used as a basis for observing vacuum induced changes in the mechanical properties of the material: (1) Young's initial modulus, (2) maximum stress, and (3) fracture (total) energy. These parameters are defined in Figure 2. The observed vacuum induced changes are shown in Figures 3 thru 5, in which the aforementioned parameters are plotted as a function

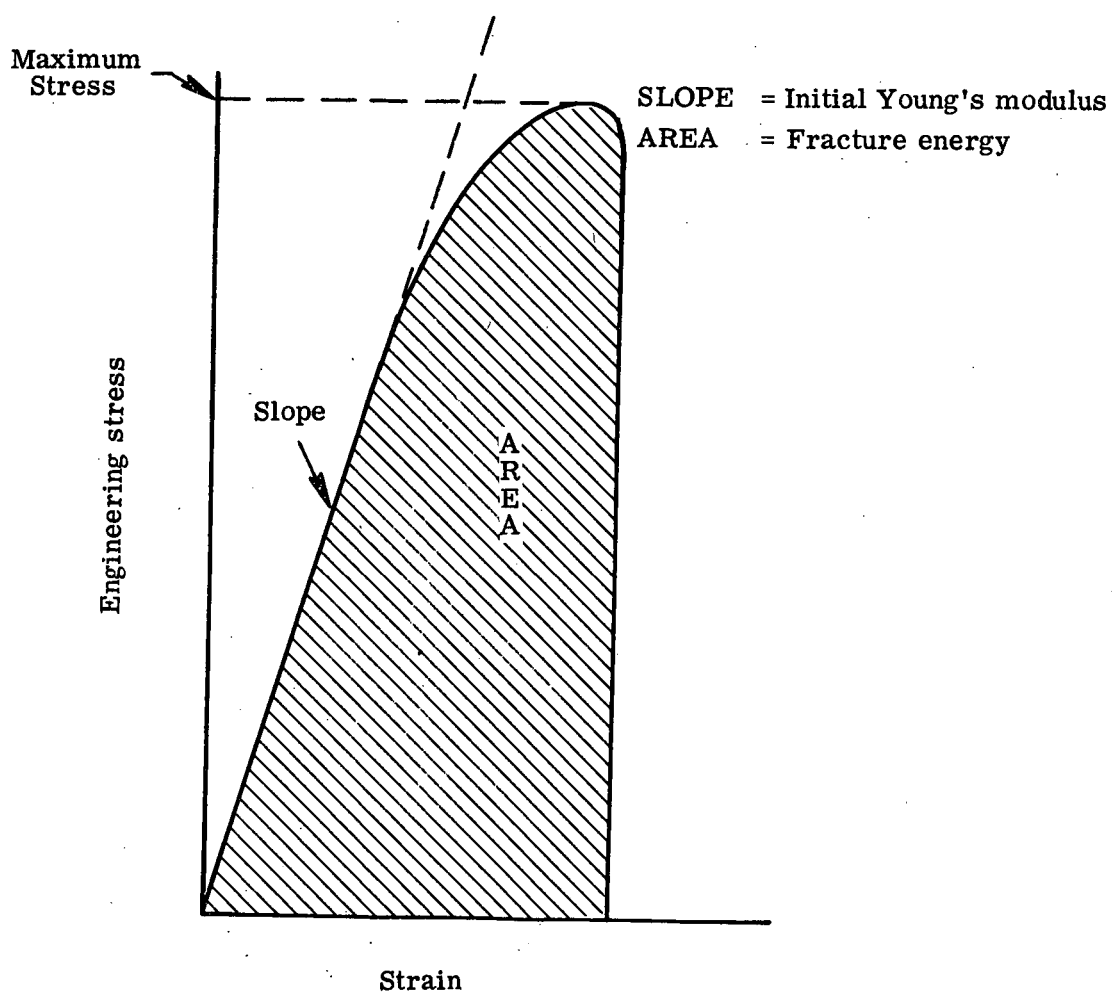


Figure 2. - Typical stress-strain curve for TPH 3105.

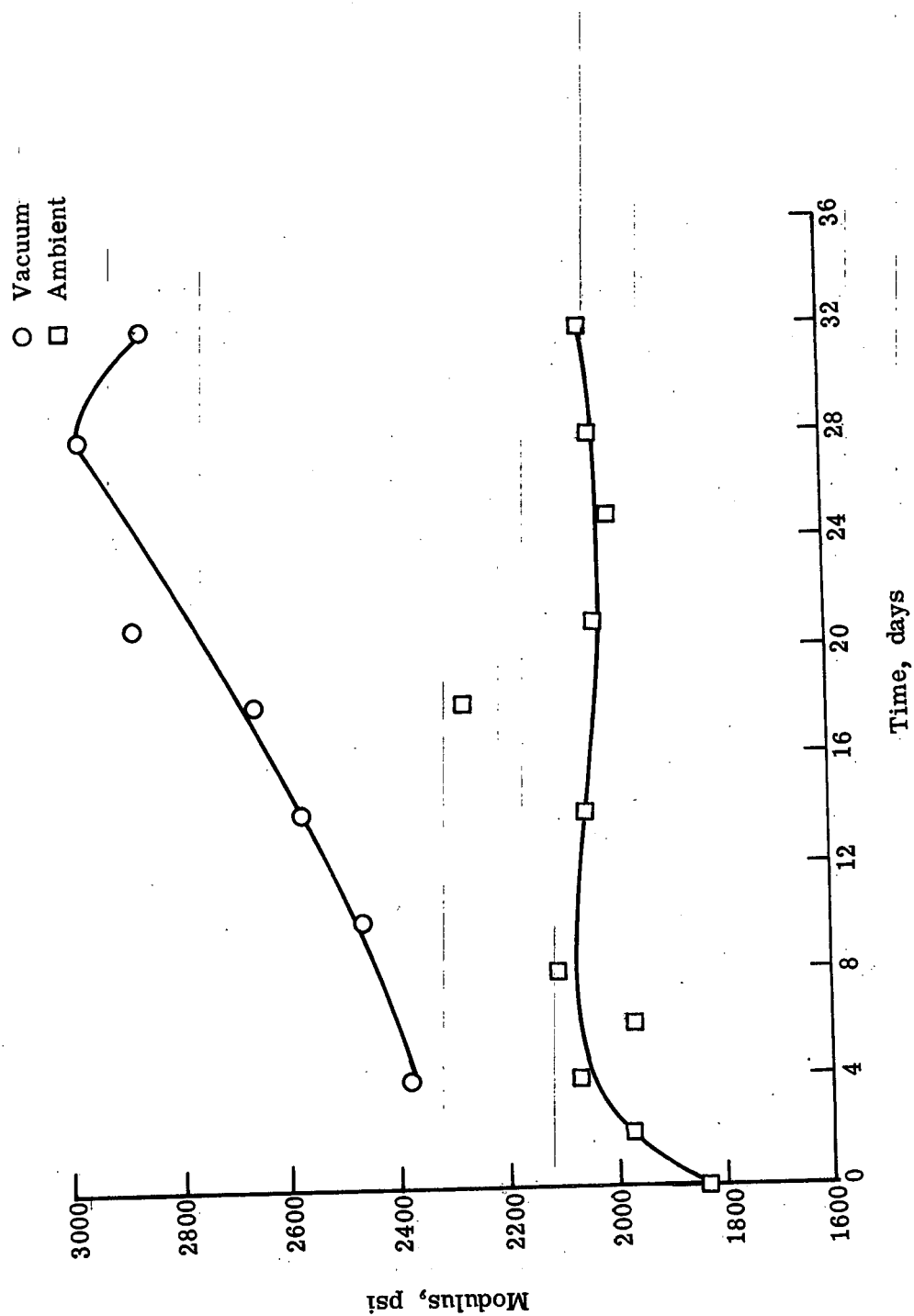


Figure 3. - Variation of Young's modulus of TPH 3105 with storage time.

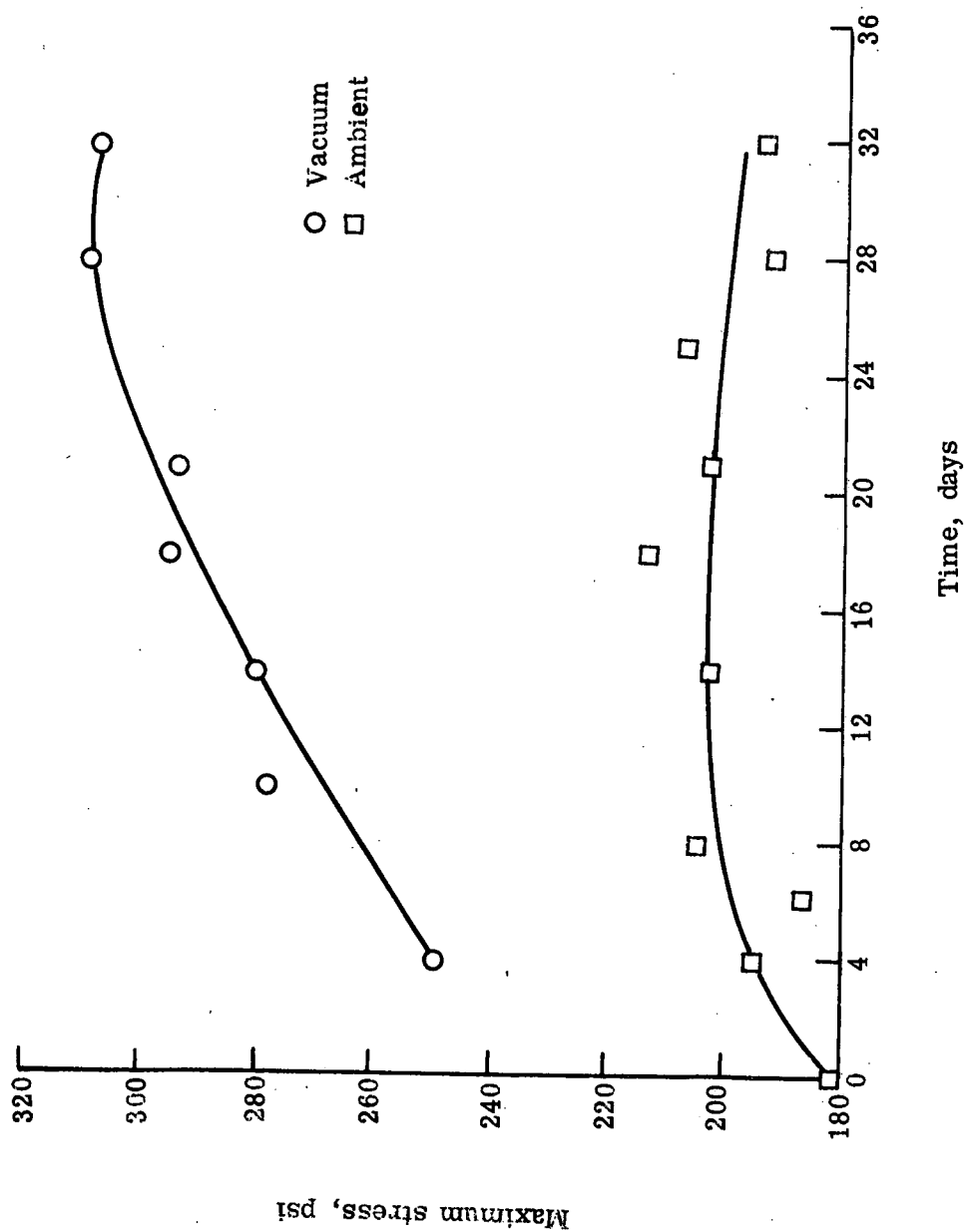


Figure 4. - Variation of maximum stress of TPH 3105 with storage time.

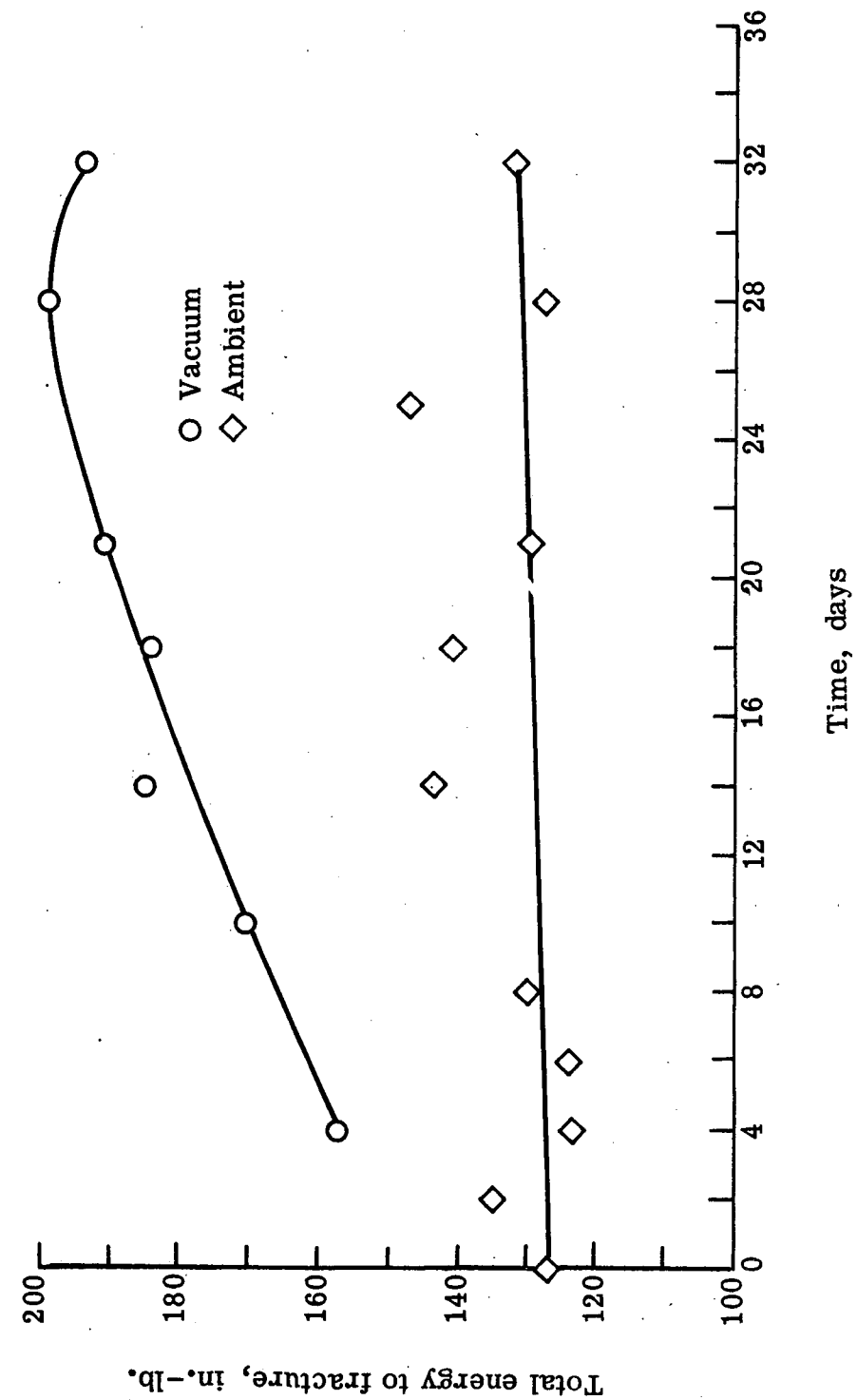


Figure 5. - Energy required to fracture TPH 3105.

of storage time. It is noted that Young's modulus, maximum stress, and fracture energy increase for this material as vacuum storage time increases, whereas measurements on ambient stored samples indicate little change in these parameters. The vacuum induced changes are of the order of 50% higher as compared to the ambient values. These results indicate that the tensile strength of TPH 3105 is significantly increased as the result of the storage of the material in the vacuum environment. Discussions in reference 4 indicated that this strengthening of the material was due to the removal of water from the material by vacuum outgassing. This water loss theory was supported by mass spectrometer data which showed that water was constantly being removed from the material in vacuum. Supplementary tensile testing indicated that the storage of TPH 3105 in other drying environments, such as dry nitrogen, produced similar strengthening effects but of a lesser magnitude than observed in vacuum. The need for making in situ mechanical property measurement is demonstrated in reference 4, in that samples exposed to vacuum for 32 days and then returned to ambient conditions for tensile testing exhibited much smaller property changes than observed in the in situ 32-day vacuum measurements. Table II illustrates these results. Several of the bonding mechanisms and deformation processes occurring in the material were discussed as to their sensitivity to the water content of the material. It was concluded that a number of these processes may be affected by water and the filler-binder bond is probably most moisture sensitive.

TABLE II

TENSILE PROPERTIES OF TPH 3105 AS DETERMINED FROM CONSTANT STRAIN RATE TESTING AT 2 INCHES PER MINUTE (REF. 4)

Property	Environmental Condition		
	Ambient	Vacuum	Re-exposed
Maximum Stress, psi	193	307	244
Modulus, psi	2046	2851	2408
Fracture Energy, in-lb.	131	193	154

Ambient Storage - 31 day storage at:

760 torr

room temperature

50% relative humidity

Vacuum Storage - 32 day storage at:

$10^{-8}$  torr

room temperature

Reexposure - 32 day vacuum storage at:

Storage             $10^{-8}$  torr

room temperature

plus

24 hour air storage at:

760 torr

unknown humidity

room temperature

Description of Mechanical Behavior

The development of idealized models describing the mechanical behavior of filled elastomeric systems has been studied in some detail. These descriptions range from macroscopic models, based on combining springs and dashpots (Kelvin, Voight, and Maxwell models) to account for observed mechanical behavior of the material, to microscopic models that envision individual filler particle-polymer chain reactions. The model to be discussed in this section is microscopic in nature, but is suitable for describing the macroscopic behavior of the material. In addition, several techniques which have been applied for correlation and prediction of the mechanical behavior of filled systems will be discussed.

Mechanical Property Model

From the literature (9-13) a model can be developed to explain the mechanical behavior of filled elastomers. This model separates the mechanical behavior into three distinct regions or stages:

- (1) Viscoelastic Region
- (2) Dewetting Region
- (3) Filled-foam Region

Each of these regions is characterized by different material behavior and each will be discussed. First, however, the general state of a filled elastomer prior to straining will be considered. A filled elastomer is made up of a network of long and highly cross-linked

polymer chains. Prior to material straining, this network consists of an entanglement of coiled, unstretched, polymer chains. Embedded in this network are filler particles. There are bonds between the polymer network (binder) and the filler particles, and these bonds are an influencing factor on the mechanical behavior of the material. The nature and strength of the filler-binder bond is largely responsible for the improved strength of the filled elastomer as compared to the unfilled elastomer. In this model, the polymer network is assumed to be somewhat elastic; whereas, the filler particles are assumed rigid. The mechanical behavior of the material is dependent on the properties of the filler and binder themselves, as well as on the nature of the filler-binder bond. Three basic groups of processes can occur during straining of a filled elastomer: (1) binder response, (2) binder-particle interaction, and (3) particle-particle interaction.

Viscoelastic Region. When the material is first strained, the viscoelastic region of mechanical behavior is entered. In this region, the material behaves as a viscoelastic solid where stress is proportional to strain and to the time derivative of strain. In this region, as the material is strained the cross-linked polymer network is uncoiled and stretched. During this straining, the long polymer chains slip past one another. A few cross-linked chains may be broken as a result of immobility of the highly cross-linked network, but in general the network remains intact. The mechanical behavior of the material in the viscoelastic region is characterized by the properties of the

polymer network such as cross-link density, molecular weight distribution of the polymer chains, and average molecular weight of the network. The filler-binder bonds do not significantly affect the mechanical behavior of the material in this region. Figure 6 illustrates the material behavior in the viscoelastic region. Figure 6a illustrates the filled elastomer prior to straining; Figure 6b is illustrative of the material in the viscoelastic region.

Dewetting Region. With continual straining, the material reaches the point at which internal voids begin to form in the material. At this point, the material leaves the viscoelastic region of behavior and enters the dewetting region. In this region straining causes the binder to separate from the filler and hence the filler is said to be dewetted of the binder. The mechanism of initial void formation is not understood. This mechanism may be a cohesive failure (tear) in the binder near the filler interface which propagates to the filler interface, or, it may be an adhesive failure of the filler-binder bond at the filler interface. In any event, the strength of the filler-binder bond strongly influences the degree of void formation and it is generally accepted that once dewetting is initiated, the void formation (vacuole) occurs around the filler particle. As a result of the internal growth of these vacuoles with straining, the volume of the material is increased. The dewetting process occurs over a range of strain, with filler particles being dewetted at various strain levels. As straining continues, a point is reached where the material is referred to as

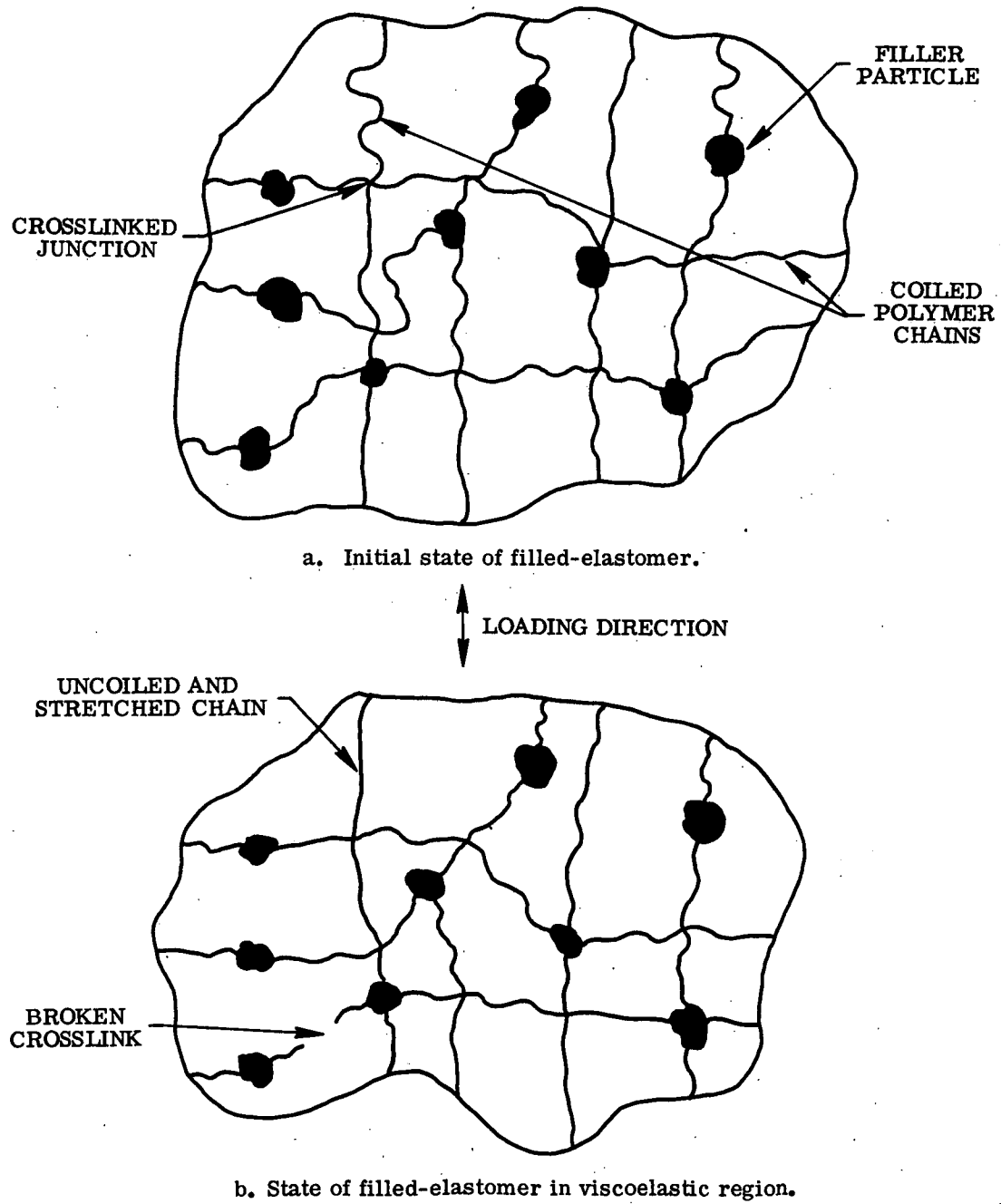


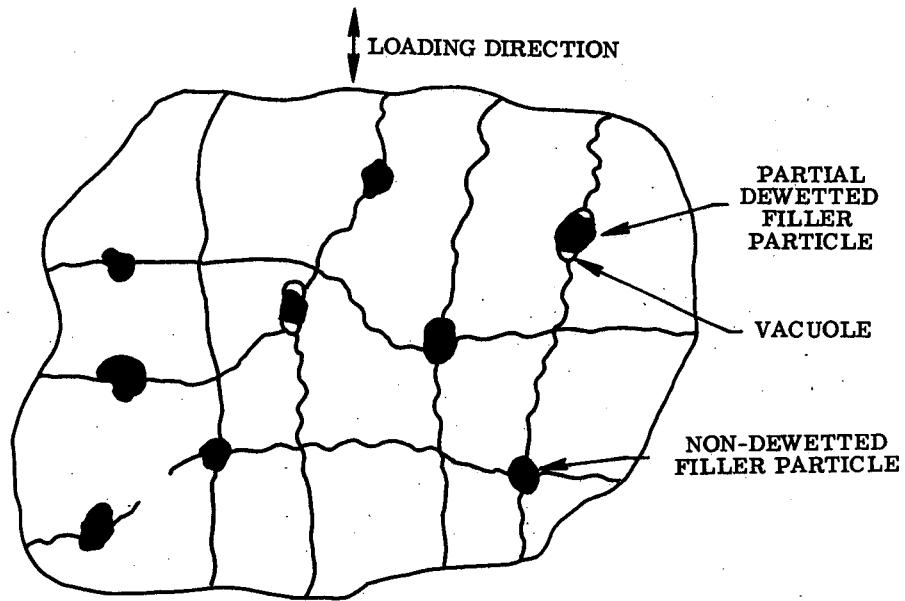
Figure 6. - Internal structure of filled elastomer.

being completely dewetted.\* Beyond this strain level, additional filler particles are not dewetted and continual straining results in only enlargement of the already existing vacuoles. Figure 7 illustrates the dewetting behavior of the material. Figure 7a shows the material in the initial stages of dewetting in which only a few filler particles have been dewetted. Figure 7b illustrates the completely dewetted state. In this state a large percentage of the filler particles are dewetted with large vacuoles surrounding the dewetted filler particles. In this model, it is assumed that the primary bonds between the dewetted fillers and the binder have been broken upon reaching the completely dewetted state.

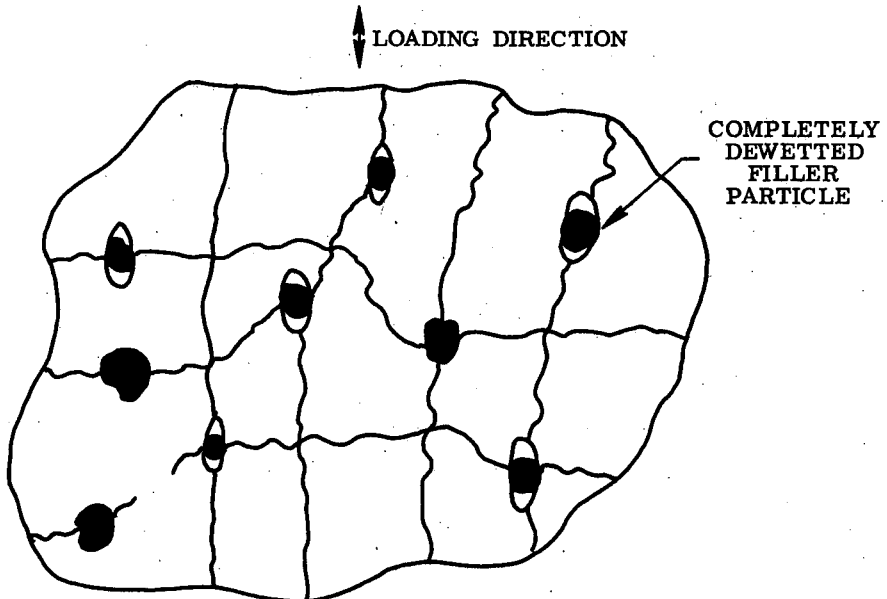
Filled-Foam Region. As the material is strained beyond the completely dewetted state, it enters the filled-foam region of behavior. In the filled-foam region, the polymer network is being pulled over the filler particles. There is a frictional bond or force between the filler and network and this force influences the mechanical behavior of the material in this region. Also in this region, the polymer network is again being stretched, with the result that longitudinal chains (in direction of loading), as well as cross-linked chains, are broken. Increased breakage of these chains as the result of failure of the

---

\*The term completely dewetted does not necessarily mean that all filler particles in the material have been dewetted. However, it does mean that all those filler particles that will dewet have already done so; this may or may not be all the filler particles in the material.



a. State of filled-elastomer just after initiation of dewetting.



b. State of filled elastomer at point of complete dewetting.

Figure 7. - Internal structure of filled elastomer in dewetting region.

dewetted filler to support a load eventually causes the failure of the material. The stretching and breaking of the polymer chains is believed to control the mechanical behavior of the material in this region. Therefore, the properties of the polymer network (cross-link density, etc.) determine the response of the material in this region. The volume increase of the material is proportional to strain level in this region as the result of the completely dewetted state of the filler particles. Figure 8 illustrates the state of the material in the filled-foam region.

An ideal strain-time response of a filled elastomer to a uniaxial constant tensile force is shown in Figure 9 to illustrate that the three regions of behavior as depicted by the model are distinct with definable transition points. However, in practice the location of the two transition points (point of initiation of dewetting and point of complete dewetting) are not always apparent. The three regions of mechanical behavior may overlap each other to some extent, not invalidating the model, but making it difficult to locate the transition points from experimental data. The application of the above model to the explanation of the mechanical behavior of a material does require that these two points be located. The next section of this investigation is concerned with the techniques available for locating these transition points.

#### Techniques for Locating the Mechanical Behavior Regions

The model proposed for the explanation of the mechanical behavior of filled elastomers separates the material's behavior into three

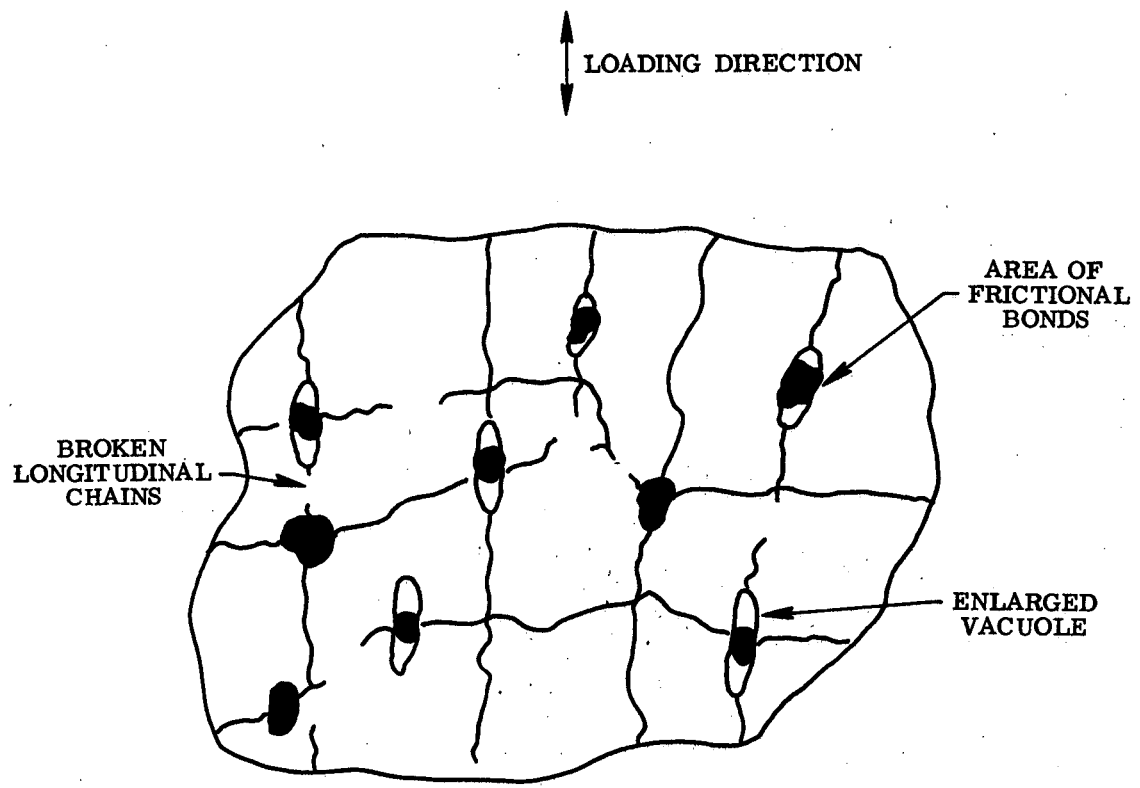


Figure 8. — Internal structure of filled elastomer in filled-foam regions.

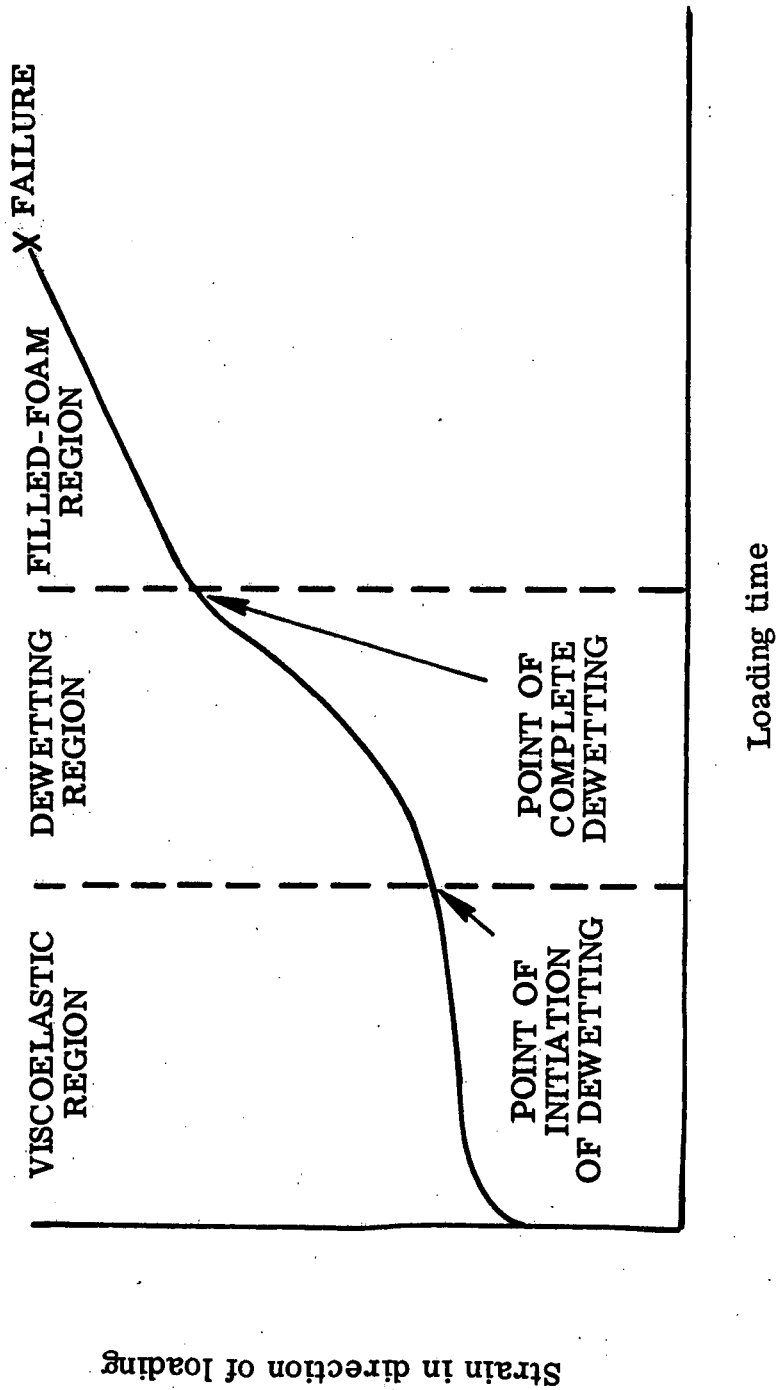


Figure 9. - Ideal strain-time response of a filled elastomer to uniaxial constant tensile force.

distinct regions of stress-strain-time behavior. The transition points associated with these three regions are the point of initiation of dewetting (initiation point) and the point of complete dewetting (completely dewetted point). As previously mentioned, the accurate location of the two transition points is a necessity if the proposed model is to be used in the explanation of the mechanical behavior of a given material. The literature documents several techniques which have been used for locating these transitional points. No one of these techniques has been accepted as a standard; hence, each of these techniques will be considered. These techniques are

- (1) Creep curve technique
- (2) strain energy technique
- (3) Dilatational technique
- (4) Poisson's ratio technique

Creep curve technique. The creep curve technique locates the two transitional points from the true strain-time response of the material during tensile uniaxial constant-force or constant-stress creep testing (14). Figure 10 illustrates the ideal creep response of a filled elastomer for constant force loading. The point of initiation of dewetting is defined as that point at which the derivative of strain with respect to time deviates from its previously constant value. (The initial strain behavior due to the instantaneous loading is neglected.) The point of complete dewetting is defined as that time at which the derivative returns to a constant value. Creep curves similar to that shown in

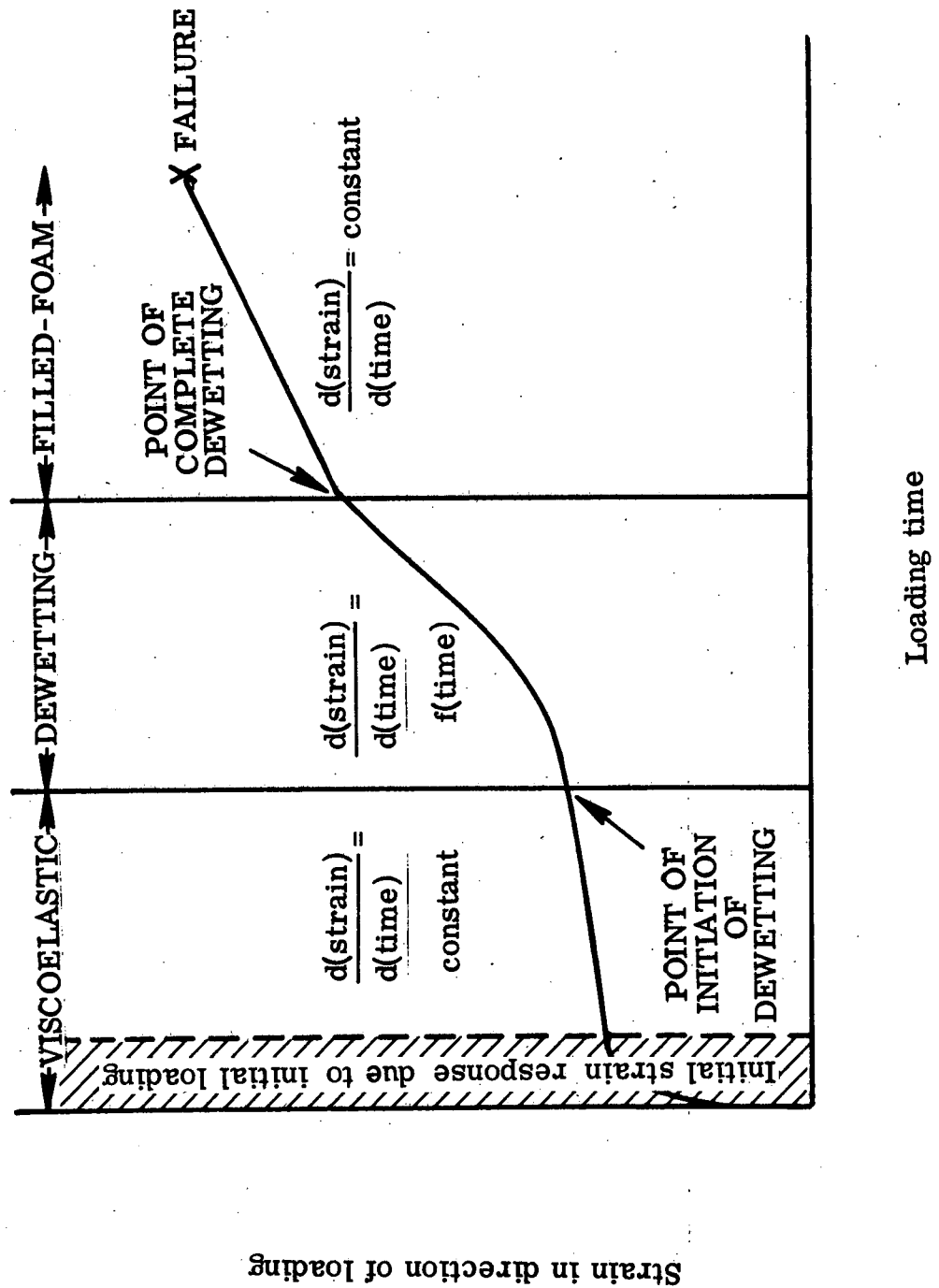
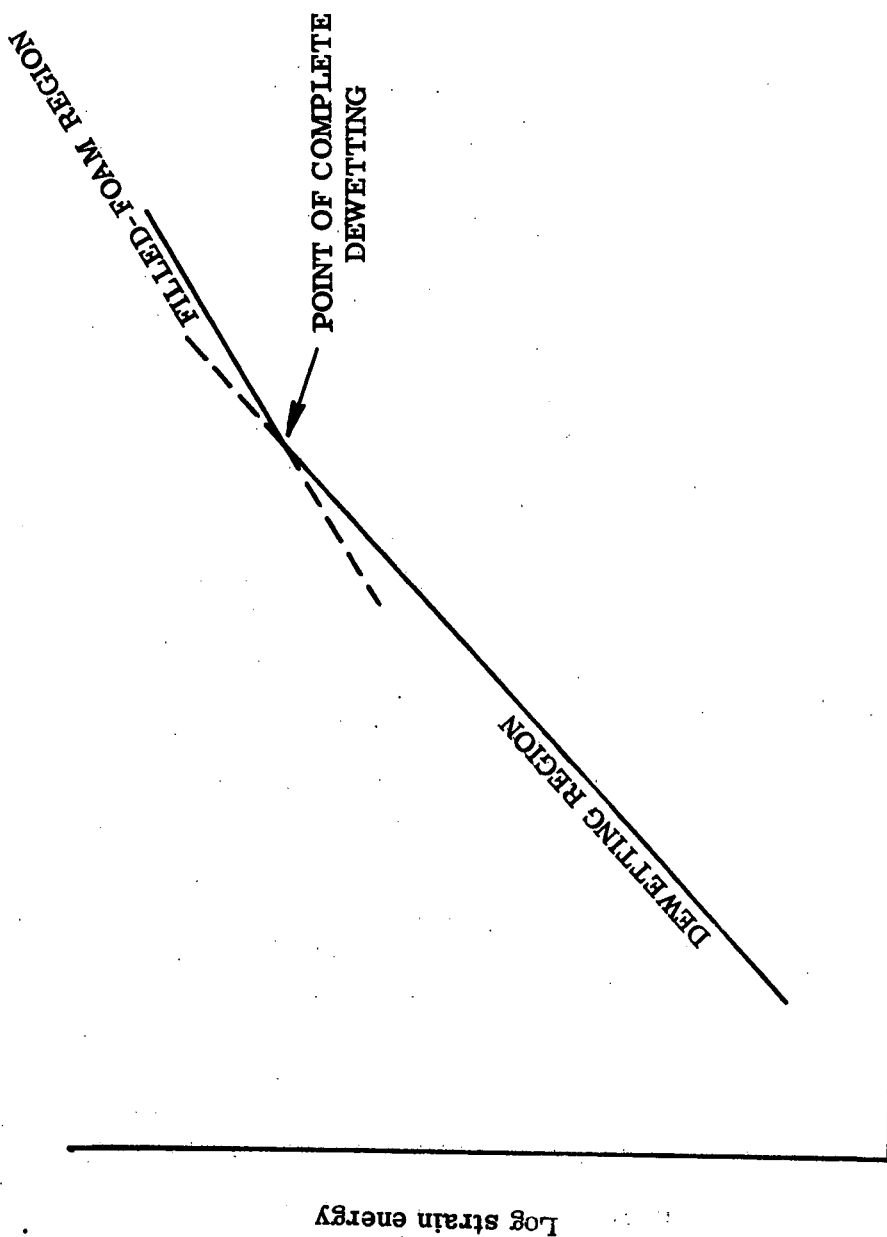


Figure 10. - Ideal creep curve illustrating location of transition points.

Figure 10 have been experimentally observed for filled elastomers (14, 15).

Strain energy technique. The strain energy technique is used for locating the point of complete dewetting. The strain energy technique considered is that applied in reference 12. This technique is supported analytically by Blatz and Ko (16-18). To apply the strain energy technique, the logarithm of the strain energy (area under the stress-strain curve) is plotted against the logarithm of the true strain in the direction of loading (see Figure 11). The two straight line regions of this curve represent the dewetting and filled-foam regions of behavior and the intersection point is defined as the point of complete dewetting. This technique (4, 12) is frequently used to locate the complete dewetting point for constant strain rate testing.

Dilatational Technique. The dilatational technique can be used to locate both the point of initiation of dewetting and the point of complete dewetting. The technique is based on a model proposed by Farris (13) for the explanation of the dilatational behavior of filled elastomers. The dilatational model, developed in detail in Appendix A, is consistent with the mechanical behavior model already discussed. Only the results from Appendix A which are pertinent to the location of the two transition points will be discussed. This technique is based on the volume change behavior of the material during straining and the dilatational model is developed by focusing attention on the



Log strain in direction of loading

Figure 11. - Strain energy technique for locating completely dewetted point.

vacuole formation around an individual filler particle during the straining process. The result of interest from Appendix A is equation A-22,

$$\frac{\Delta V}{V_0} = C \int_0^{\epsilon_1} V_{fd} d\epsilon \quad (6.1)$$

where:  $\Delta V$  = volume change of the material

$V_0$  = initial volume at zero strain

$V_{fd}$  = volume fraction of dewetted filler

$\epsilon_1$  = strain in loading direction

The volume fraction of dewetted filler is the ratio of the volume of those filler particles dewetted to the initial volume of the composite material. The value of  $V_{fd}$  at a given strain level is a measure of the quantity of filler that has been dewetted up to that strain level. The mechanical behavior model assumes that no dewetting occurs in the viscoelastic region and that additional filler particles are not dewetted beyond the completely dewetted point. In terms of  $V_{fd}$ , then

$V_{fd} = 0$  viscoelastic region

$V_{fd} = \text{Constant}$  filled foam region

and with these conditions and equation 6.1, the dilatational behavior of a filled elastomer is as shown in Figure 12. Dilatational responses of this type have been observed (12) for several filled elastomers and under a variety of uniaxial tensile loading histories. As seen from Figure 12, the point of initiation of dewetting and the point of

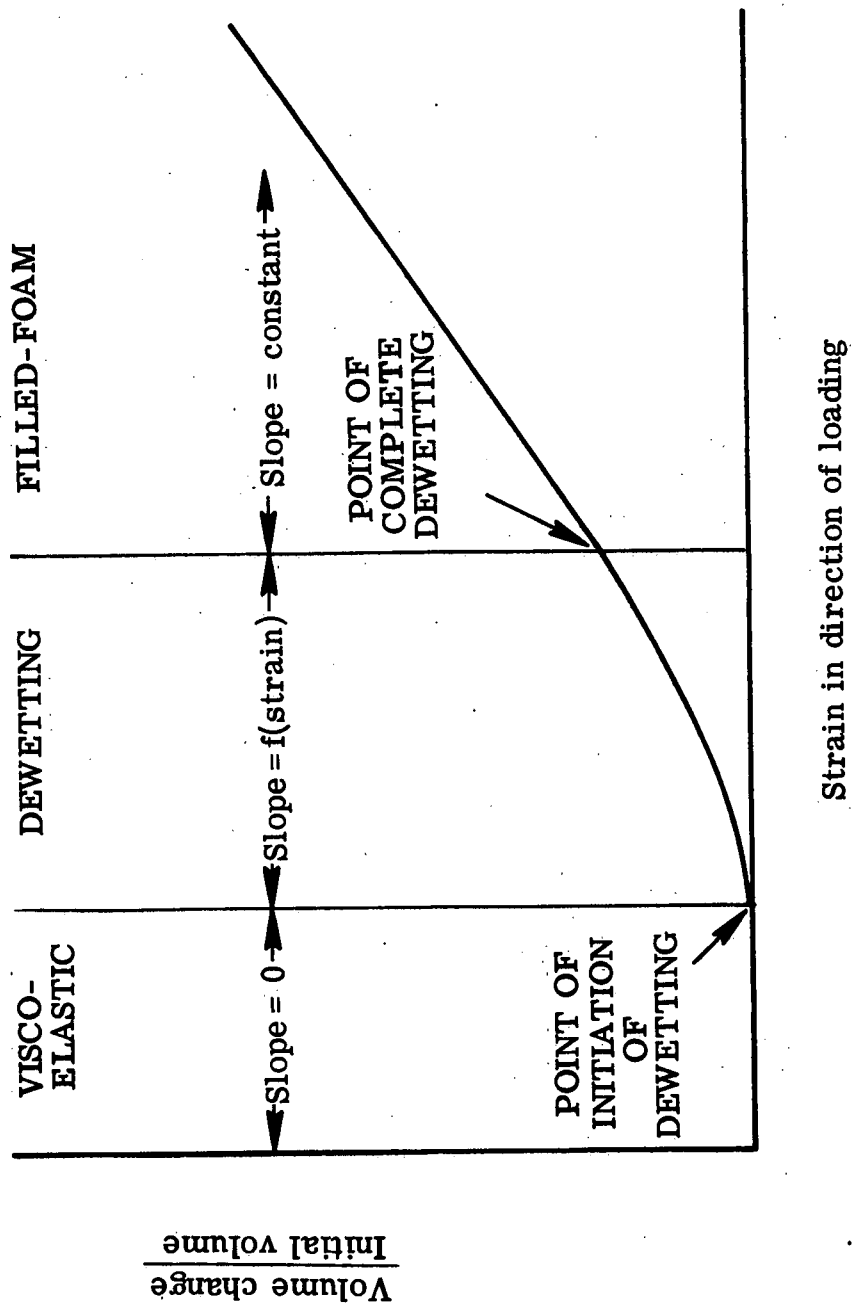


Figure 12. - Location of transition points from dilatational data.

complete dewetting are defined as that point at which a volume change is first noted and that point beyond which  $d(\Delta V/V_0)/d\varepsilon$  is constant, respectively.

Poisson's ratio technique. The Poisson's ratio technique is used for locating the point of initiation of dewetting. This technique is based upon comparison, at a particular strain level, of Poisson's ratio as determined experimentally for the material with Poisson's ratio of an incompressible material at the same strain level. The theory is that the material behaves as an incompressible solid prior to vacuole formation, and in the dewetting region, as the result of the volume increase, the material no longer appears incompressible. Figure 13 illustrates the technique. Reference 19 makes limited use of this technique for locating the initiation point.

Techniques for Correlating Mechanical Property Behavior.

With the advent of space flight there is much interest in characterizing the mechanical behavior of materials in various environments. Not only is the behavior of materials in the earth's environment (pressure, temperature, humidity, etc.) under study but the effects of the space environment, reentry environment, and other planetary atmospheres are being considered. In characterizing the behavior of materials in the various environments, it is desirable to develop correlation techniques which, when applied to experimental mechanical property data for a material, will result in an equation-of-state which in turn can be used

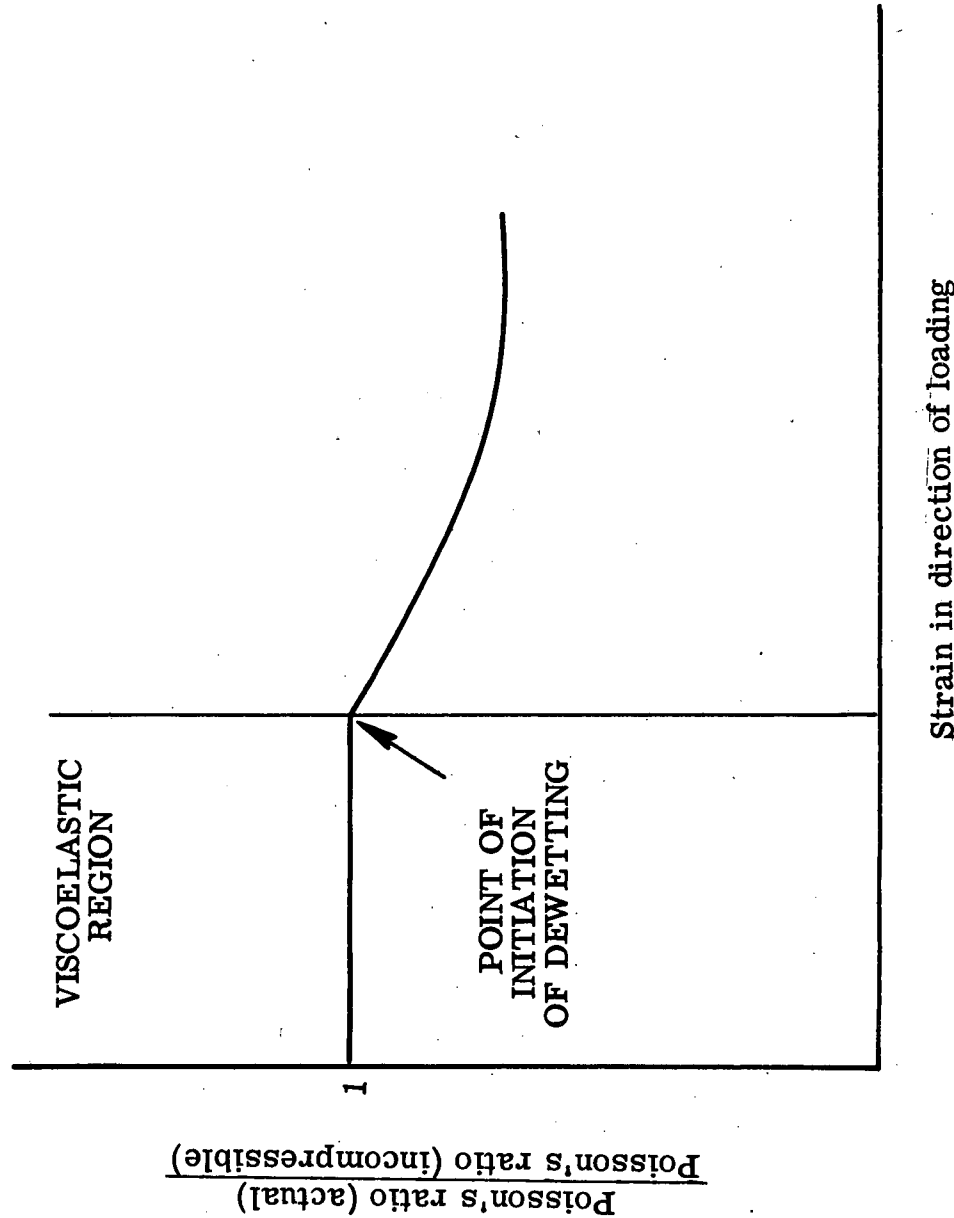


Figure 13. - Poisson's ratio technique for locating initiation point.

to calculate the mechanical behavior of the material. References 14, 20, 21, 22, and 23 deal with the development and use of such techniques for characterizing filled elastomers in various environments. The past application of these techniques have been in the earth's environment, investigating the effects of pressure, temperature, and humidity on the mechanical behavior of filled elastomers. Several of the more successful techniques will now be discussed: (1) the Arrhenius technique, (2) the dilatational technique, and (3) the compliance shift technique.

Arrhenius technique. The Arreheinuis technique is an activation energy concept based upon the general Arreheinuis equation

$$A = A_0 \exp \left[ -\frac{E_0}{RT} \right] \quad (6.2)$$

where:  $A$  = reaction rate

$A_0$  = pre-exponential function

$E_0$  = activation energy

$R$  = universal gas constant

$T$  = temperature

Activation energies are associated with many types of processes including the deformation of materials under imposed stresses. In the Arrhenius approach it is assumed that there are available to the material's "reaction units" an initial state, an activated state, and a final state. (See Figure 14) For a reaction or process to occur, the reacting units must go from the initial state to the final state

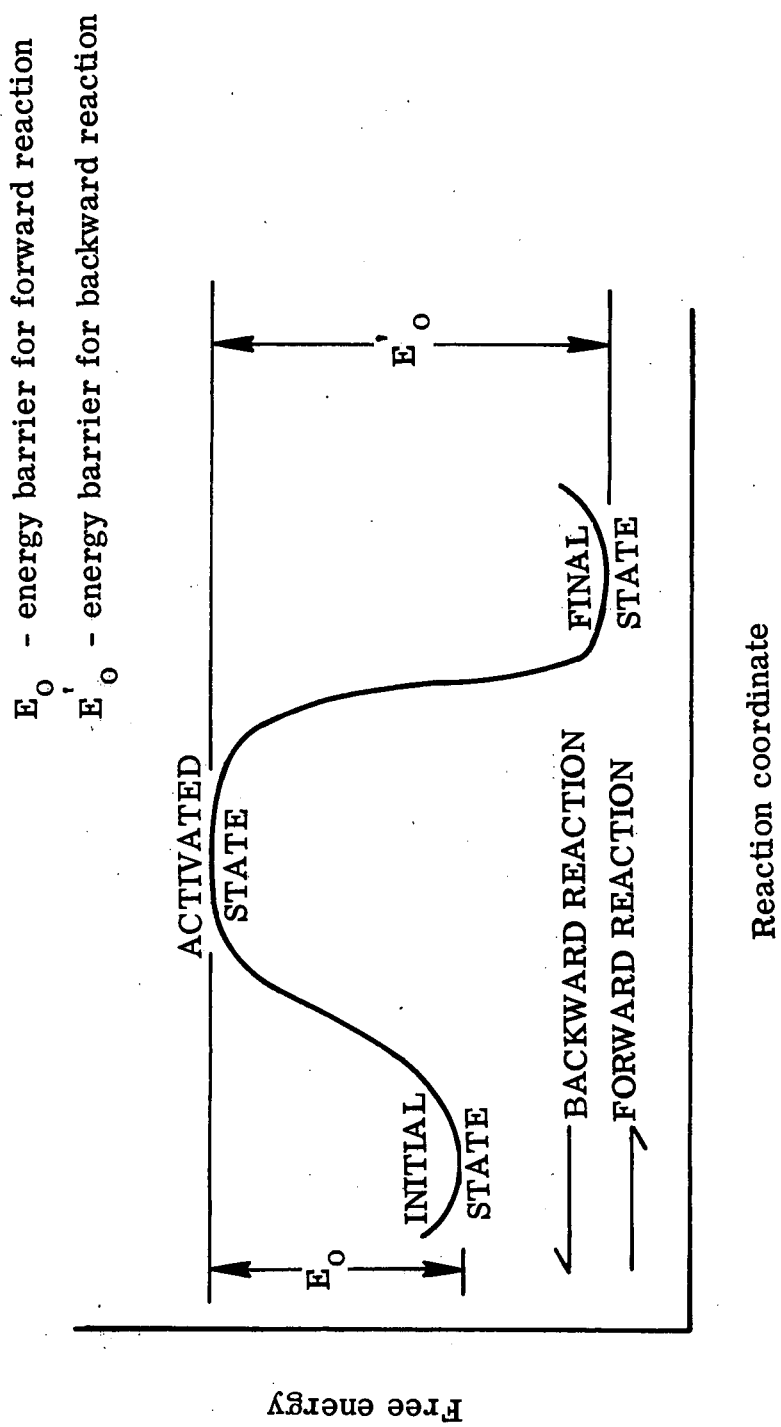


Figure 14. — Basic energy diagram for Arrhenius theory.

or from the final state to the initial state. In order to accomplish this the reaction units must enter the activated state and in doing so an amount of energy,  $E_0$ , is absorbed by the material. The rate of the reaction in one direction is given by an equation of the form of equation 6.2.

The normal application of the Arrhenius approach deals with empirically determining an activation energy from measurements taken at various temperatures. This activation energy is then related to the mechanisms controlling the behavior of the material in the temperature range considered. Graham, in references 14 and 24, applied the Arrhenius technique to the mechanical behavior of a solid propellant. From constant force uniaxial creep tests at ambient pressure in the temperature range of  $-50^{\circ}\text{C}$  to  $60^{\circ}\text{C}$ , Graham determined an activation energy which was associated with the fracture process. From this creep determined activation energy he showed that fracture times for the same material can be calculated for constant strain rate loading conditions. Graham did not define the relationship between the measured activation energy and the deformation processes occurring.

In some situations, due to additional test requirements, it is not desirable to vary temperature for application of the Arrhenius approach. In this case, an Arrhenius approach similar to that developed by Graham is developed for isothermal testing. In this approach, creep measurements are made at various stress levels rather than at various temperatures. In Appendix B, the Arrhenius equation is developed for

isothermal testing at different stress levels. The equation of interest is equation (B-14) and is

$$\ln(t_f T \sigma) = -C\sigma + \frac{E_0}{RT} + \ln \frac{h}{kC} \quad (6.3)$$

where:  $t_f$  = fracture time

$T$  = temperature

$\sigma$  = stress

$C$  = material constant determined by the Arrhenius technique

$E_0$  = activation energy

$R$  = universal gas constant

$h$  = Planck's constant

$k$  = Boltzman's constant

The derivation of equation 6.3 and the equation used by Graham assumes a constant stress loading on the material, whereas in the actual measurement a constant force loading is applied. The variation of stress during a constant force loading is generally small and can be neglected in equation 6.3. By plotting the results for a series of constant force creep measurements at a given temperature, as shown in Figure 15, and by applying equation 6.3,  $E_0$  and  $C$  can be determined from the intercept and slope of this curve. An equation-of-state based on the creep-measured activation energy can be developed (see Appendix B) and can be used to predict the fracture time of a material given a stress-time history. Figure 16 shows the results of this technique obtained by Graham (24) for a cyclic stress history. Note that the agreement

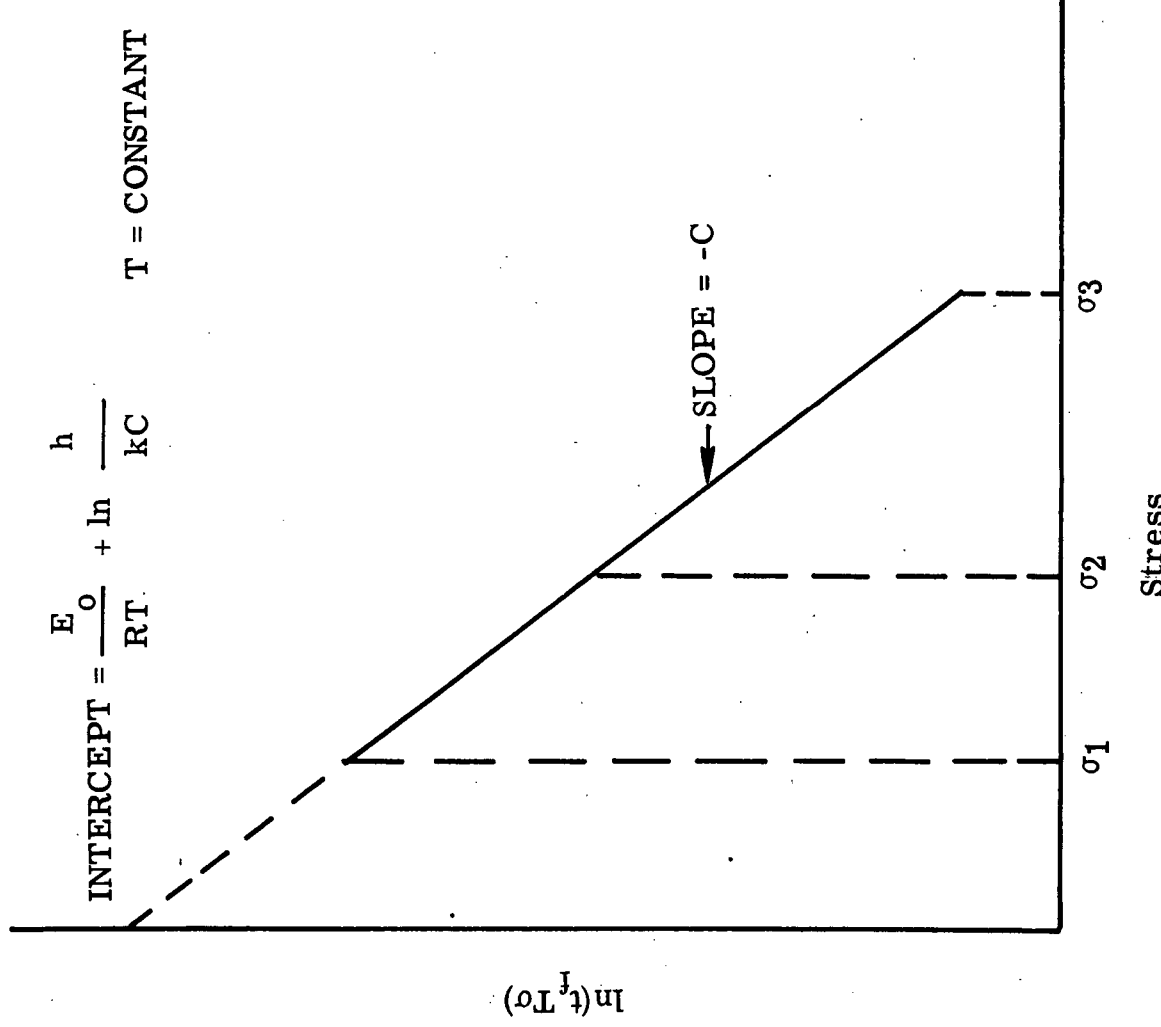


Figure 15. — Arrhenius plot for isothermal application of reaction-rate technique.

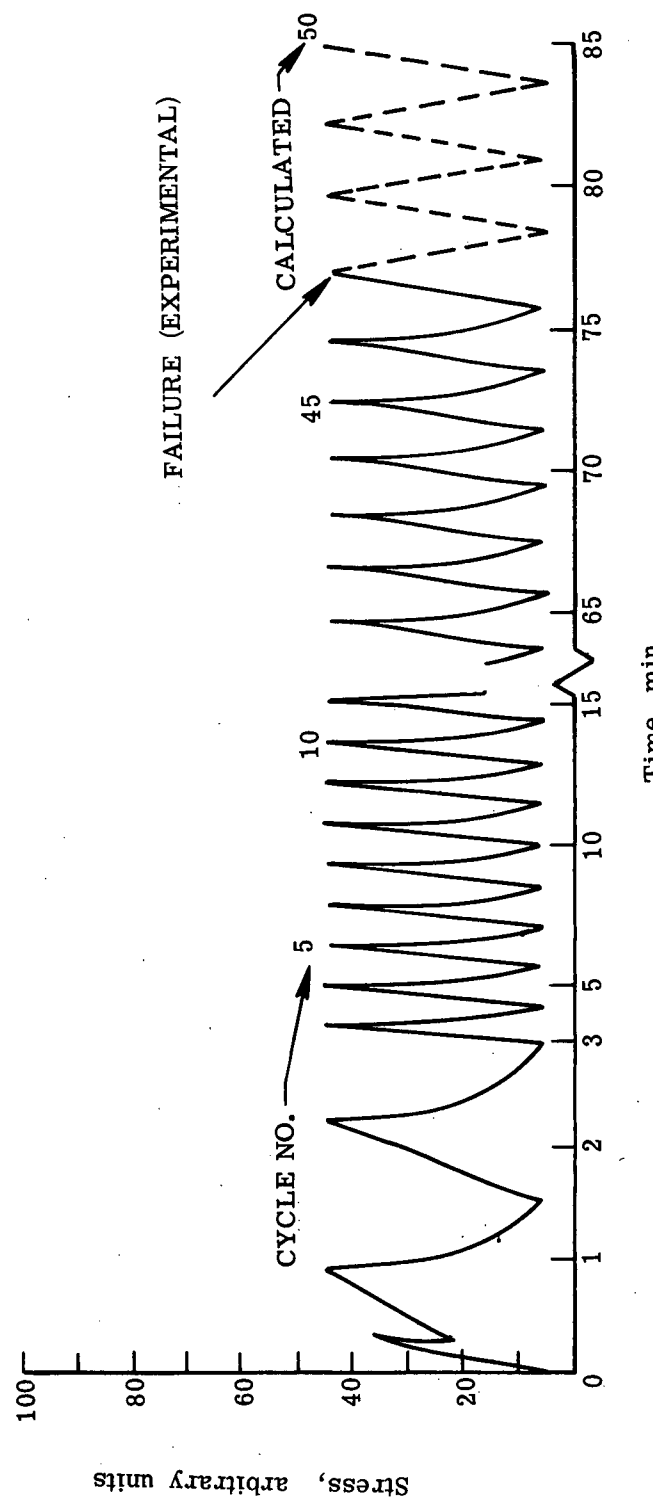


Figure 16. - Comparison of calculated and experimental failure for cyclic loading of a solid propellant.

between calculated failure (85 minutes) and the experimentally measured failure time (77 minutes) is good.

Dilatational technique. The dilatational technique is based on the volume change (dilatational) behavior of a material while it is being strained. As illustrated in the filled elastomer mechanical behavior model, the material dilates (increases its volume) in two regions of behavior, the dewetting and filled foam regions. The dilatational behavior of filled elastomers is frequently measured (10, 12, 20, 21, 23, 25) in association with mechanical property testing. The dilatational behavior is known to depend upon the nature of the filler-elastomer bond. Oberth has illustrated that weak filler elastomer bonds promote the dewetting process and that strong bonds tend to retard the dewetting process. The dilatational technique is based on the dilatational model as presented in Appendix A. The equations of interest in the development of this correlation technique are equations A-22, A-19, and A-20. These equations are as follows:

$$\frac{\Delta V}{V_0} = C \int_0^{\epsilon} 1 v_{fd} d\epsilon \quad (6.4)$$

$$\frac{d\left(\frac{\Delta V}{V_0}\right)}{d \epsilon} = C v_{fd} \quad (6.5)$$

$$\frac{d^2\left(\frac{\Delta V}{V_0}\right)}{d \epsilon^2} = C \frac{d(v_{fd})}{d \epsilon} \quad (6.6)$$

where the terms are as previously defined.

The experimental requirements of this technique are that the volume change of the material must be measured as a function of the length strain (in the direction of loading). The dilatational response of a filled elastomer under an uniaxial tensile load is shown in Figure 12 and has been previously discussed. This type of curve has been observed for various uniaxial tensile loading histories (21). Differentiation of the dilatational data of Figure 12 with respect to strain results in Figures 17 and 18 for the first and second derivatives, respectively. Figures 12, 17, and 18 are represented by equation 6.4, 6.5, and 6.6 respectively. Then from the model, Figure 18 is a plot of the frequency of dewetting versus strain. (The frequency of dewetting,  $\frac{d(V_{fd})}{d \epsilon}$ , is interpreted as an indication of that volume fraction of filler particles that are dewetted at a particular strain value). The format of Figure 18 is similar to that of a normal distribution curve of a random variable and thus can be represented statistically by a probability distribution function (26) (PDF) of the type

$$C \frac{d(V_{fd})}{d \epsilon} = \frac{1}{\sqrt{2 \pi} S} \exp \left[ \frac{-(\epsilon - \bar{\epsilon})^2}{2 S^2} \right] \quad (6.7)$$

where  $\bar{\epsilon}$  is the mean of the PDF and  $S$  is the standard deviation of the PDF. From statistics then

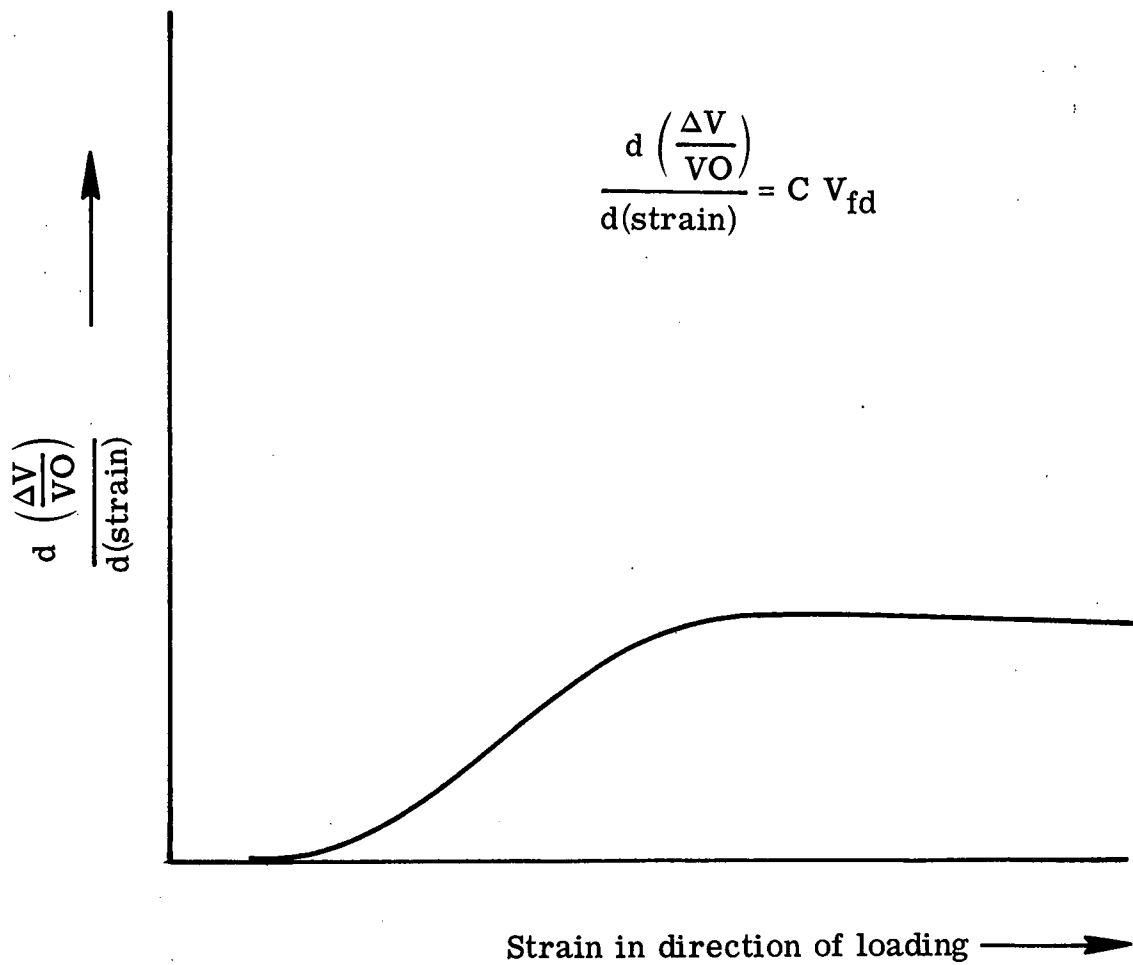


Figure 17. - First derivative of dilatation data.

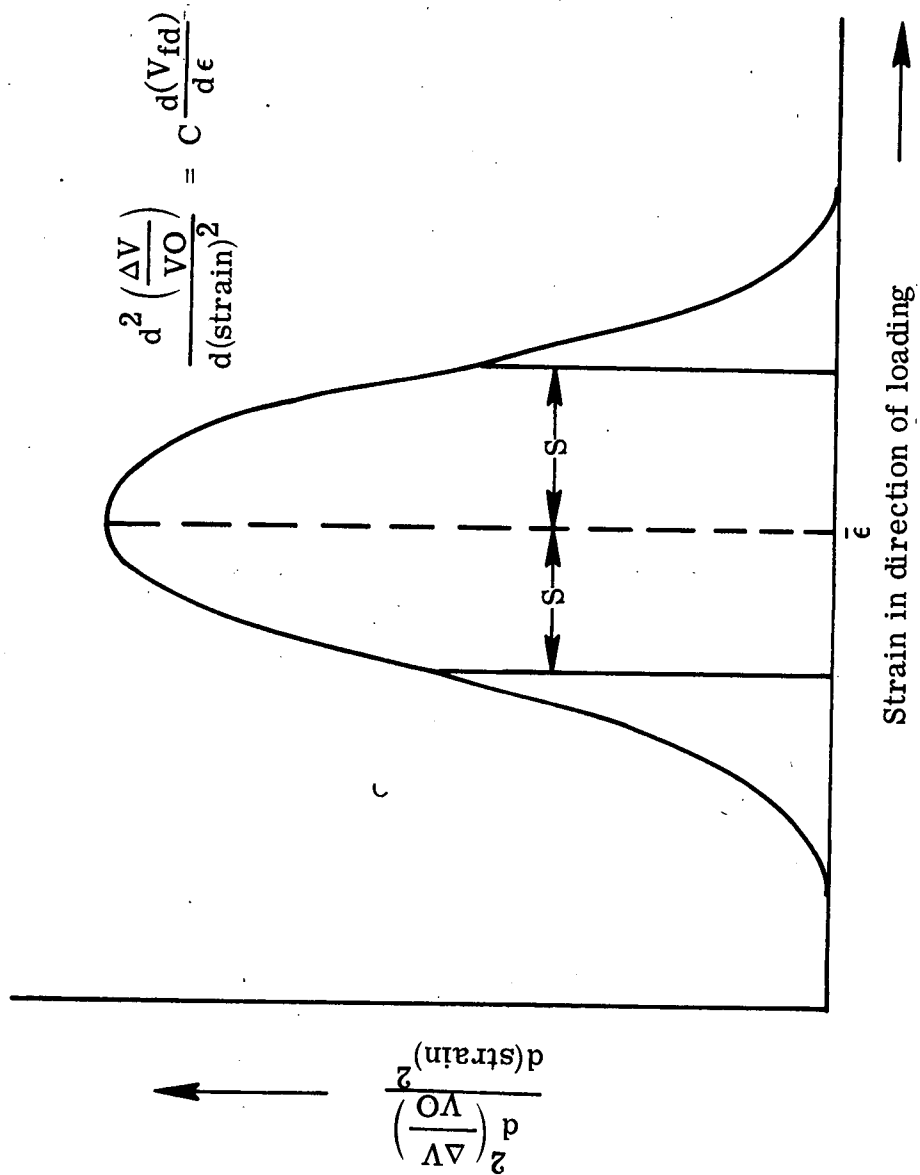


Figure 18. - Second derivative of dilatation data.

$$\int_{-\infty}^{\infty} \frac{1}{\sqrt{2 \pi} S} \exp \left[ \frac{-(\epsilon - \bar{\epsilon})^2}{2 S^2} \right] d\epsilon = 1 \quad (6.8)$$

and from the dilatational model

$$\int_{-\infty}^{\infty} \frac{d(V_{fd})}{d\epsilon} d\epsilon = V_{fmax} - V_{fdo} \quad (6.9)$$

where  $V_{fmax}$  is the final or total volume fraction of filler particles dewetted and  $V_{fdo}$  is the volume fraction dewetted at zero strain. It is assumed in Appendix A that  $V_{fdo}$  is zero due to the initial unstrained condition of the material. Therefore, equations 6.8 and 6.9 determine the value of  $C$  as being  $(V_{fmax})^{-1}$  and hence equation 6.7 becomes

$$\frac{d(V_{fd})}{d\epsilon} = \frac{V_{fmax}}{\sqrt{2 \pi} S} \exp \left[ \frac{-(\epsilon - \bar{\epsilon})^2}{2 S^2} \right] \quad (6.10)$$

Integration of equation 6.10 with respect to strain results in the cumulative distribution function (CDF)

$$V_{fd} = \frac{V_{fmax}}{\sqrt{2 \pi}} \int_{-\infty}^{n_1} \exp \left[ \frac{-n^2}{2} \right] dn \quad (6.11)$$

where  $n$  is a dummy variable defined as  $(\epsilon - \bar{\epsilon})/S$ . Equation 6.11 represents the volume fraction of filler which has been dewetted from strain zero to strain  $\epsilon_1$ . Integration of equation 6.11 in a similar manner gives

$$\int_0^{\bar{\epsilon}_1} v_{fd} d\epsilon = \frac{S V_{fmax}}{\sqrt{2 \pi}} \int_{-\infty}^{n_1} \int_{-\infty}^{n_1} \exp \left[ -n^2 / 2 \right] dn dn \quad (6.12)$$

Noting equation 6.4 and the value of  $C$ , equation 6.12 becomes

$$\frac{\Delta V}{V_0} = \frac{S}{\sqrt{2 \pi}} \int_{-\infty}^{n_1} \int_{-\infty}^{n_1} \exp \left[ -n^2 / 2 \right] dn dn \quad (6.13)$$

Equation 6.13 analytically describes the dilatational-strain behavior of the material. The parameters  $\bar{\epsilon}$  and  $S$  can be obtained from the measured dilatational behavior of the material as shown in Figure 19. From equation 6.13 and its derivative forms, equation 6.10 and 6.11, parameters can be defined whose magnitude and behavior are related to the dewetting process. These parameters are listed in Table III along with a brief description of their importance to the dewetting process.

Since the magnitude of  $S$  and  $\bar{\epsilon}$  are expected to depend on the stress history imposed on the material,  $S$  and  $\bar{\epsilon}$  must be determined as a function of stress. Only after the stress dependence of  $S$  and  $\bar{\epsilon}$  is determined, can a path-independent equation-of-state be considered.

Compliance Shift Technique. Numerous applications of shifting techniques have been used in mechanical property testing of polymeric materials (15, 21, 27-30). One well known shift technique is time-temperature superposition (27, 28, 31) in which the modulus or compliance of a material is measured as a function of time at various temperatures. Then by a horizontal translation of the isothermal data along

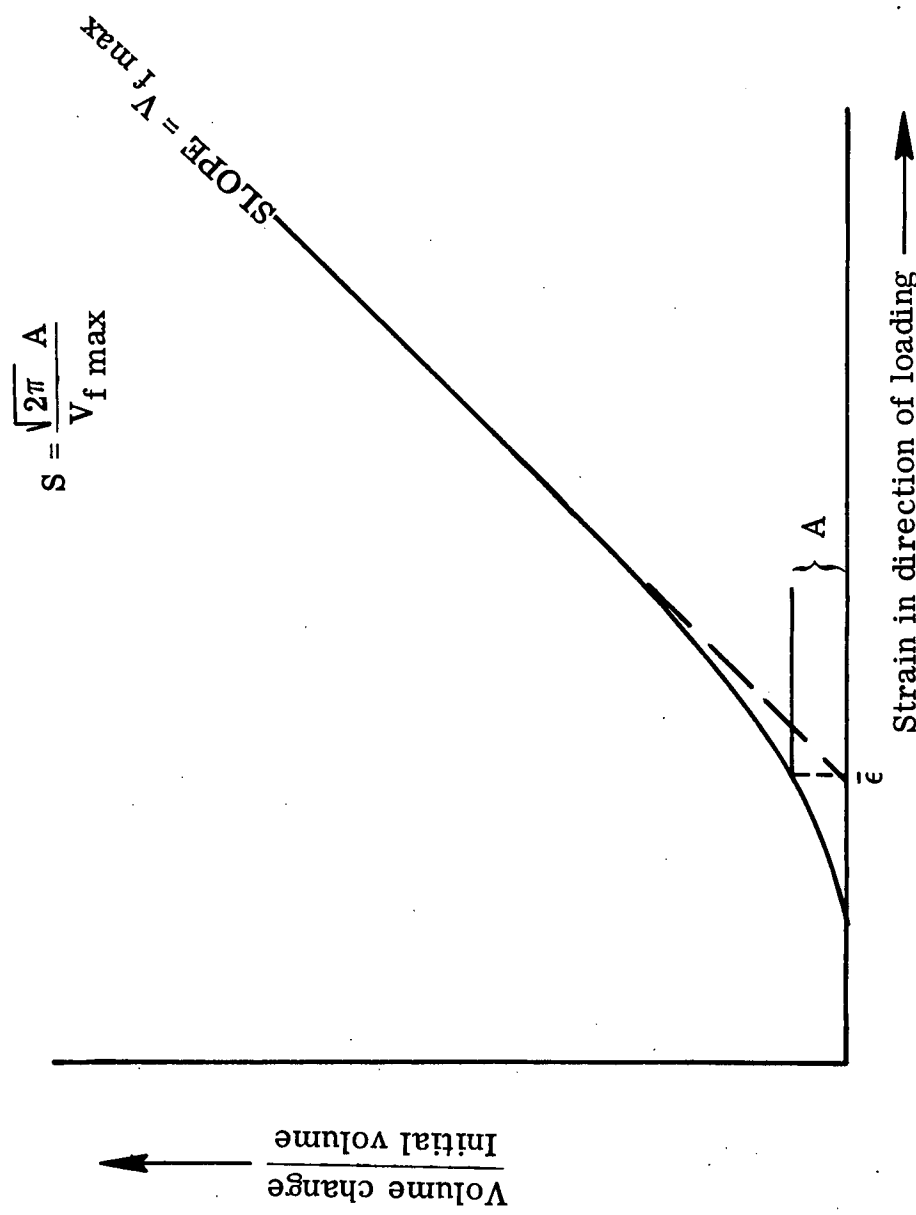


Figure 19. - Identification of parameters for statistical dilatational equation.

TABLE III  
PARAMETERS OF IMPORTANCE TO THE DEWETTING PROCESS

Parameter	Symbol	Source	Parameter Importance
Standard Deviation	S	Experimental Dilatational Data (Figure 19)	This parameter is an indication of the band width (strain width) over which the dewetting process is occurring.
Mean of the Strain Distribution	$\bar{\epsilon}$	Experimental Dilatational Data (Figure 18 or 19)	This parameter is that strain at which the frequency of dewetting $(\frac{dV_{fd}}{d\epsilon})$ is a maximum.
Volume Fraction Dewetted Filler Particles	$V_{fd}$	Equation 6-11	The value of this parameter at any particular strain value, $\epsilon_1$ , is an indication of the quantity of filler particles which have been dewetted from strain zero to strain $\epsilon_1$ .
Frequency of Dewetting	$\frac{d(V_{fd})}{d\epsilon}$	Equation 6.10	This parameter is an indication as to the rate (with respect to strain) at which the dewetting process is progressing.
Total volume fraction of Filler particles dewetted	$V_{fmax}$	Figure 19	This parameter indicates the volume fraction of filler particles that are dewetted in the material during the straining process. At a maximum this parameter is the volume fraction of the filler in the material.

the time axis (superposition), the isothermal curves are combined into a single curve (master curve) at some reference temperature. The goal of time-temperature superposition is to be able to predict the modulus or compliance of the material at long times from measurements at shorter times. Figure 20 illustrates the manner in which each isothermal curve is shifted to form the master curve. Analytically the horizontal shift employed in Figure 20 is represented as

$$J_{T_0} (t) = J_T \left( \frac{t}{a_T} \right)^* \quad (6.14)$$

or in terms of log time

$$J_{T_0} (\log t) = J_T (\log t - \log a_T) \quad (6.15)$$

where:

$J_T$  = compliance at temperature  $T$

$J_{T_0}$  = compliance at reference temperature,  $T_0$

$t$  = time under load

$\log a_T$  = log shift factor - number of log cycles an isothermal curve is shifted to form the master curve

Implicit in the application of time-temperature superpositioning are the assumptions: (1) no new mechanisms are introduced over the temperature range considered, and (2) that temperature affects only the rate of response of the material. Following the example set by time-temperature

\*This notation indicates that both  $J_{T_0}$  and  $J_T$  are identical functions of the independent variable; i.e.  $J_{T_0} = f(x) = J_T$ , but for  $J_{T_0}$ ,  $x$  is  $t$  and for  $J_T$ ,  $x = t/a_T$ .

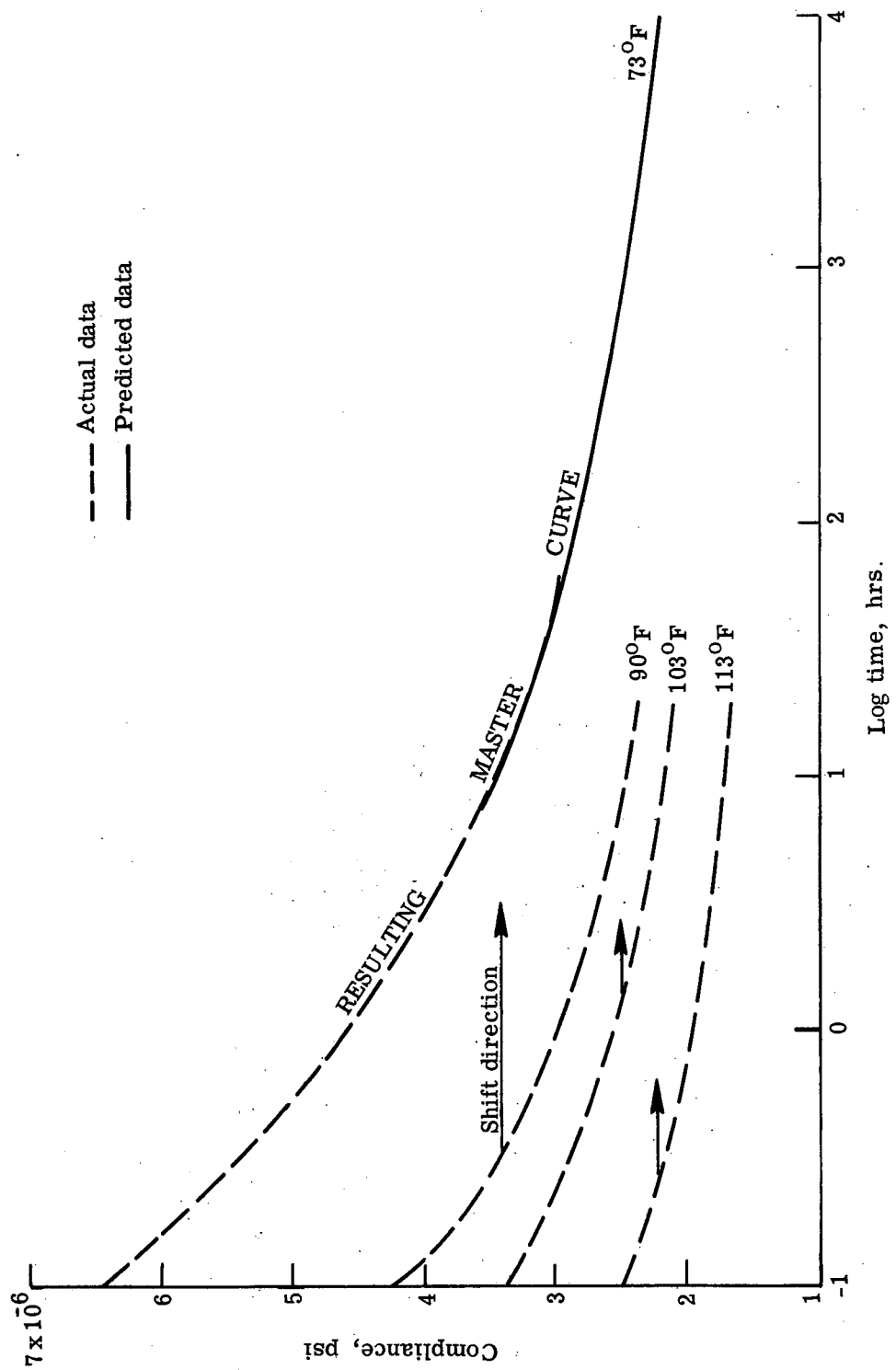


Figure 20. - Time-temperature superposition applied to polyethylene (27).

superpositioning and numerous experimental verifications of the technique, shift techniques have been used to generate master curves for various environments, such as stress (15) and humidity (21). For example, for the stress environment equation 6.14 becomes

$$J_{\sigma_0}(t) = J_{\sigma}(t/a_{\sigma}) \quad (6.16)$$

where:

$J_{\sigma}$  = compliance at stress  $\sigma$

$J_{\sigma_0}$  = compliance at reference stress,  $\sigma_0$

$a_{\sigma}$  = stress shift factor

For combinations of environments such as temperature, stress, and vacuum

$$J_{T_0, \sigma_0, V_0}(t) = J_{T, \sigma, V} \left( \frac{t}{a_T a_{\sigma} a_V} \right) \quad (6.17)$$

or in log time nomenclature

$$J_{T_0, \sigma_0, V_0}(\log t) = J_{T, \sigma, V} (\log t - \log a_T - \log a_{\sigma} - \log a_V) \quad (6.18)$$

where:

$J_{T, \sigma, V}$  = compliance at temperature, T; vacuum exposure, V; stress loading,  $\sigma$

$J_{T_0, \sigma_0, V_0}$  = compliance at reference environment

$t$  = time under load

$\log a_T$  = log shift factor for temperature — number of log cycles each isothermal curve is shifted to form master

$\log a_{\sigma}$  = log shift factor for stress — number of log cycles each iso-stress curve is shifted to form master curve

$\log a_v = \log$  shift factor for vacuum---number of log cycles  
each vacuum isochronal curve is shifted to form  
master curve

Implicit in equations 6.17 and 6.18 are the assumptions: (1) no new mechanisms are introduced over the temperature, stress, and vacuum environments considered, (2) change in an environmental parameter affects only the rate of response, (3) shift factors are dependent only on the indicated environmental parameter; i.e.,  $a_T$  is a function of temperature but not a function of stress or vacuum.

Summary

The literature review has shown a sparseness of *in situ* vacuum studies on the mechanical behavior of filled elastomeric materials. The existing investigations indicate that vacuum can and does cause sizeable changes in the mechanical properties of this class of materials. Existing studies concentrate on documenting the magnitude and direction of particular mechanical property changes for specific materials. A comprehensive understanding of the vacuum-material interaction occurring is not available from the literature. However, the literature does provide a mechanical properties model which is used to explain the behavior of filled elastomers in the earth's environments of pressure, temperature, and humidity. In addition, the literature reveals several experimental and analytical techniques which have been used in understanding the mechanical behavior of filled elastomers in the earth's environment. The nature and, in some cases, the incompleteness of the existing vacuum results make it impossible to apply the model and these techniques to an understanding of the vacuum-material interactions.

Based on the literature review, a research program was initiated to study the mechanical behavior of a particular filled elastomer with emphasis on understanding the vacuum-material interactions occurring and on the development of analytical techniques which are useful for predicting vacuum behavior. The program was oriented such that the model and techniques which have been most successful in explaining material behavior in the earth's environment could be applied to the vacuum results.

C2

## VII. THE INVESTIGATION

### Test Technique and Material Selection

The creep test was selected for use in characterizing the mechanical behavior of the test material. This technique has long been recognized as one of the more fundamental techniques for determining the effects of surrounding environments on the mechanical behavior of materials (32). In this application, the creep testing sequence consisted of applying a uniaxial constant force to the test material and measuring the time required to fail (rupture) the material. Longitudinal and diametrical deformation of the material was measured as a function of loading time. Correlation of these measured parameters as a function of vacuum storage time for the material provided the basis for studying the vacuum-material interactions that occurred. Incorporation of these results into the analytical techniques described in Section VI added further insight into these interactions as well as providing a basis for analytically describing the mechanical behavior of the material in vacuum.

Selection of the test material was based on the following criteria:

- (1) The material must be representative of filled elastomers in general use.
- (2) While still a representative filled elastomer, the material's composition should be simple, i.e., at best a single filler in a single matrix.

- (3) The material's mechanical properties must have been shown to be sensitive to the vacuum environment.

A review of the literature indicated that a filled elastomer was available which met the above conditions. The material selected for the investigation was an ammonium perchlorate filled butadiene-acrylic acid copolymer, known in the industry as a composite solid propellant. The particular formulation of interest was TPH 3105.

#### Research Program

The purpose of the research program was three-fold: (1) to determine the effects of vacuum on the creep properties of TPH 3105, (2) to investigate the possibility of analytically describing the vacuum behavior of TPH 3105, and (3) to investigate the vacuum-material interaction occurring for TPH 3105. To accomplish these purposes, samples of TPH 3105 were creep tested in a vacuum and in a reference ambient environment. A total of 138 samples were tested of which 66 were tested in vacuum. All creep measurements were made at  $83^{\circ}\text{F} \pm 0.5^{\circ}\text{F}$  and all test samples were preconditioned for a minimum of 35 days at  $83^{\circ}\text{F} \pm 0.5^{\circ}\text{F}$  and 50% R.H.  $\pm 2\%$ . Vacuum samples were stored in a vacuum chamber at  $81^{\circ}\text{F} \pm 3^{\circ}\text{F}$  and were exposed to vacuum for periods up to 14 days. Vacuum environments ranged from  $5 \times 10^{-6}$  torr (after 2 hours of pumping) to  $5 \times 10^{-8}$  torr (after 14 days of pumping). Samples were creep tested after having been exposed to the vacuum environment for approximately 2, 7, and 14 days. Reference environment samples were stored in the test chamber for 1 day prior to testing, and the

test chamber environment was identical to the preconditioning environment. Creep measurements were made at three stress levels: 51, 56, and 61 psi.

#### Test Apparatus

The test apparatus consisted of a vacuum chamber, a pre-conditioning chamber, a creep testing apparatus, and various types of instrumentation. The vacuum chamber was a stainless steel cylinder approximately 32 inches in diameter and 4 feet in length and is described in detail in reference 2. With its liquid nitrogen-trapped diffusion pump system, the chamber can attain, from atmospheric pressure (without test samples), a vacuum of  $10^{-9}$  torr after approximately 4 hours of pumping. For these investigations the chamber pressure with test samples installed ranged from  $5 \times 10^{-6}$  torr after 2 hours of pumping to about  $5 \times 10^{-8}$  torr after 14 days of pumping. Figure 21 shows a typical pressure-time history for the vacuum exposures. The chamber pressure was continuously monitored with a Bayard Alpert ionization gage. Frequent mass spectrometer measurements were made to identify the gas composition in the chamber. Temperature control of the chamber was provided by resistance heaters at the base of the chamber. This system maintained the test sample (sample being creep tested, sample position 1 as shown in Figure 28) at  $83^{\circ}\text{F} \pm 0.5^{\circ}\text{F}$ . However, as a result of the heating system, a  $\pm 3^{\circ}\text{F}$  temperature differential existed among the different sample storage positions in the test chamber ( $78^{\circ}\text{F}$  to  $84^{\circ}\text{F}$ ).

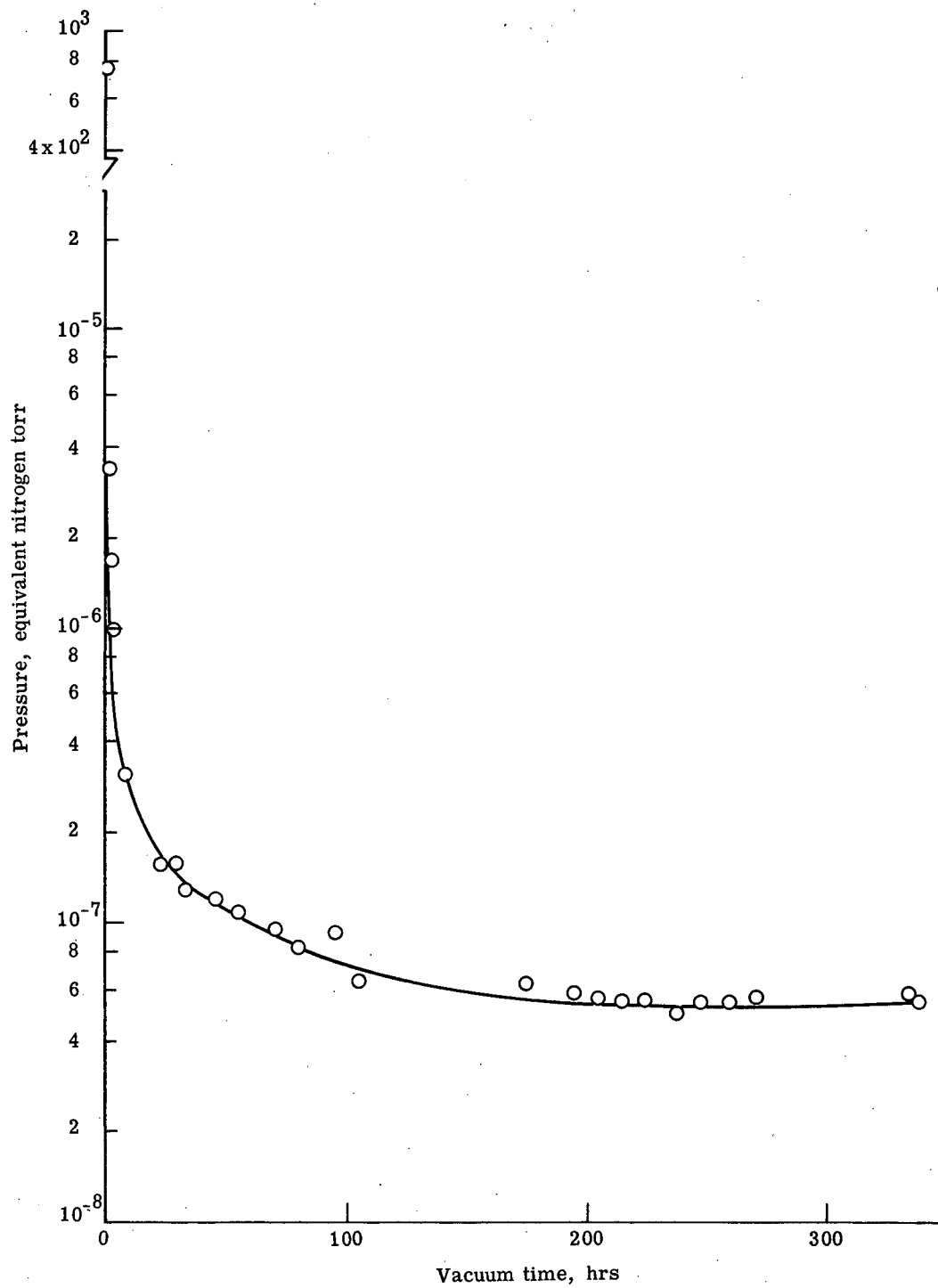


Figure 21. - Typical pressure-time history for vacuum samples.

The preconditioning chamber was used for preconditioning the test samples prior to vacuum and reference environment testing. The chamber consisted of a temperature and humidity controlled glove box with an internal volume of approximately 16 ft<sup>3</sup>. The glove box was equipped with an ante-chamber arrangement for entry into the interior volume and featured shoulder length gloves for manipulation of objects within the box. A water-glycerin solution was used to maintain the humidity at 50% ±2% and frequent refractive index measurements were made of these solutions to ensure humidity control. Humidity solutions were changed as required (usually about every 10 days) and the contents of the preconditioning chamber were exposed to the surrounding room environment (50% R.H. ±10%, 77° ±10°F) for approximately 10 minutes during a solution change. A forced convection heater installed inside the glove box maintained the samples at 85°F ±0.5°F during preconditioning. The heater employed a continuously operating fan and a resistance heater whose output was controlled by a proportional temperature controller. The input signal to the proportional controller was an air temperature probe located in the glove box. Samples preconditioned in the preconditioning chamber were sealed in plastic bags before being removed from the preconditioning environment.

The creep testing apparatus was specially designed and installed in the vacuum chamber in order to perform the required in situ

measurements. The apparatus had two basic functions: (1) to provide in situ storage of a relatively large number of test samples, and (2) to allow any given sample to be creep tested at any given time. The test apparatus was designed to store and test 24 samples in one given chamber pumpdown and was constructed primarily of stainless steel and aluminum. Figure 22 shows a photograph of the apparatus identifying its major components: (1) storage table, (2) sample jaw, (3) loading train, and (4) test weight.

#### Storage Table

The storage table, shown in the vacuum chamber in Figure 23, was a 30-inch diameter gear, supported on a central shaft which was free to rotate a full  $360^\circ$ . A matching pinon gear and rotary feedthru allowed external indexing of the storage table. (The central shaft, pinon gear, and feedthru cannot be seen in the photograph). The 30-inch diameter gear had 24 equally spaced slots, along its circumference, for locating the sample jaws.

#### Sample Jaw

Sample jaws (Figure 23) slide thru the slots on the storage table and are supported on the top side of the table by rectangular washers. The sample jaws are designed with a T-bolt on top for lifting the sample and a machined slot on the bottom for receiving a circular washer attached to the top of the sample.

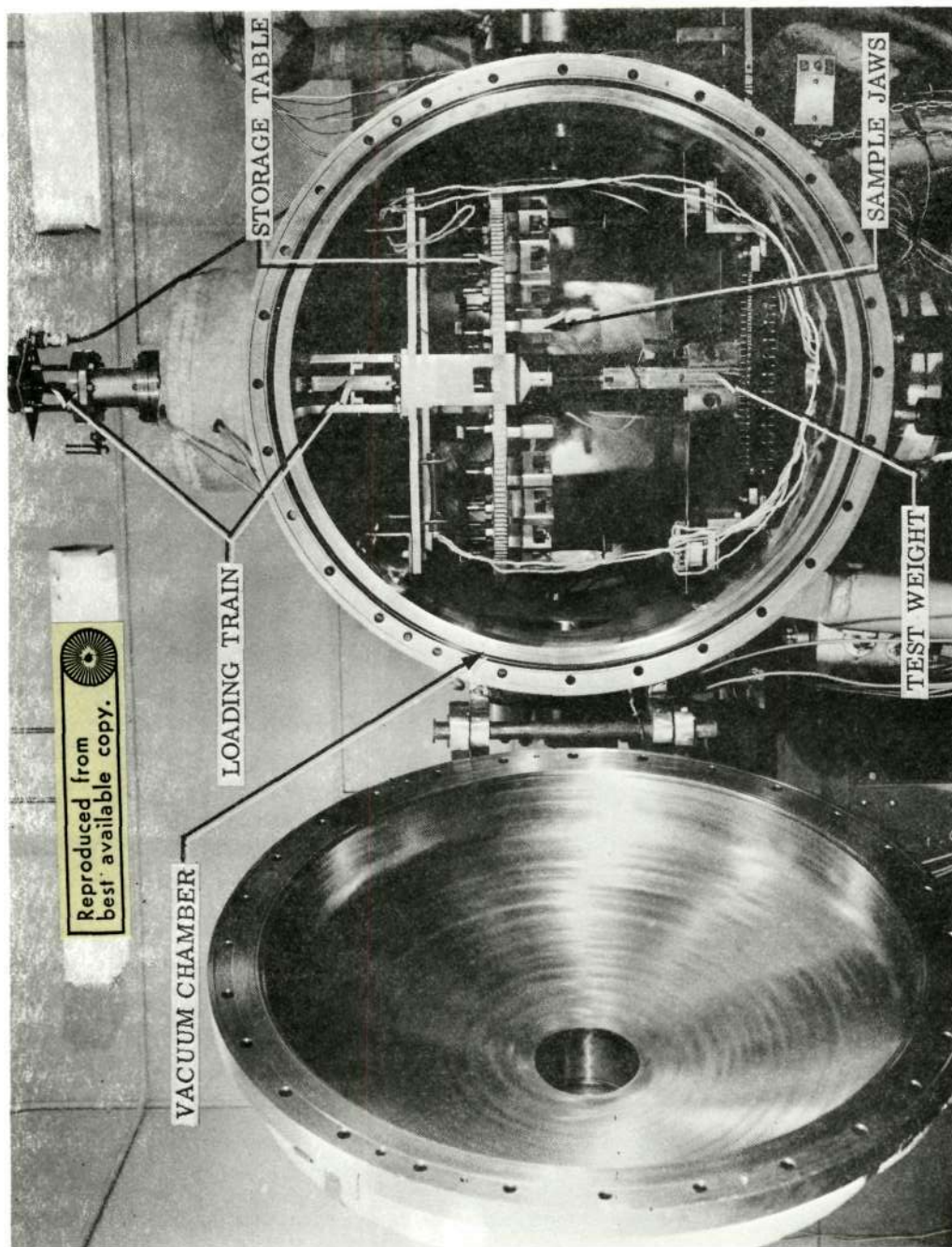


Figure 22. - Photograph of test apparatus.

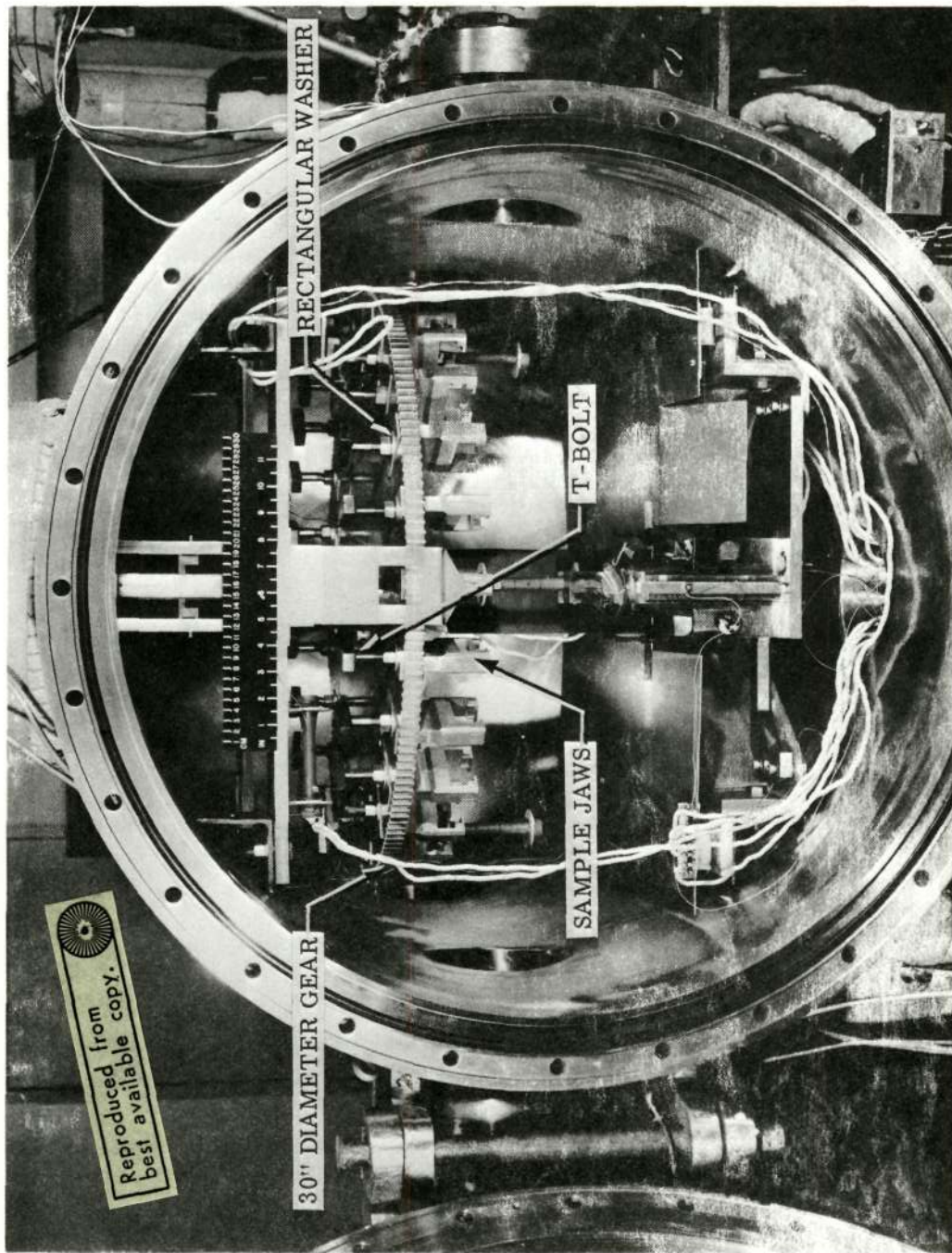


Figure 23. - Close-up photograph of creep apparatus.

Loading Train

The loading train provided the linear motion for lifting the test sample and the test weight. External rotary motion from a 300 rpm electric motor was transformed by a jack screw arrangement into linear motion which lifted the T-bolt, test sample, and test weight. Continuous operation of the electric motor lifted the test weight at a linear rate of 2.4 in./min. Return of the loading train to its starting position allowed the next test sample to be rotated into the test position.

Test Weight

The test weight (Figure 24) was a hollow stainless steel container whose weight was varied from 10 lb. to 12 lb. by adding mercury. A tapered slot machined in the top of the weight received the sample's bottom washer. With the sample jaw resting on the storage table, the bottom washer of the sample was free to pass thru the weight. Guide posts were attached to the sides of the weight to ensure that the weight returned to its initial position on the weight platform after sample failure. With the weight in the up position (sample loaded configuration) the weight was free swinging and thus assured uniaxial loading. The weight and weight platform had built-in electrical circuits which activated the sample timer for measuring loading time and an alarm if the weight was in contact with the weight platform during the creep measurement.

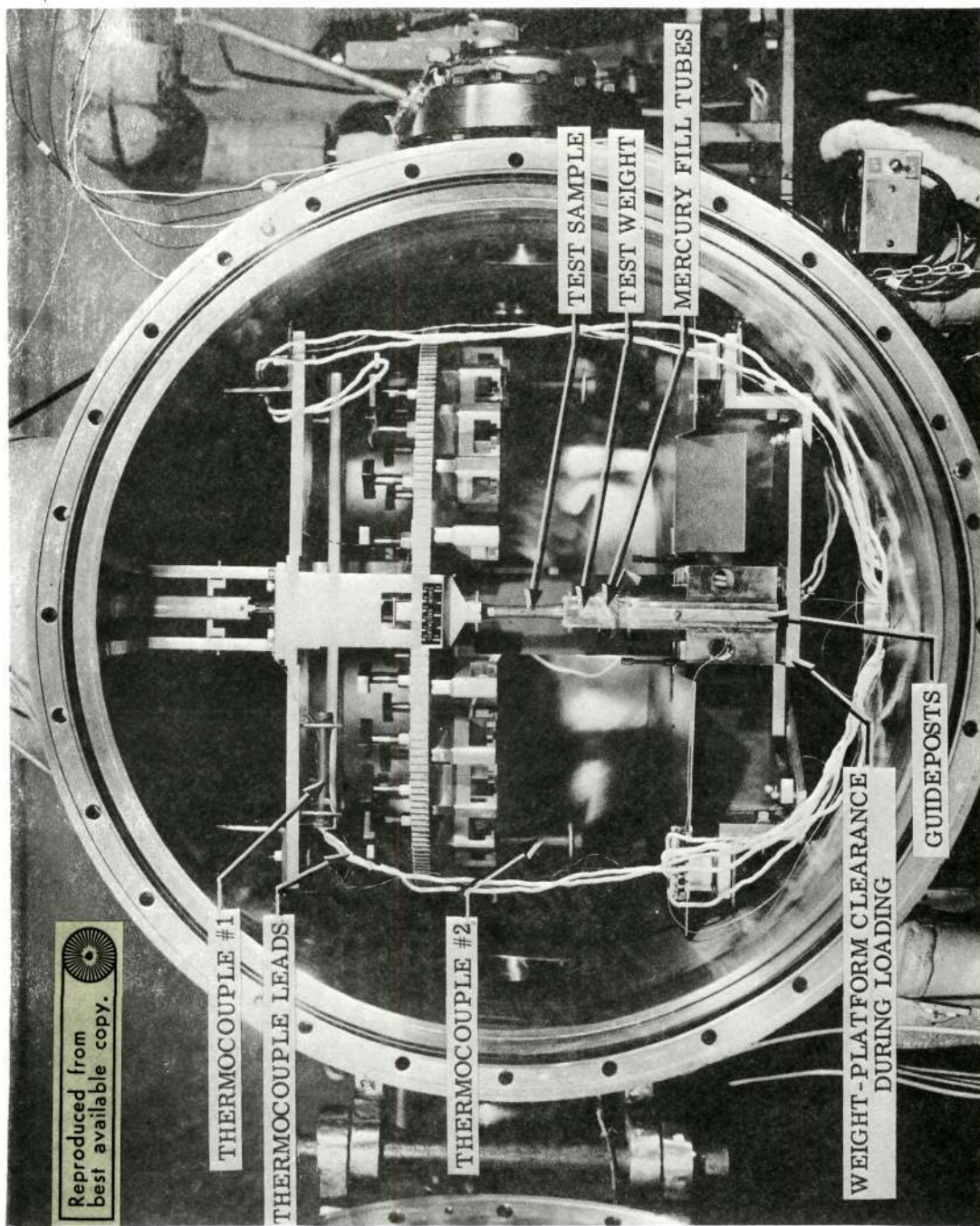


Figure 24. - Photograph of creep apparatus with sample loaded.

Instrumentation associated with the creep measurement consisted of the sample timer, the temperature monitoring system, and the strain-monitoring system. The sample timer was a 1000-minute, in increments of 0.1 minute, electric clock, automatically activated and stopped by the lifting of the weight and the return of the weight to the weight platform, respectively. The temperature monitoring system employed thermocouples embedded in two test samples. Thermocouple 1 was embedded in a sample attached to the support frame of the test apparatus near the test position (see Figure 24). This thermocouple indicated the temperature of a sample during the creep measurement and controlled the heat input to the vacuum chamber's temperature control system. Thermocouple 2 was embedded in a sample located on one of the 24 sample slots of the storage table. This thermocouple indicated the temperature difference among the samples stored at various locations around the table. This temperature variation was at a maximum 6°F. Outputs from both thermocouples were recorded on a millivolt chart recorder. The straining monitoring technique featured a pre-programmed time sequence photographing of the test samples. The diameter change and elongation between bench marks on the sample were recorded on 70 mm film using the sample timer as the time reference. Figure 25 shows a photograph of the vacuum chamber with the test camera in position. Both control and vacuum creep measurements were performed on the above apparatus and in the vacuum chamber. For control samples, the vacuum chamber was maintained at atmospheric pressure with 50% r. h. ( $\pm 2\%$ ) air and 83°F ( $\pm 0.5^{\circ}\text{F}$ ).

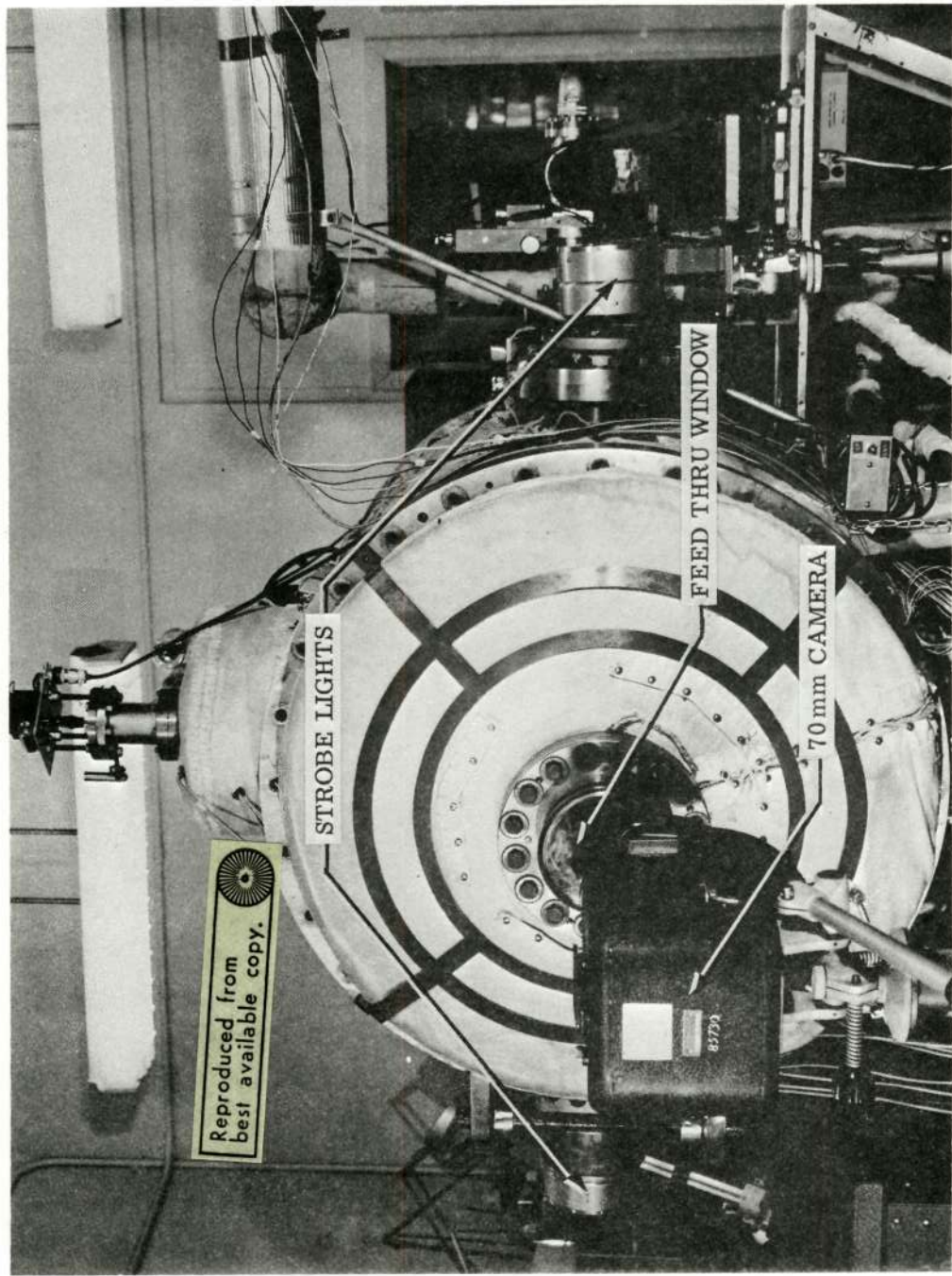


Figure 25. - Test camera location.

Sample Preparation

The filled elastomer used in this investigation was a 82% (by weight) ammonium perchlorate filled butadiene-acrylic acid copolymer known in the industry as TPH 3105, a composite solid propellant. The propellant was manufactured for the subject investigation under contract (33) by the Elkton, Maryland Division of the Thiokol Chemical Corporation. The detailed composition of the propellant is classified information but can be obtained by appropriate request from the author, National Aeronautics and Space Administration, Langley Research Center, Hampton, Virginia. The propellant batch report supplied with the tensile samples is given in Table IV. Four hundred cast circular samples of the configuration shown in Figure 26 were X-rayed for voids and supplied to the author. Sample washers (aluminum) were attached perpendicular to the axis of the samples with an epoxy and served as sample grips during creep testing. After fabrication the samples were stored at room temperature and 52% r.h. until shipped to the author. Upon receipt of the samples they were immediately placed on specially designed racks (Figure 27) and were stored at 50% R.H.  $\pm 10\%$  and  $77^{\circ}\text{F} \pm 10^{\circ}\text{F}$  until placed in the preconditioning chamber. Groups of 50 test samples were bench marked, and placed in the preconditioning environment of 50% r.h.  $\pm 2\%$  and  $83^{\circ}\text{F} \pm 0.5^{\circ}\text{F}$ . All samples remained in this preconditioning environment for at least 35 days. Samples were sealed in plastic bags and then removed from the preconditioning chamber for transfer to the vacuum chamber for either vacuum testing or control testing.

TABLE IV  
PROPELLANT BATCH REPORT ON TPH 3105

Mix Date : March 9, 1970

Release Date : April 9, 1970

In-Process Tests

Total Solids (%)	82.00
Theoretical Uncured Density (g/cc)	1.623

Physical Properties (Cured)

Cured Density (g/cc)	1.617
Modulus, E <sub>(2.6)</sub> *(psi)	886
Maximum Stress (psi)	125
Maximum Strain at Maximum Stress, e <sub>(2.6)</sub> *(in./in.)	0.243

\*Based on an assumed gage length of 2.6 inches

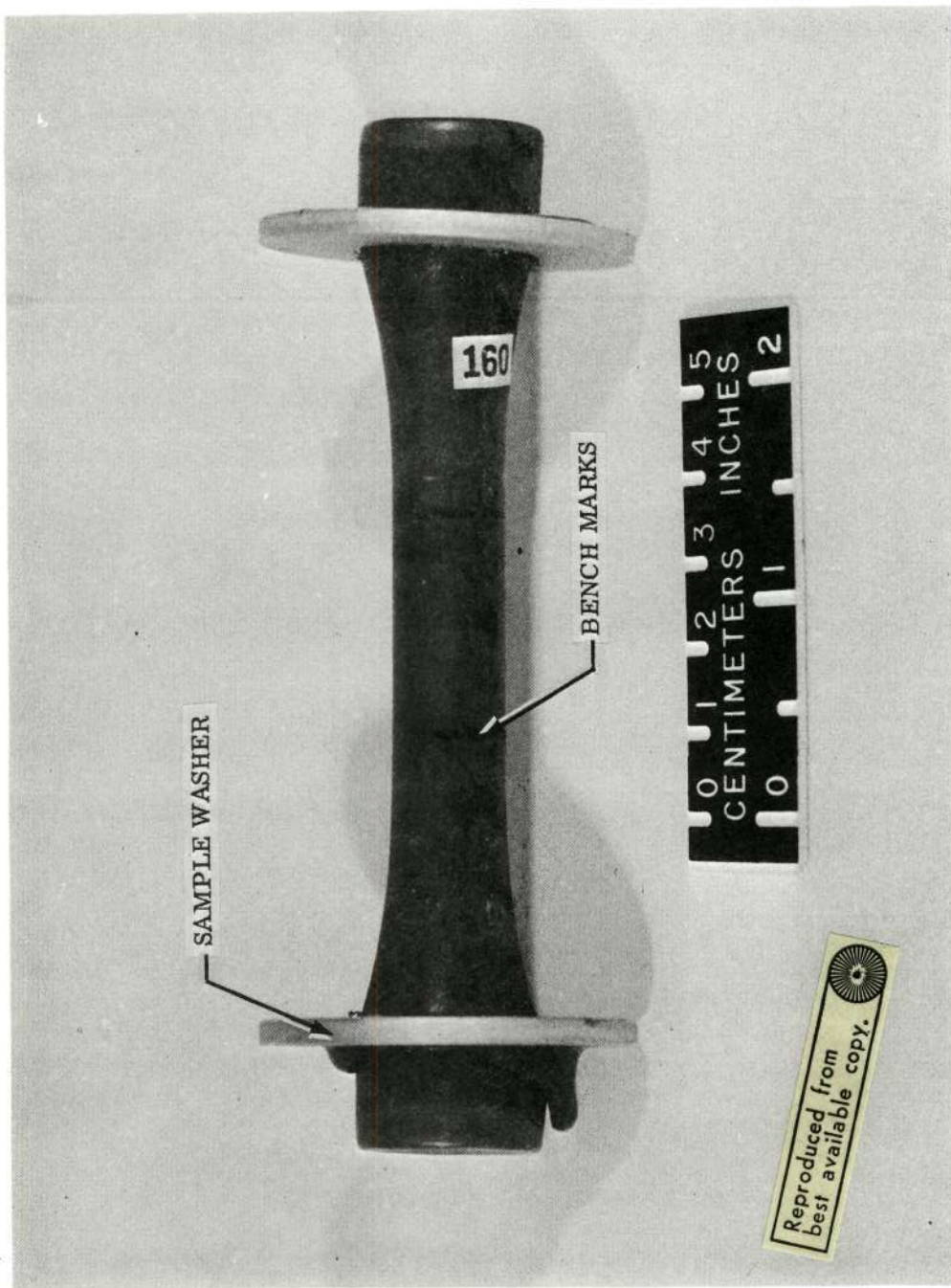


Figure 26. - Photograph of test sample.

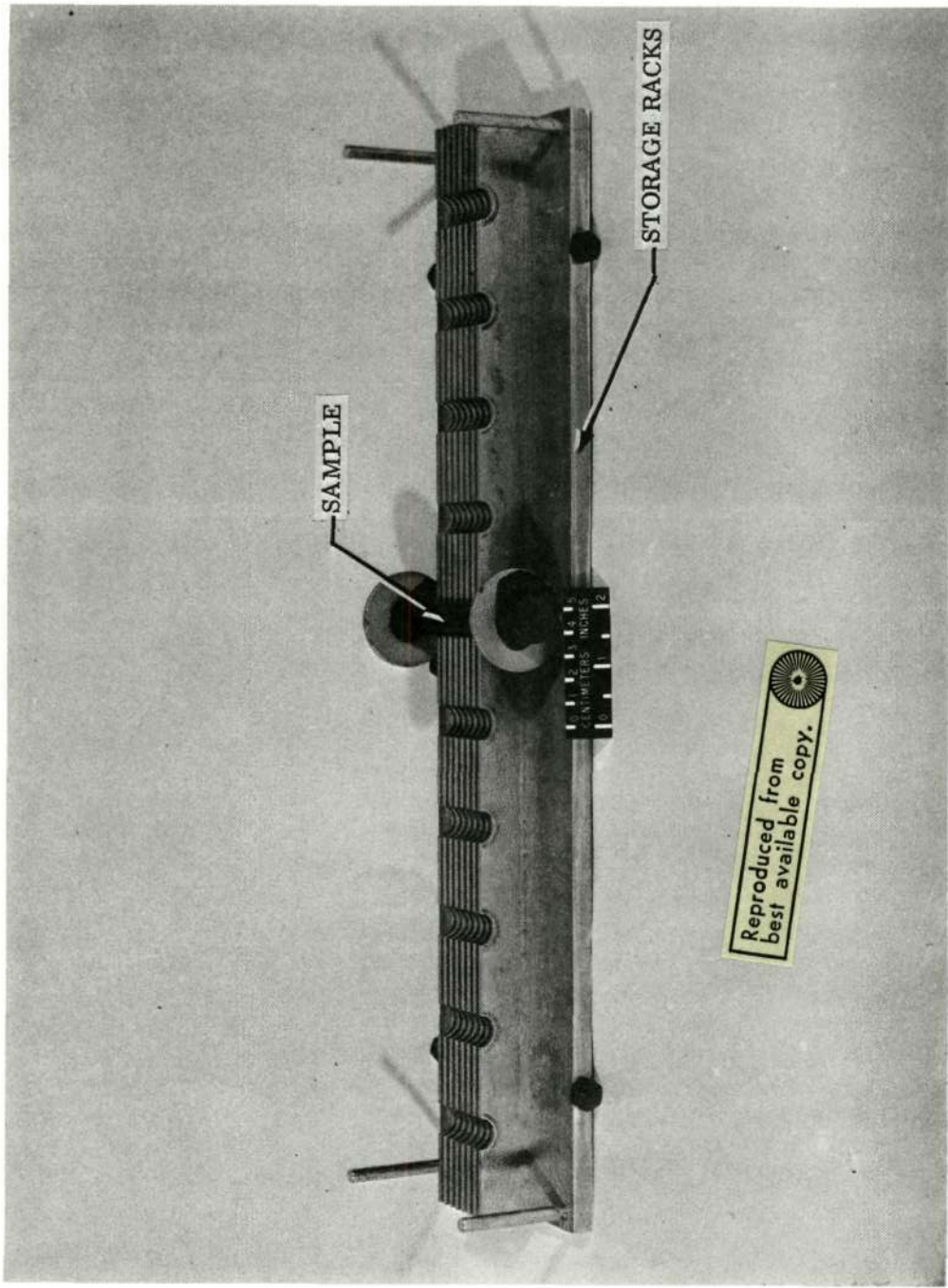


Figure 27. - Preconditioning storage racks.

Test Procedures

The test procedures followed during the experimental portion of this investigation are described in this section. Three separate procedures are given: (1) Control Sample Procedure, (2) Vacuum Sample Procedure, and (3) Creep Measurement Procedure.

Control Sample Procedure

After a minimum of 35 days of preconditioning, test samples were sealed in plastic bags and then removed from the preconditioning environment. The samples (groups of 10, 20, or 22) were taken to the vacuum chamber (located in another building), removed from the bags, and installed in the creep apparatus. Prior to removal of the samples from the plastic bags, the relative humidity and temperature of the room were measured (see Table V\*). Alignment checks were then made on the samples and sample jaws to ensure that uniaxial tensile loading would occur.

Approximately 150 in.<sup>3</sup> of water-glycerin solution was placed in containers (100 in.<sup>2</sup> in surface area) located in the vacuum chamber. Approximately 2 hours elapsed between removal of the samples from the preconditioning environment and the sealing of the vacuum chamber door. After the temperature control system of the chamber was started, one hour was required for the temperature of the samples to reach 85° F ± 0.5° F. After 24 hours of storage under these conditions, the test samples were tested in accordance with the "Creep Measurement Procedure." One to two days,

---

\*The 90% confidence interval column of Table V is discussed in the Data Reduction section.

TABLE V  
SAMPLE GROUP DATA LISTING

Stress psi	Environment Group	Room Environment During Chamber Loading		Number of Samples Tested	Number of Samples Falling within 90% Failure time Confidence Interval	Vacuum Exposure Time Variation Within the Group, hrs	
		Temperature °F	Humidity % r.h.			Minimum	Average
51	Air, 50% r.h.	74	72	42	9	46.0	55.6
	Vacuum, 51 hrs.	75	40	10	6		
	Vacuum, 173 hrs.	75	40	7	3		
	Vacuum, 348 hrs.	75	40	6	4		
56	Air, 50% r.h.	72	32	20	5	44.9	47.9
	Vacuum, 47 hrs.	73	37	8	4		
	Vacuum, 170 hrs.	73	37	7	4		
	Vacuum, 338 hrs.	73	37	7	4		
61	Air, 50% r.h.	79	48	10	5	45.0	47.3
	Vacuum, 46 hrs.	72	39	8	4		
	Vacuum, 171 hrs.	72	39	7	4		
	Vacuum, 337 hrs.	72	39	6	2		

depending on the failure time of the samples, were required to complete the testing of each sample group. After completion of the creep testing, the chamber was opened and a refractive index measurement made of the humidity solution. For all reference environment tests, the relative humidity remained at 50%  $\pm 2\%$ . This same procedure was followed for each reference environment test conducted.

#### Vacuum Sample Procedure

The "Vacuum Sample Procedure" is identical to that of the "Control Sample Procedure" up to the point where the humidity solution is installed in the chamber. At this point the chamber door was sealed and the vacuum pumps and temperature control system was started. Due to the influence of the liquid nitrogen trap, a time interval of approximately two hours was required to stabilize the temperature at  $83^{\circ}\text{F} \pm 0.5^{\circ}\text{F}$ . As noted earlier, in the vacuum mode there existed temperature differences among the various sample positions (see Figure 28). By testing the samples in table sequence and by rotating the table in one direction as shown in Figure 28, the sample being tested was always at equilibrium at  $83^{\circ}\text{F} \pm 0.5^{\circ}\text{F}$ . Because of convection currents in the chamber, this problem did not occur in the reference environment tests. For each pumpdown, samples (groups of 6, 7, or 8 samples) were creep tested after being exposed to vacuum for approximately 2, 7, or 14 days (48, 168, or 336 hours). Vacuum storage time differences between samples of a given group are shown in Table V. These time differences were at maximum on the order of several hours for the 2-day samples and of a day

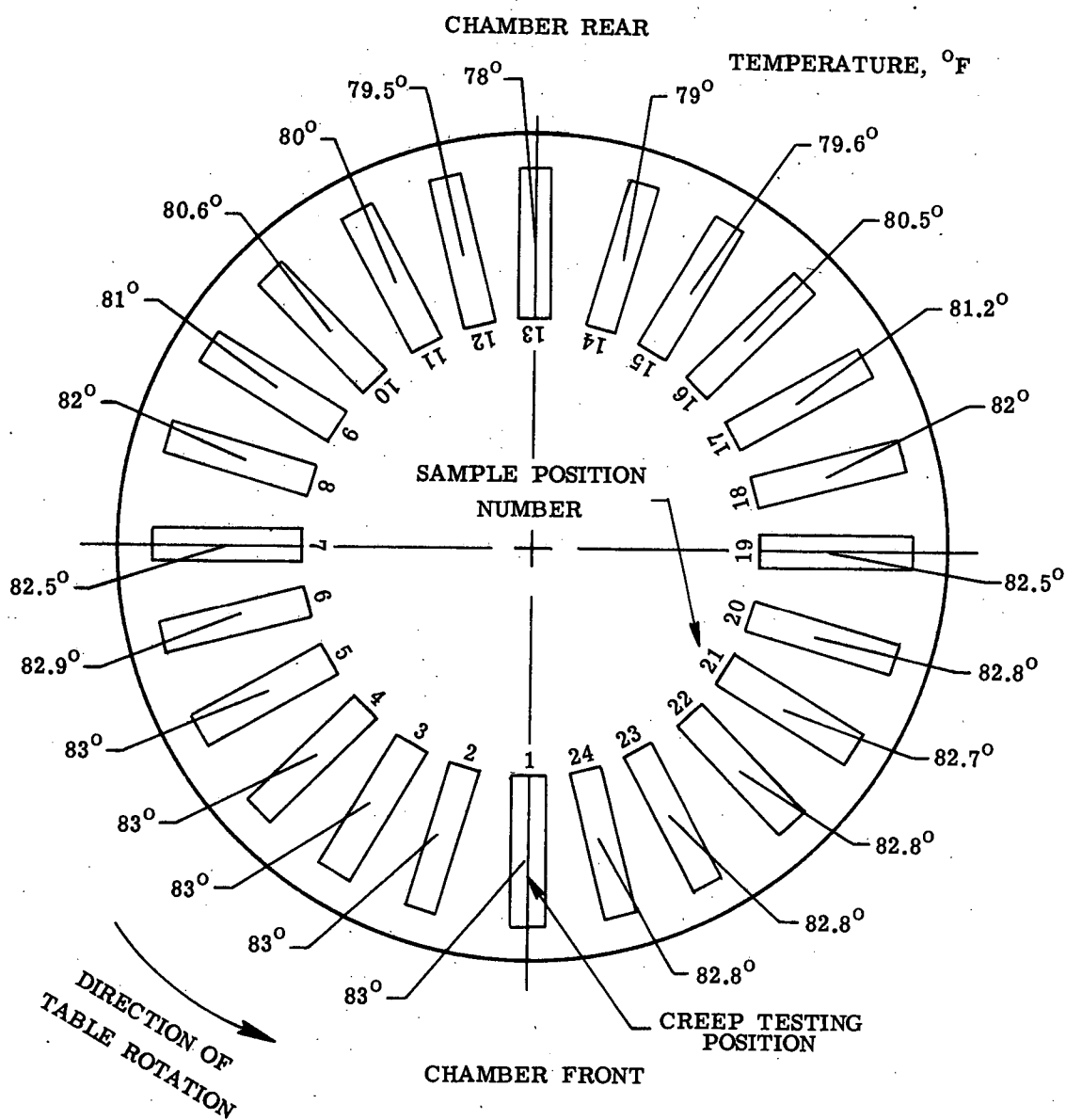


Figure 28. - Storage table temperature gradient.

for the 14-day samples. During each vacuum exposure sequence, mass spectrometer measurements were made at frequent intervals. After completion of the creep measurements, the chamber was vented to atmosphere and the fractured samples were removed. This same procedure was followed for each vacuum exposure.

#### Creep Measurement Procedure

Having positioned the sample to be tested in the test position of the creep apparatus, the sample was slowly raised until the bottom sample washer entered the tapered slot of the test weight. Visual inspection insured that during this operation the sample was not loaded. At this stage in the procedure all instrumentation was calibrated and photographs of the unloaded sample were taken. At the prescribed time the test sample was loaded and the sample timer was automatically started when the test weight left the weight platform. To allow for the creep of the sample the test weight was lifted approximately 1 inch from the weight platform. Immediately upon start of the sample timer, photographs were taken of the loaded sample in a pre-programmed sequence. With sample failure, the falling weight short circuited the sample timer's electrical circuit and the camera photographed the fractured sample. The sample jaw was then lowered to its original position in the storage table. The storage table was then rotated to the next sample and the creep measurement procedure repeated. Both control and vacuum samples were tested by these procedures.

Data Reduction

In this section the data reduction procedures required to convert the measured parameters into the mechanical properties of the material are discussed. Concurrently, the effects of sample-to-sample variations in the measured parameters (failure time, length strain, and diameter strain) are discussed along with the effects of these variations on the data reduction techniques applied by the author.

Failure Time

The failure time representing the behavior of the material in a given environment was taken to be the average failure time of the sample group calculated by

$$\bar{t}_f = \frac{\sum t_f}{n} \quad (7.1)$$

where:  $\bar{t}_f$  = mean failure time of  $n$  samples.

$t_f$  = failure time of an individual sample.

$n$  = number of samples tested in a given environment

Stress

The stress values reported in this investigation are the engineering stresses, calculated by dividing the test weight (lb) by the sample original cross sectional area ( $in.^2$ ). The cross sectional area of the test samples was taken to be  $0.196\ in.^2$  (nominal 0.5-inch diameter sample). Diameter measurements showed negligible variations among samples.

Length Strain

The sample elongation and diameter change during a creep measurement were photographed at pre-programmed times during the loading history. By measuring on the photograph the distance between the bench marks as the sample elongated and knowing this distance for the unstrained sample (photographs taken of the unloaded sample), the length strain as a function of loading time for each sample tested was calculated as follows:

$$\epsilon_{1i} = \frac{L_i - L_o}{L_o} \times 100 \quad (7.2)$$

where:  $\epsilon_{1i}$  = length strain at time  $i$ , %.

$L_i$  = distance between bench marks at time  $i$ .

$L_o$  = distance between bench marks at zero time; i.e., for unstrained sample.

Diameter Strain

The diameter strains were obtained from the same photographs as the length strains. By measuring the diameter change of a sample on the film and knowing the original diameter (unstressed sample), the diameter strain is given by

$$\epsilon_{2i} = \frac{D_o - D_i}{D_o} \times 100 \quad (7.3)$$

where:  $\epsilon_{2i}$  = diameter strain at time  $i$ , %.

$D_i$  = sample diameter at time  $i$ .

$D_o$  = sample diameter at zero time.

In this manner, the diameter strain as a function of loading time was obtained for each sample tested.

#### Observed Sample-to-Sample Variations

Sample to sample variations for the measured parameters, failure time, length strain, and diameter strain were not negligible and had to be considered in the data reduction. Typical failure time variations for the sample groups tested in this study are shown in Table VI. "P" values (maximum and minimum) for the sample groups tested in 50% r.h. air are shown. "P" is defined as the ratio of a sample's failure time to the average failure time of the sample group. Also shown for comparison are "P" values associated with other creep measurements in the literature. Considering that the air group tested at the 51 psi stress level had the largest observed failure time variations of any sample group tested in this investigation, it is seen that observed failure time variations were within reported limits.

The typical range in variation of the length strain measurement for a particular sample group is illustrated in Figure 29. This figure is a length strain-loading time plot for the samples tested at 51 psi stress and 50% r.h. air. Shown in this figure are strain curves for four samples taken from a sample group of 42 samples. Curves 1 and 4 are the strain curves for the samples in the sample group having the highest and lowest creep rates, respectively, and indicates the magnitude of observed sample-to-sample variations for the length strain measurement. Other sample groups had similar variations in the length

TABLE VI  
FAILURE TIME VARIATIONS WITHIN SAMPLE GROUPS

Material	Stress (PSI)	Temperature (°F)	P (Minimum)	P (maximum)	Number of samples tested
Propellant*	76	77	0.5	2.0	—
Propellant**	68	79	0.4	3.0	29
Propellant**	76	79	0.2	3.0	35
Propellant***	47	142	0.4	1.9	4
TPH 3105	51	83	0.4	3.0	42
TPH 3105	56	83	0.6	1.8	20
TPH 3105	61	83	0.7	1.4	10

\*from: Final Report Solid Propellant Structural Test Vehicle,  
Cumulative Damage and Systems Analysis. Lockheed Propulsion Co.,  
AFRPL-TR-68-130, Oct. 1968.

\*\*from: Final Report Solid Propellant Cumulative Damage  
Program. Aerojet General Corporation, AFRPL-68-131, Oct. 1968.

\*\*\*from: Final Report Solid Propellant Mechanical Behavior  
Studies. Atlantic Research Corporation, AFRPL-69-124, May 1969.

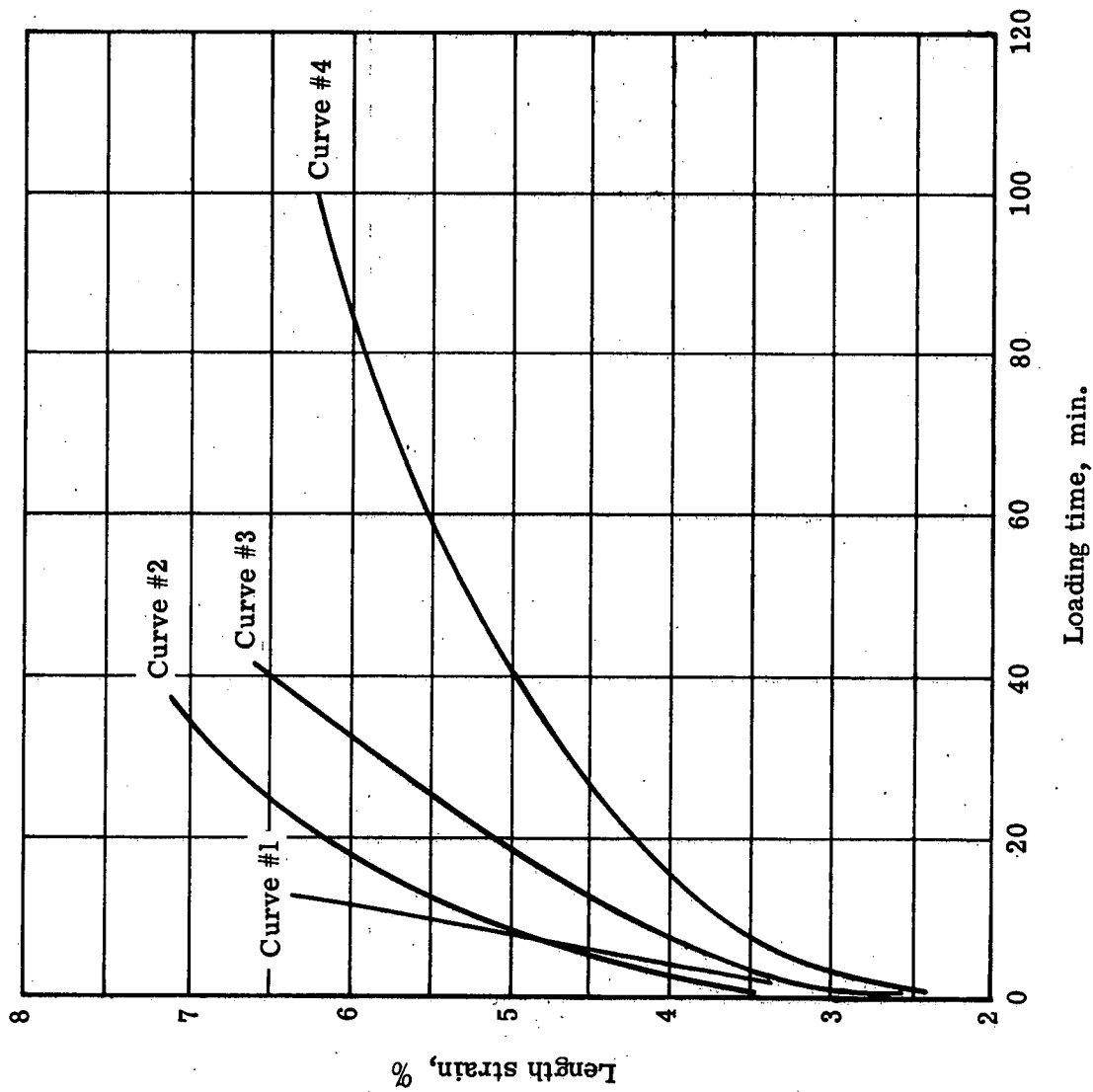


Figure 29. - Variation of the strain measurement for the sample group tested at 51 psi in 50% r.h. air and at 83°F.

strain measurement. Curves 2 and 3 are strain curves for two additional samples in the sample group.

Sample-to-sample variations for the diameter strain measurement were as large as 0.004 in./in. (0.4% strain), but were more typically of the order of 0.2% strain.

Causes of sample-to-sample variations in mechanical property testing of filled elastomers are discussed in Appendix C.

#### Data Reduction Techniques

The sample-to-sample variations in the measured parameters (failure time, length strain, and diameter strain) were an influencing factor in the selection of the data reduction techniques used to report the strain behaviors of TPH 3105. Data reduction technique 1 (DRT 1) consisted of averaging at each loading time the strain of the individual samples within a sample group. The strain-loading time behavior for each sample group was taken to be the average strain at the corresponding loading time. For the length strain, this technique (DRT 1) resulted in length strain-loading time curves which had discontinuities (step changes in strain) at each loading time where a particular sample of the sample group failed. These discontinuities were most apparent for sample groups of less than 20 samples and were large enough to invalidate reported length strain values for loading times beyond the point of the first sample failure. Similar discontinuities existed for the diameter strain-loading time curves calculated by DRT 1. In order to extend the strain behavior of the material beyond the point of

failure of the first sample and out to the mean failure time for the sample group, data reduction technique two (DRT 2) was applied to the measured strains. DRT 2 was based on the calculation of a standard 90 percent confidence interval (90% C.I.) on the mean failure time of the sample group. Only those samples which had failure times within the confidence interval were selected for the analysis. (See Table V for the number of samples in a given sample group which failed within the confidence intervals.) The strain-loading time behavior of the material was then calculated by averaging at each loading time the strain of those samples falling within the confidence interval. The 90 percent confidence interval was calculated from

$$\bar{t}_f \pm \frac{t_{\alpha/2, n-1} s_t}{\sqrt{n}} \quad (7.4)$$

where:  $\bar{t}_f$  = mean failure time of  $n$  samples.  
 $t_{\alpha/2, n-1}$  = students "t" statistic.  
 $\alpha$  = statistical significance level.  
 $s_t$  = failure time standard deviation,  $n$  samples.  
 $n$  = number of samples tested in a given environment.

The upper limit of the confidence interval is given by

$$\bar{t}_f + \left( t_{\alpha/2, n-1} s_t \right) / \sqrt{n} \quad \text{and the lower limit, } \bar{t}_f - \left( t_{\alpha/2, n-1} s_t \right) / \sqrt{n} .$$

Comparison of length strain and diameter strain results calculated by the two methods (DRT 1 and DRT 2) are shown in Appendix D. All strains reported in this thesis, with the exception of those in Figure 29 and in Appendix D, were calculated by DRT 2.

### Derived Parameters

Using the results from DRT 2, three mechanical properties were calculated: creep compliance, Poisson's ratio, and volume change.

Creep Compliance. Creep compliance as a function of loading time was calculated for each sample group using equation 7.5.

$$J_i = \frac{\bar{\epsilon}_{1i}}{\sigma} \quad (7.5)$$

where:  $\bar{\epsilon}_{1i}$  = average length strain at time  $i$ , %

$\sigma$  = applied stress, psi.

Poisson's Ratio. Poisson's ratio as a function of loading time was calculated using equation 7.6.

$$\text{Poisson's ratio} = \frac{\bar{\epsilon}_{2i}}{\bar{\epsilon}_{1i}} \quad (7.6)$$

where:  $\bar{\epsilon}_{2i}$  = average diameter strain at time  $i$ , %

$\bar{\epsilon}_{1i}$  = average length strain at time  $i$ , %.

Volume Change. The volume change as a function of loading time was calculated (assuming a cylindrical gage section) for each sample group using equation 7.7.

$$\left. \frac{\Delta V}{V_0} \right|_i = \left[ \left( 1 - \frac{\bar{\epsilon}_{2i}}{100} \right)^2 \left( 1 + \frac{\bar{\epsilon}_{1i}}{100} \right) - 1 \right] \times 100 \quad (7.7)$$

where:  $\left. \frac{\Delta V}{V_0} \right|_i$  = volume change at time  $i$ , %  
(based on initial volume,  $V_0$ ).

$\bar{\epsilon}_{2i}$  = average diameter strain at time  $i$ , %.

$\bar{\epsilon}_{1i}$  = average length strain at time  $i$ , %.

Test Results

For clarity of presentation, the results of this thesis are presented in tabular form in this section. The tabulated results are those results calculated according to data reduction technique 2. The range columns of each table indicate the magnitude of sample-to-sample variations for the strain measurement for those samples which failed within the 90% C.I. of the mean failure time. The plus and minus range values for a given strain grouping apply to any strain value in the grouping.

TABLE VIII.-CREEP MEASURED PROPERTIES OF TPH 3105

Stress: 51 psi      Temperature: 85° F      Environment: AIR, 50% r.h.  
 Mean failure time: 35.4 min.      90% Confidence interval: 29.7 to 41.1 min.

Loading time, min	Average	Range	Average	Range	Compliance, (psi) <sup>-1</sup> x 10 <sup>4</sup>	Poisson's ratio	Volume change, original volume
0.6	2.74	1.36	1.27	+0.39	5.39	0.45	0.00
0.8	2.75	+0.54	1.29	-0.21	5.39	0.46	0.16
1.0	2.86	1.36	-0.25	1.31	5.61	0.45	0.22
1.2	3.02	-0.25	1.36	-0.21	5.92	0.45	0.25
1.4	3.08	1.31	-0.25	1.31	6.05	0.43	0.40
1.6	3.15	+0.79	1.37	+0.21	6.18	0.43	0.34
1.8	3.17	1.31	1.32	-0.22	6.22	0.41	0.48
2.0	3.27	-0.41	1.36	-0.22	6.42	0.40	0.56
3.0	3.37	-0.41	1.37	-0.22	6.62	0.40	0.58
4.0	3.68	1.37	-0.25	1.37	7.23	0.37	0.86
5.0	3.86	+0.78	1.35	+0.17	7.58	0.35	1.07
6.0	4.15	1.36	1.36	-0.19	8.14	0.35	1.34
7.0	4.26	-0.48	1.35	-0.19	8.36	0.32	1.44
8.0	4.27	1.36	1.38	-0.19	8.38	0.32	1.47
9.0	4.45	-0.48	1.38	-0.19	8.70	0.31	1.57
10.0	4.53	+0.69	1.35	+0.28	8.90	0.30	1.73
12.0	4.68	1.40	1.40	-0.28	9.19	0.27	2.01
14.0	4.90	-0.38	1.41	-0.29	9.61	0.29	1.98
16.0	5.10	1.37	1.41	-0.29	10.0	0.28	2.16
18.0	5.29	-0.38	1.48	-0.37	10.4	0.26	2.42
20.0	5.38	+0.78	1.38	+0.24	10.6	0.26	2.49
22.0	5.57	1.42	1.42	-0.24	11.0	0.25	2.59
24.0	5.59	1.40	1.40	-0.30	11.0	0.25	2.65
26.0	5.78	-0.48	1.42	-0.30	11.4	0.25	2.80
28.0	5.99	1.48	1.48	-0.25	11.8	0.25	2.88

TABLE VII. -CREEP MEASURED PROPERTIES OF TPH 3105 - Concluded

Stress: 51 psi Temperature: 83° F Environment: AIR, 50% r.h.

Mean failure time: 35.4 min. 90% Confidence interval: 29.7 to 41.1 min.

Loading time, min	Length strain, %			Diameter strain, %	Compliance, (psi) <sup>-1</sup> × 10 <sup>4</sup>	Poisson's ratio	Volume change, original volume
	Average	Range	Average	Range			
30.0	6.13	1.44	1.44	+0.16	12.0	0.24	3.10
32.0	6.26	+0.57	1.43		12.3	0.23	3.24
34.0	6.49	1.44	1.41	-0.13	12.7	0.22	3.45
35.4	6.71	-0.40	1.41		13.2	0.21	3.72

TABLE VIII.- CREEP MEASURED PROPERTIES OF TPH 3105

Stress: 51 psi      Temperature: 83° F      Environment: VACUUM, 51 hours  
 Mean failure time: 37.4 min.      90% Confidence interval: 31.1 to 42.7 min.

Loading time, min	Average	Range	Average	Range	Diameter strain, %	Compliance, (psi) <sup>-1</sup> x 10 <sup>4</sup>	Poisson's ratio	Volume change, original volume
0.6	2.50	1.27	1.29	+0.20	4.91	0.51	0.00	0.00
0.8	2.55	+0.29	1.25	-0.22	5.01	0.51	0.00	0.00
1.0	2.58	-0.24	1.25	-0.22	5.07	0.50	0.00	0.00
1.2	2.67	-0.24	1.25	-0.22	5.24	0.47	0.12	0.18
1.4	2.73	-0.24	1.25	-0.22	5.36	0.46	0.18	0.18
1.6	2.80	-0.19	1.25	-0.39	5.50	0.45	0.25	0.25
1.8	2.86	-0.19	1.28	-0.39	5.62	0.45	0.25	0.25
2.0	2.91	-0.24	1.26	-0.24	5.71	0.43	0.33	0.33
2.0	2.99	-0.24	1.29	-0.24	5.87	0.43	0.35	0.35
3.0	3.09	-0.09	1.30	-0.07	6.07	0.42	0.43	0.43
4.0	3.16	-0.37	1.31	+0.34	6.20	0.42	0.43	0.43
5.0	3.27	-0.32	1.32	-0.25	6.42	0.40	0.58	0.58
6.0	3.32	-0.32	1.32	-0.25	6.52	0.40	0.61	0.61
7.0	3.42	-0.32	1.32	-0.25	6.72	0.39	0.71	0.71
8.0	3.54	-0.32	1.33	-0.25	6.95	0.38	0.80	0.80
9.0	3.65	+0.26	1.36	+0.32	7.23	0.37	0.88	0.88
10.0	3.81	+0.26	1.36	+0.32	7.48	0.36	1.00	1.00
12.0	3.95	-0.28	1.38	-0.22	7.76	0.35	1.10	1.10
14.0	4.05	-0.28	1.39	-0.22	7.95	0.34	1.18	1.18
16.0	4.18	-0.28	1.39	-0.22	8.21	0.33	1.30	1.30
18.0	4.40	-0.40	1.47	+0.33	8.64	0.33	1.35	1.35
20.0	4.58	-0.40	1.44	-0.33	8.99	0.31	1.39	1.39
22.0	4.77	-0.31	1.47	-0.22	9.37	0.31	1.71	1.71
24.0	4.93	-0.31	1.51	-0.22	9.68	0.31	1.79	1.79
26.0	5.08	-0.31	1.54	-0.22	9.97	0.30	1.87	1.87

TABLE VIII.- CREEP MEASURED PROPERTIES OF TPH 3105 - Concluded

Stress: 51 psi      Temperature: 83° F      Environment: VACUUM, 51 hours  
 Mean failure time: 37.4 min.      90% Confidence interval: 31.1 to 42.7 Min.

Loading time, min	Length strain, %		Diameter strain, %	Compliance, $\text{psi}^{-1} \times 10^4$		Poisson's ratio	Volume change, original volume
	Average	Range	Average	Range	(psi) $^{-1}$ $\times 10^4$		
30.0	5.30	+0.12	1.52	+0.24	10.4	0.29	2.12
32.0	5.25	-	1.60	-	10.3	0.31	1.91
34.0	5.32	-	1.64	-	10.5	0.31	1.89
36.0	5.51	-0.06	1.60	-0.36	10.8	0.29	2.16
37.4	5.65	-	1.64	-	11.1	0.29	2.21

TABLE IX .- CREEP MEASURED PROPERTIES OF TPH 3105

Stress: 51 psi      Temperature: 83° F      Environment: VACUUM, 173 hours  
 Mean failure time: 83.8 min.      90% Confidence interval: 67.1 to 100.5 min.

Loading time, min	Length strain, %	Diameter strain, %	Compliance, $(\text{psi})^{-1} \times 10^4$	Poisson's ratio	Volume change, % original volume
Average	Range	Average	(psi) $^{-1}$	ratio	
0.6	2.05	1.19	4.03	0.58	0.00
0.8	2.17	+0.29	4.26	0.53	0.00
1.0	2.18	1.15	4.28	0.54	0.00
1.2	2.23	-0.16	4.38	0.53	0.00
1.4	2.23	1.19	4.38	0.52	0.00
1.6	2.25	1.15	4.38	0.51	0.00
1.8	2.24	+0.24	4.40	0.53	0.00
2.0	2.25	1.18	4.38	0.53	0.00
2.0	2.28	-0.19	4.48	0.53	0.00
2.0	2.31	1.17	4.54	0.51	0.00
5.0	2.30	1.17	4.52	0.51	0.00
6.0	2.32	+0.27	4.56	0.52	0.00
7.0	2.40	1.20	4.71	0.49	0.00
8.0	2.40	-0.36	4.71	0.51	0.00
9.0	2.42	1.23	4.75	0.50	0.00
10.0	2.51	1.23	4.93	0.49	0.00
12.0	2.51	+0.21	4.93	0.50	0.00
14.0	2.62	1.32	5.14	0.50	0.00
16.0	2.67	-0.38	5.24	0.47	0.00
18.0	2.70	1.28	5.30	0.47	0.00
20.0	2.78	1.38	5.46	0.50	0.00
22.0	2.89	+0.22	5.67	0.45	0.25
24.0	2.95	1.31	5.79	0.45	0.27
26.0	3.07	-0.35	6.03	0.42	0.28
28.0	3.14	1.23	6.16	0.39	0.62

TABLE IX .- CREEP MEASURED PROPERTIES OF TPH 3105 - Concluded

Stress: 51 psi      Temperature: 83° F      Environment: VACUUM, 173 hours  
 Mean failure time: 83.8 min.      90% Confidence interval: 67.1 to 100.5 min.

Loading time, min	Length strain, %			Diameter strain, %	Compliance, (psi) <sup>-1</sup> × 10 <sup>4</sup>		Poisson's ratio	Volume change, % original volume
	Average	Range	Average	Range	(psi) <sup>-1</sup> × 10 <sup>4</sup>	ratio		
30.0	3.24	+0.15	1.28	+0.11	6.36	0.40	0.61	
32.0	3.33	+0.13	1.34	+0.12	6.54	0.38	0.70	
34.0	3.42	-0.13	1.35	-0.08	6.72	0.39	0.67	
36.0	3.49	+0.13	1.29	+0.10	6.85	0.39	0.71	
38.0	3.54	+0.13	1.29	+0.10	6.95	0.36	0.89	
40.0	3.57	+0.25	1.38	+0.25	7.01	0.39	0.73	
42.0	3.71	+0.25	1.36	+0.25	7.28	0.37	0.91	
44.0	3.77	+0.25	1.35	+0.25	7.40	0.36	0.99	
46.0	3.89	-0.17	1.39	-0.17	7.64	0.36	1.02	
48.0	3.93	+0.13	1.34	+0.13	7.72	0.34	1.16	
50.0	3.96	+0.27	1.43	+0.24	7.77	0.36	1.01	
52.0	4.09	+0.27	1.37	+0.24	8.03	0.34	1.26	
54.0	4.14	+0.27	1.44	+0.24	8.13	0.35	1.16	
56.0	4.20	-0.18	1.34	-0.14	8.25	0.32	1.43	
58.0	4.22	+0.22	1.46	+0.22	8.29	0.35	1.20	
60.0	4.28	+0.29	1.41	+0.24	8.40	0.35	1.36	
65.0	4.38	+0.29	1.39	+0.24	8.60	0.32	1.50	
70.0	4.52	+0.15	1.44	+0.12	8.87	0.32	1.53	
75.0	4.71	-0.15	1.47	-0.12	9.25	0.31	1.65	
80.0	4.88	+0.17	1.47	+0.17	9.58	0.30	1.82	
83.8	4.84	+1.32			9.50	0.27	2.09	

TABLE X. - CREEP MEASURED PROPERTIES OF TPH 3105

Stress: 51 psi      Temperature: 83° F      Environment: VACUM, 348 hours  
 Mean failure time: 239.6 min.      90% Confidence interval: 184.0 to 295.2 min.

Loading time, min	Length strain, %			Diameter strain, %*	Compliance, (psi) <sup>-1</sup> × 10 <sup>4</sup>		Poisson's ratio**	Volume change, % original volume***
	Average	Range	Average	Range	(psi) <sup>-1</sup> × 10 <sup>4</sup>	ratio**	Volume change, % original volume***	
0.6	1.97	+0.10			3.86	< 0.08	1.66 <	< 2.28
0.8	1.96				3.84	< 0.08	1.65 <	< 2.27
1.0	1.96	-0.16			3.84	< 0.08	1.65 <	< 2.27
1.2	1.96				3.89	< 0.08	1.65 <	< 2.27
1.4	1.98				3.88	< 0.08	1.67 <	< 2.29
1.6	2.04	+0.47			4.00	< 0.07	1.73 <	< 2.35
1.8	2.08	+0.47			4.08	< 0.07	1.77 <	< 2.39
2.0	2.08				4.08	< 0.07	1.77 <	< 2.39
3.0	2.10	-0.28			4.12	< 0.07	1.79 <	< 2.41
4.0	2.12				4.16	< 0.07	1.81 <	< 2.43
5.0	2.14	+0.46			4.19	< 0.07	1.83 <	< 2.45
6.0	2.21				4.34	< 0.07	1.90 <	< 2.52
7.0	2.28				4.48	< 0.07	1.97 <	< 2.59
8.0	2.31	-0.33			4.54	< 0.06	2.00 <	< 2.62
9.0	2.40				4.71	< 0.06	2.09 <	< 2.71

\* The diameter strain was within the limits of detection of the measuring technique; i.e.,  
 $-0.15\% < \epsilon_2 < +0.15\%$ .

\*\* Based on  $|\epsilon_2| < 0.15\%$

\*\*\* Upper and lower limits were calculated corresponding to diameter strains of +0.15% and -0.15%, respectively. Actual volume change was within the indicated range.

TABLE X. - CREEP MEASURED PROPERTIES OF TPH 3105 - Continued

Stress: 51 psi      Temperature: 83° F      Environment: VACUUM, 348 hours  
 Mean failure time: 239.6 min.      90% Confidence interval: 184.0 to 295.2 min.

Loading time, min	Length strain, %			Diameter strain, %*	Compliance, (psi) <sup>-1</sup> × 10 <sup>4</sup>	Poisson's ratio**	Volume change, % original volume***
	Average	Range	Average	Range			
10.0	2.47	+0.38			4.84	< 0.06	2.16 < 2.78
12.0	2.51				4.92	< 0.06	2.20 < 2.82
14.0	2.64	-0.50			5.17	< 0.06	2.33 < 2.95
16.0	2.72	-0.50			5.33	< 0.06	2.41 < 3.03
18.0	2.70				5.29	< 0.06	2.39 < 3.01
20.0	2.77	+0.50			5.44	< 0.05	2.46 < 3.08
22.0	2.74				5.38	< 0.05	2.43 < 3.05
24.0	2.79	-0.53			5.48	< 0.05	2.48 < 3.10
26.0	2.78	-0.53			5.46	< 0.05	2.47 < 3.09
28.0	2.80				5.50	< 0.05	2.49 < 3.11
30.0	2.85	+0.43			5.60	< 0.05	2.54 < 3.16
32.0	2.86	-0.52			5.62	< 0.05	2.55 < 3.17
34.0	2.92				5.73	< 0.05	2.61 < 3.23
36.0	3.04				5.97	< 0.05	2.72 < 3.35
38.0							
40.0	3.09	+0.42			6.07	< 0.05	2.78 < 3.40
42.0	3.08				6.05	< 0.05	2.77 < 3.39
44.0	3.15	-0.53			6.18	< 0.05	2.84 < 3.46
46.0	3.18				6.23	< 0.05	2.87 < 3.49
48.0	3.23				6.33	< 0.05	2.92 < 3.54
50.0							
52.0	3.26	+0.36			6.40	< 0.05	2.95 < 3.57
54.0	3.33	-0.56			6.53	< 0.05	3.02 < 3.64
56.0	3.35				6.57	< 0.04	3.04 < 3.66
58.0	3.37				6.61	< 0.04	3.06 < 3.68

TABLE X. - CREEP MEASURED PROPERTIES OF TPH 3105 - Concluded

Stress: 51 psi      Temperature: 83° F      Environment: VACUUM, 348 hours

Mean failure time: 239.6 min. 90% Confidence interval: 184.0 to 295.2 min.

Loading time, min	Length strain, %		Diameter strain, %*		Compliance, (psi) <sup>-1</sup> × 10 <sup>4</sup>	Poisson's ratio**	Volume change, % original volume***
	Average	Range	Average	Range			
60.0	3.38	+0.39			6.63	< 0.04	< 3.69
70.0	3.42				6.71	< 0.04	< 3.73
80.0	3.49	-0.44			6.85	< 0.04	< 3.80
90.0	3.60				7.07	< 0.04	< 3.91
100.0	3.62				7.11	< 0.04	< 3.93
110.0	3.66				7.18	< 0.04	< 3.97
120.0	3.80	+0.35			7.46	< 0.04	< 4.11
130.0	3.93				7.71	< 0.04	< 4.24
140.0	4.00	-0.43			7.86	< 0.04	< 4.31
150.0	4.05				7.96	< 0.04	< 4.36
160.0	4.15				8.15	< 0.04	< 4.46
170.0	4.28	+0.55			8.40	< 0.04	< 4.59
180.0	4.44				8.71	< 0.03	< 4.75
190.0	4.53	-0.45			8.89	< 0.03	< 4.84
200.0	4.63				9.08	< 0.03	< 4.94
210.0	4.84				9.50	< 0.03	< 5.15
220.0	4.86	+0.52			9.54	< 0.03	< 5.17
230.0	4.92				9.65	< 0.03	< 5.23
239.6	5.01	-0.52			9.85	< 0.03	< 5.33

TABLE XI.- CREEP MEASURED PROPERTIES OF TPH 3105

Stress: 56 psi      Temperature: 83° F      Environment: AIR, 50% r.h.  
 Mean failure time: 6.6 min.      90% Confidence interval: 5.8 to 7.3 min.

Loading time, min	Length strain, %		Diameter strain, %	Compliance, $(\text{psi})^{-1} \times 10^4$		Poisson's ratio	$\frac{\text{Volume change, \%}}{\text{original volume}}$
	Average	Range	Average	Range	(psi) $^{-1}$		
0.6	2.76		1.48		4.93	0.54	0.00
0.8	2.93	+0.32	1.47	+0.04	5.23	0.50	0.00
1.0	3.13		1.49		5.58	0.48	0.08
1.2	3.27	-0.26	1.53	-0.02	5.83	0.47	0.14
1.4	3.46		1.48		6.17	0.43	0.42
1.6	3.67		1.54		6.55	0.42	0.51
1.8	3.83	+0.39	1.56	+0.15	6.84	0.41	0.62
2.0	3.95		1.62		7.05	0.41	0.61
3.0	4.57	-0.49	1.57	-0.11	7.81	0.36	1.12
4.0	4.73		1.71		8.45	0.36	1.18
5.0	5.94		1.83		10.6	0.31	2.10
6.0	6.49		1.87		11.6	0.29	2.54
6.6	7.19		1.89		13.4	0.26	3.18

TABLE XIII.-CREEP MEASURED PROPERTIES OF TPH 3105

Stress: 56 psi      Temperature: 85° F      Environment: VACUUM, 47 hours  
 Mean failure time: 9.9 min.      90% Confidence interval: 8.3 to 11.4 min.

Loading time, min	Average	Length Range	Strain, %	Diameter strain, %	Compliance, $(\text{psi})^{-1} \times 10^4$		Poisson's ratio	Volume change, original volume
					(psi)	Range		
0.6	2.91	1.01	+0.13	5.19	0.35	0.84		
0.8	3.04	1.04	-0.13	5.43	0.34	0.91		
1.0	3.26	1.01	-0.14	5.82	0.31	1.18		
1.2	3.32	-0.28	1.08	5.93	0.33	1.10		
1.4	3.37	1.13	-0.14	6.02	0.33	1.05		
1.6	3.51	1.15	+0.18	6.26	0.35	1.14		
1.8	3.63	1.13	1.11	6.47	0.31	1.30		
2.0	3.78	-0.17	1.13	6.75	0.29	1.49		
3.0	3.92	1.24	-0.12	6.99	0.29	1.58		
4.0	4.21			7.52	0.29	1.64		
5.0	4.37	1.31						
6.0	4.55	+0.25	1.27	+0.28	7.80	0.30	1.65	
7.0	4.81		1.29		8.11	0.28	1.91	
8.0	5.16	-0.45	1.39	-0.25	8.59	0.27	2.12	
9.0	5.39		1.40		9.22	0.27	2.26	
9.9	5.53		1.40		9.63	0.26	2.46	
					9.87	0.25	2.60	

TABLE XIII.- CREEP MEASURED PROPERTIES OF TPH 3105

Stress: 56 psi      Temperature: 83° F      Environment: VACUUM, 170 hours  
 Mean failure time: 32.6 min.      90% Confidence interval: 25.6 to 39.6 min.

Loading time, min	Length strain, %		Diameter strain, %	Compliance, (psi) <sup>-1</sup> × 10 <sup>4</sup>		Poisson's ratio	Volume change, % original volume
	Average	Range	Average	Range	(psi) <sup>-1</sup> × 10 <sup>4</sup>		
0.6	2.25	+0.21	0.81	+0.16	4.02	0.36	0.61
0.8	2.26		0.81		4.03	0.36	0.62
1.0	2.32	-0.13	0.83	-0.16	4.15	0.36	0.63
1.2	2.32		0.80		4.15	0.35	0.69
1.4	2.38		0.86		4.25	0.36	0.63
1.6	2.40	+0.24	0.83	+0.10	4.29	0.34	0.72
1.8	2.43		0.81		4.34	0.33	0.78
2.0	2.48		0.80		4.42	0.32	0.85
3.0	2.57	-0.18	0.84	-0.11	4.59	0.33	0.85
4.0	2.66		0.82		4.75	0.31	0.99
5.0	2.75	+0.16	0.84	+0.07	4.90	0.31	1.03
6.0	2.86		0.85		5.11	0.30	1.13
7.0	2.83		0.85		5.05	0.30	1.10
8.0	3.04	-0.25	0.85	-0.12	5.43	0.28	1.30
9.0	3.12		0.86		5.57	0.28	1.35
10.0	3.14		0.87		5.61	0.28	1.36
12.0	3.27	+0.19	0.87	+0.06	5.84	0.27	1.48
14.0	3.33		0.89		5.95	0.27	1.50
16.0	3.53	-0.21	0.93	-0.09	6.31	0.26	1.61
18.0	3.71		0.90		6.62	0.24	1.86

TABLE XIII. - CREEP MEASURED PROPERTIES OF TPH 3105 - Concluded

Stress: 56 psi    Temperature: 83° F    Environment: VACUUM, 170 hours

Mean failure time: 32.6 Min.    90% Confidence interval: 25.6 to 39.6 min.

Loading time, min	Length strain, %		Diameter strain, %		Compliance, $(\text{psi})^{-1} \times 10^4$		Poisson's ratio	Volume change, % original volume
	Average	Range	Average	Range	(psi) $^{-1}$ $\times 10^4$	ratio		
20.0	4.03	0.89	0.89	+0.05	7.19	0.22	2.23	
22.0	4.28	+0.30	0.93	0.94	7.64	0.22	2.35	
24.0	4.47	0.94	0.95	-0.10	7.99	0.21	2.53	
26.0	4.62	-0.37	0.95	0.93	8.25	0.21	2.64	
28.0	4.70	0.93	0.93		8.40	0.20	2.76	
30.0	4.86	0.91	0.91		8.68	0.19	2.96	
32.0	4.83	1.02	1.02		8.62	0.21	2.70	
32.6	4.86	0.99	0.99		8.68	0.20	2.79	

TABLE XIV.- CREEP MEASURED PROPERTIES OF TPH 3105

Stress: 56 psi      Temperature: 83° F      Environment: VACUUM, 338 hours  
 Mean failure time: 67.4 min.      90% Confidence interval: 58.4 to 76.4 min.

Loading time, min	Length strain, %			Diameter strain, %	Compliance, (psi) <sup>-1</sup> × 10 <sup>4</sup>	Poisson's ratio	Volume change, % original volume
	Average	Range	Average	Range			
0.6	1.98	+0.37	0.83	+0.17	3.54	0.42	0.29
0.8	1.99	0.81	0.83	0.17	3.55	0.41	0.34
1.0	2.04	0.83	0.83	-0.08	3.64	0.40	0.36
1.2	1.99	-0.29	0.83	-0.08	3.55	0.42	0.30
1.4	2.08	0.81	0.81	-0.08	3.72	0.39	0.44
1.6	2.09	0.83	0.83	+0.17	3.73	0.40	0.40
1.8	2.12	+0.34	0.83	+0.17	3.80	0.39	0.43
2.0	2.17	0.83	0.83	-0.07	3.88	0.38	0.49
2.2	2.21	-0.27	0.82	-0.07	3.94	0.37	0.54
2.4	2.23	0.85	0.85	-0.07	3.98	0.38	0.51
5.0	2.31	0.82	0.82	-0.03	4.13	0.36	0.64
6.0	2.38	+0.40	0.84	+0.23	4.25	0.35	0.66
7.0	2.42	0.84	0.84	-0.11	4.33	0.35	0.71
8.0	2.44	-0.32	0.85	-0.11	4.35	0.35	0.71
9.0	2.46	0.83	0.83	-0.11	4.39	0.34	0.76
10.0	2.55	+0.24	0.83	+0.17	4.55	0.32	0.87
12.0	2.64	0.83	0.86	-0.17	4.72	0.31	0.94
14.0	2.70	-0.29	0.82	-0.11	4.82	0.32	0.95
16.0	2.75	-0.29	0.84	-0.11	4.91	0.30	1.07
18.0	2.85	0.84	0.84	-0.11	5.10	0.29	1.14
20.0	2.93	0.86	0.86	-0.06	5.23	0.29	1.17
22.0	2.98	+0.22	0.86	+0.16	5.33	0.29	1.22
24.0	3.11	0.89	0.89	-0.09	5.55	0.28	1.29
26.0	3.18	-0.27	0.85	-0.09	5.68	0.27	1.43
28.0	3.26	0.87	0.87	-0.09	5.82	0.27	1.48

TABLE XIV. - CREEP MEASURED PROPERTIES OF TPH 3105 - Concluded

Stress: 56 psi      Temperature: 83° F      Environment: VACUUM, 338 hours  
 Mean failure time: 67.4 min.      90% Confidence interval: 58.4 to 76.4 min.

Loading time, min	Length strain, %		Diameter strain, %		Compliance, (psi) <sup>-1</sup> × 10 <sup>4</sup>	Poisson's ratio	Volume change, original volume
	Average	Range	Average	Range			
30.0	3.28	0.86	0.86	+0.27	5.86	0.26	1.52
32.0	3.40	+0.32	0.87	-0.27	6.07	0.25	1.62
34.0	3.40	0.86	0.86	-0.11	6.07	0.25	1.63
36.0	3.47	-0.36	0.86	0.95	6.20	0.25	1.69
38.0	3.54	-0.36	0.95	0.95	6.32	0.27	1.59
40.0	3.64	0.90	0.90	-0.14	6.50	0.25	1.78
42.0	3.81	+0.63	0.91	+0.14	6.80	0.24	1.94
44.0	3.84	0.95	0.95	-0.16	6.86	0.25	1.89
46.0	3.97	-0.38	0.94	-0.16	7.09	0.24	2.02
48.0	4.02	0.91	0.91	-0.16	7.18	0.23	2.13
50.0	4.11	0.95	0.95	+0.15	7.34	0.23	2.15
52.0	4.25	+0.68	0.94	+0.15	7.59	0.22	2.30
54.0	4.30	0.90	0.90	-0.12	7.68	0.21	2.43
56.0	4.35	-0.35	0.94	-0.12	7.77	0.22	2.41
58.0	4.51	0.93	0.93	-0.06	8.06	0.21	2.57
60.0	4.62	1.01	1.01	-0.01	8.25	0.22	2.51
65.0	4.98	1.05	1.05	-0.05	8.89	0.21	2.78
67.4	5.25	1.02	1.02	-0.02	9.36	0.19	3.11

TABLE XV. - CREEP MEASURED PROPERTIES OF TPH 3105

Stress: 61 psi      Temperature: 83° F      Environment: AIR, 50%, r.b.  
 Mean failure time: 3.3 min.      90% Confidence interval: 2.8 to 3.7 min.

Loading time, min	Average	Range	Average	Range	Diameter strain, %	Compliance, $(\text{psi})^{-1} \times 10^4$	Poisson's ratio	Volume change, % original volume
0.6	3.41		1.51		+0.16	5.58	0.44	0.31
0.8	3.52	+0.23	1.51			5.76	0.43	0.42
1.0	3.67		1.58			6.00	0.43	0.56
1.2	3.80	-0.23	1.55	-0.10		6.35	0.41	0.60
1.4	4.23		1.55			6.91	0.37	1.02
1.6	4.52		1.58			7.39	0.35	1.24
1.8	4.76	+0.31	1.58	+0.15		7.79	0.33	1.48
2.0	5.04		1.61			8.24	0.32	1.68
2.2	5.27	-0.34	1.62	-0.11		8.63	0.31	1.89
2.4	5.41		1.65			8.86	0.30	1.96
2.6	5.71		1.65			9.35	0.29	2.25
2.8	6.06	+0.45	1.59	+0.24		9.91	0.26	2.71
3.0	6.39		1.68			10.5	0.26	2.84
3.2	6.68	-0.34	1.70	-0.16		10.9	0.25	3.08
3.3	6.96		1.77			11.4	0.25	3.21

TABLE XVI.—CREEP MEASURED PROPERTIES OF TPH 3105

Stress: 61 psi      Temperature: 83° F      Environment: VACUUM, 46 hours  
 Mean failure time: 5.4 min.      90% Confidence interval: 4.8 to 6.0 min.

Loading time, min	Length strain, %		Diameter strain, %		Compliance, $(\text{psi})^{-1} \times 10^4$		Poisson's ratio	Volume change, original volume
	Average	Range	Average	Range	$(\text{psi})^{-1} \times 10^4$	ratio		
0.6	2.36	+0.32	0.90	+0.05	3.88	0.38	0.53	0.53
0.8	2.53	0.93	0.86	-0.08	4.05	0.57	0.63	0.63
1.0	2.57	-0.37	0.90	-0.10	4.22	0.33	0.82	0.82
1.2	2.73	0.93	0.93	-0.02	4.48	0.33	0.88	0.88
1.4	2.94				4.82	0.52	1.03	1.03
1.6	3.09	0.89	0.91	+0.13	5.06	0.29	1.01	1.01
1.8	3.19	+0.25	0.91	-0.10	5.22	0.29	1.32	1.32
2.0	3.27	0.91	0.91	-0.10	5.36	0.28	1.39	1.39
3.0	3.65	-0.29	0.91	0.93	5.98	0.25	1.77	1.77
4.0	4.22	0.93	0.93	0.09	7.09	0.21	2.40	2.40
5.0	4.73	0.85	0.91	0.91	7.75	0.18	2.97	2.97
5.4	5.09	0.91			8.34	0.18	3.19	3.19

TABLE XVII.-CREEP MEASURED PROPERTIES OF TPH 3105

Stress: 61 psi      Temperature: 83° F      Environment: VACUUM, 171 hours  
 Mean failure time: 16.6 min.      90% Confidence interval: 14.2 to 19.1 min.

Loading time, min	Length strain, %		Diameter strain, %*	Compliance, (psi) <sup>-1</sup> × 10 <sup>4</sup>		Poisson's ratio*	Volume change, % original volume*
	Average	Range	Average	Range	(psi) <sup>-1</sup> × 10 <sup>4</sup>		
0.6	2.28		+0.14			5.72	
0.8	2.24					3.65	
1.0	2.27					3.71	
1.2	2.30		-0.23			3.75	
1.4	2.39					3.91	
1.6	2.46					4.02	
1.8	2.69		+0.14			4.39	
2.0	2.74					4.47	
3.0	2.85		-0.22			4.66	
4.0	2.88					4.72	
5.0	3.09					5.06	
6.0	3.25		+0.14			5.31	
7.0	3.36					5.50	
8.0	3.48		-0.36			5.69	
9.0	3.72					6.08	
10.0	3.85					6.30	
12.0	4.07		+0.33			6.66	
14.0	4.33					7.08	
16.0	4.80		-0.52			7.85	
16.6	4.98					8.18	

\* Poor film resolution made diameter strain measurements unreliable

TABLE XVIII.- CREEP MEASURED PROPERTIES OF TPH 3105

Stress: 61 psi      Temperature: VACUUM, 337 hours  
 Mean failure time: 56.5 min.      90% Confidence interval: 44.2 to 68.8 min.

Loading time, min	Average	Length strain, %	Diameter strain, %	Compliance, $(\text{psi})^{-1} \times 10^4$	Poisson's ratio	Volume change, % original volume
		Range *	Average	Range *	$(\text{psi})^{-1} \times 10^4$	
0.6	2.27	0.80	0.80	3.72	0.35	0.54
0.8	2.35	0.86	0.86	3.85	0.37	0.60
1.0	2.27	0.91	0.91	3.72	0.40	0.42
1.2	2.31	0.80	0.80	3.79	0.35	0.68
1.4	2.43	0.76	0.76	3.98	0.31	0.88
1.6	2.47	0.74	0.74	4.05	0.30	0.96
1.8	2.59	0.88	0.88	4.24	0.34	0.79
2.0	2.59	0.74	0.74	4.24	0.29	1.08
2.0	2.59	0.89	0.89	4.24	0.34	0.77
4.0	2.75	0.88	0.88	4.51	0.32	0.95
5.0	2.83	0.88	0.88	4.64	0.31	1.03
6.0	2.91	0.82	0.82	4.77	0.28	1.23
7.0	3.03	0.88	0.88	4.97	0.29	1.23
8.0	2.99	0.88	0.88	4.90	0.29	1.19
9.0	3.11	0.89	0.89	5.10	0.29	1.28
10.0	3.30	0.89	0.89	5.41	0.27	1.47
12.0	3.38	0.89	0.89	5.54	0.26	1.55
14.0	3.58	0.86	0.86	5.87	0.24	1.81
16.0	3.58	0.88	0.88	5.87	0.25	1.77
18.0	3.66	0.88	0.88	6.00	0.24	1.84

\* For this sample group, two samples fell within the 90% confidence interval, but only one of these samples had film which could be read; therefore, data tabulated are for that one sample.

TABLE XVIII.- CREEP MEASURED PROPERTIES OF TPH 3105 - Concluded

Stress: 61 psi      Temperature:      Environment: VACUM, 337 hours  
 Mean failure time: 56.5 min.      90% Confidence interval: 44.2 to 68.8 min.

Loading time, min	Length strain, %			Diameter strain, %	Compliance, $(\text{psi})^{-1} \times 10^4$	Poisson's ratio	Volume change, % original volume
	Average	Range *	Average	Range *			
20.0	3.74		0.91		6.13	0.24	1.86
22.0	3.82		0.91		6.26	0.24	1.94
24.0	3.78		0.97		6.19	0.26	1.78
26.0	3.94		0.89		6.46	0.23	2.10
28.0	4.22		0.89		6.92	0.21	2.37
30.0	4.22		0.91		6.92	0.22	2.33
32.0	4.30		0.91		7.05	0.21	2.41
34.0	4.26		0.97		6.98	0.23	2.25
36.0	4.22		1.05		6.92	0.25	2.04
38.0	4.30		1.05		7.05	0.24	2.12
40.0	4.30		1.06		7.05	0.25	2.10
42.0	4.30		0.97		7.05	0.23	2.29
44.0	4.50		0.89		7.37	0.20	2.65
46.0	4.74		0.93		7.77	0.20	2.80
48.0	4.70		0.97		7.70	0.21	2.68
50.0	4.82		0.99		7.90	0.21	2.75
52.0	4.94		0.91		8.10	0.18	3.04
54.0	4.86		0.99		7.96	0.20	2.79
56.0	4.98		0.93		8.16	0.19	3.04
56.5	5.01		0.95		8.21	0.19	3.02

## VIII. ACCURACY AND ERRORS

The errors associated with the research measurements will be discussed. The probable accuracy of each measured quantity will be noted along with its effect on the accuracy of the calculated quantities of compliance, percent volume change, and Poisson's Ratio. The reported accuracies are for individual sample measurements and not for sample group averages or confidence interval groupings.

### Vacuum Exposure Time

The vacuum storage time for all tests was measured with an electric clock, believed to be accurate to within  $\pm 1$  minute over a two-week period. Minimum vacuum storage times for samples were two days, in which case, any error in vacuum storage time is negligible.

### Sample Loading Time

Loading time was measured by an electric panel clock, accurate and readable to within  $\pm 0.1$  minute. Considering that the clock was started and stopped by the movement of the test weight, sample loading times and failure times are accurate to at least  $\pm 0.1$  minute.

### Temperature

Sample temperatures were measured with chromel-alumel thermocouples embedded in selected propellant samples as previously discussed. Thermocouple outputs were recorded on a continuous balanced servo potentiometer accurate to  $\pm 0.002$  mv ( $0.1^{\circ}\text{F}$ ). Although an instrument

accuracy of  $\pm 0.1^{\circ}\text{F}$  was available, calibration of the thermocouples and readout instrumentation (ice and steam point calibration) showed a temperature accuracy of  $\pm 0.5^{\circ}\text{F}$ . All reported temperature measurements are accurate to  $\pm 0.5^{\circ}\text{F}$ .

#### Pressure

Pressure was measured with a Bayard Alpert ionization gage calibrated for nitrogen gas. All reported pressures are in equivalent nitrogen torr and believed to be accurate to within  $\pm 8\%$  of the reported value (35).

#### Humidity

The humidity in the preconditioning chamber was calculated from the measured refractive index of the humidity solution. As shown in reference 36 this method of determining humidity is at least accurate to  $\pm 1\%$  r.h. Humidity measurements of the room environment during chamber loading were made with a wet-dry bulb psychrometer accurate to within  $\pm 2\%$  r.h.

#### Sample Cross-Sectional Area

Measurement of diameter of the test samples with micrometer calipers (accurate to 0.001") indicated a diameter accuracy of  $\pm 0.001"$ , which in turn, resulted in an area accuracy of  $\pm 0.002 \text{ in}^2$ . Each sample cross section area was taken to be  $0.196 \pm 0.002 \text{ in}^2$ .

Test Weight

Prior to each test sequence, the test weight was filled with mercury and then weighed to within  $\pm 0.5$  oz. After each test, the weight was re-weighed to ensure its value did not change. For these investigations, the test weights were accurate to  $\pm 0.5$  oz. or, in equivalent stress units,  $\pm 0.2$  psi.

Length Strain

Application of the photographic technique to measuring length strain of a stainless steel sample with machined bench marks indicated an accuracy of  $\pm 0.0008$  in/in strain could be approached. For the actual test measurements, the composition of the material and the bench marking technique made it impossible to reach this accuracy. The controlling factor for the accuracy of measurement of length strain in the samples was the repeatability to which the bench marks were located on the 70 mm film. A statistical analysis on this repeatability showed that at a 90% confidence level, length strain measurements were accurate to within  $\pm 0.0023$  in/in strain.

Diameter Strain

Application of the diameter strain measurement to a stainless steel cylinder showed that diameter changes of 0.0005 inch could be detected. Statistical tests on the repeatability of the diameter strain measurement showed that with a 90% confidence level, strain measurements were accurate to within  $\pm 0.0015$  in/in strain. (To obtain this accuracy, each diameter change was read from the film four times and the

average of these readings was used in the strain calculation.) Reported diameter strain measurements are believed to be accurate to within  $\pm 0.0015$  in/in. strain. In addition, diameter strains below 0.0015 in/in. cannot be detected.

#### Compliance

Defining compliance as the ratio of length strain to applied stress, the accuracy of the compliance calculation (37) can be obtained from

$$\delta J = \left[ \left( \left| \frac{\partial J}{\partial \varepsilon_1} \right| \delta \varepsilon_1 \right)^2 + \left( \left| \frac{\partial J}{\partial \bar{A}} \right| \delta \bar{A} \right)^2 + \left( \left| \frac{\partial J}{\partial F} \right| \delta F \right)^2 \right]^{1/2} \quad (8.1)$$

where  $J$ ,  $\varepsilon_1$ ,  $\bar{A}$ , and  $F$  are respectively the compliance, length strain, cross sectional area, and force. Results from this analysis indicate that compliance accuracies range from  $0.38 \times 10^{-4}$  to  $0.47 \times 10^{-4}$   $(\text{psi})^{-1}$ , with the largest error occurring at the lower strains and test weights.

#### Percent Volume Change

Considering the definition of "percent volume change" (eqn. 7.7) and using an analogy similar to that of equation 8.1, the accuracy of "percent volume change" was calculated to be .4% ( $\pm 0.004$  in.<sup>3</sup>/in.<sup>3</sup>) for the range of strains observed in this investigation. The volume change accuracy was relatively independent of the strain magnitudes for this investigation.

Poisson's Ratio

Using the definition of Poisson's Ratio (diameter strain/length strain) the probable accuracies range from  $\pm 0.12$  at 2% length strain to  $\pm 0.02$  at 7% strain. At strain values greater than 3% a Poisson's Ratio accuracy greater than  $\pm 0.07$  can be assumed.

## IX. DISCUSSION OF RESULTS

### Introduction

The results obtained during this investigation are presented and discussed in detail in this section. As previously noted, all discussions are based on the results of data obtained by averaging, at each loading time, the strain behavior of those samples within a sample group which failed within the 90 percent confidence interval of the mean failure time of the sample group. (See tabulated data of Tables VII thru XVIII and the Data Reduction section of this thesis.) Application of the correlation techniques discussed in the Literature Review to the experimental data are also presented along with their applicability for predicting vacuum effects. The final discussion of this section focuses on the nature of the mechanisms controlling the mechanical behavior of TPH 3105.

### Observed Vacuum Behavior

#### Length Strain

The length strain behavior as a function of loading time and for the different stress levels is shown in Figures 30, 31, and 32. Four curves are shown on each figure. These are the 50% r.h. air sample groups and three vacuum exposure groups with exposure times of approximately 2 days (46 to 51 hours), 1 week (170 to 173 hours, and 2 weeks (337 to 348 hours). The effects of vacuum on the strain behavior of TPH 3105 is illustrated in Figure 30 (51 psi stress level). In vacuum,

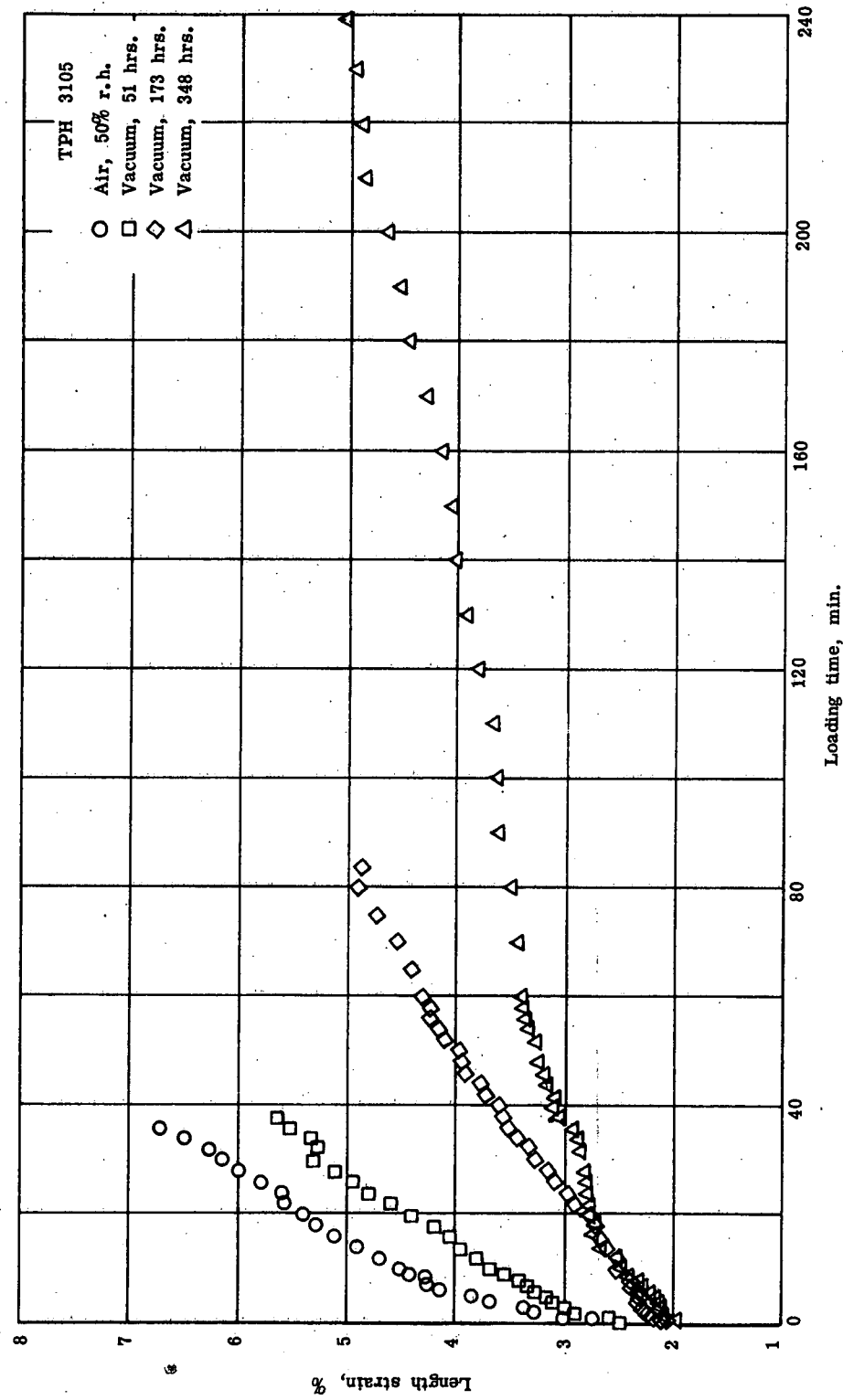


Figure 30. - Length strain results at a stress of 51 psi and at 83°F.

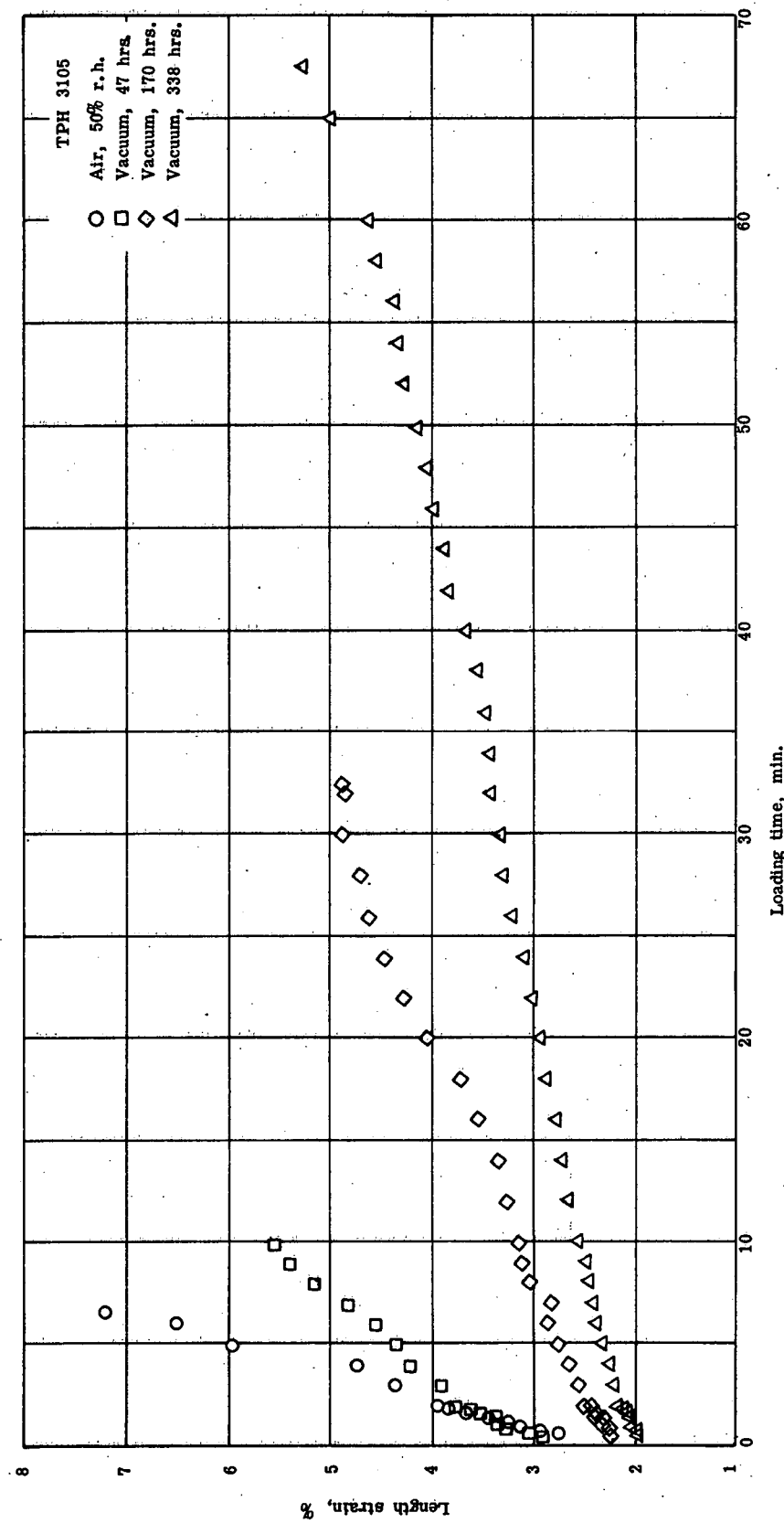


Figure 31. - Length strain results at a stress of 56 psi and at 83°F.

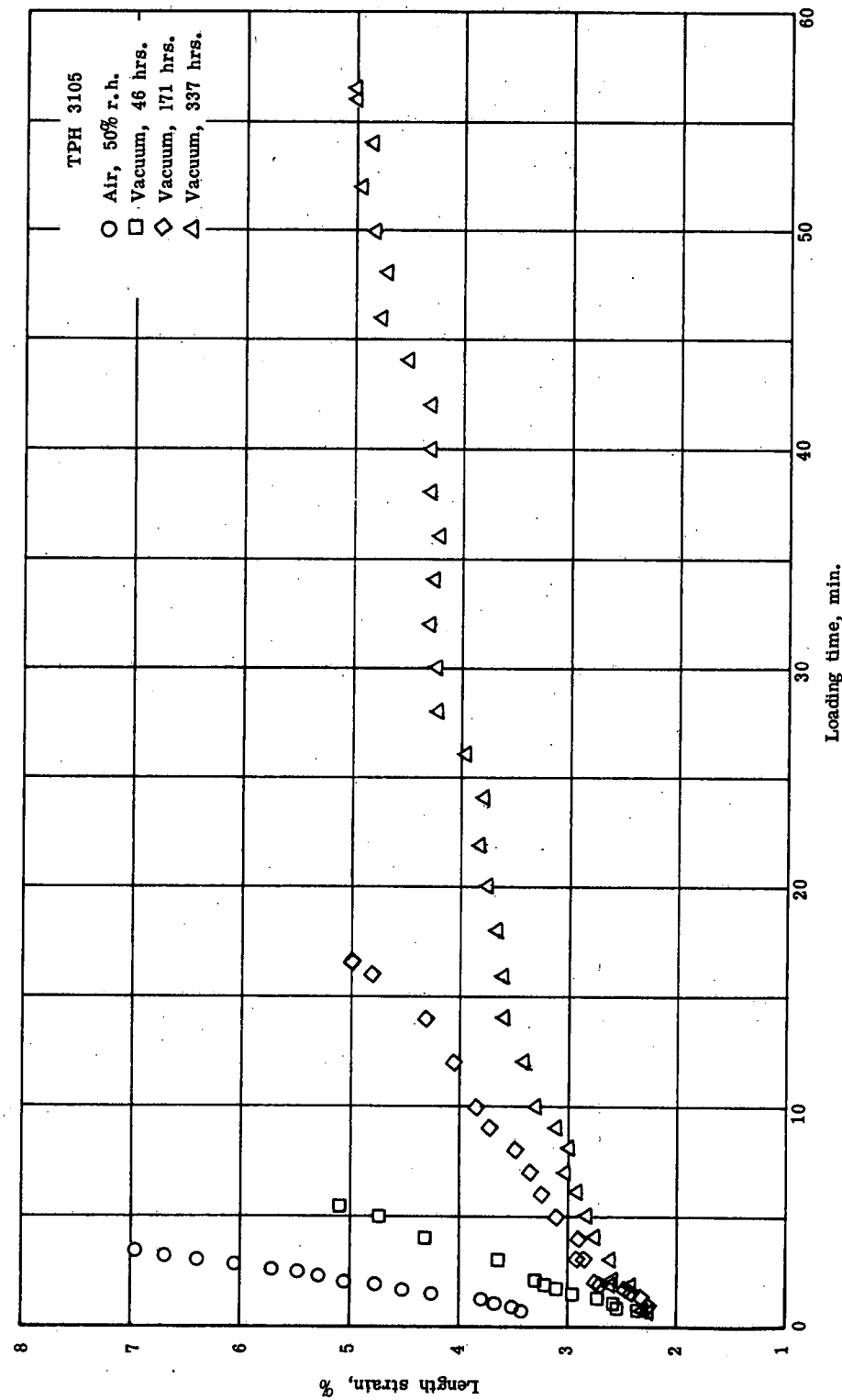


Figure 32. - Length strain results at a stress of 61 psi and at 83°F.

length strains were lower than those in air at corresponding loading times. For example, at 30 minutes into the loading cycle the length strain in air was on an average 6.15%. After 51 hours of vacuum the strain at 30 minutes was 5.30%; after 348 hours, 2.8%. In other words, after 348 hours of vacuum the strain at 30 minutes of loading was approximately 55% lower as compared to the air results. Similar decreases were noted at the other loading times and stress levels. (See Figures 31 and 32.)

#### Compliance

Creep compliance curves calculated from the experimental data are shown in Figures 33, 34, and 35. In each environment, compliance generally increased with increasing loading time indicating the creep of the material under the applied force. Increasing the vacuum exposure time resulted in lower compliances at virtually all loading times. Reductions as large as 50% occurred after approximately two weeks of vacuum exposure. This type of behavior indicates that those relaxation mechanisms which operate to dissipate stress or strain were retarded by the vacuum. Similar effects were observed in vacuum studies (4) of sterilized TPH 3105 in which the constant strain rate test method was employed. In those studies Young's modulus increased 20% after two weeks of vacuum exposure. Modulus and compliance measurements cannot be quantitatively related in these cases for a number of reasons. First, moduli and compliances are not simply related in viscoelastic materials; secondly, the limits of linear viscoelasticity were exceeded in both

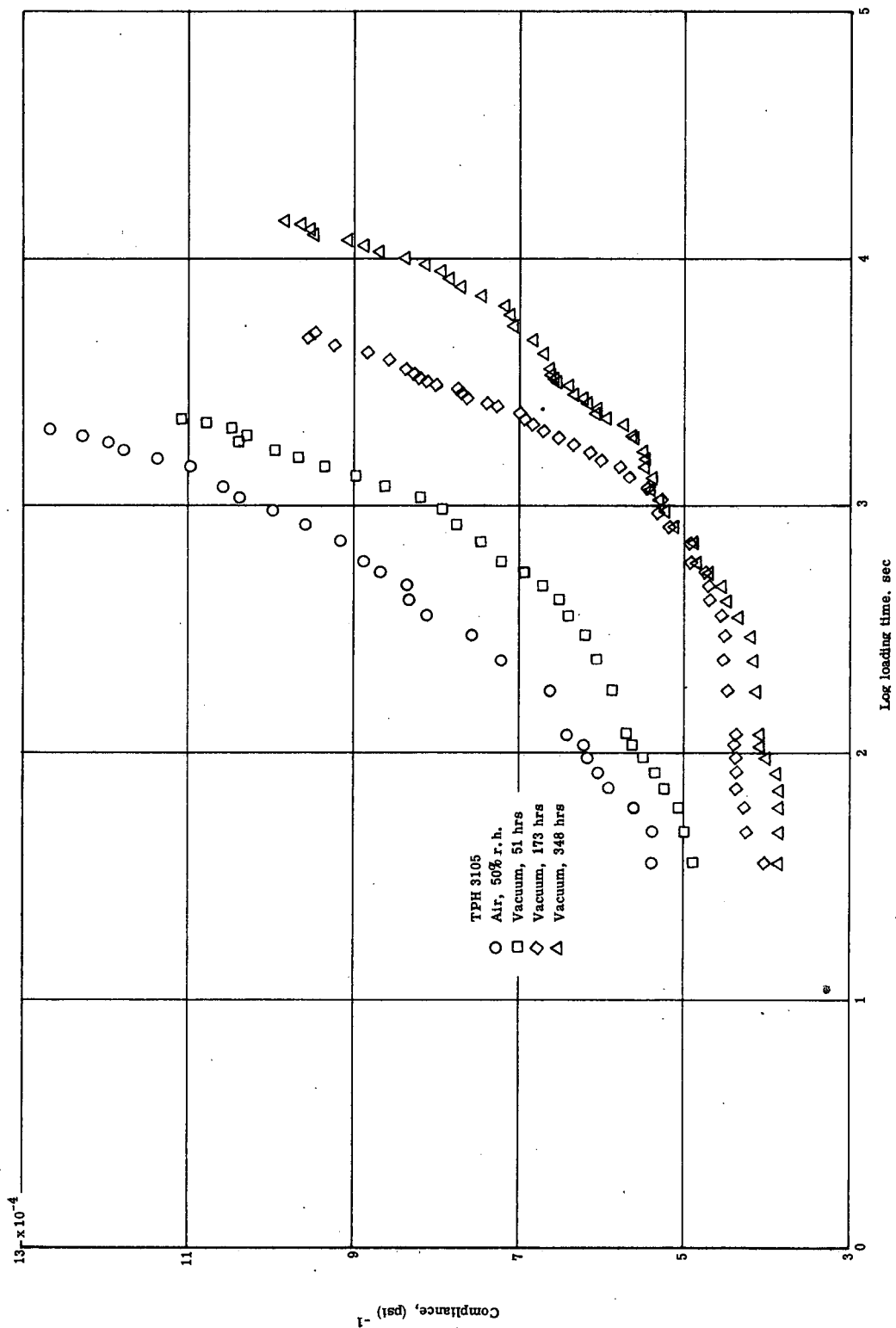


Figure 33. - Compliance results at 51 psi stress and 83°F.

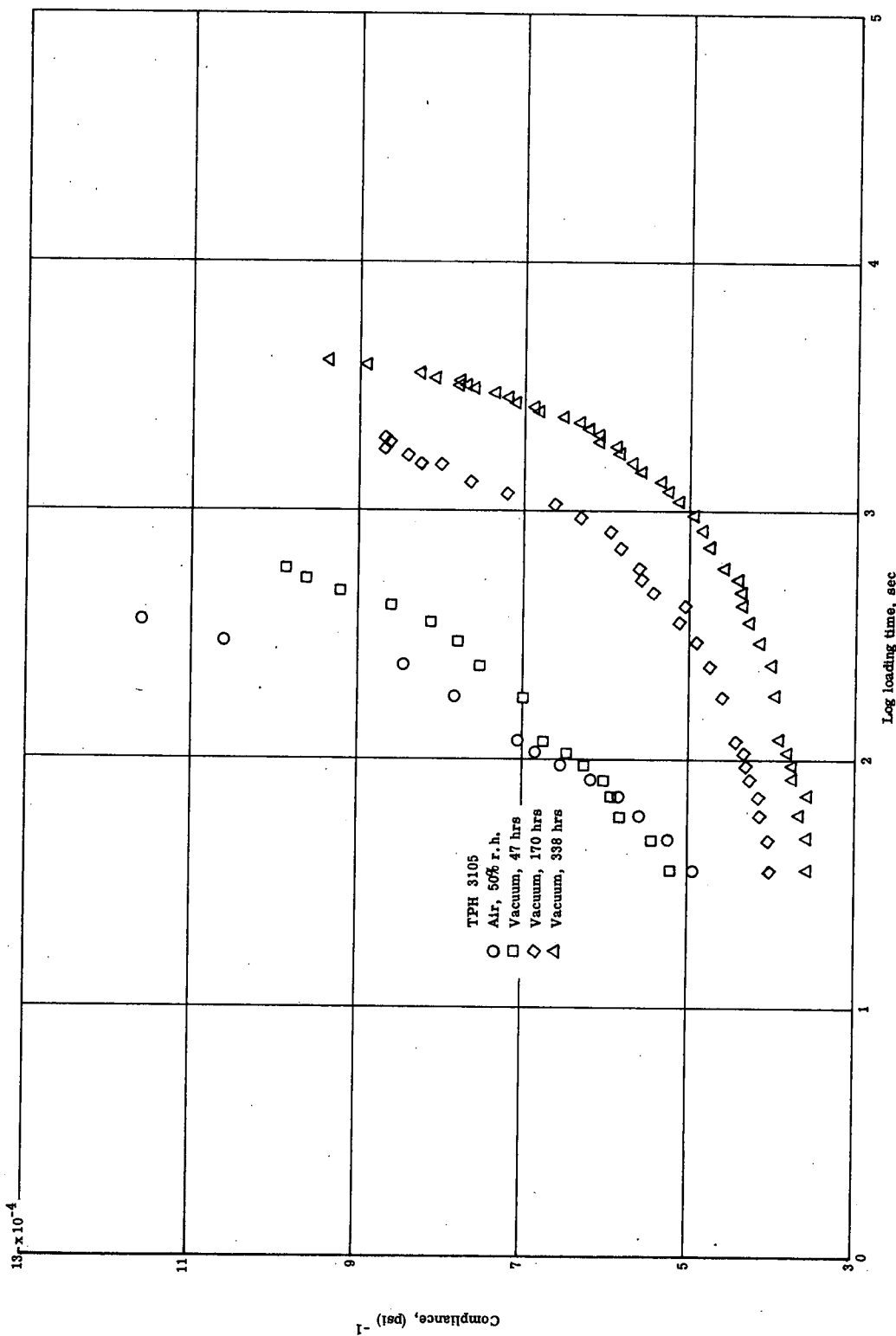


Figure 34. - Compliance results at 56 psi stress and 83° F.

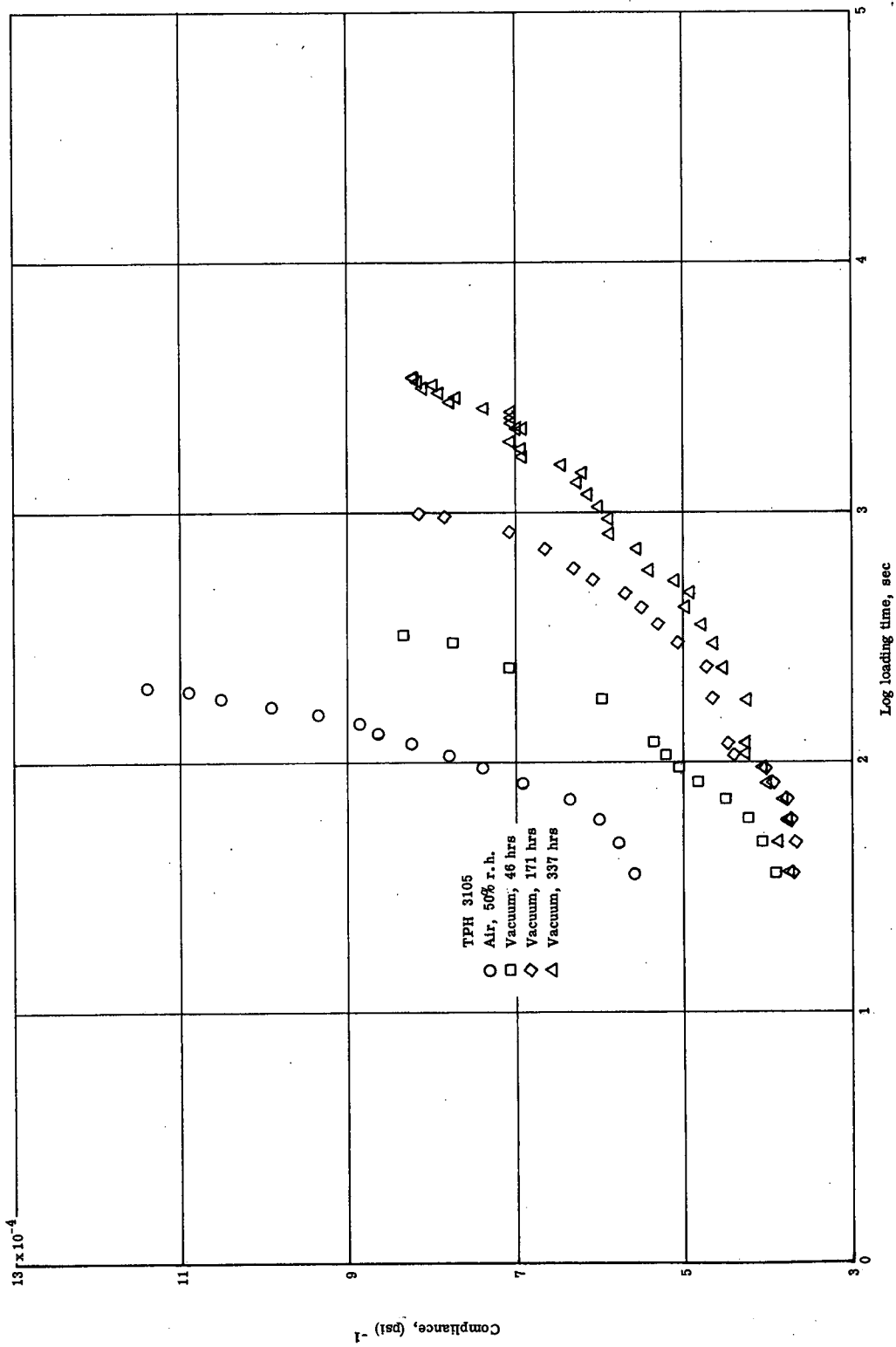


Figure 35. - Compliance results at 61 psi stress and 83°F.

tests; and thirdly, there were differences in the preconditioning of the material (sterilized and unsterilized). Qualitatively, the increase in modulus and decrease in compliance with vacuum exposure time indicate similar changes in the relaxation mechanisms occurring within the material.

As expected (30, 34) and as shown for similar environments, the effect of increasing the applied stress is to increase the compliance of the material at virtually all loading times.

#### Poisson's Ratio

Poisson's ratio as a function of length strain is shown in Figures 36, 37 and 38. (Poisson's ratio greater than 0.5 does not exist in nature, but may occur as the result of measurement inaccuracies.) Shown for comparison on each figure is Poisson's ratio calculated for an incompressible viscoelastic material (38). In each case, immediately upon loading, Poisson's ratio departed from that of an incompressible material. Poisson's ratio - length strain behavior of the type shown in Figures 36, 37 and 38 is typically observed in the mechanical property testing of propellants (39), other highly filled composites (40), and foamed materials (41). Generally, the effect of vacuum exposure was to decrease Poisson's ratio at each value of length strain. However, this decrease did not occur immediately upon exposing the material to vacuum. For each stress level, two critical vacuum exposure times were identified: one exposure time such that shorter exposure times had no effect on the Poisson's ratio - length strain behavior and for

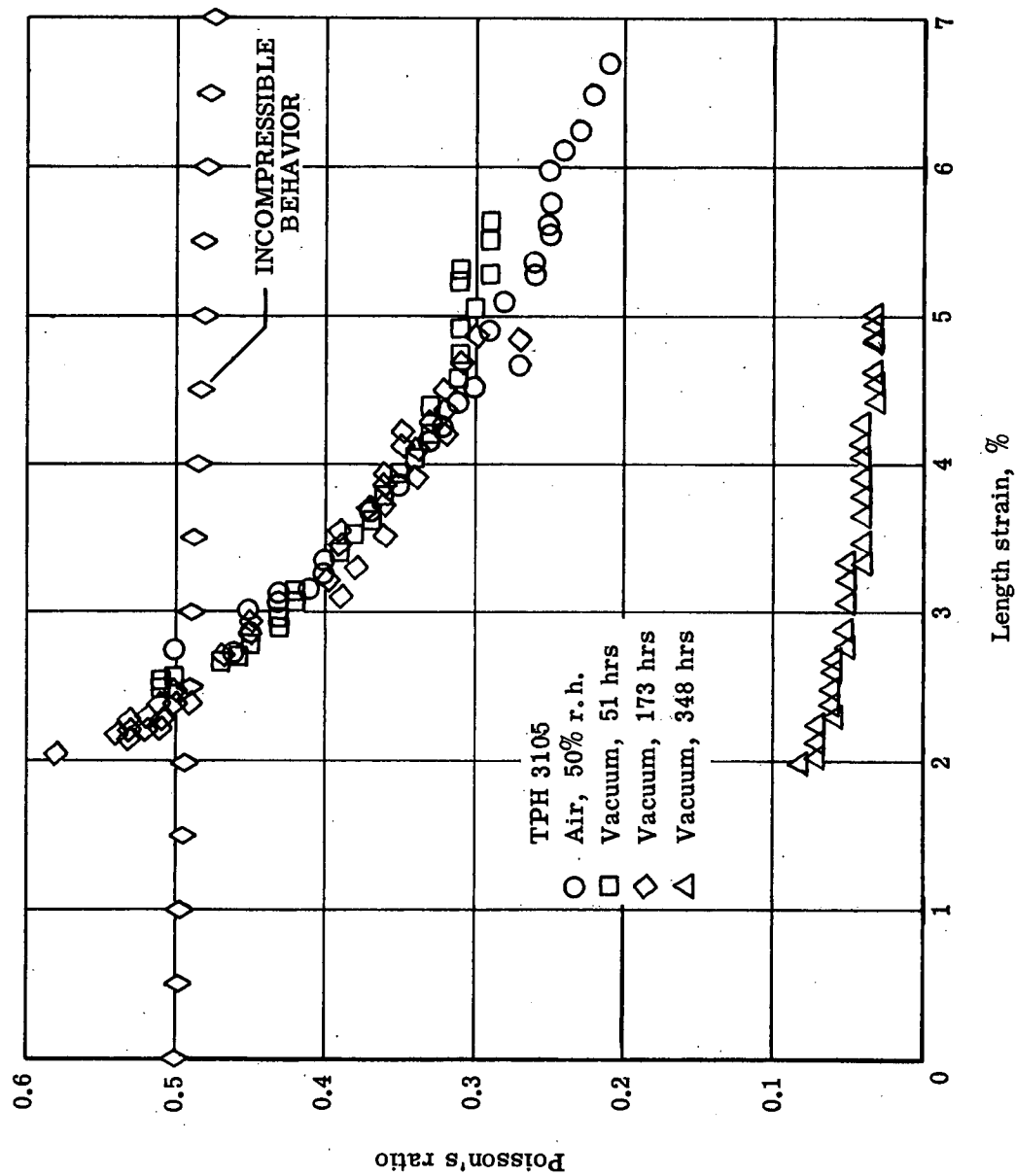


Figure 36. - Poisson's ratio results at 51 psi stress and 83°F.

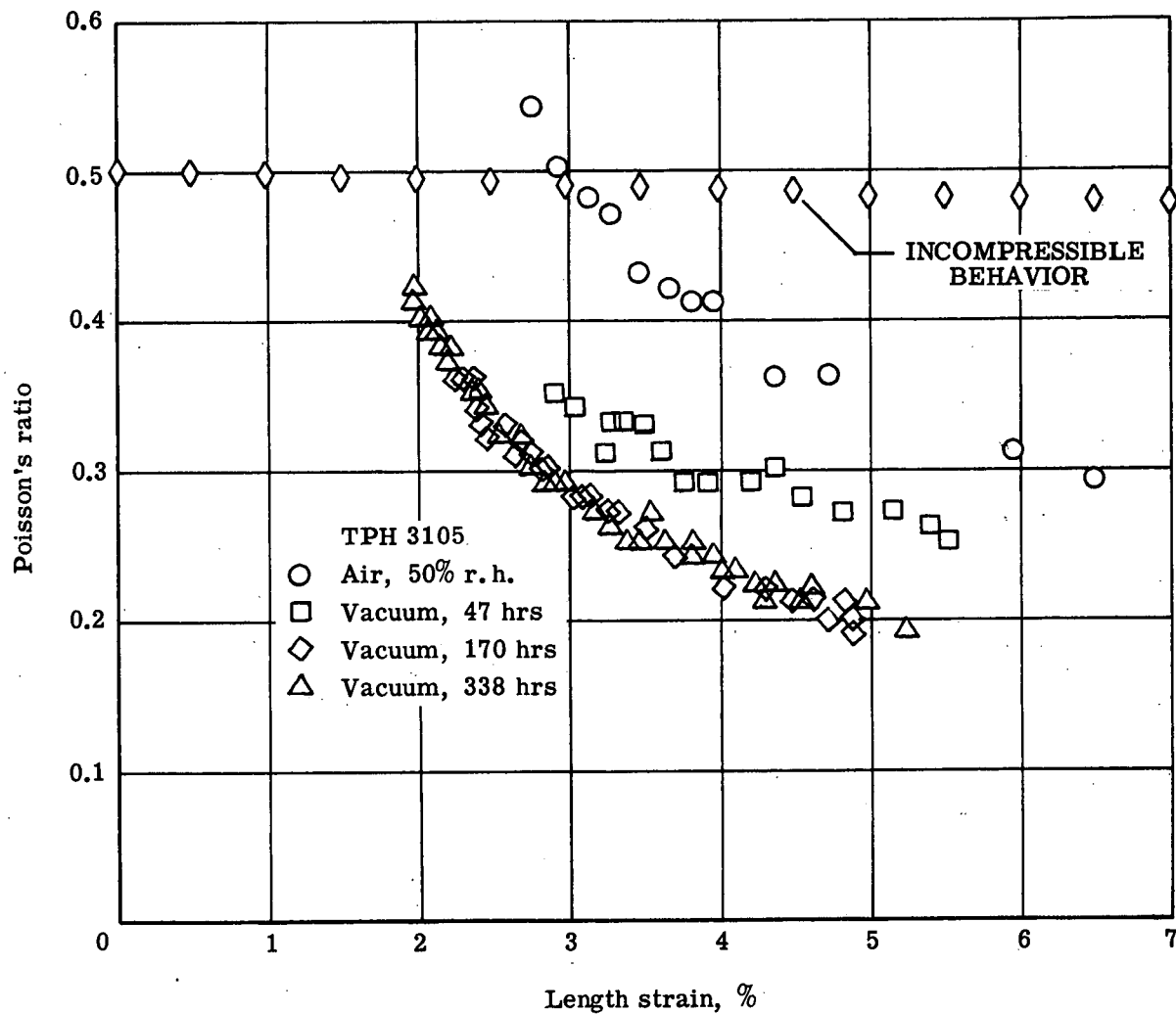


Figure 37. - Poisson's ratio results at 56 psi stress and 83°F.

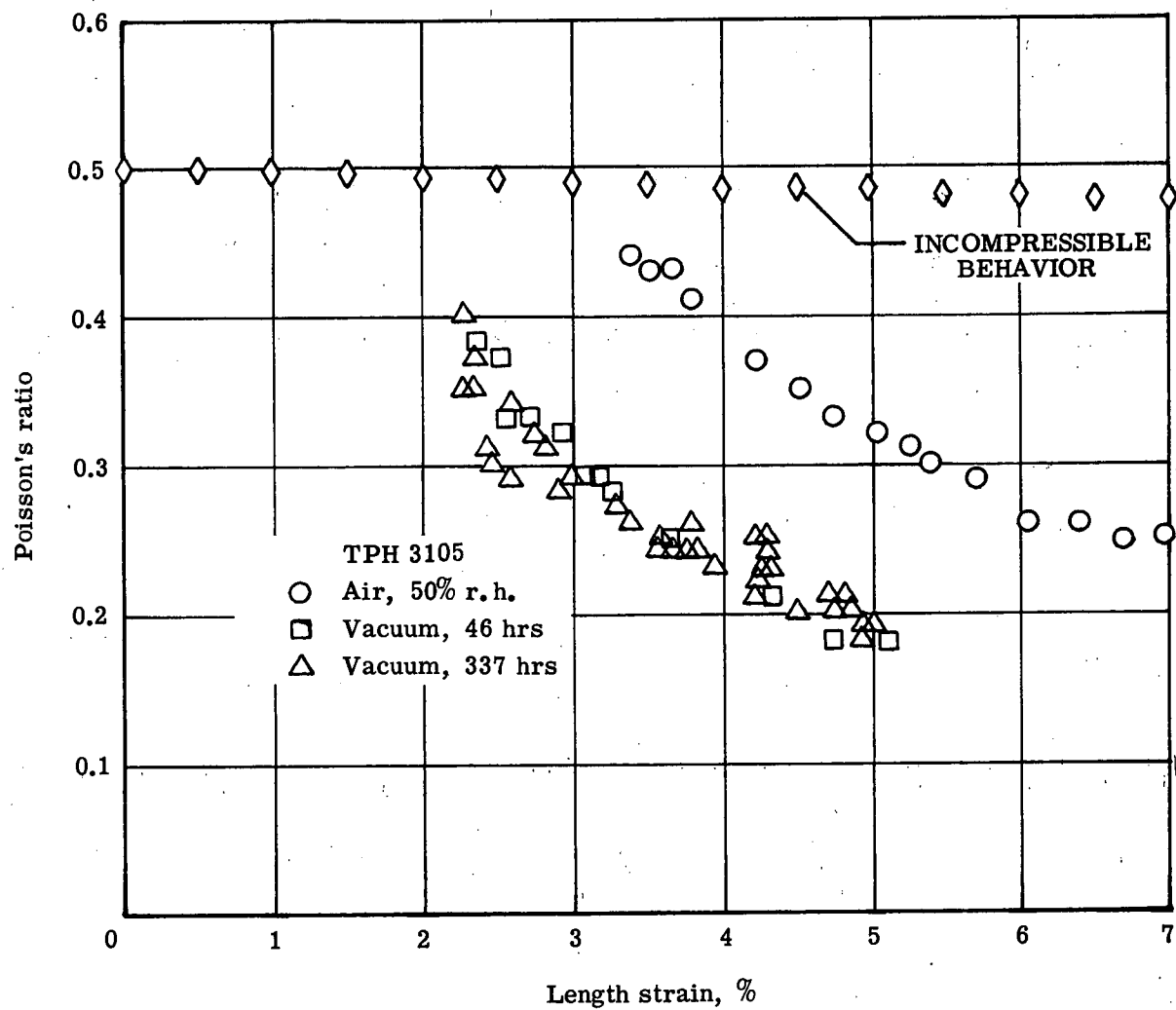


Figure 38. - Poisson's ratio results at 61 psi and 83° F.

longer exposure times beyond this time Poisson's ratio - length strain behavior was a function of vacuum time; a second vacuum time (longer than the first), such that additional vacuum exposure beyond this time caused no further changes in Poisson's ratio behavior with length strain. For example, from Figure 36 (51 psi), vacuum exposure times up to 173 hours had no effect on Poisson's ratio behavior with strain as compared to the air results; whereas, after 348 hours of vacuum much smaller values occurred at all strain levels. At 56 psi (Figure 37) Poisson's ratio changes occurred after 47 hours of exposure but after 170 hours of exposure additional changes were not observed. At 61 psi (Figure 38), the change occurred at or before 46 hours of vacuum and additional exposures up to 337 hours produced no further changes in the Poisson's ratio - length strain behavior of the material. Thus, there was a coupling between the applied stress and vacuum exposure time which influenced the Poisson's ratio behavior of the material — the changes in the Poisson's ratio - length strain behavior occurred at shorter exposure times at the higher stresses. It should be noted at this point that the stress level alone influences the Poisson's ratio - length strain behavior of the material (compare the air results of Figures 36, 37 and 38), but these changes were much much less than the vacuum induced changes. No explanation is apparent which would explain the low Poisson's ratio values observed at 51 psi and 348 hours in vacuum.

Volume Change

Plots of volume change versus length strain are shown in Figures 39, 40 and 41. Note that in Figure 39 the volume change for the samples exposed to 348 hours of vacuum is shown as a shaded area. This was the only sample group in which diameter strains were within the limits of detection of the strain monitoring technique (i.e.,  $-0.15\% < \epsilon_2 < 0.15\%$ ). The shaded area represents the range of the volume change for this sample group, based on equation 7.5 and the limits of detection of the diameter strain measurement. The actual volume change for this sample group lies in the shaded area.

The volume change (dilatational) behavior of TPH 3105 was similar for each environment in that volume changes were observed to increase approximately linearly with increasing length strain. The initial volume change in the material as the result of load application ranged from zero to 2.25% with the higher initial volume change generally occurring for the longer vacuum exposure times. Maximum volume changes for the material were approximately 5%. In every case but one, the linear increase of volume change with respect to length strain occurred immediately upon sample loading thus suggesting that the material was behaving as a filled foam (13). At 51 psi and following 173 hours of vacuum (Figure 39), the volume change did not increase immediately upon sample loading. For these samples the volume change was zero from the initial strain of 2% to approximately 2.85% strain (20 minutes into the loading cycle). Straining beyond 2.85% resulted in the linear increase in volume change as observed for the other sample groups. For this one

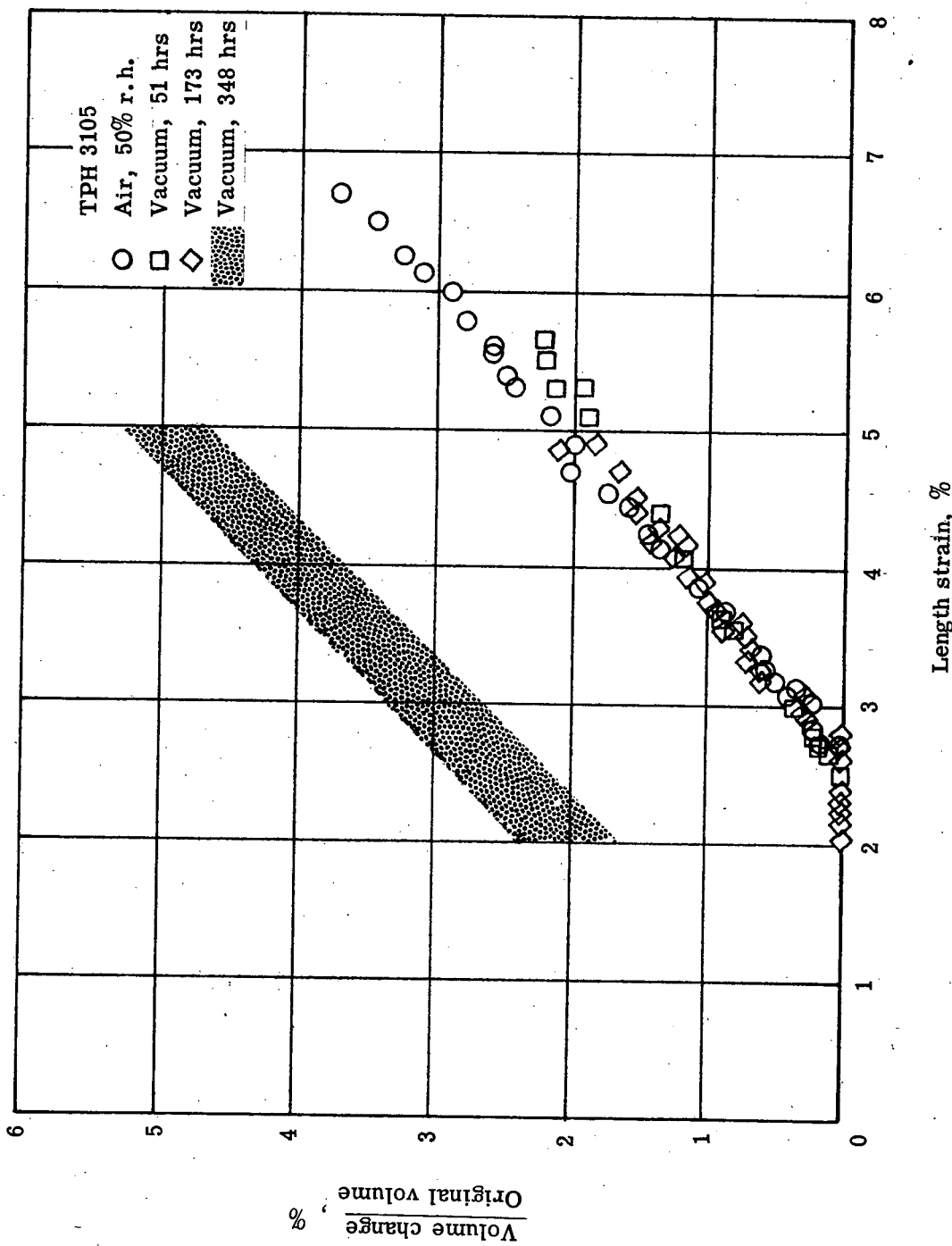


Figure 39. - Volume change results at 51 psi and 83°F.

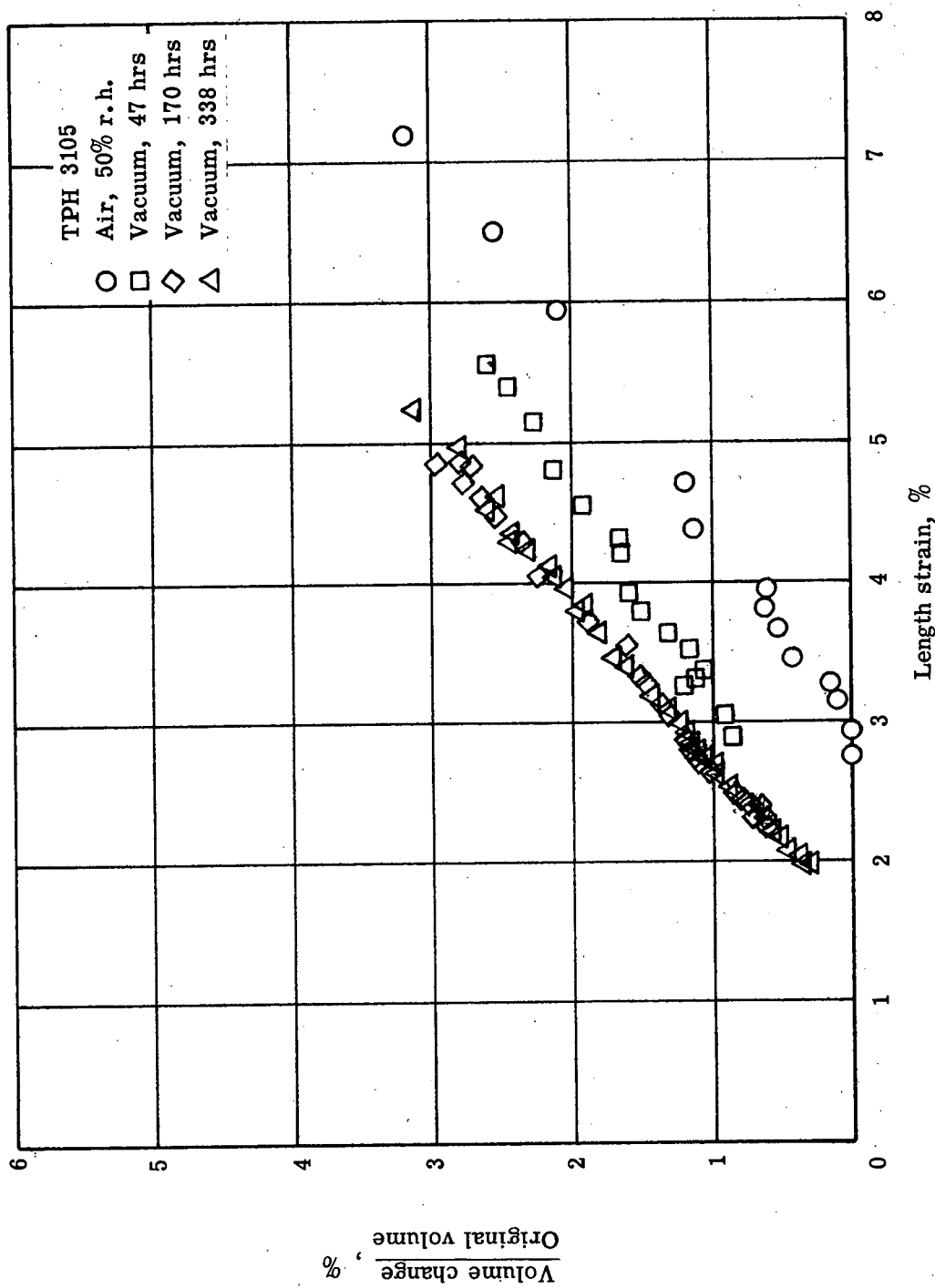


Figure 40. - Volume changes results at 56 psi and 83°F.

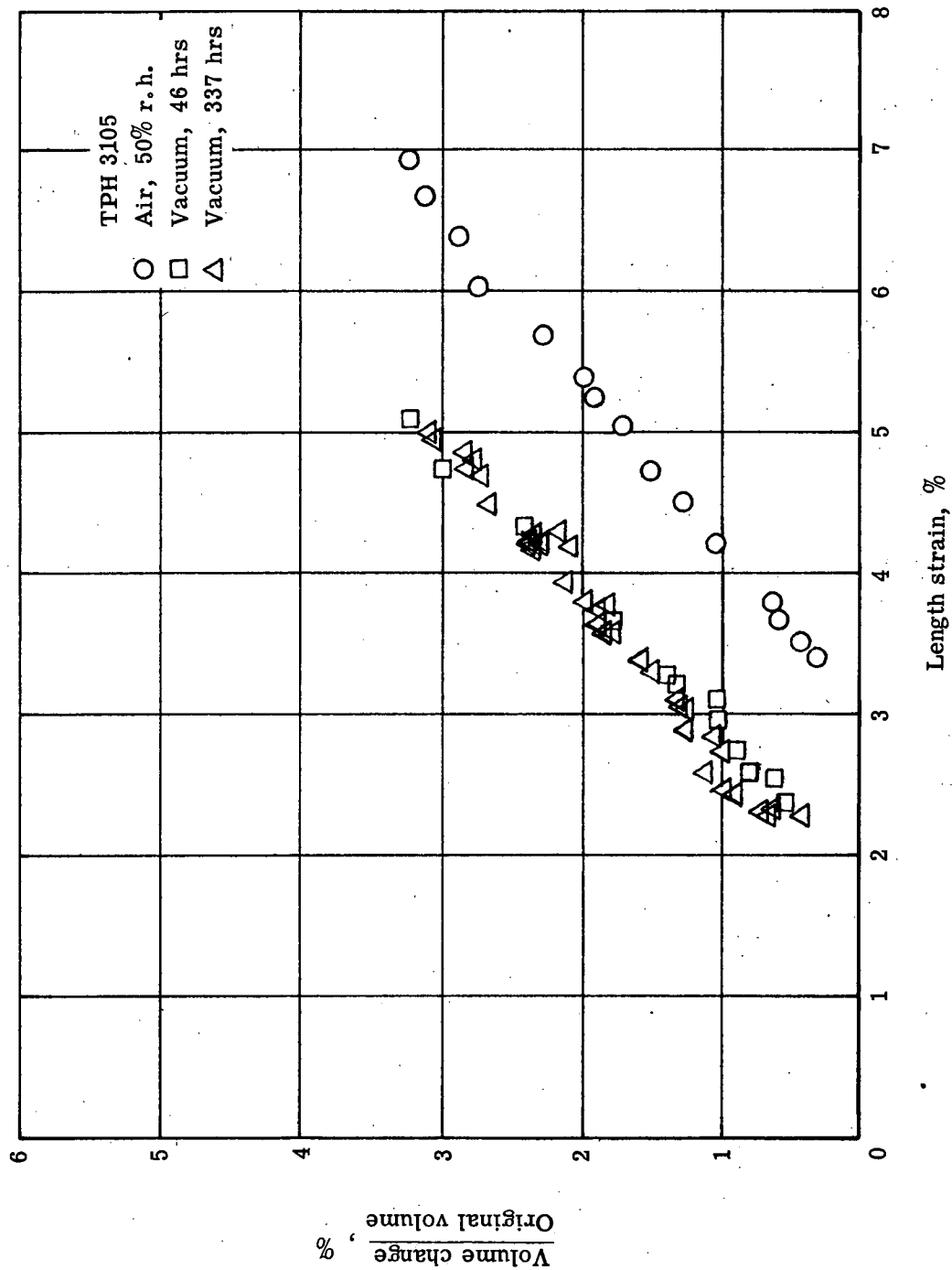


Figure 41. - Volume change results at 61 psi and 83°F.

case, the volume change behavior suggests that initially the material was viscoelastic ( $\frac{\Delta V}{V_0} = 0$ , Poisson's ratio is that of an incompressible material) and at 2.85% strain, transition to filled foam behavior occurred almost instantaneously.

As discussed in the mechanical properties model,  $\frac{d \frac{\Delta V}{V}}{d \epsilon_{li}}$  at any time "i", measures the quantity of filler dewetted in the material in time "i". Assuming, as predicted by this model, that in the filled foam region additional filler particles do not dewet and vacuoles around existing dewetted particles only enlarge, then  $\frac{d \frac{\Delta V}{V}}{d \epsilon_{li}}$  in this region measures the total quantity of filler dewetted in the straining process. Slopes of least squares straight lines fitted to each curve in Figures 39, 40 and 41 (excluding the data of the zero volume change region at 51 psi and 173 hours of vacuum) ranged from 0.65 to 1.0 with no trend to the variations. The 90% confidence interval for the mean of the slopes (0.84) was 0.79 to 0.89 which agrees with an expected slope of 0.82 for a 82% filled composite in which all filler particles dewet (13).

As seen from the previous discussion, exposure of TPH 3105 to vacuum had little effect as compared to air results on the manner in which the volume change of the material varied with increasing length strain. Rather, the effect of vacuum was to increase the magnitude of the initial volume change of the material as the result of the stress loading. As was the case for Poisson's ratio, a given vacuum exposure time was required before changes in the volume behavior became apparent.

Similarly, a second exposure time existed beyond which additional exposure of TPH 3105 to vacuum had no further effect on the volume change. As was the case for Poisson's ratio, the magnitude of these critical vacuum exposure times was stress dependent. For example, at the 51 psi stress level (Figure 39) the volume change - length strain behavior after 51 and 173 hours of vacuum exposure was similar to that observed for the material in air (excluding the zero volume change region at 173 hours), while after 348 hours of vacuum the volume change at every length strain was approximately 2.5% higher than the volume change in air at corresponding length strains. In other words, the initial volume change of the material at loading increased 2.5%, but the linear increase in volume with increasing length strain was similar to that observed in air, after 51 hours of vacuum, and after 173 hours of vacuum. At 56 psi stress and after 47 hours of vacuum, the initial volume change at loading increased approximately 0.8% while after 170 hours of vacuum exposure, the increase was 1.25% as compared to the results in air. Again the linear increase of volume change with length strain was similar to that observed in air at the 56 psi stress level. Additional exposures beyond 170 hours had no further influence on the volume change - length strain behavior. At 61 psi stress similar volume change increases occurred. After 46 hours in vacuum the volume change increased 1.3% (as compared to air results) and additional exposures up to 337 hours resulted in essentially no further changes. As noted for Poisson's ratio and as evident from the volume change results, the effects of vacuum are apparently coupled to a stress level effect.

Applying the statistical representation of the dilatation equation (equation 6.13 and Figure 19), the length strain,  $\bar{\epsilon}_1$ , about which dewetting occurred was determined from the point of intersection of the least squares lines fitted to the volume change - length strain curves (Figures 39, 40 and 41) with the zero volume change line (abscissa). Table XIX shows the results of the analysis. Vacuum exposure decreases the strain about which the dewetting process occurs. Thus after vacuum exposure TPH 3105 dewets at smaller length strain than in air. (As will be discussed later, the increase in the viscous mechanisms within the material reduces the mobility of the binder network, thus causing dewetting to occur at smaller elongations.)

#### Failure Time

The effect of vacuum exposure on the mean failure time of the sample group is shown in Figure 42. The 90% confidence interval on the mean failure times is indicated by the error bars on the data. The effect of vacuum was to increase the mean failure time at each stress level. Failure times ranged from 3.3 minutes (61 psi stress, zero vacuum) to 239.6 minutes (51 psi stress, 348 hours of vacuum). After approximately 2 weeks of vacuum, failure times at 51, 56 and 61 psi stress increased approximately 600, 900 and 1600%, respectively, when compared to results in air. Failure times were longer at the lower stress levels and the longer exposures.

By applying the Arrhenius equation (equation 6.3) to the failure times of the air samples, an activation energy for the failure process

TABLE XIX  
STRAIN MEAN FOR DEWETTING

Sample Group	Stress (psi)	$\bar{\varepsilon}_1$ (%)
Air, 50% r.h.	51	2.67
Vacuum, 51 hours	51	2.48
Vacuum, 173 hours	51	2.61
Vacuum, 348 hours	51	$-0.31 < \bar{\varepsilon}_1 < 0.07$
Air, 50% r.h.	56	2.89
Vacuum, 47 hours	56	1.64
Vacuum, 170 hours	56	1.55
Vacuum, 338 hours	56	1.58
Air, 50% r.h.	61	3.01
Vacuum, 46 hours	61	1.88
Vacuum, 337 hours	61	1.58

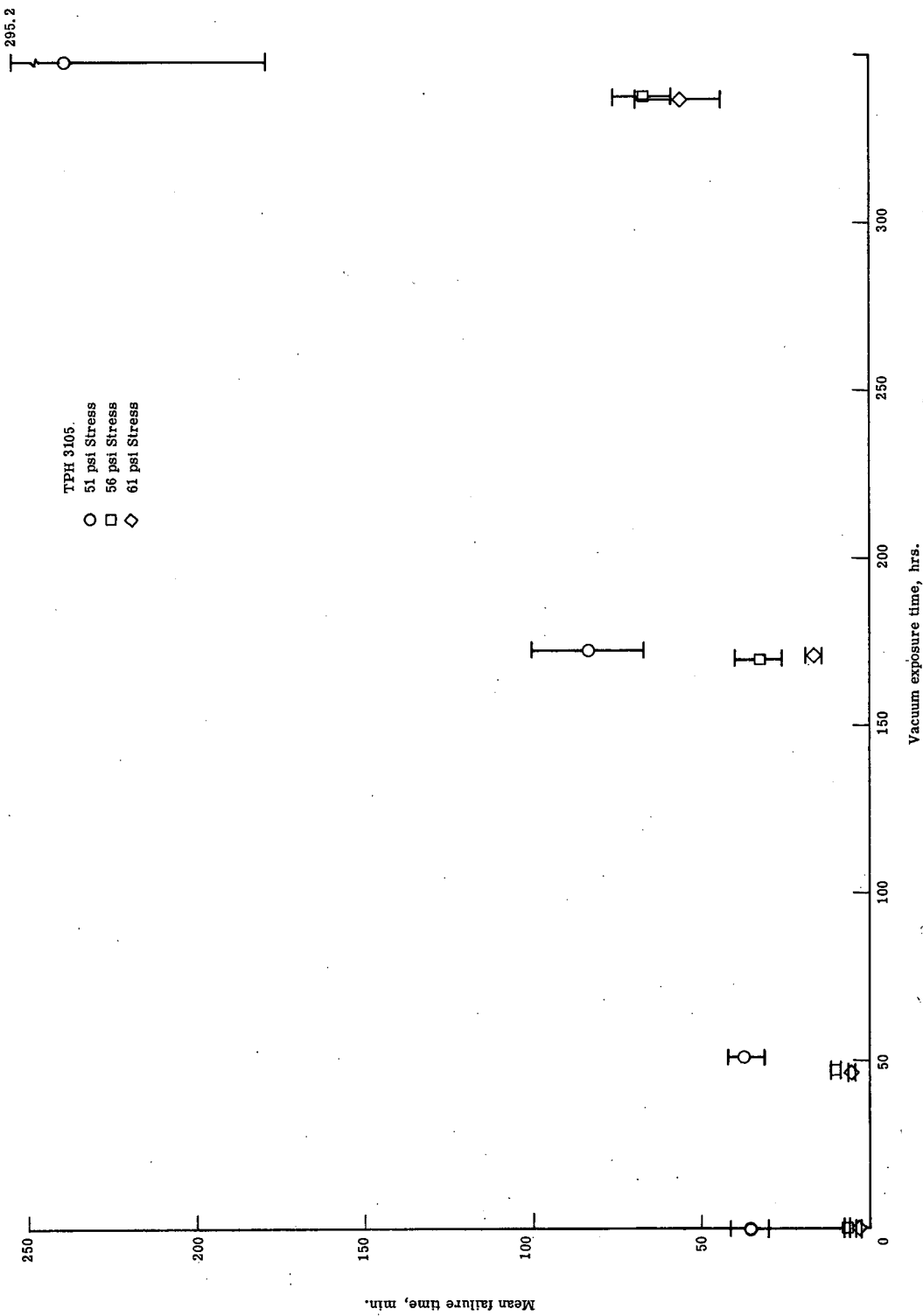


Figure 42. - Failure time results at 83° F.

was calculated to be 30 kilo-cal /gm -mole. It is noted that the measured activation energy was well below that required for breaking a carbon-carbon bond (C - C; 90 kilo-cal /gm -mole) (42) but only slightly above that recognized for most elastic or viscous retardation processes (15 to 25 kilo-cal /gm -mole)<sup>3</sup>. From the activation energy concept, it appears that those mechanisms controlling the failure process in air are viscous and elastic retardation processes. Activation energies were not calculated for the vacuum data because the coupling between applied stress and vacuum exposure time was believed to have violated assumptions used in deriving equation 6.3; in particular, the assumption that the failure mechanisms were not changed by the testing at different stress levels.

#### Analytical Correlation of Experimental Results

In the Literature Review several techniques were discussed which had potential for the development of an analytical expression to describe the mechanical behavior of TPH 3105 in vacuum. The compliance-shift technique did correlate the vacuum behavior of the material and predict the compliance behavior in vacuum. The application of this technique is discussed in detail after first pointing out the problems associated with the other techniques.

#### Dilatational Technique

The dilatational technique as discussed in the Literature Review could not be applied to the TPH 3105 results. The application of this technique requires volume change data of the type shown in Figure 12

in order that both  $S$  and  $\bar{\epsilon}_1$  be determined for use in equation 6.13. As previously discussed, only the volume change behavior in the filled foam region was obtained and hence  $S$  could not be determined. The dilatational behavior of each sample group was analytically described by least squares straight lines fitted to the volume change - length strain data. Attempts to correlate the least square analysis into a general mechanical behavior equation for TPH 3105 were not successful. The failure of the dilatational technique was due to the limited range of the experimental data rather than to an inadequate dilatational model.

#### Arrhenius Technique

Because of the coupling effects that existed between applied stress and vacuum exposure time, activation energies could not validly be calculated for the vacuum exposed samples. However, the Arrhenius correlation technique was applied to the air data. Using the activation energy obtained by the Arrhenius analysis (30 kilo-cal /gm -mole) and the Arrhenius constant,  $C$ , ( $3 \times 10^{-5} \text{ m}^2/\text{Nt}$ ), equation 6.17 was solved on the computer using finite difference iteration. Four stress levels were chosen for comparison of predicted and experimental results. Table XX shows the results of calculated and of measured failure times. Considering that the activation energy and Arrhenius constant were obtained from least squares straight lines fitted to three data points, the agreement of measured and calculated failure times is good. It should be noted that the 41 psi samples were not tested to failure.

TABLE XX

COMPARISON OF PREDICTED FAILURE TIMES  
TO MEASURED FAILURE TIMES IN 50% R.H. AIR

Stress psi	Measured Failure min.	Predicted Failure min.
41	—	273
51	35.4	27.3
56	6.6	8.4
61	3.3	3.7

However, the volume change of the material after 100 minutes of loading ( $\frac{\Delta V}{V_0} \approx 2\%$ ) indicated that the material was not near failure; thus the predicted failure time of 273 minutes is reasonable.

#### Compliance - Shift Technique

As discussed in the Literature Review, numerous applications of the shift factor concept have been made. In this investigation, the goal of the technique is to develop a "master" compliance curve or curves in a reference environment (50% r.h. air) and from the curves to predict the creep compliance of TPH 3105 after vacuum exposures up to two weeks. Having developed equation 6.18 for the environments of temperature, stress, and vacuum exposure,

$$J_{T_o, \sigma_o, V_o} (\log t) = J_{T, \sigma, V} (\log t - \log a_T - \log a_\sigma - \log a_v) \quad (6.18)$$

the equation becomes

$$J_{T_o, \sigma_o, V_o} (\log t) = J_{T_o, \sigma, v} (\log t - \log a_\sigma - \log a_v) \quad (9.1)$$

for the experimental constraint of isothermal testing. As noted earlier, the form of equation 6.18 and hence equation 9.1 assumes  $a_\sigma$  is independent of vacuum exposure and  $a_v$  is independent of applied stress; thus,  $a_\sigma$  can be determined at any vacuum exposure and  $a_v$  can be determined at any stress level.

Using the 51 psi data (Figure 33) and the 50% r.h. air measurements as the reference environment, the vacuum effect shift factor for the 51 hour vacuum exposed samples was obtained by horizontally shifting

to the left the 51-hour vacuum compliance curve until the area (as visually determined) between the vacuum curve and air curve was minimal (i.e. the two curves approximately coincided). The vacuum effect shift factor ( $\log a_v$ ) is the number of log time cycles the vacuum curve was shifted. Performing similar shifts for the other two vacuum exposure groups on Figure 33 results in a single "master" compliance - log time curve (at 51 psi and 50% r.h. air) and two additional shift factors. This master curve is shown in Figure 43. The dependency of the vacuum effects shift factors on vacuum exposure time is shown in Figure 46. Master curves and vacuum effect shift factors were obtained in a similar manner at the other two stress levels and are shown in Figures 45, 46 and 47. Comparison of the vacuum effect shift factors at the three stress levels (Figure 46) showed that they were essentially stress independent; thus, justifying the separation of  $a_\sigma$  and  $a_v$  and validating assumption 3 in the development of equation 6.18. The vacuum effect shift factors for TPH 3105 were taken to be arithmetic averages (Figure 46) of those at the three stress levels for a given exposure.

Attempts to generate a single master curve and a set of stress shift factors by applying the shift technique to the master curves of Figures 43, 44 and 45 were unsuccessful. The master curve at each stress level was different shaped and would not shift; thus, stress shift factors,  $\log a_\sigma$ , (equation 9.1) could not be determined. Based on reference 15 a possible explanation for the different shaped master curves is as follows:

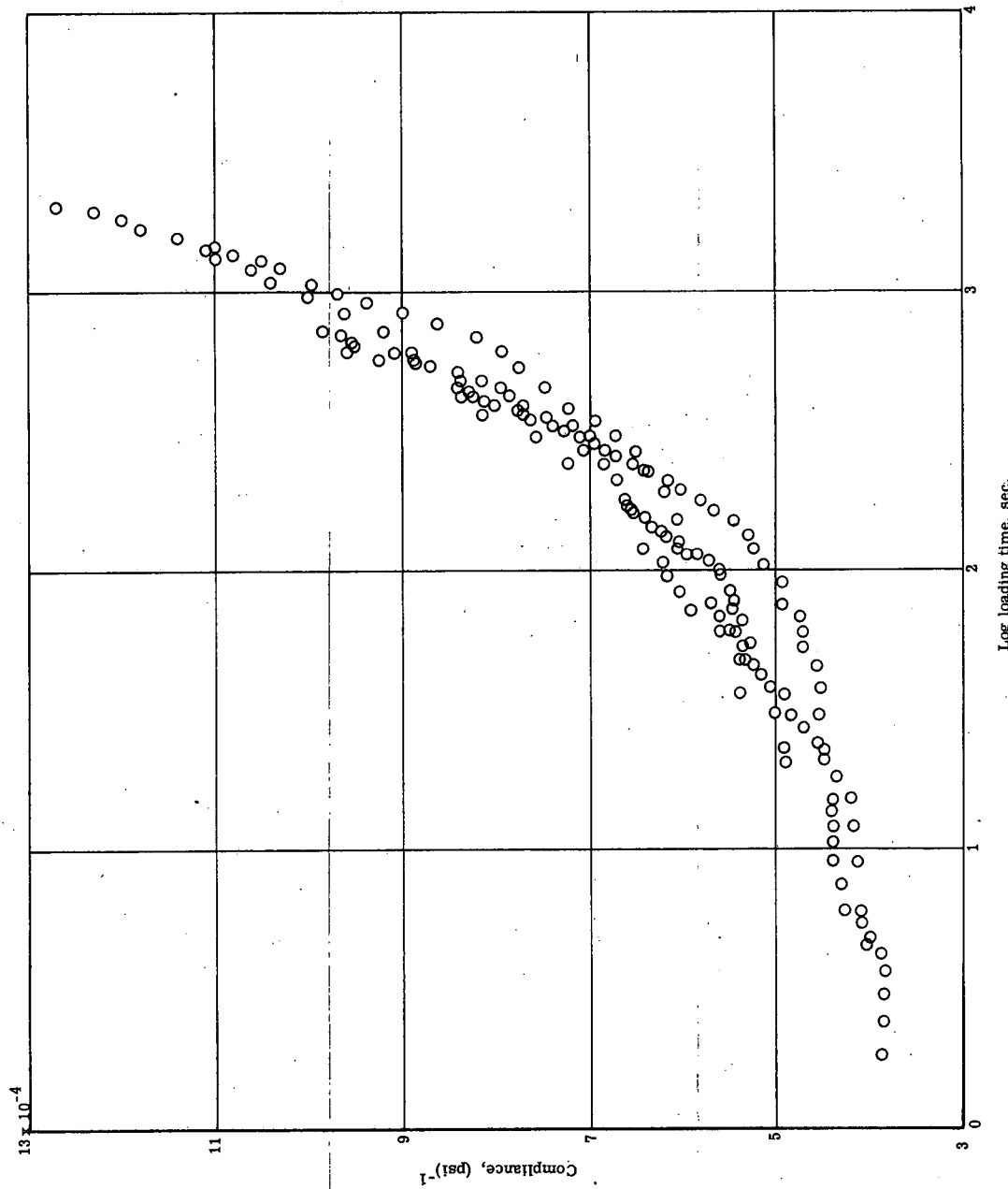
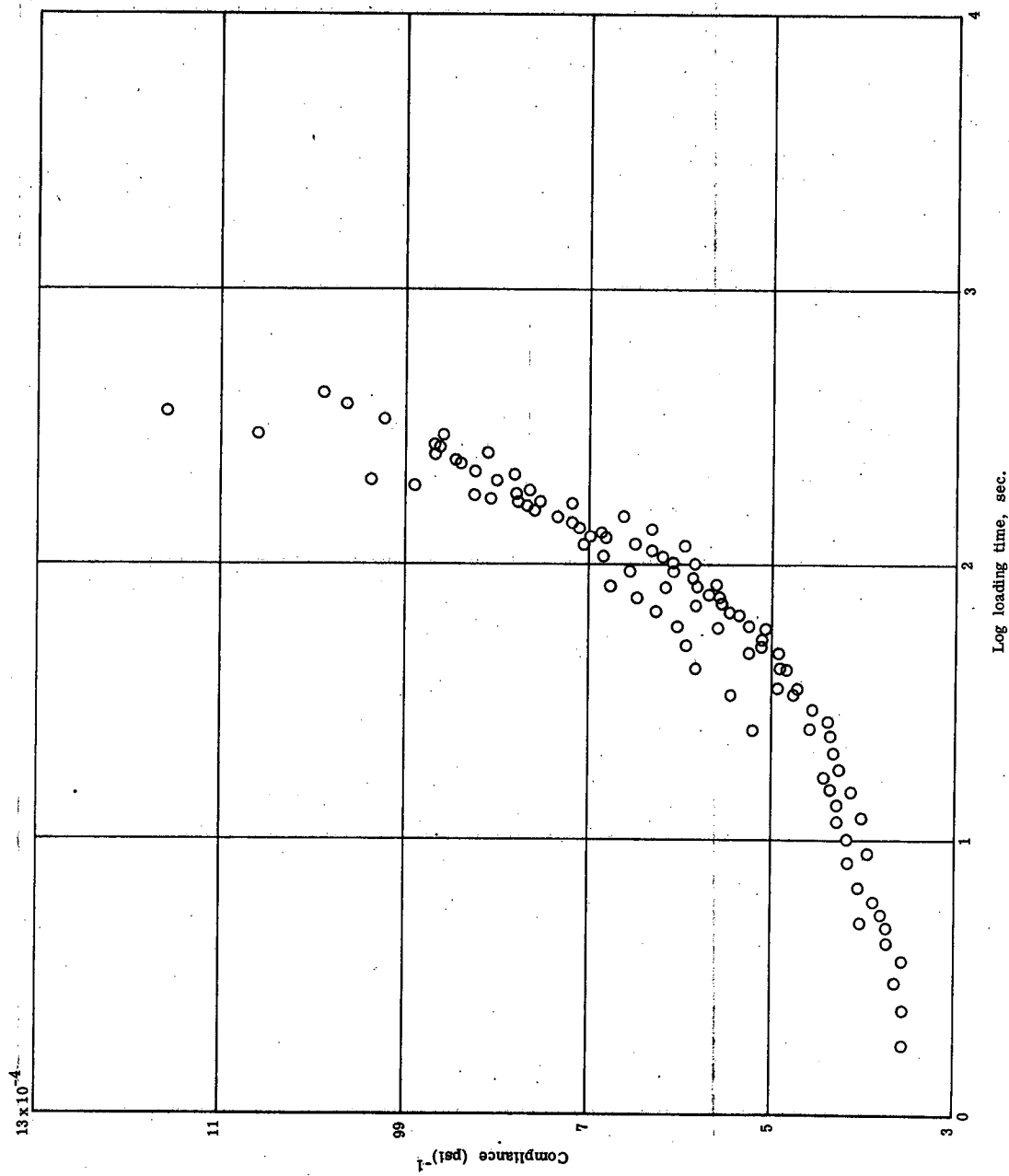


Figure 43. - Compliance master curve for TPH 3105 at 51 psi stress and 50% r.h. air.



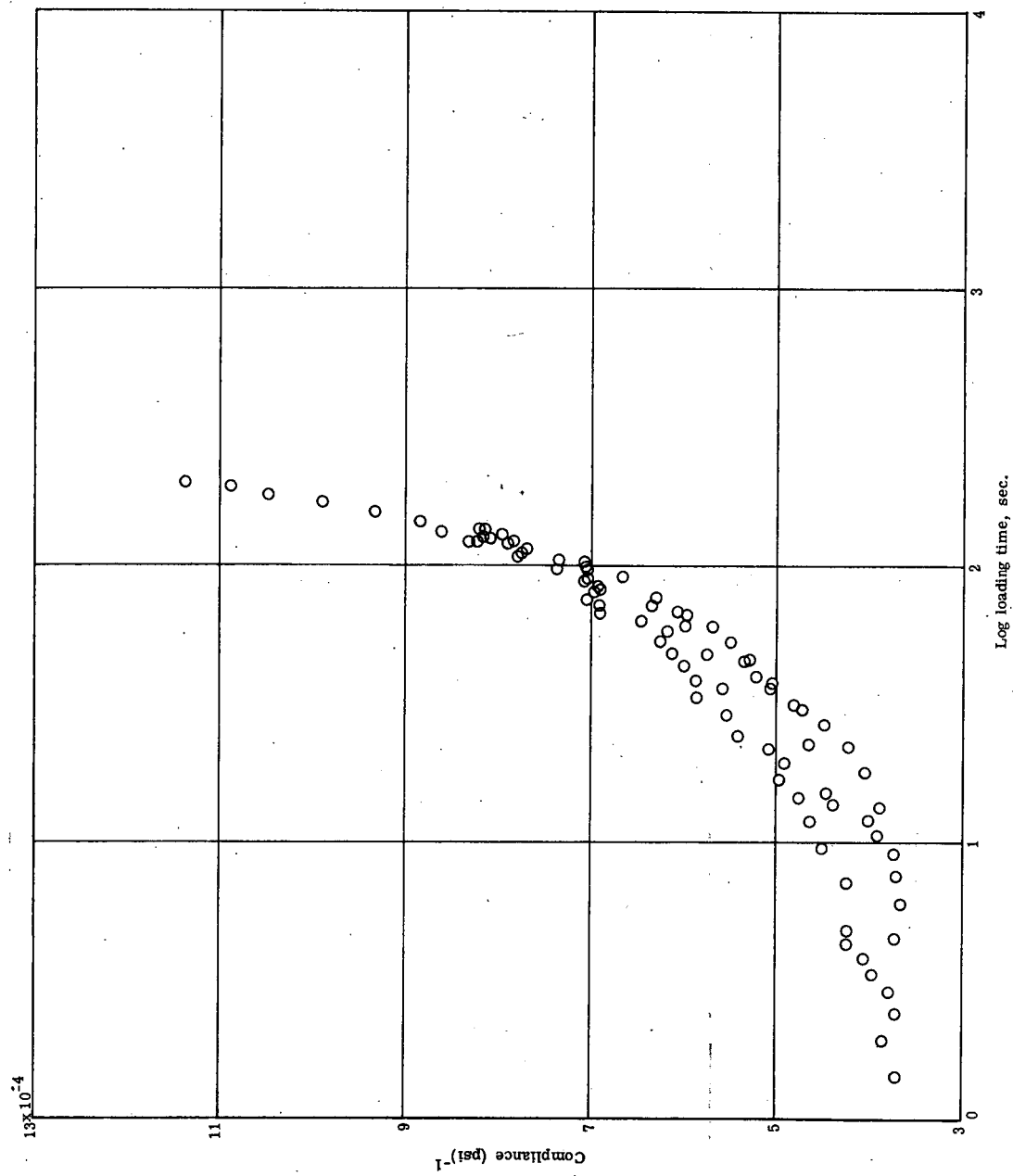


Figure 45. - Compliance master curve for TPH 3105 at 61 psi stress and 50% r.h. air.

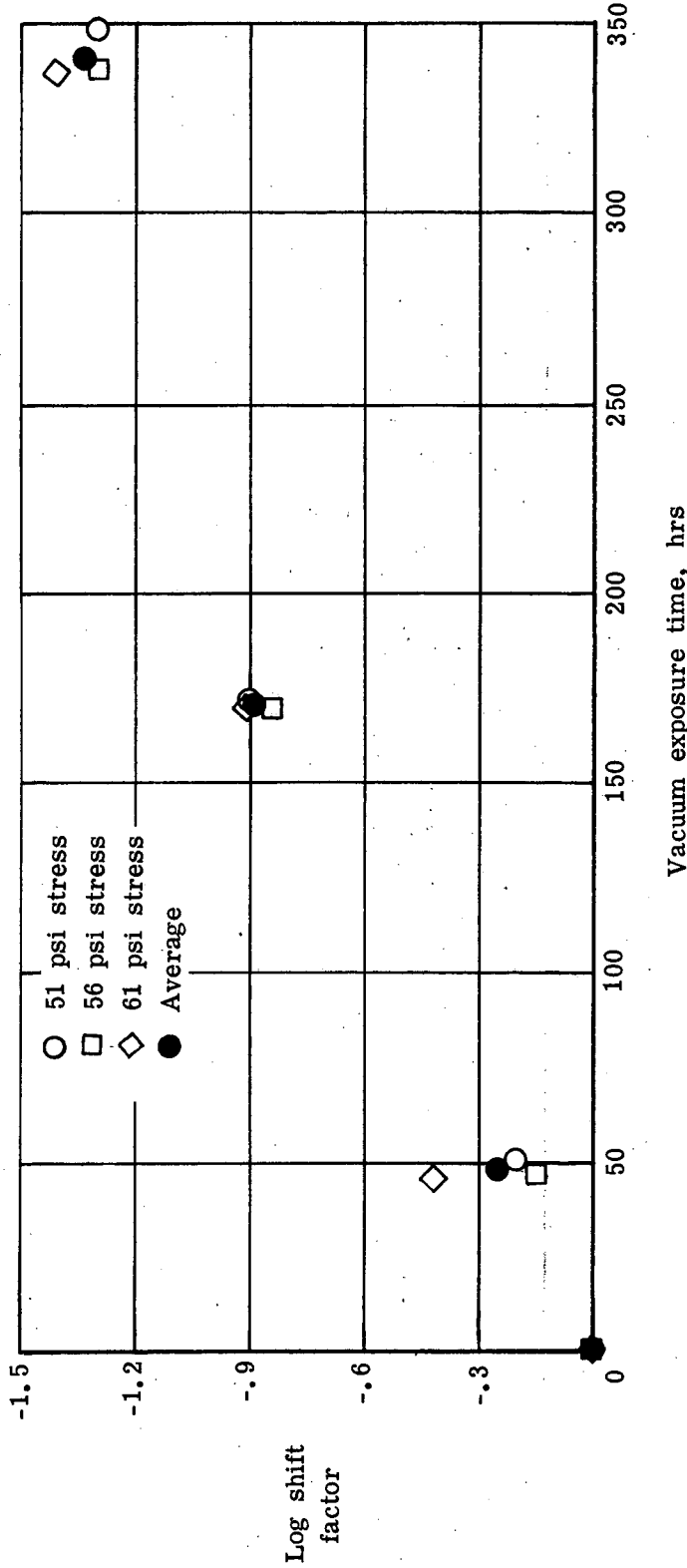


Figure 46. - Vacuum effect shift factors for TPH 3105.

For this material creep in the filled foam region of mechanical behavior is envisioned as being governed by vacuole growth which in turn is dependent on local stresses in the material. For low filler content materials, individual vacuole growth is independent of neighboring vacuole growth and the local stress distribution is dependent on the applied stress. Thus compliance - time curves at different stress levels are similar in shape and can be shifted to produce a master curve. For a highly filled composite (like TPH 3105), neighboring vacuole growths are not independent of each other and thus local stresses are dependent upon neighboring vacuole growth as well as applied stress. Similar shaped compliance curves are not obtained and master curves cannot be constructed. For the highly filled composites, higher stresses result in steeper compliance-time curves.

Examination of Figures 43, 44 and 45 showed that the master curves at the higher stresses had the steeper slopes.

Eliminating the stress shift factor from equation 9.1 gives

$$J_{T_o, \sigma_i, V_o} (\log t) = J_{T_o, \sigma_i, V} (\log t - \log a_v), \quad i = 1, 2, 3 \quad (9.2)$$

a set of three equations, one at each stress. Equations 9.2, the average vacuum effect shift factor curve (Figure 46), and the three 50% r.h. air master curves (Figures 43, 44 and 45) describe the vacuum behavior of TPH 3105 illustrated in Figures 33, 34 and 35. Equation 9.2 implies that the vacuum behavior of TPH 3105 at stress,  $\sigma_x$ , can be obtained by applying the appropriate vacuum shift factor to compliance measurements obtained in 50% r.h. air and at  $\sigma_x$ . Figure 47 is a comparison of compliances calculated from equation 9.2 (using the average vacuum shift factor and the master curve at 51 psi stress) and those measured for TPH 3105 after 348 hours of vacuum. This comparison is not intended as validation of this technique for predicting vacuum behavior from compliance measurements in air, but does illustrate the

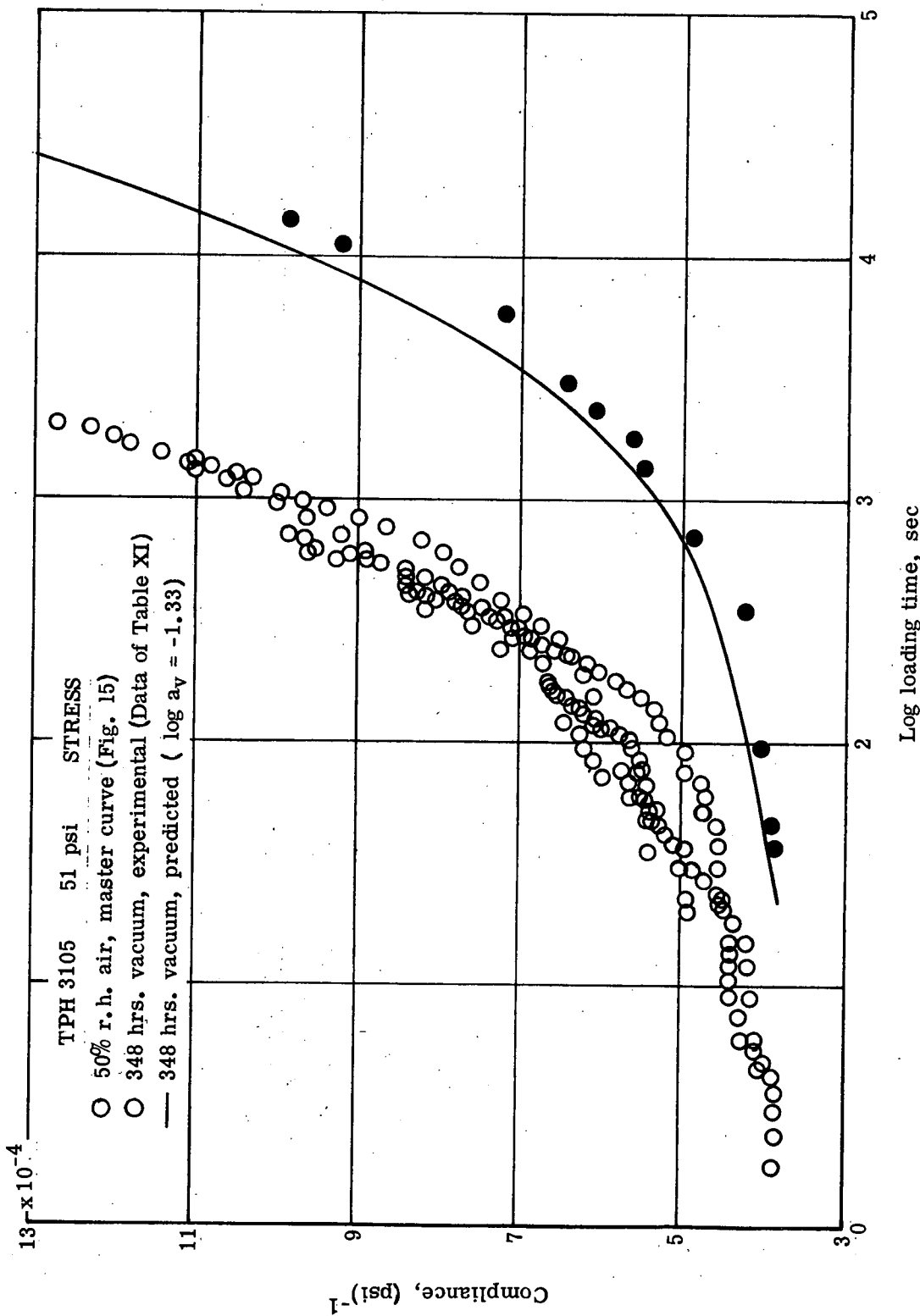


Figure 47. - Comparison of predicted and experimental compliances.

mechanics of the technique. In order to get a sound verification of the approach, compliance measurements at  $\sigma_x$  would have to be made.

#### Mechanisms of Mechanical Behavior

The results of the experimental program were analyzed to identify the microscopic mechanisms controlling the mechanical behavior of TPH 3105. Two classes of mechanisms were identified: (1) those controlling the time response of the material after stress loading and (2) those controlling the initial deformation (vacuole volume) of the material as the result of applying the stress. Other work done under NASA contract (33) indicated that chemical changes such as additional crosslinking or chain scission did not occur upon exposing TPH 3105 to vacuum. Comparison of crosslink density and sol content measurements on samples of TPH 3105 (from the same batch as material used in the author's investigation) exposed to vacuum or to 52% r.h. air for up to 32 days showed no significant changes in these properties. (See Figures 48 and 49). Moreover, any observed small changes in crosslink density and sol content in air and vacuum were always coincident with respect to exposure time, thus leading to the conclusion that vacuum had no influence on crosslinking. Based on these results, the controlling mechanisms are believed to be associated with changes in the material which are not related to the chemical structure of the binder. It should be stated at this point that the experimental results do not identify those mechanisms occurring. However, in the discussion to follow the author presents, in his opinion and based on the available literature, those mechanisms that occurred.

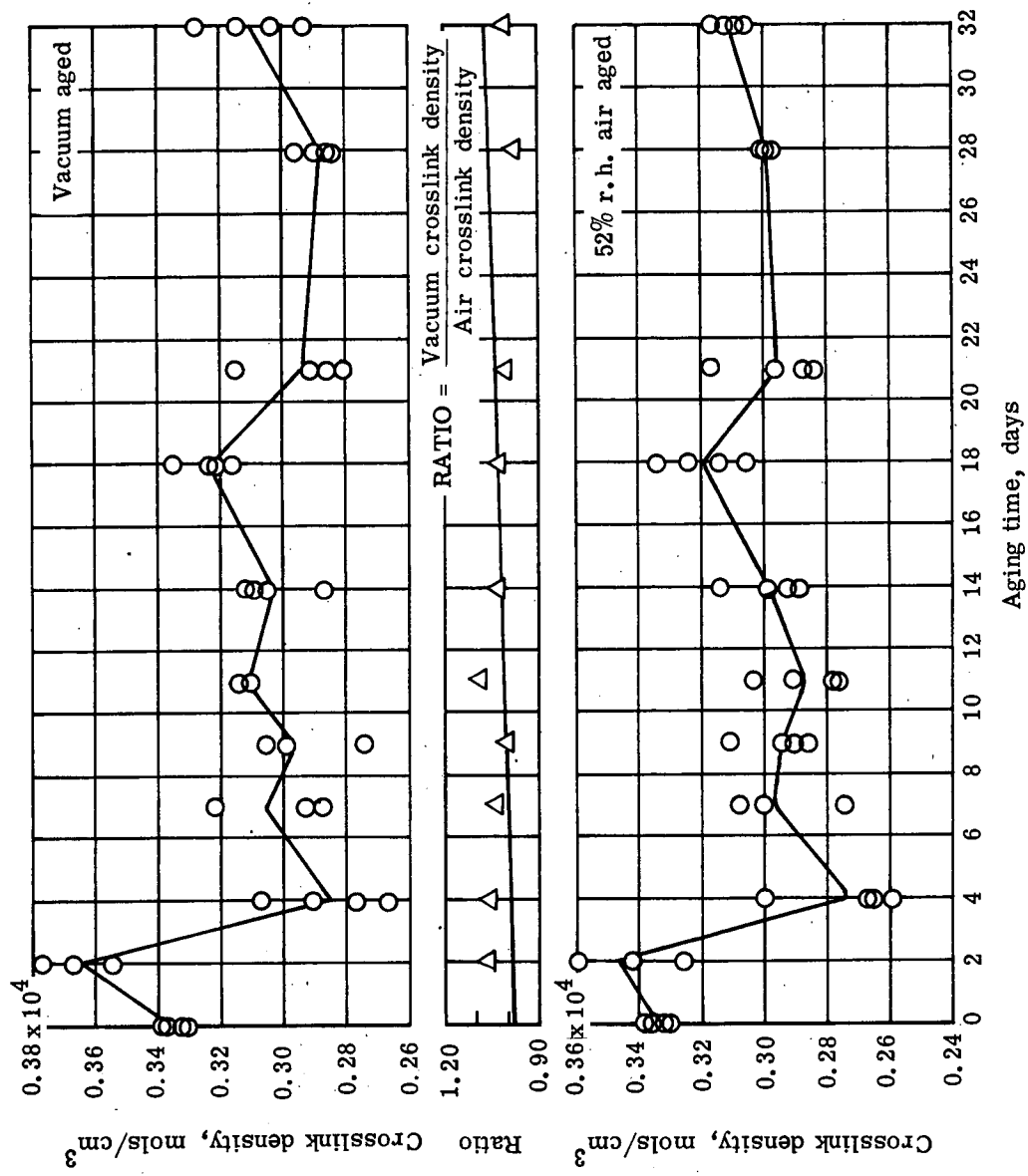


Figure 48. - Crosslink density of aged samples of TPH 3105 (room temperature).

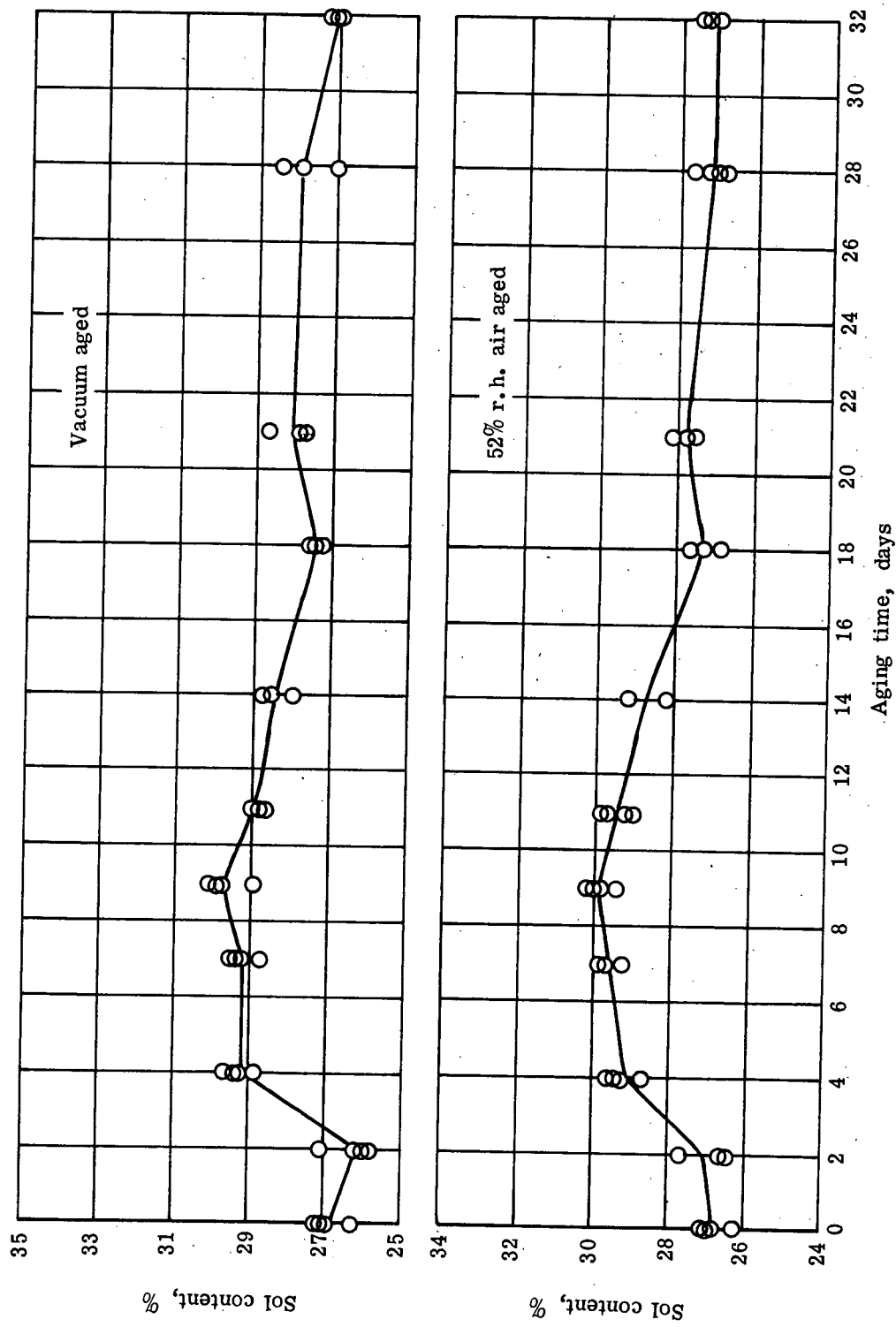


Figure 49. - Sol Content of aged samples of TPH 3105 (room temperature).

The time response of the material after stress loading (designated class 1 mechanisms for convenience of notation) is believed to be controlled by the mobility or viscosity (stretching, uncoiling, bending and diffusion) of the binder network. Assuming no primary bonding changes in the chemical structure, this will be regulated largely by the concentration of dissolved "plasticizers" in the binder phase. Loss of water (a plasticizer) due to vacuum outgassing (Figure 50) decreases the mobility (increases the viscosity) of the binder network and hence the material requires longer times to accommodate to a given strain (see Figures 30, 31 and 32). In other words, in the creep experiment stress is constant and a viscosity increase results in a decrease in the rate of straining.

$$\text{Viscosity} = \frac{\text{Stress}}{\text{Rate of Strain}} \quad (9.3)$$

The fact that master curves may be successfully generated from the creep data obtained implies that the controlling deformation mechanisms for tensile creep in air and vacuum are similar. At least it indicates that the vacuum exposure is affecting each of the various molecular relaxation mechanisms in the material (which operate to produce the overall compliance curve) in exactly the same way, a highly improbable result unless the air and vacuum processes are identical. This reasoning parallels assumption 1 in the derivation of equation 6.18 in that master curves can be generated, provided new failure mechanisms are not introduced. In addition, this conclusion is supported by Figures 36 thru 41, in that, when the time response of the material is eliminated as in the volume change and Poisson's ratio plots of these figures, the

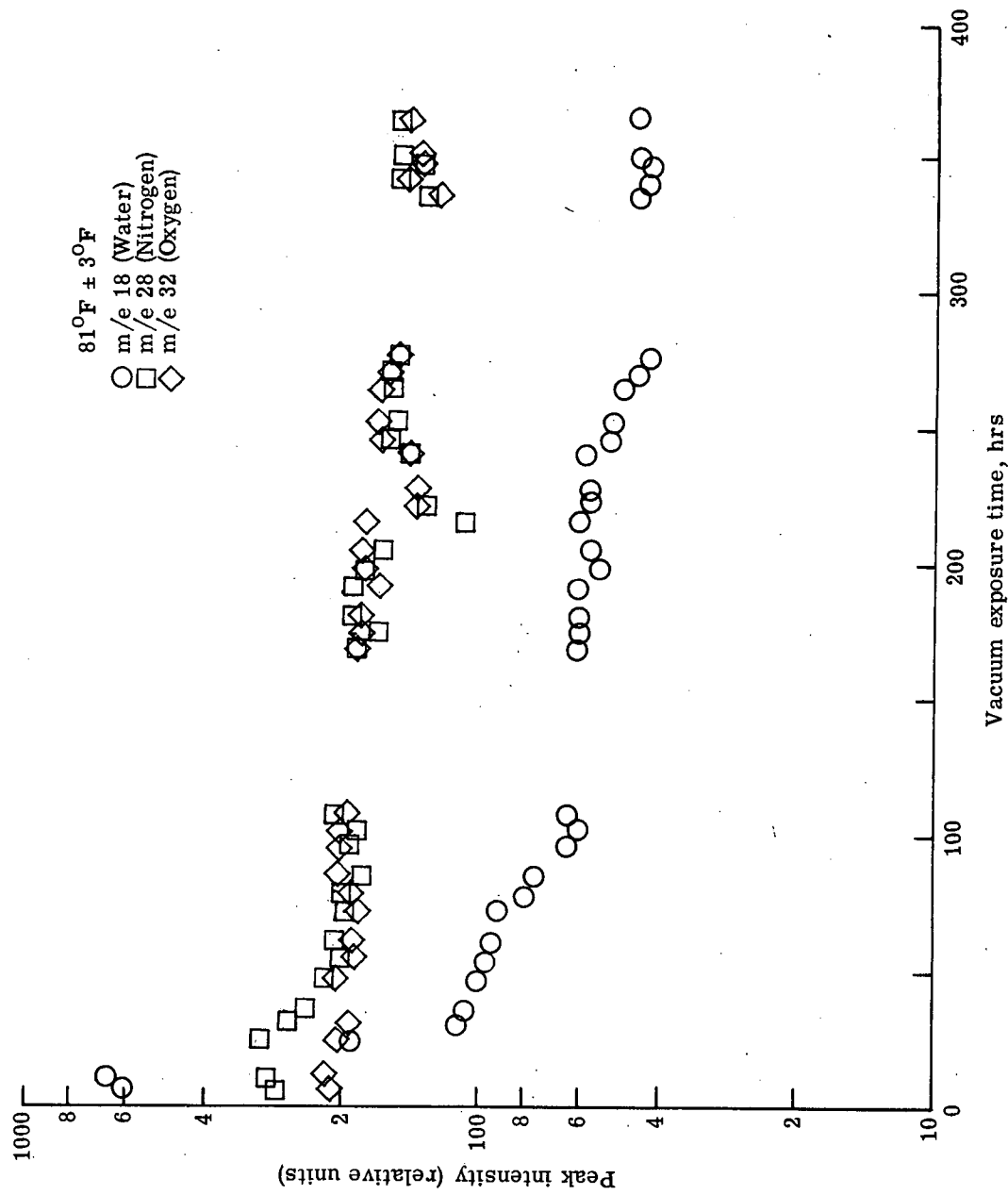


Figure 50. - Major outgassing constituents from TPH 3105.

air and vacuum results are identical prior to any changes in the material as the result of the second class of mechanisms.

The effect of the second class of mechanisms on the mechanical behavior of TPH 3105 was to control the magnitude of vacuole formation within the material during the stress loading period. In vacuum, the vacuole volume due to the initial stress loading was larger than in air. As previously discussed, at each stress level a finite vacuum time occurred prior to any observed changes (and hence the onset of the mechanism in question) in the initial vacuole volume in the material as the result of applying the stress. In addition the process was saturable such that after a given vacuum exposure any further exposure caused no additional increase in the vacuole volume as the result of stress loading. This mechanism appeared to have no influence on subsequent vacuole growth with straining of the material as evident by the slope of the volume change - length strain curves. The proposed mechanism is as follows:

Assume the mechanism involves a binder-binder response and the only function of the filler particles is to provide sites about which vacuoles occur. Assume that water loss from the material in vacuum is the driving force of the mechanism. As pictured by the mechanical properties model, on application of stress (large enough to completely dewet the material) ellipsoidal vacuoles are formed around the filler particles with minor axes equal to the radii of the particles and major axes in the direction of the applied stress. (See Figure 8.) The author suggests that the progression of the vacuoles in the loading direction during the initial loading (i.e., the length of the major axes of the ellipsoids) is a type of tear phenomena, the extent of which is governed by the viscoelasticity of the binder (43,44) and the magnitude of the overall applied stress. The viscous response of the material in a rapid straining process

(stress application in a creep test) governs the microscopic mobility of the binder network and hence the material's most effective method of relieving localized stresses. In vacuum the increase in local viscosity (decrease in mobility) of the binder due to water outgassing results in a less effective method for relieving localized stresses.

In summary, both classes of mechanisms are dependent upon the viscous nature of the material's binder, which in vacuum is believed to have increased. In addition, both mechanisms appear to occur completely independent of the other; that is, the fact that mechanism 2 is occurring does not affect mechanism 1 and mechanism 1 does not affect mechanism 2. Although the proposed mechanisms cannot fully be verified from the results of the investigation current research in the area further supports the author's viewpoint. Investigations by Ward (45) to measure *in situ* in vacuum ( $10^{-5}$  torr) the storage modulus (elastic behavior) and the loss modulus (viscous behavior) of TPH 3105 indicates that the viscous processes in the material increase with increasing vacuum exposure. (Samples were from the same batch of material as used for the author's creep measurements and were preconditioned for two weeks in 50% r. h. air.) The loss modulus as determined by Ward is shown in Figure 51. Measurements were made with a torsional pendulum apparatus (46) modified for *in situ* vacuum use. The instrument applied a small torsional strain (approximately 1% at a frequency of approximately 0.25 Hz) to the material and analyzed the response. At this low strain and frequency, the loss modulus is a very good measure of the viscosity of the binder, which from Figure 51 is seen to be steadily increasing with vacuum exposure.

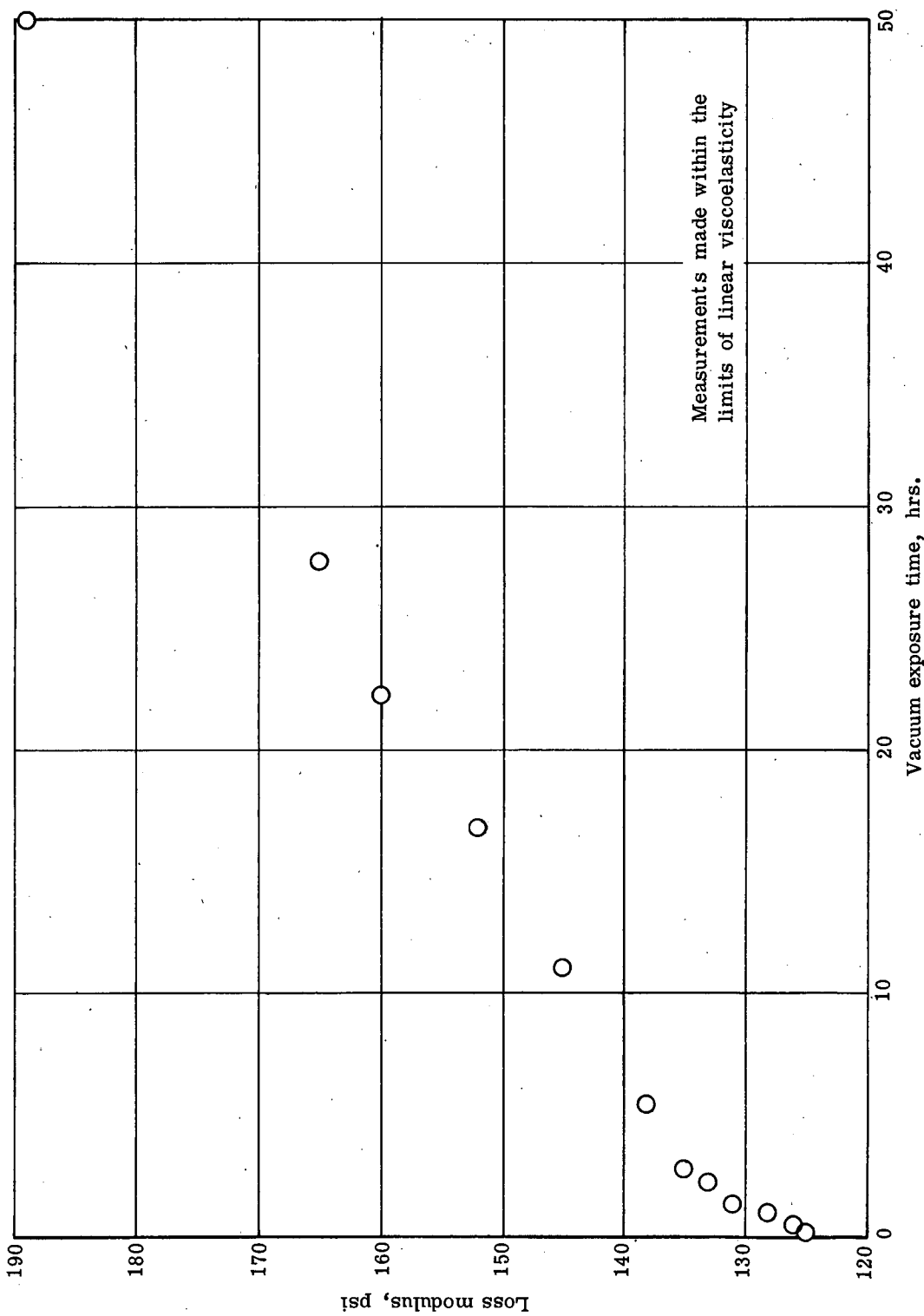


Figure 51. - Loss modulus of TPH 3105,  $10^{-5}$  torr and  $77^{\circ}\text{F}$ .

## X. SUMMARY

With the continuation of the space program there has developed the need to advance the understanding of material-environmental interactions which result in engineering property changes of spacecraft materials and to develop test techniques which can be used to predict environmental effects on materials.

A review of the literature showed that mechanical properties of spacecraft materials in the environment of space are of key concern. In particular the mechanical behavior of filled elastomeric materials in vacuum is of much interest. The literature showed that a model does exist for explaining the mechanical behavior of filled elastomers and that this model appears suitable for explaining vacuum effects on mechanical behavior. In addition a number of techniques were identified which have been used to predict mechanical behavior of materials in various environments. Neither the mechanical behavior model nor the predictive techniques had been employed in the vacuum environment.

A test program was conducted to measure in situ, in vacuum, the mechanical behavior (tensile creep) of a filled elastomer and to apply the results to develop an understanding of the material-environment interactions occurring. The test results indicated that two separate classes of mechanisms are involved in the observed property changes in vacuum. The first class controls the time response of the material to an applied stress; the second determines the initial internal state of the material as the result of applying a stress. Both classes of

mechanisms are believed to be controlled by the viscous nature of the relaxation processes occurring in the material.

In addition, techniques from the literature suitable for predicting environmental effects on materials were applied to the tensile creep measurements. Compliance decreases as large as 50 percent after approximately two weeks of vacuum exposure were accurately predicted from compliance measurements in air.

## XI. CONCLUSIONS

The purpose of the subject program was threefold: (1) to determine the effects of vacuum on the creep properties of TPH 3105, (2) to investigate the possibility of analytically describing the vacuum behavior of TPH 3105, (3) to investigate the vacuum-material interaction occurring for TPH 3105. Uniaxial constant force creep measurements were performed in situ in the vacuum environment ( $10^{-6}$  to  $10^{-8}$  torr) on samples of TPH 3105 which were preconditioned for a minimum of 35 days in 52% r.h. air. Vacuum effects on TPH 3105 were determined by comparison of in situ vacuum measurements with measurements made in situ in 52% r.h. air. Chemical tests were performed to measure possible chemical changes in the binder of TPH 3105 as the result of vacuum exposure. In addition, mass spectrometer measurements were made to identify the primary outgassing constituents of TPH 3105. From the results the following conclusions were reached:

1. The effect of vacuum exposure was to decrease the compliance of TPH 3105 at virtually all loading times. After approximately two weeks of vacuum exposure, compliances were observed to have decreased as much as 50% as compared to results in air.
2. Generally for both air and vacuum environments, the volume change of TPH 3105 increased linearly with increasing length strain. Vacuum exposure had no effect on this linear relationship, but did increase the initial volume change of the material due to stress loading.

Initial volume changes ranged from 0 to 2.5% and volume changes as large as 5% were observed at sample failure.

3. Failure time of creep tested samples increased as the result of vacuum exposure indicating that in vacuum longer times were required for the material to respond to a given stress and strain. Failure times were increased as much as 1600% as a result of two weeks of vacuum exposure.

4. In both air and vacuum, increasing the stress level of the experiment increased the internal response of the material to stress; that is, at the higher stresses, samples failed sooner and compliance increased more rapidly as a function of loading time. This effect was most obvious in that the observed vacuum behavior of TPH 3105 was dependent on the stress level. At higher stress levels, vacuum induced changes in the material's behavior occurred after shorter vacuum exposure times.

5. The compliance shift technique was found to be suited for predicting vacuum induced changes in the compliance of TPH 3105. Compliance increases of 50% as the results of two weeks of vacuum exposure can be predicted from air compliance measurements provided air results are obtained at the vacuum stress level of interest.

6. The mechanical property model satisfactorily described the mechanical behavior of TPH 3105 as observed for both the vacuum and air environments.

7. The TPH 3105 binder was not changed chemically as the result of vacuum exposure. Both crosslink density and sol content of the binder were relatively insensitive to vacuum exposure.

8. Mechanical property changes in TPH 3105 were attributable to changes in the relaxation processes occurring in the material. These changes were brought about by outgassing of water (a plasticizer) which tended to increase the viscous response of the relaxation processes (decrease the internal mobility of the polymer network) to stress and strain.

## XII. RECOMMENDATIONS

From the results of the research program the following are suggested for future investigations:

- (1) Investigate in vacuum the dilatation and strain behavior of a butadiene foam (void content of 82%). This recommendation is based on the author's opinion that little, if any, filler-binder interactions affected the observed behavior of TPH 3105. Therefore, similar results might be obtained on a material of the same composition as TPH 3105, but with the filler particles replaced by voids.
- (2) Evaluate the dilatational model (in all three regions of mechanical behavior) for describing vacuum induced changes in the mechanical behavior of a filled elastomer.
- (3) Examine the applicability of the compliance shift technique in the viscoelastic and dewetting regions of mechanical behavior.
- (4) Investigate the dependency of the vacuum shift factor on vacuum exposure time.

### XIII. ACKNOWLEDGMENTS

The author takes this opportunity to express his appreciation to the members of his Thesis Committee: Professor Henry L. Wood, Chairman, Professor J. B. Jones, Associate Professors R. K. Will and J. W. Layman, and Adjunct Professor J. P. Mugler, Jr. for the helpful suggestions and criticisms received during this investigation.

Furthermore, he wishes to thank the National Aeronautics and Space Administration, Langley Research Center, who made possible this research program. In addition, the author thanks Dr. T. C. Ward of the chemistry department of Virginia Polytechnic Institute and State University for his stimulating discussions with the author during the preparation of this thesis.

The author expresses his appreciation to the competent staff of technicians who assisted in the operation of the vacuum facility during the research program, to include Messrs. C. P. Moore, Jr., B. R. Emerson, M. G. Beasley, C. D. King, C. H. Hudgins, J. R. Smith, and J. R. Morris.

Finally the author wishes to express his gratitude to his parents, Mr. and Mrs. David W. Gregory, Sr., for their encouragement and sacrifices during his formal education, and to his wife, Carol, and children, Dean and Tamera, for their patience and help during the preparation of this thesis.

#### XIV. BIBLIOGRAPHY

1. Comparin, R. A. and Wilson, W. G.: Vacuum Thermal Conductivity Measurements of NASA E4A1 Elastomeric Heat Shield Material. NASA CR-66629, 1968.
2. Greenwood, L. R. and Fleming, R. M.: Thermal Conductivity Measurements of Candidate Viking Heat Shield Materials After Exposure to Sterilization, Vacuum, and a Simulated Martian Atmosphere. ASTM/IES/AIAA Space Simulation Conference, Sept. 1970.
3. Bueche, F.: Strength of Filled Rubbers: Temperature, Rate, and Oxygen Effects. *J. Appl. Poly. Sci.*, Vol 7, 1963, pp. 1165-1174.
4. Greenwood, Lawrence R.: The Effect of Vacuum on the Mechanical Properties of a Solid Propellant During Space Storage. Phd. Thesis, Virginia Polytechnic Institute, 1967.
5. Thiokol Chemical Corporation: Development of Solid Propellant Systems Capable of Withstanding Extended Storage in Space Environment. (CONFIDENTIAL)
6. Battelle Memorial Institute: Evaluation of Solid Propellants and Solid Propellant Systems for Space Application, 1963.
7. Space Storage Capability of Solid-Rocket Motors. Report 8708-67, August 1966, (CONFIDENTIAL)
8. Chemical Propulsion Information Agency: ICRPG Solid Propellant Mechanical Behavior Manual. CPIA publication number 21, June 1963.
9. Tobolsky, Arthur and Eyring, Henry: Mechanical Properties of Polymeric Materials. *J. Chem. Phy.*, Vol. II, March 1943, pp. 125-134.
10. Oberth, A. E.: Principle of Strength Reinforcement in Filled Rubbers. *Rubber Chem. and Tech.*, Vol. 40, No. 5, Dec. 1967, pp. 1337-1363.
11. Nielsen, Lawrence E.: Simple Theory of Stress-strain Properties of Filled Polymers. *J. Appl. Poly. Sci.*, Vol. 10, 1966, pp. 97-103.
12. Fishman, Norman and Rinde, James A.: Solid Propellant Mechanical Properties Investigations. Report no. 12 (AF04611-8388), Stanford Research Institute, Menlo Park, California, Nov. 1963.
13. Farris, R. J.: Strain Dilatation in Solid Propellants. Bulletin of 3rd Meeting ICRPG Working Group on Mechanical Behavior, CPIA publication 61 U, October 1964, pp. 291-302.

14. Graham, Phillip H. and Robinson, Courtland N.: Analysis of Tensile Creep Data for a Composite Plastisol Propellant by Reaction Rate Methods. Bulletin of 6th Meeting ICRPG Working Group on Mechanical Behavior, CPIA publication 158, Vol. 1, 1967, pp. 299-310.
15. Bree, H. W.; Schwarzl, F. R.; and Struik, L. O. E.: Mechanical Properties of Highly Filled Elastomers. Central Laboratory T. N. O., DELEFT, Report CL/65/58, 1965.
16. Blatz, P. J.: Studies of the Mechanical Behavior of Ammonium Perchlorate Particles, A Glass-Bead Filled Polyurethane Binder, and a Typical Continuum Binder. Firestone Flight Services Laboratory, Graduate Aeronautical Laboratories, California Institute of Technology, GALCIT SM 63-28, 1963.
17. Ko, William L.: Application of Finite Plastic Theory to the Behavior of Rubber-Like Materials. Ph.D. Thesis, California Institute of Technology, 1963.
18. Blatz, Paul J. and Ko, William L.: Application of Finite Elastic Theory to the Deformation of Rubbery Materials. Tran. Soc. Rheol., Vol. VI, 1962, pp. 223-251.
19. Landel, R. F. and Moser, B. G.: The Effects of Moisture on the Dynamic Mechanical Properties of Ammonium Perchlorate - Polyurethane Propellants. Jet Propulsion Laboratory, Technical Report 32-389 (NAS7-100), 1963.
20. Farris, R. J.: The Character of the Stress-Strain Function for Solid Propellant. Bulletin of 5th Meeting ICRPG Working Group on Mechanical Behavior, Vol. I, CPIA Publication 119, 1966, pp. 143-156.
21. Fishman, Norman and Rinde, James A.: Development of Dilatational Equation-of-State. Bulletin of 3rd Meeting ICRPG Working Group on Mechanical Behavior, CPIA publication 61V, October 1964, pp. 267-289.
22. Martin, Donald L. Jr.: Microstructural Response and Failure Mechanism in Solid Propellants Bulletin of 5th Meeting ICRPG Working Group on Mechanical Behavior, Vol. 1, CPIA publication 119, 1966, pp. 191-226.
23. Fishman, Norman: The Relationship Between Filler Distribution and Uniaxial Rupture of Composite Solid Propellants. Bulletin of 4th Meeting ICRPG Working Group on Mechanical Behavior, CPIA publication 94U, 1965, pp. 65-79.

24. Robinson, C. N.; Graham, P. H.; and Moore, F. C.: Solid Propellant Mechanical Behavior Studies, Volume II, Application of Reaction Rate Theory to Solid Propellant Mechanical Behavior. Atlantic Research Corporation, Contract F04611-68-C-0015, AFRPL-TR-69-124, May 1969.
25. Thiokol Chemical Corp.: Investigation of Broad Spectrum Volumetric Response in Solid Propellants. AFRPL-TR-65-133, 1965.
26. Bowker, Albert H. and Liberman, Gerald J.: Engineering Statistics. Prentice-Hall, Inc., 1959.
27. Seitz, J. T. and Balazs, C. F.: Application of Time-Temperature Superposition Principle to Long Term Engineering Properties of Plastic Materials. Polymer Engineering and Science, April 1968, pp. 151-159.
28. Greenwood, L. R. and Ward, T. C.: Prediction of Long-Term Vacuum Effects on Mechanical Properties of a Heat Shield Material. 1971 Proceedings of Institute of Environmental Sciences, pp. 435-439.
29. Leeming, H. and Williams, M. L.: Final Report Solid Propellant Structural Test Vehicle Cumulative Damage and Systems Analysis. Lockheed Propulsion Company, Contract F04611-67-C-0100, AFRPL-TR-68-130, Oct. 1968.
30. Schwarzl, F. R., Struik, L. C. E., and Bree, H. W.: Influence of Filler Characteristics on Tensile Creep at Large Deformations. Bulletin of 6th Meeting ICRPG Working Group on Mechanical Behavior, CPIA publication 158, Oct. 1967, pp. 335-351.
31. Tobolsky, Arthur V.: Properties and Structure of Polymers. John Wiley and Sons, Inc., 1960.
32. American Society for Testing and Materials: Recommended Practices for Testing Long-Time Creep and Stress Relaxation of Plastics Under Tension or Compression Loads at Various Temperatures. 1968 Book of ASTM Standards, ASTM D 674-56.
33. Brownell, Robert M.: Determination of Crosslink Densities and Percentages of Sol in TPH 3105 Propellant Specimens Aged in Vacuum and under 50 Percent Relative Humidity. Thiokol Chemical Corp., Elkton Division, Contract NAS1-9397, NASA CR-111775, 1970.
34. Bills, K. W., Jr.; Sampson, R. C.; and Steele, R. D.: Solid Propellant Cumulative Damage Program. Aerojet General Corporation, Contract F04611-67-C-D102, AFRPL-TR-68-131, October 1968.

35. Melfi, L. T. and Kern, F. A.: Variations in Gage Constant as a Function of Emission Current in an Unshielded Open-End Grid Bayard-Alpert Ionization Gage. NASA/Langley, TN D-3811, 1967.
36. American Society for Testing and Materials: Recommended Practices for Maintaining Constant Relative Humidity By Means of Aqueous Solutions. 1968 Book of ASTM Standards, ASTM E 104-51.
37. Kline, S. J. and McClintock, F. A.: Describing Uncertainties in Single-Sample Experiments. Mechanical Engineering, Volume 75, Jan. 1953, pp. 3-8.
38. Rigbi, Z.: The Value of Poisson's Ratio of Viscoelastic Materials. Applied Polymer Symposia, No. 5, 1967, pp. 1-8.
39. Francis, E. C. and Carlton, C. H.: Some Aspects of Nonlinear Mechanical Behavior of a Composite Propellant. J. Spacecraft, Vol. 6, No. 1, Jan. 1969. pp. 65-69.
40. Smith, T. L.: Volume Changes and Dewetting in Glass Bean-Polyvinyl Chloride Elastomeric Composites under Large Deformations Trans. of the Society of Rheology, Vol. III, 1959, pp. 113-136.
41. Ko, W. L.: Deformation of Foamed Elastomers. J. of Cellular Physics, Vol. 1, No. 1, Jan. 1965, pp. 45-50.
42. Tobolsky, A. V.; Prettyman, I. B.; and Dillon, J. H.: Stress Relaxation of Natural and Synthetic Rubber Stocks. J. Applied Physics, Vol. 15, 1944, pp. 380-395.
43. Kraus, Gerard: Reinforcement of Elastomers. Interscience Publishers, 1965.
44. Oberth, A. E. and Bruenner, R. S.: Tear Phenomena around Solid Inclusions in Castable Elastomers. Transactions of the Society of Rheology, Vol. 9, No. 2, 1965, pp. 165-185.
45. Ward, T. C.: Private communication of work under NASA contract NAS1-10043, Chemistry Dept., Virginia Polytechnic and State University, Blacksburg, Va.
46. Nielsen, L. E.: A Recording Torsion Pendulum for the Measurement of the Dynamic Mechanical Properties of Plastics and Rubbers, Review of Scientific Instruments, Vol. 22, No. 9, Sept. 1951, pp. 690-692.
47. Glasstone, Samuel; Laidler, Keith J.; and Eyring, Henry: The Theory of Rate Processes. McGraw Hill Book Co., 1941.

XV VITA

The author, Gerald Lee Gregory, was born [REDACTED]

[REDACTED] He attended school in Norfolk and Virginia Beach, Virginia, and graduated from Princess Anne High School in June, 1960.

Upon graduation from high school he entered the Norfolk Division of Virginia Polytechnic Institute to pursue a Bachelor of Science degree in Mechanical Engineering. In the fall, 1962, the author transferred to Virginia Polytechnic Institute and while an undergraduate was a member of Pi Tau Sigma, Tau Beta Pi, Omicron Delta Kappa, Phi Kappa Phi, and ASME. In June 1964, the author received a Bachelor of Science degree in Mechanical Engineering from VPI.

After graduation he was employed by the National Aeronautics and Space Administration, Langley Research Center, Hampton, Virginia. The author is assigned to the Mission Environmental Effects Section of the Environmental Effects Branch of the Space Technology Division.

In September 1964, the author became a participant in the graduate study program at the Langley Research Center. In June 1967, he completed the requirements for the Master of Science degree in Mechanical Engineering. In September 1967, he was enrolled as a graduate student at the Virginia Polytechnic Institute where he pursued a course of study leading to the degree of Doctor of Philosophy in Mechanical Engineering.

[REDACTED]

## XVI. APPENDICES

### Appendix A: Dilatational Model for a Filled Elastomer

The dilatational model presented is that developed by Farris in reference 13. The purpose of the model is to develop an equation which relates the volume change (dilatation) of a filled-elastomer to the strain history of the material. Attention is focused on a single filler particle surrounded by an elastic matrix and then the results summed over all filler particles. Five basic assumptions as to the material's behavior are required:

1. Dilatation in the material results from vacuoles or voids around the filler.
  2. The filler is rigid and the particles are spherical but may be of various radii.
  3. Each vacuole is ellipsoidal with the minor axis equal to the diameter of the particle.
  4. The major axis of a vacuole increases linearly with strain at a rate proportional to the minor axis.
  5. A vacuole may be formed at any magnitude of strain.
- Consider a single filler particle contained in a highly filled elastomeric matrix. The matrix is being strained at a rate so that the particle, the elastomer, and the particle-elastomer interface are all subjected to constant or increasing stresses. When the stress exceeds the energy of the bond between the filler and the matrix, the elastomer and particle separate,

thus forming a vacuole at this interface. The vacuole is ellipsoidal with its major axis parallel to the direction of strain. The length of the minor axis is maintained constant at the diameter of the particle. The major axis of the ellipsoidal vacuole increases linearly with strain, with its rate of growth proportional to the filler diameter. Based on this explanation the following equations are developed. The volume of the  $r^{\text{th}}$  solid filler particle,  $v_{pr}$ , is given by

$$v_{pr} = \frac{4}{3} \pi a_r^3 \quad (\text{A-1})$$

and  $a_r$  is the radius of the  $r^{\text{th}}$  particle  
the volume of the  $r^{\text{th}}$  ellipsoid,  $Vel_r$ , is

$$Vel_r = \frac{4}{3} \pi a_r^2 b_r \quad (\text{A-2})$$

and  $b_r$  is the major axis of the  $r^{\text{th}}$  ellipsoid. The void volume,  $V_r$ , is obtained by subtracting equation A-1 from equation A-2

$$V_r = \frac{4}{3} \pi a_r^2 (b_r - a_r) \quad (\text{A-3})$$

The following definitions arise

$$b_r - a_r > 0 \quad \text{dewetting} \quad (\text{A-4})$$

$$b_r - a_r = 0 \quad \text{no dewetting} \quad (\text{A-5})$$

The assumption that continued straining increases the length of the major axis of a vacuole at a constant rate proportional to the particle radius can be expressed as

$$d \frac{(b_r - a_r)}{d\epsilon} = C a_r \quad (A-6)$$

or

$$\frac{d \left( \frac{b_r - a_r}{a_r} \right)}{d\epsilon} = C \quad (A-7)$$

where  $\epsilon$  is strain in direction of loading and  $C$  is a constant.

Taking the strain derivative of equation A-3

$$\frac{d V_r}{d\epsilon} = \frac{4}{3} \pi a_r^2 \frac{d (b_r - a_r)}{d\epsilon} \quad (A-8)$$

or in another form

$$\frac{d V_r}{d\epsilon} = \frac{4}{3} \pi a_r^3 \frac{d \left( \frac{b_r - a_r}{a_r} \right)}{d\epsilon} \quad (A-9)$$

The total volume change at a given strain may be expressed as the sum of all the void volumes up to that strain provided it is assumed that the elastomer is incompressible and that the filler is of high modulus to prevent filler dilatation. Therefore,

$$\Delta V = \sum_{r=1}^N v_r \quad (A-10)$$

where:

 $\Delta V$  = total volume change of the material $v_r$  = volume of  $r^{\text{th}}$  void $N$  = number of filler particles in specimen

Forming the strain derivative of equation A-10

$$\frac{d (\Delta V)}{d\epsilon} = d \left( \sum_{r=1}^N v_r \right) \quad (A-11)$$

or

$$\frac{d(\Delta V)}{d\epsilon} = \sum_{r=1}^N \frac{dV_r}{d\epsilon} \quad (A-12)$$

Noting that at a given strain, the total number of filler particles,  $N$ , is made up of  $n$  dewetted particles and  $(N-n)$  non-dewetted particles, then equation A-12 becomes

$$\frac{d(\Delta V)}{d\epsilon} = \sum_{r=1}^n \frac{dV_r}{d\epsilon} + \sum_{r=n+1}^N \frac{dV_r}{d\epsilon} \quad (A-13)$$

The volume change associated with the non-dewetted particles as shown in equations A-3 and A-5 is zero, thus equation A-13 becomes

$$\frac{d(\Delta V)}{d\epsilon} = \sum_{r=1}^n \frac{dV_r}{d\epsilon} \quad (A-14)$$

With the aid of equations A-1, A-7, and A-9, equation A-14 becomes

$$\frac{d(\Delta V)}{d\epsilon} = C \sum_{r=1}^n v_{pr} \quad (A-15)$$

Noting that the volume of dewetted solid filler particles,  $v_{ds}$ , can be defined as

$$v_{ds} = \sum_{r=1}^n v_{pr} \quad (A-16)$$

then equation A-15 reduces to

$$\frac{d(\Delta V)}{d\epsilon} = C v_{ds} \quad (A-17)$$

Incorporating the initial volume of the material,  $v_0$ , into equation A-17 and defining the volume fraction of dewetted filler as

$$v_{fd} \equiv \frac{v_{ds}}{v_o} \quad (A-18)$$

then equation A-17 becomes

$$\frac{d \left( \frac{\Delta V}{v_o} \right)}{d \epsilon} = C v_{fd} \quad (A-19)$$

Taking the strain derivative of equation A-19 gives

$$\frac{d^2 \left( \frac{\Delta V}{v_o} \right)}{d \epsilon^2} = C \frac{d(v_{fd})}{d \epsilon} \quad (A-20)$$

Equation A-19 states that the first derivative of dilatation (volume change) with respect to strain is proportional to the volume fraction of filler particles which have been dewetted up to that strain. The second derivative of dilatation, equation A-20, is proportional to the volume fraction of filler dewetted at a particular strain. Integrating equation A-20 twice with respect to strain gives a general equation for the dilatation of the filled elastomer material.

$$\frac{\Delta V}{v_o} = C \int_0^{\epsilon_1} v_{fd} d\epsilon + v_{fdo} \epsilon \quad (A-21)$$

In equation A-21,  $v_{fdo}$  is the initial volume fraction of filler dewetted at strain zero and  $v_{fd}$  is a function of strain. In the studies at hand  $v_{fdo}$  is zero and equation A-21 becomes

$$\frac{\Delta V}{v_o} = C \int_0^{\epsilon_1} v_{fd} d\epsilon \quad (A-22)$$

Equation A-19, A-20 and A-22 are the equations of interest for discussing the dilatational behavior of TPH 3105.

Appendix B: Arrhenius Equation for Isothermal  
Creep Test at Constant Stress

The Arrhenius equation is used to describe the behavior of various types of processes which are assumed to be rate dependent. The Arrhenius equation has been applied to the deformation of various materials. In this section the Arrhenius equation developed for the deformation of a material under an isothermal constant stress loading will be presented. In addition, a technique, based on the Arrhenius activation energy, for predicting material rupture or failure will be discussed.

Definition of Symbols

C - material constant obtained from the Arrhenius equation

$h$  - Planck's constant

$e_0$  - activation energy per reaction unit

$E_0$  - activation energy per mole of reaction unit

$K$  - Boltzmann's constant

$K_b$  - rate constant for reverse reaction (final to activated state)

$K_f$  - rate constant for forward reaction (initial to activated state)

$K_n$  - net rate constant for the process

$N$  - number of reaction units per cross-sectional area

$N_0$  - number of reaction units at time zero

$R$  - universal gas constant

$T$  - temperature

$t_f$  - fracture time of the material

$U$  - ratio of reaction units in initial state at time =  $t$  to  
reaction units in initial state at time zero

$\sigma$  - engineering stress

$\lambda$  - distance reaction unit must travel to reach the final state

#### Arrhenius Equation Development (47)

In any process requiring an activation energy the reacting units must first reach an activated state. The reaction rate model envisions the reaction units or flow units, as initially at equilibrium and considers the energy barrier that these units must overcome in deforming or flowing to a final equilibrium state. This energy barrier is the result of interactions between neighboring reaction units as deformation occurs. The energy diagram for an isothermal activation process in the absence of external forces is shown in Figure B-1. The energy barrier,  $e_0$ , is assumed to be symmetrical with respect to the reaction coordinate, such that the maximum peak height occurs at  $\lambda/2$ . The rate for the forward reaction is given by

$$K_f = \frac{KT}{h} \exp \left[ -\frac{e_0}{KT} \right] \quad (B-1)$$

where  $e_0$  is the height of the energy barrier in going from the initial to the activated state. For this case the rate of the reverse reaction is also given by the right-hand side of equation B-1. Thus the net rate constant for the process,  $K_n$ , is zero; i.e.,

$$K_n = K_f - K_b = 0 \quad (B-2)$$

Now if the process being considered involves external forces such as that of the deformation of a stressed material, then the energy diagram of

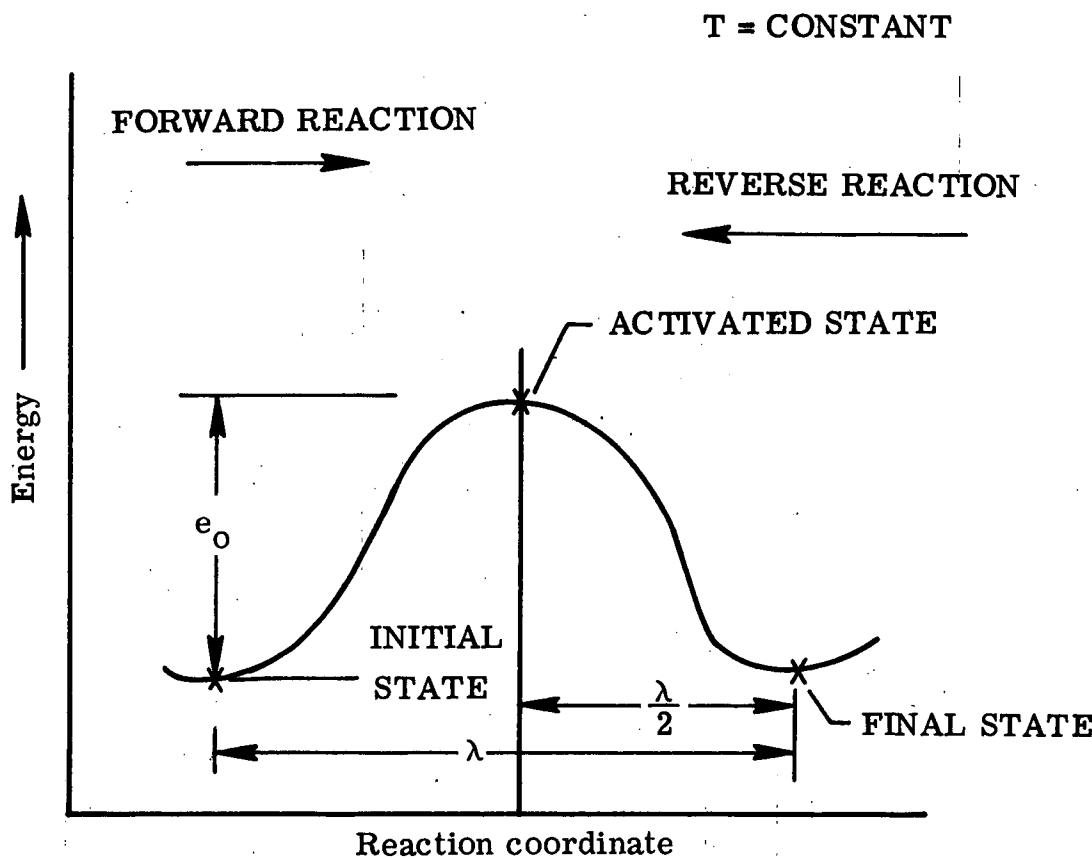


Figure B-1. - Energy diagram for isothermal activation process in absence of external forces.

Figure B-1 must be modified to include the external forces associated with the loading. As a result of the loading there will be an energy input into the initial state and this energy input changes the height of the energy barrier between the initial and activated state and between the final and activated state. The energy input to the initial state is given by equation B-3.

$$\text{Energy Input} = \frac{\sigma\lambda}{2N} \quad (\text{B-3})$$

and is obtained by multiplying the applied force per reaction unit,  $\sigma/N$ , by the distance a reaction unit moves in reaching the activated state,  $\lambda/2$ . This energy input into the initial state results in a reaction unit having a higher probability than originally (without external force) of entering the activated state. In principle this higher probability is represented by a reduction in the height of the energy barrier for the forward reaction. The amount of the reduction is  $\frac{\sigma\lambda}{2N}$ . Likewise, since these external forces are opposing the reverse reaction, the energy barrier for the reverse reaction is increased by  $\frac{\sigma\lambda}{2N}$ . The energy diagram for this process, assuming isothermal conditions, is shown in Figure B-2. The rate of the forward reaction is

$$K_f = \frac{KT}{h} \exp \left[ - \left( e_o - \frac{\sigma\lambda}{2N} \right) / KT \right] \quad (\text{B-4})$$

where the energy barrier height is  $(e_o - \frac{\sigma\lambda}{2N})$ . The rate for the reverse reaction is

$$K_b = \frac{KT}{h} \exp \left[ - \left( e_o + \frac{\sigma\lambda}{2N} \right) / KT \right] \quad (\text{B-5})$$

C 4

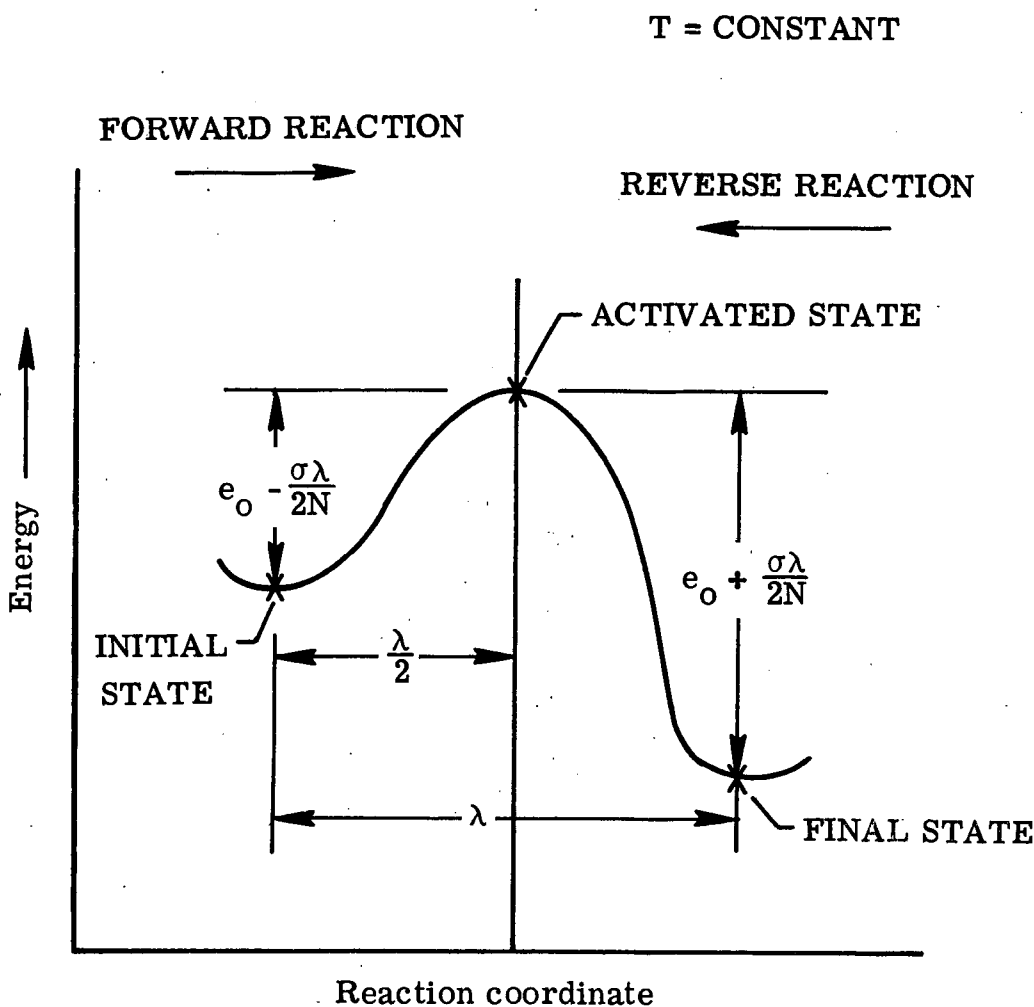


Figure B-2. - Energy diagram for isothermal constant stress deformation process.

Subtracting equation B-5 from equation B-4 gives

$$K_n = \frac{2KT}{h} \exp \left[ -\frac{E_o}{KT} \right] \operatorname{Sinh} \left[ \frac{\sigma\lambda}{2NKT} \right] \quad (\text{B-6})$$

Introducing the activation energy on a molar basis, then

$$K_n = \frac{2KT}{h} \exp \left[ -\frac{E_o}{RT} \right] \operatorname{Sinh} \left[ \frac{\sigma\lambda}{2NKT} \right] \quad (\text{B-7})$$

Noting that the net rate constant is also defined as

$$K_n = \frac{-1}{N} \frac{dN}{dt} \quad (\text{B-8})$$

Eliminating  $K_n$  from equations B-7 and B-8 gives

$$-\frac{1}{N} \frac{dN}{dt} = \frac{2KT}{h} \exp \left[ -\frac{E_o}{RT} \right] \operatorname{Sinh} \left[ \frac{\sigma\lambda}{2NKT} \right] \quad (\text{B-9})$$

If the frequency of bond repair is low, i.e. the rate constant for the reverse direction is small compared to that for the forward direction, then

$$-\frac{1}{N} \frac{dN}{dt} = \frac{KT}{h} \exp \left[ -\frac{E_o}{RT} \right] \exp \left[ \frac{\sigma\lambda}{2NKT} \right] \quad (\text{B-10})$$

Integrating equation B-10 with the boundary conditions of

$$N = N_o \quad \text{at} \quad t = 0 \quad (\text{B-11})$$

$$N = 0 \quad \text{at} \quad t = t_f \quad (\text{B-12})$$

gives

$$\frac{\exp \left[ -\frac{\sigma\lambda}{2N_o KT} \right]}{\frac{\sigma\lambda}{2N_o KT}} = \frac{KT}{h} \exp \left[ -\frac{E_o}{RT} \right] t_f \quad (\text{B-13})$$

Equation B-13 can be simplified to the form

$$\ln(t_f T\sigma) = -C\sigma + \frac{E_0}{RT} + \ln \frac{h}{KC} \quad (B-14)$$

where  $C = \frac{\lambda}{2N_0 KT}$ . For these isothermal studies both  $C$  and  $E_0$  are assumed to be material properties, hence they are not a function of loading time or stress.  $E_0$  and  $C$  are expected to be dependent on environmental conditioning, thus  $E_0$  and  $C$  must be determined at each vacuum exposure time. It should be noted that equation B-14 is derived for a constant stress loading and the application will be to constant force loadings.

#### Technique for Predicting Rupture (14)

Having determined  $E_0$  and  $C$  from equation B-14 at a specified vacuum exposure time, then an equation can be developed to predict material rupture given a stress-time loading sequence. The technique is based upon forming the ratio,  $U$ , of reaction units in the initial state at any given time to the number present in the initial state at time zero. By observing the behavior of  $U$  as a function of time, rupture is predicted. Having defined

$$U \equiv N/N_0 \quad (B-15)$$

then

$$-\frac{dU}{dt} = -\frac{1}{N_0} \frac{dN}{dt} \quad (B-16)$$

Substitution of equation B-9 into equation B-16 and using the definition of  $C$  gives

$$-\frac{d(\ln U)}{dt} = \frac{2KT}{h} \exp \left[ -\frac{E_0}{RT} \right] \sinh \left[ \frac{\sigma C}{U} \right] \quad (B-17)$$

where  $\sigma$  is a specified function of time and  $U$  is the sought unknown time function. Equation B-17 can be solved for  $U$  with the aid of the computer and the boundary conditions of

$$U = 1; \frac{d(\ln U)}{dt} = 0 \quad \text{at} \quad t = 0 \quad (B-18)$$

A typical solution of equation B-17 is plotted in Figure B-3. Material rupture is defined at that time when  $U$  rapidly decreases. This technique for predicting material rupture has been used by Graham (2) in predicting the failure of filled-elastomer systems.

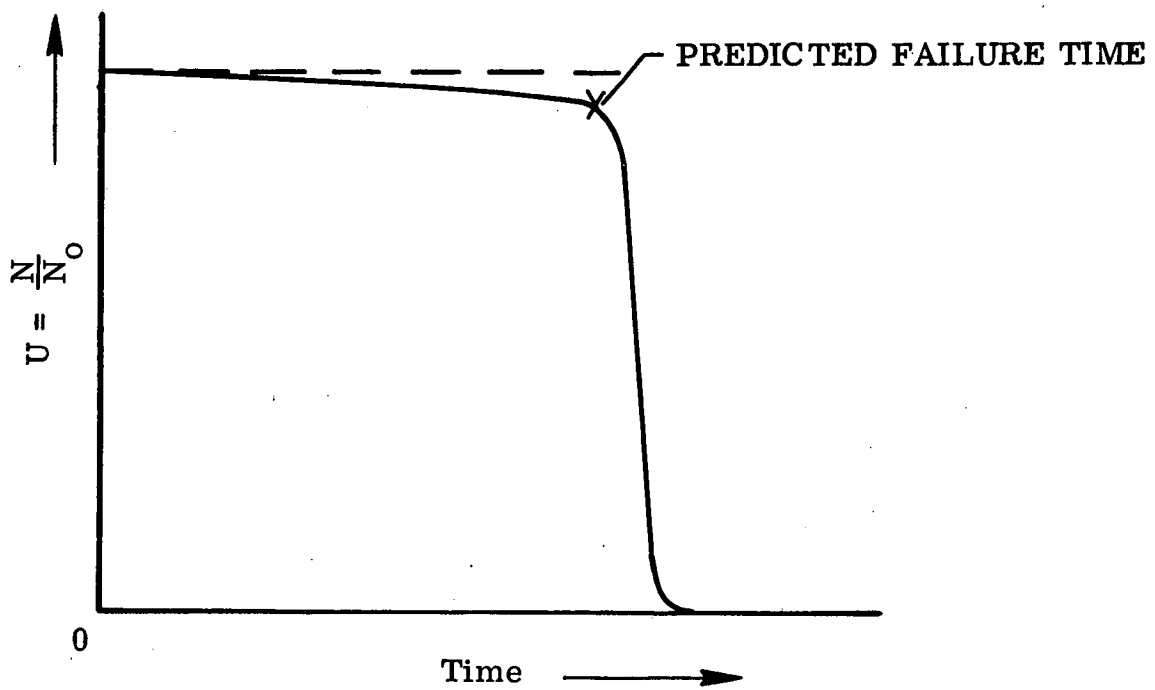


Figure B-3. - Ratio of  $\frac{N}{N_0}$  as function of loading time.

APPENDIX C: Causes of Sample-to-Sample Variations

In this appendix typical causes for sample-to-sample variations will be discussed. In addition, the influence of each cause will be discussed as to its effects on the subject investigation.

Typical causes for sample-to-sample variations in mechanical property testing of propellants are:

1. Differences in sample composition - filler content, filler distribution, crosslink density - due to non-homogeneities in formulation or curing of the material.
2. Non-uniform loading as result of misalignment of sample grips; i.e. stress concentrations due to non-uniaxial loading.
3. Deformation or contamination of sample during sample preparation.
4. Differences in sample age and aging conditions.
5. Differences in sample preconditioning - time, temperature, humidity.
6. Non-repeatable stress loading; i.e., the loading path history.
7. Accuracy of temperature and humidity control.

The influence of these factors on the present investigation can be evaluated to some extent.

Differences in propellant composition are known to exist as a result of stratification (34) during manufacture. In the propellant industry, compositional differences between samples as the result of manufacturing are referred to as batch-to-batch or within-batch variability. The nature and magnitude of these variations are a subject of

widespread investigation and are discussed in some detail in reference

34. Sample-to-sample variations for cast samples are similar to the within-batch variations.

Washer (sample grips) alignment on the test samples was definitely a problem and could be one cause of the observed sample-to-sample variations. Only those samples with the best washer alignments (as determined by visual inspection) were used in the test program.

During sample preparation and handling special emphasis was given to minimizing sample contamination and deformation. Samples were not, knowingly, subjected to undefined environments. In addition to prevent sample sagging (deformation) during the sample storage and preconditioning, samples were fully supported in specially designed racks (Figure 27) during these stages of the investigation.

Sample aging and preconditioning (cause 4 and 5) should not have been a cause of the observed sample-to-sample variations in this investigation as samples within a given sample group were aged and preconditioned side-by-side.

The manner in which the test weight is applied to the sample can affect the results, particularly when the initial loading puts the material in the filled foam region of behavior. To minimize the effects of the sample loading path on sample variations and to provide a repeatable loading path, a constant speed electric motor was used to load the samples.

Both temperature and humidity variations during testing in the vacuum chamber were found to be a cause of some of the observed sample

variations. Accuracies, as reported in Section VIII, were  $\pm 0.5^{\circ}\text{F}$  for temperature and  $\pm 2\%$  for humidity. Typical variations in sample failure times for propellant testing (34) are 7% per  $^{\circ}\text{F}$  temperature difference and 6.7% per 1% humidity change. The combined effect for a  $\pm 0.5^{\circ}\text{F}$  and  $\pm 2\%$  r.h. change is a variation of approximately 17% in the failure times. In terms of the "P" parameter, "P" would range from 0.83 to 1.17 where the average failure time in the definition of "P" is taken to be the true failure time of the material. As indicated earlier "P" values for TPH 3105 were much larger than those attributable to the observed temperature and humidity variations.

In summary, observed sample-to-sample variations were believed to be within expected limits for creep testing this type of material. The major contributors to sample-to-sample variations were believed to be differences in sample composition due to non-homogeneities, washer alignment, and temperature and humidity variation.

Appendix D: Comparison of Data Reduction Techniques

As discussed in the Data Reduction Section, two data reduction techniques were applied to the measured parameters. The first technique (DRT 1) utilized the arithmetic average of the strains of all samples within a sample group at a given loading time. This technique proved invalid for loading times longer than the shortest failure time in the sample group. Data reduction technique 2 utilized the arithmetic average of the strains of only those samples failing within the 90 percent confidence interval of the mean failure time of the sample group.

Shown in the following figures are comparisons of the strain results as determined by the two techniques. Note that the X and Y axes have been selected to correspond with Figure 30, 31, or 32, whichever is applicable. Several important points of the comparisons should be noted:

1. Both techniques give essentially the same strain results prior to the failure of the first sample.
2. DRT 2 provides a reasonable extension of the strain results to the average failure time of the sample group.
3. The time extension of the strain results is sizeable—as large as a threefold extension in some cases.

The differences in the strain values as the result of application of the two data reduction techniques were evaluated in terms of the effect on the calculated quantities—creep compliance, Poisson's ratio, and volume change. In the case of compliance, the length strain

comparison curves indicate the effects of the two data reduction techniques on compliance, since stress is constant in each comparison. Some changes in the calculated quantities of Poisson's ratio and volume change did occur as the result of the two data reduction techniques. However, these changes were less than environmentally induced changes and had little effect on the overall description of the mechanical behavior of the material.

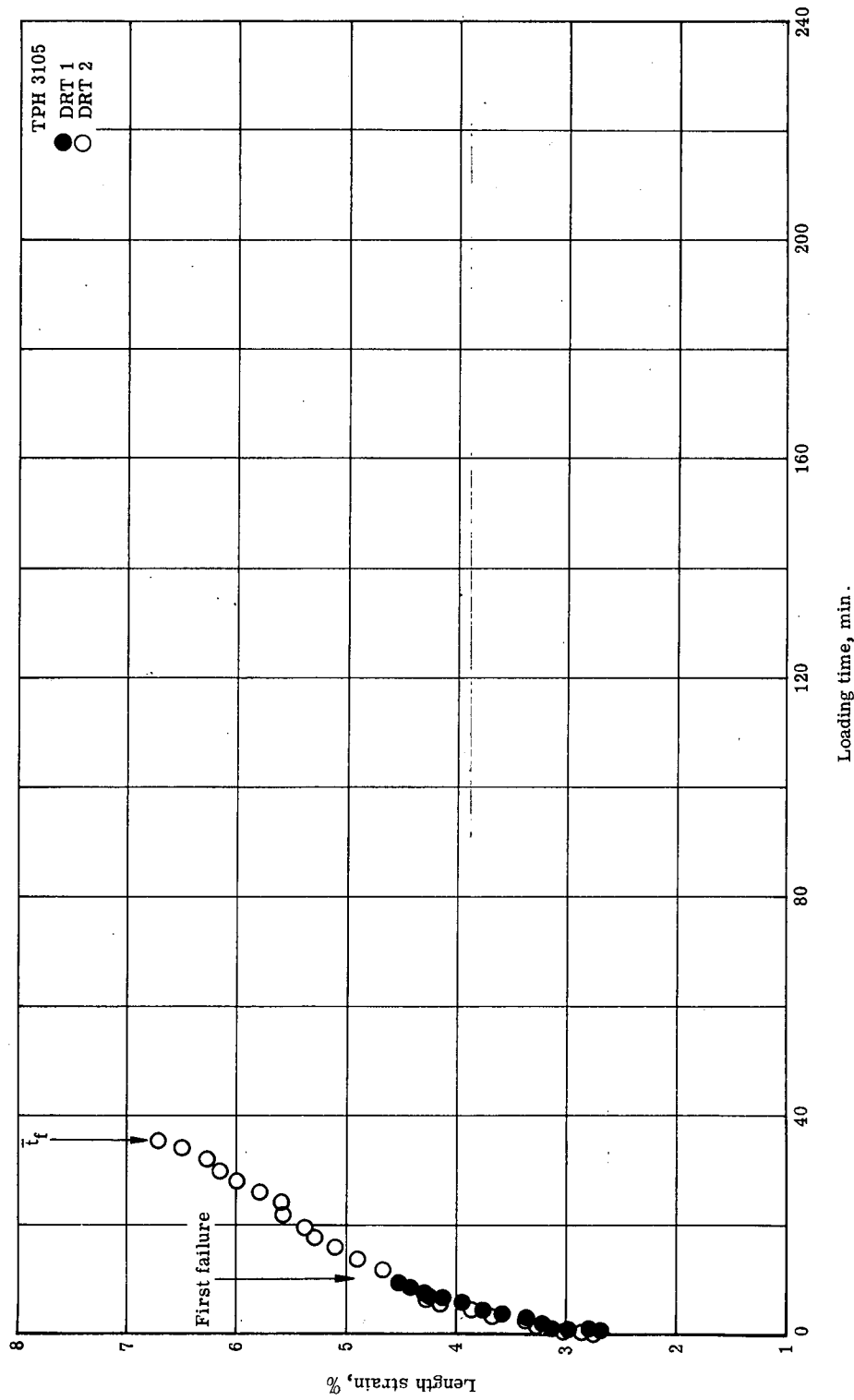


Figure D-1. - Length strain comparison, 51 psi stress, 50% r.h. air.

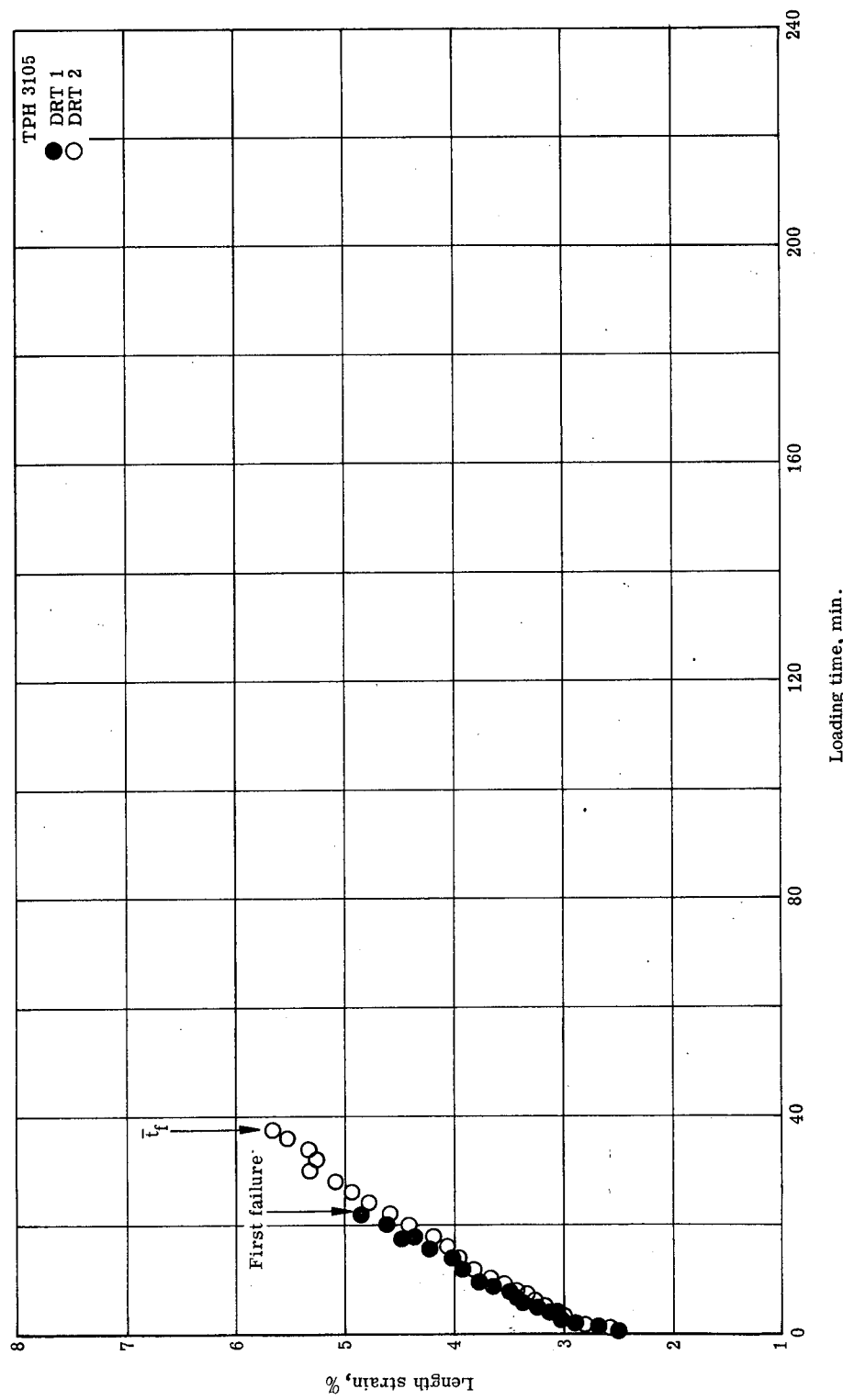


Figure D-2 . - Length strain comparison, 51 psi stress, 51 hours vacuum.

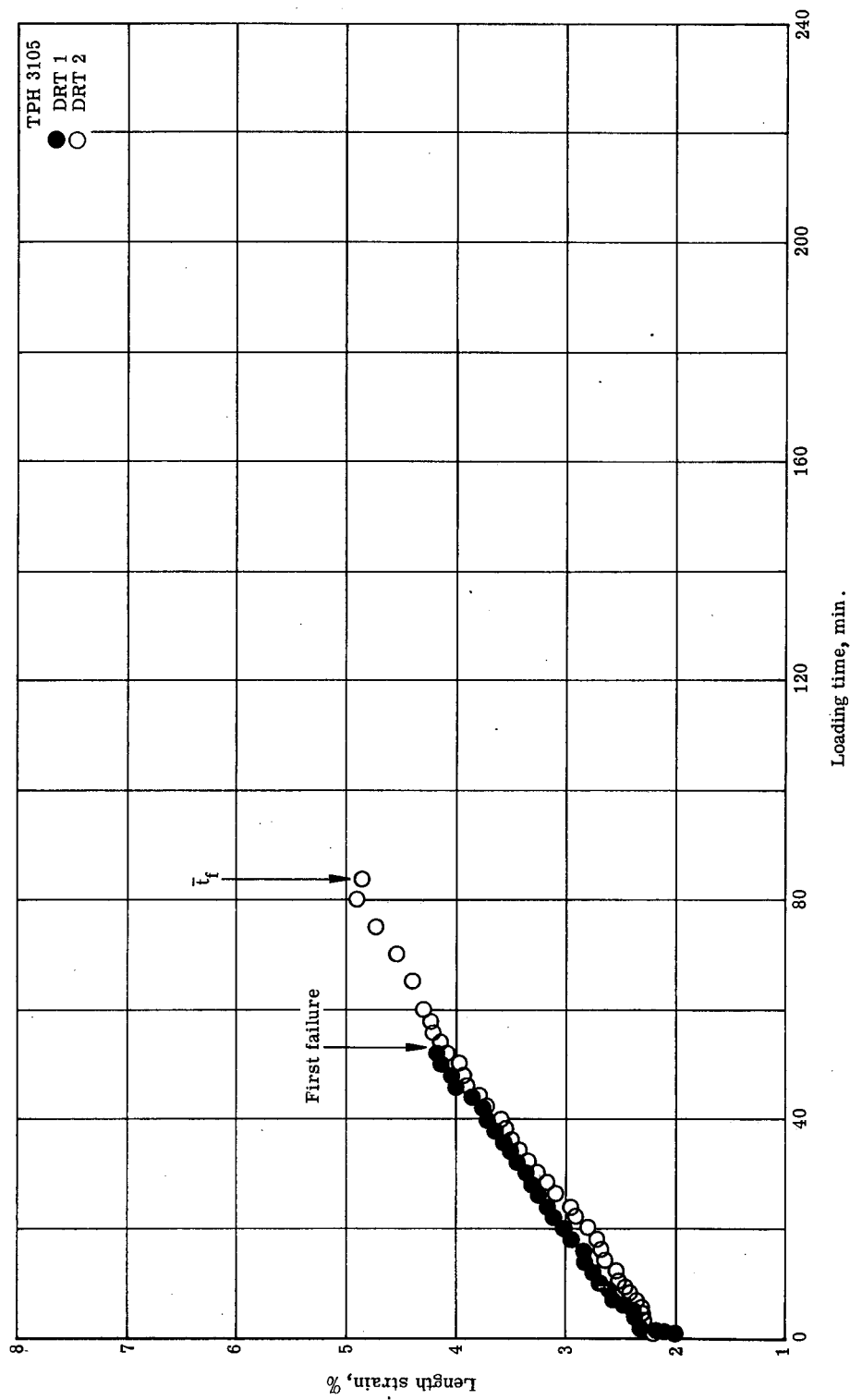


Figure D-3. - Length strain comparison, 51 psi stress, 173 hours vacuum.

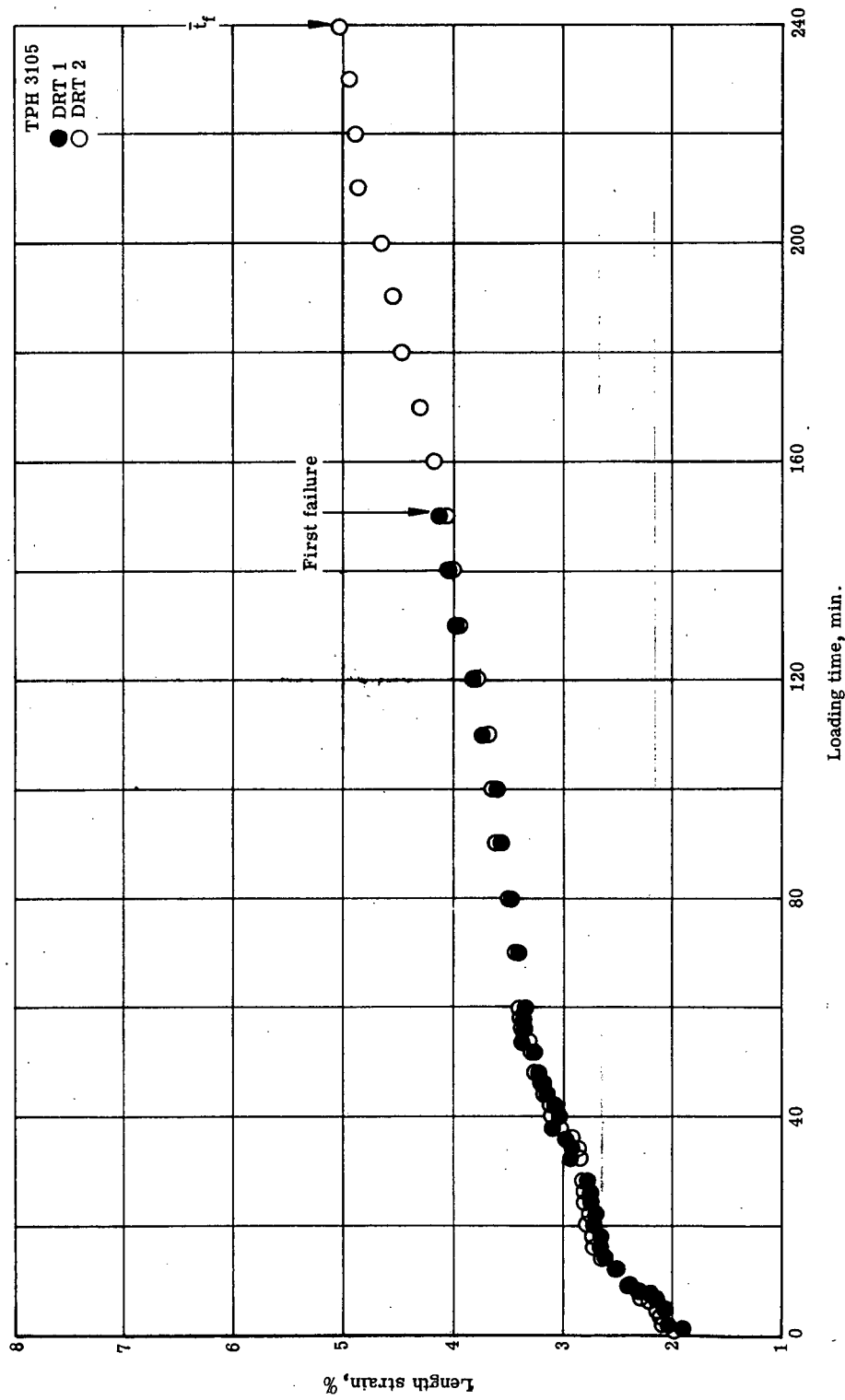


Figure D-4. - Length strain comparison, 51 psi stress, 348 hours vacuum.

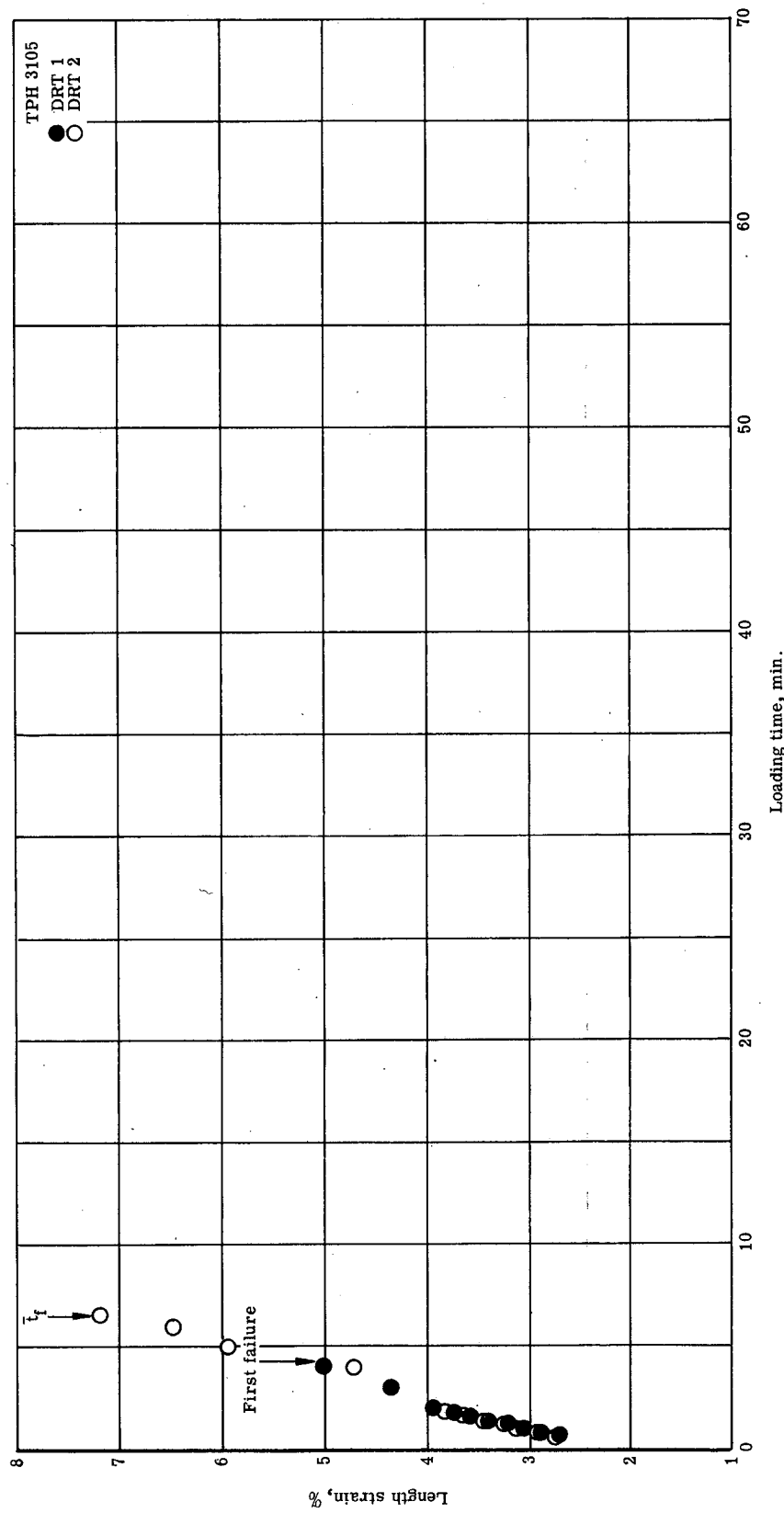


Figure D-5. - Length strain comparison, 56 psi stress, 50% r.h. air.

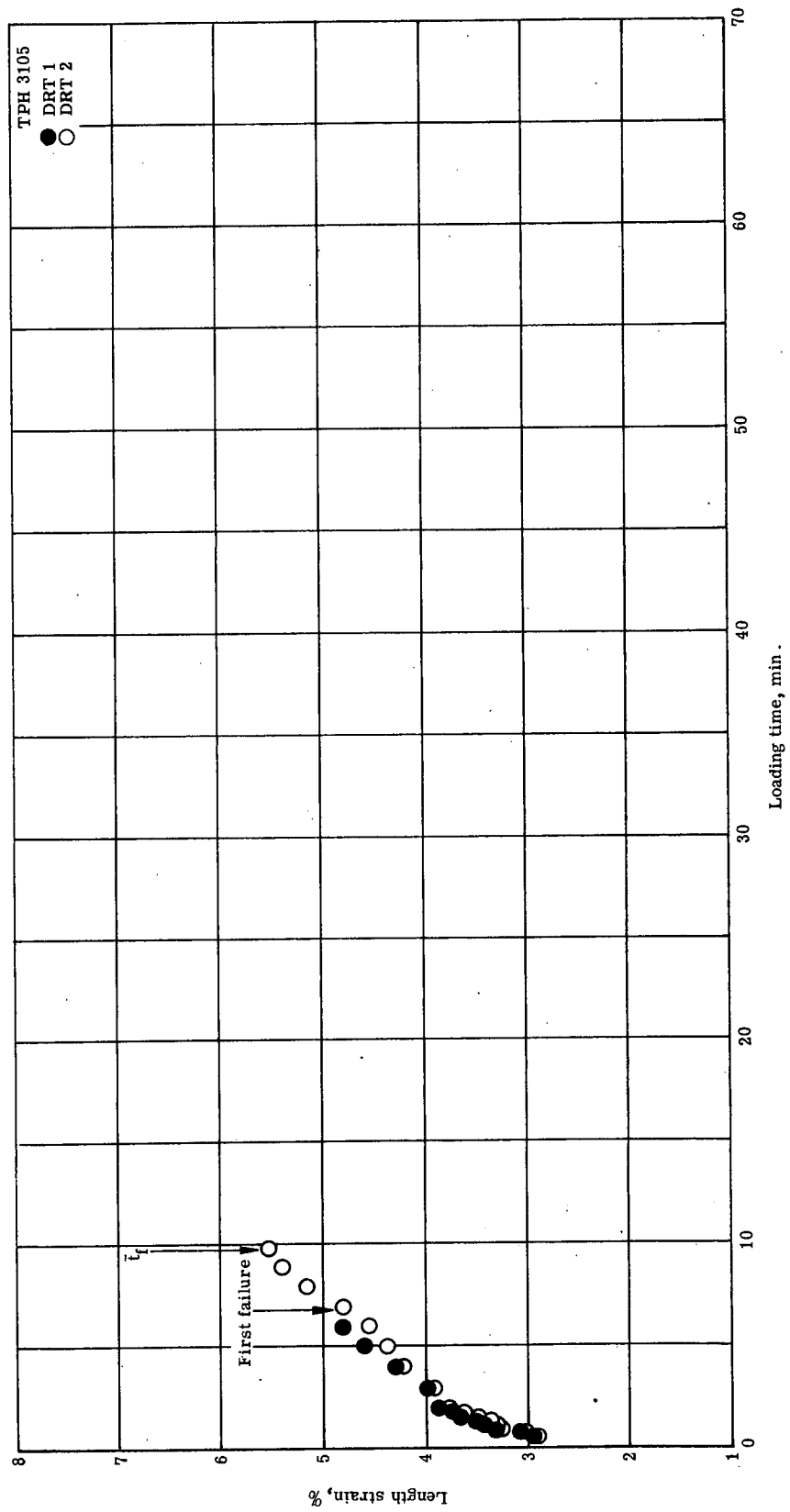


Figure D-6. - Length strain comparison, 56 psi stress, 47 hours vacuum.

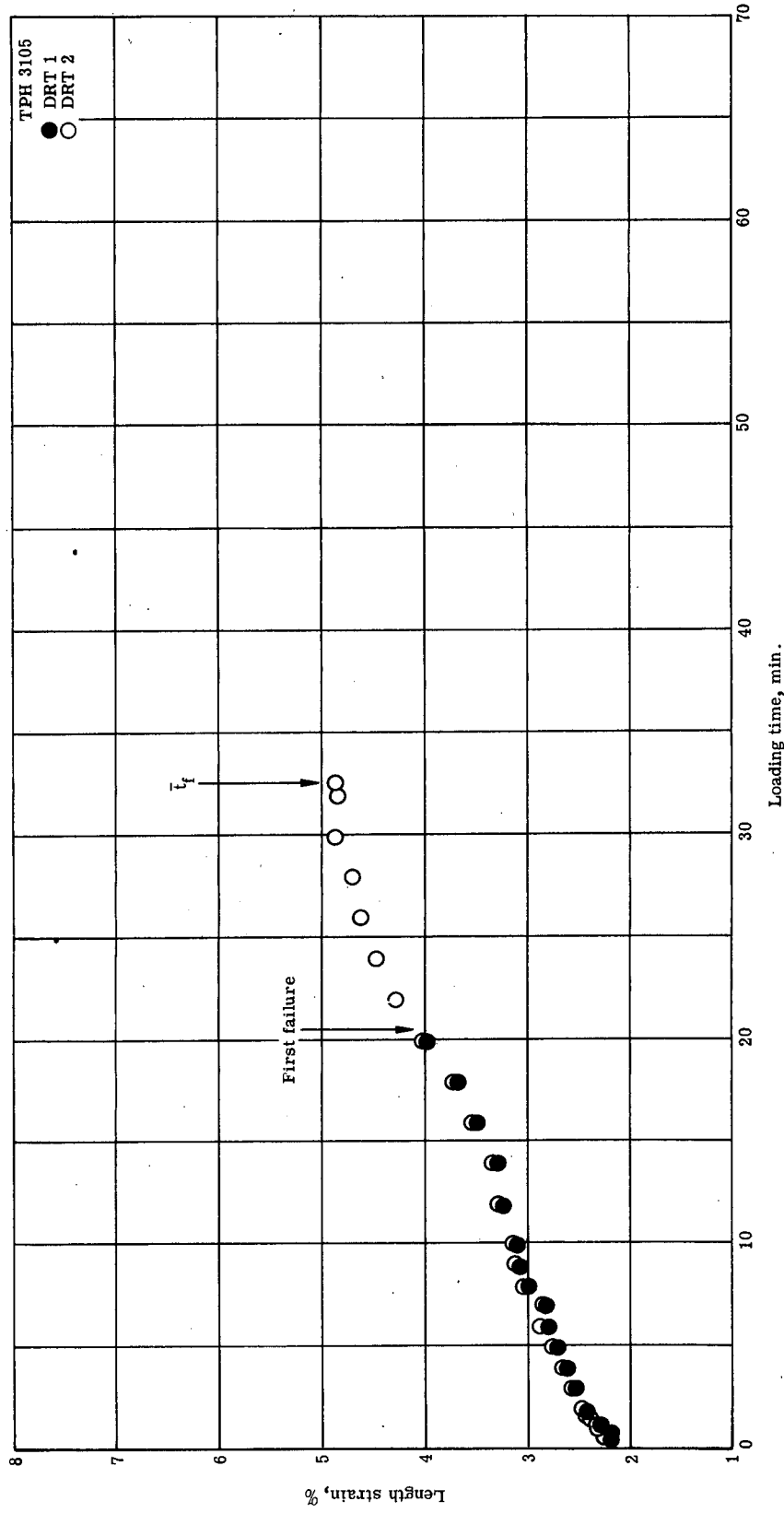


Figure D-7. - Length strain comparison, 56 psi stress, 170 hours vacuum.

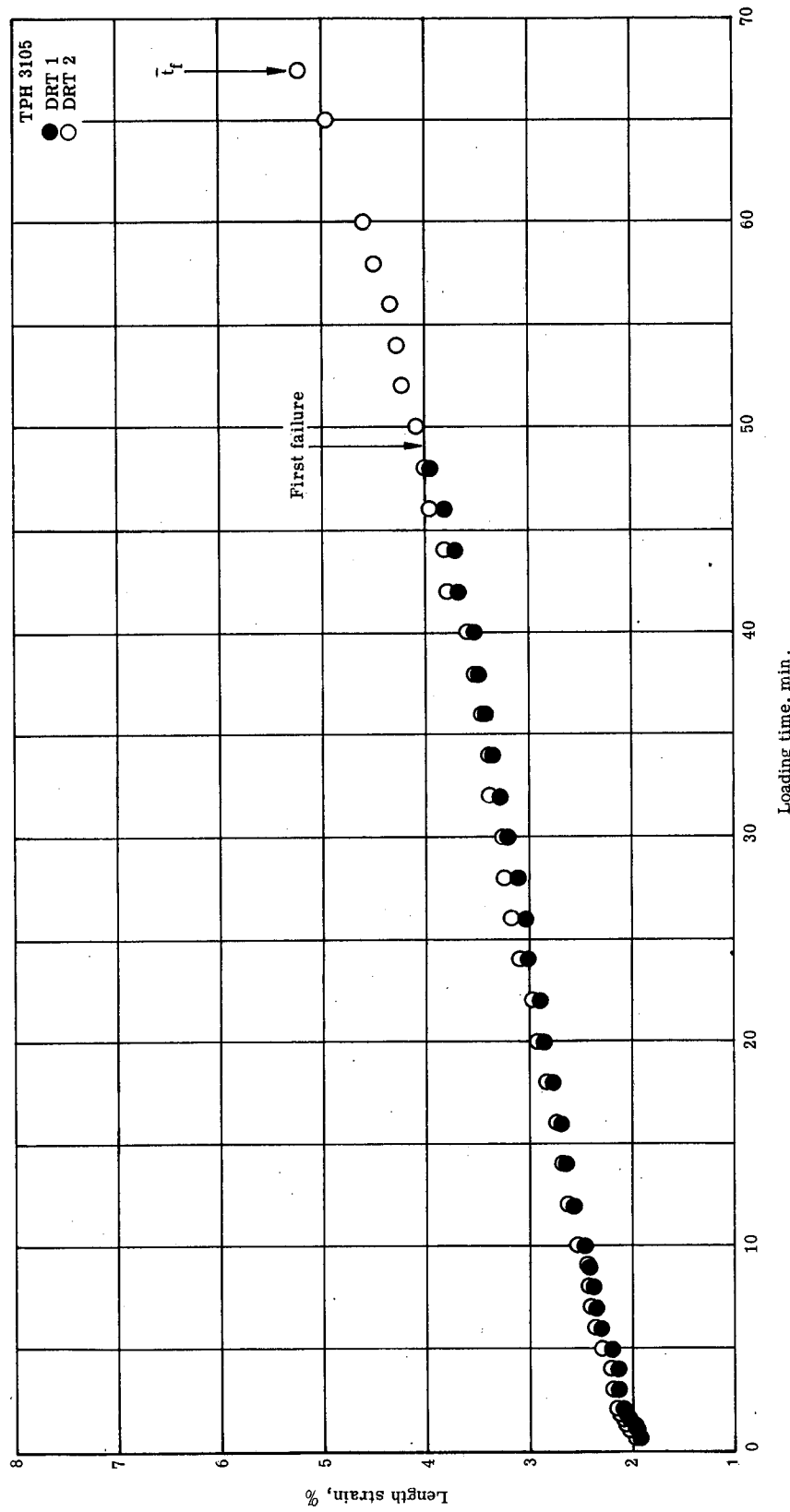


Figure D-8. - Length strain comparison, 56 psi stress, 338 hours vacuum.

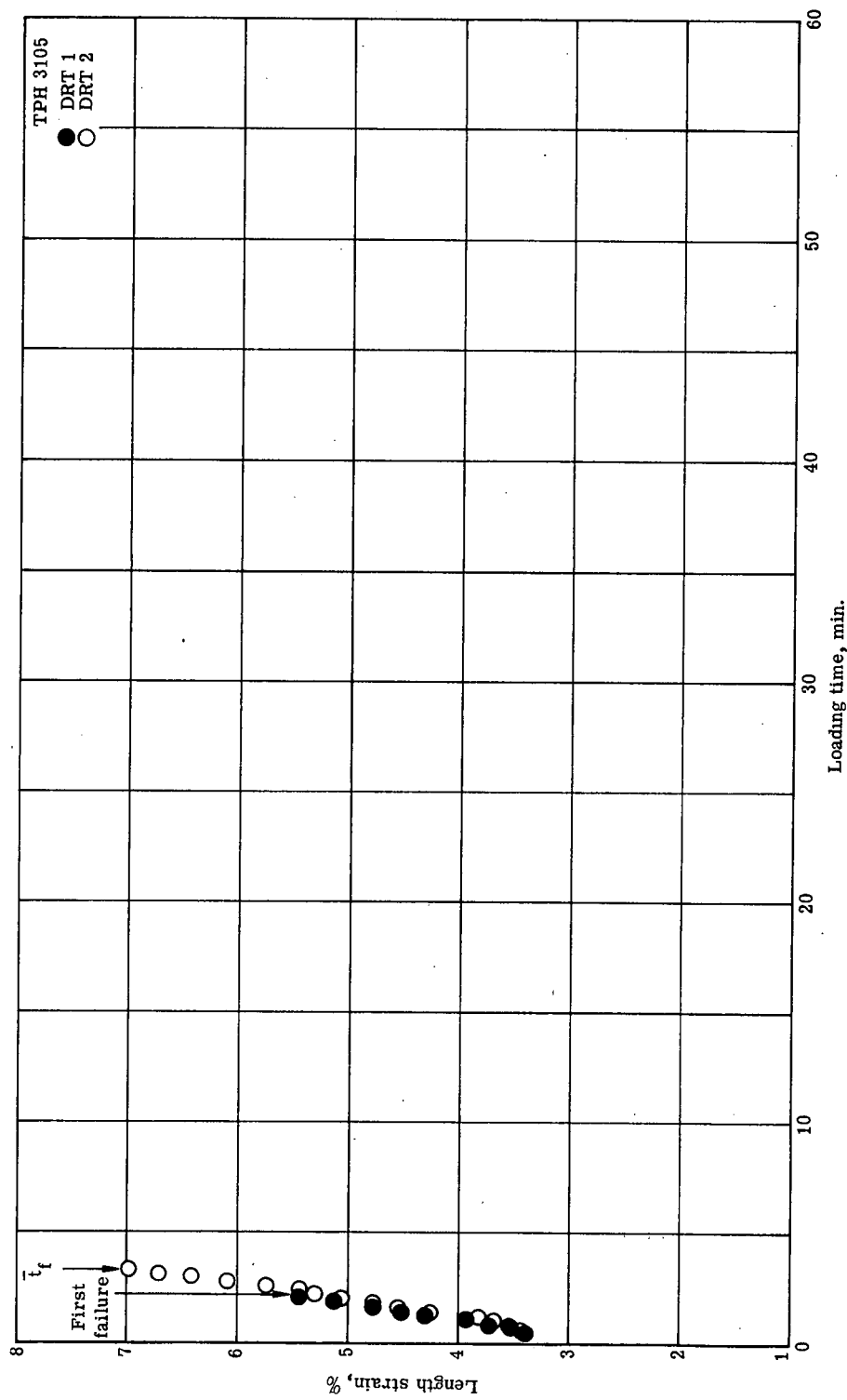


Figure D-9. - Length strain comparison, 51 psi stress, 50% r.h. air.

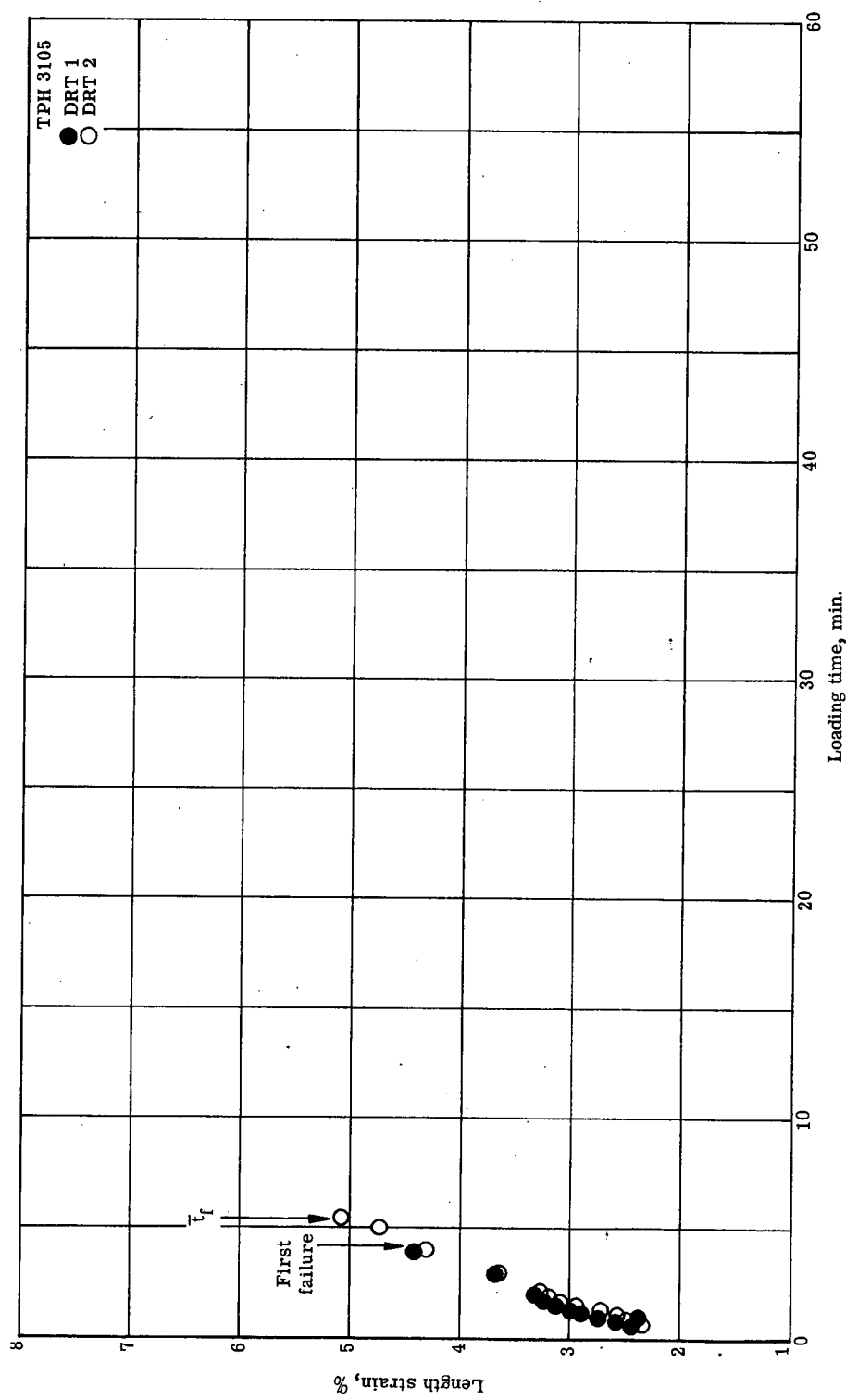


Figure D-10. - Length strain comparison, 61 psi stress, 46 hours vacuum.

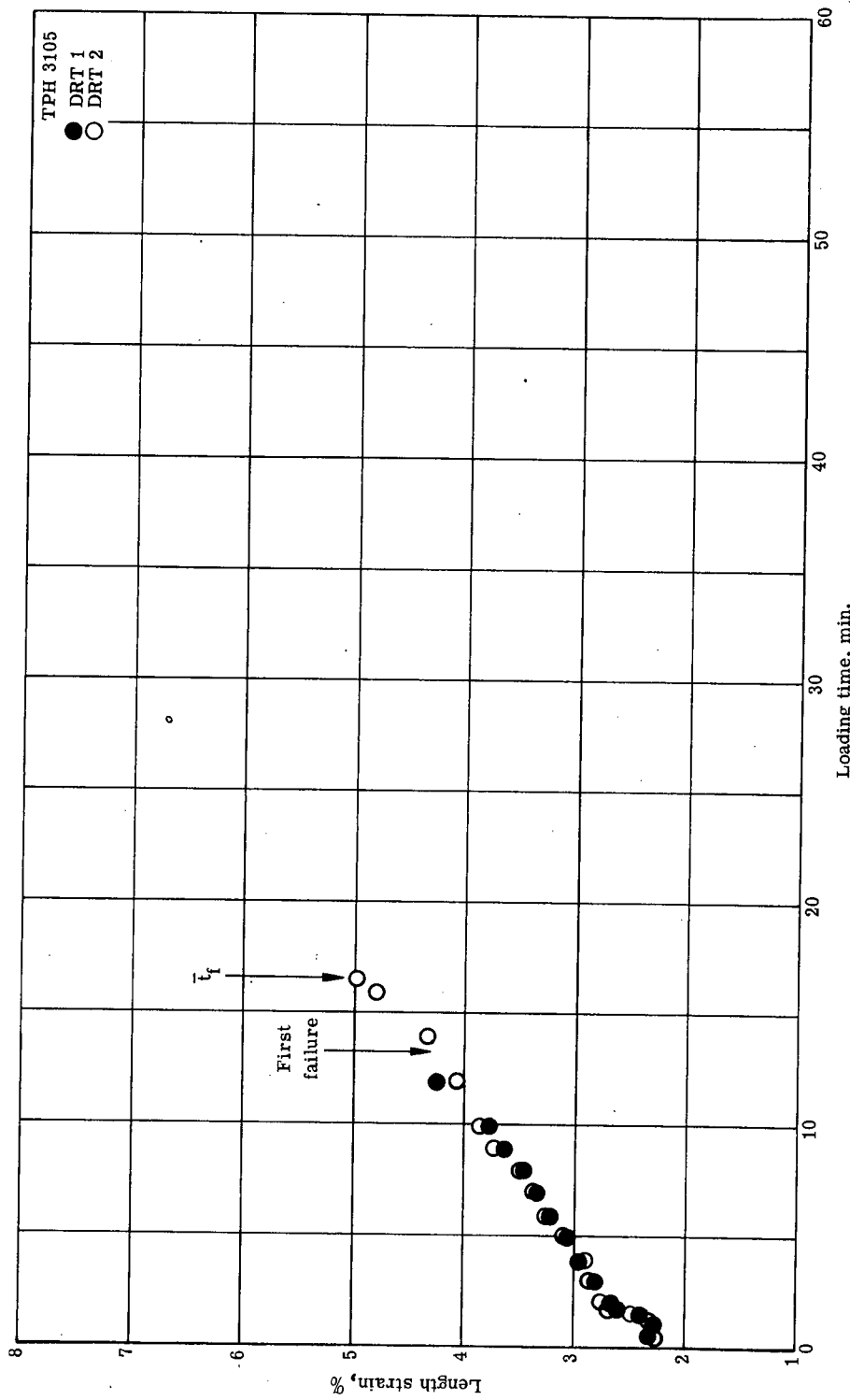


Figure D-11. - Length strain comparison, 61 psi stress, 171 hours vacuum.

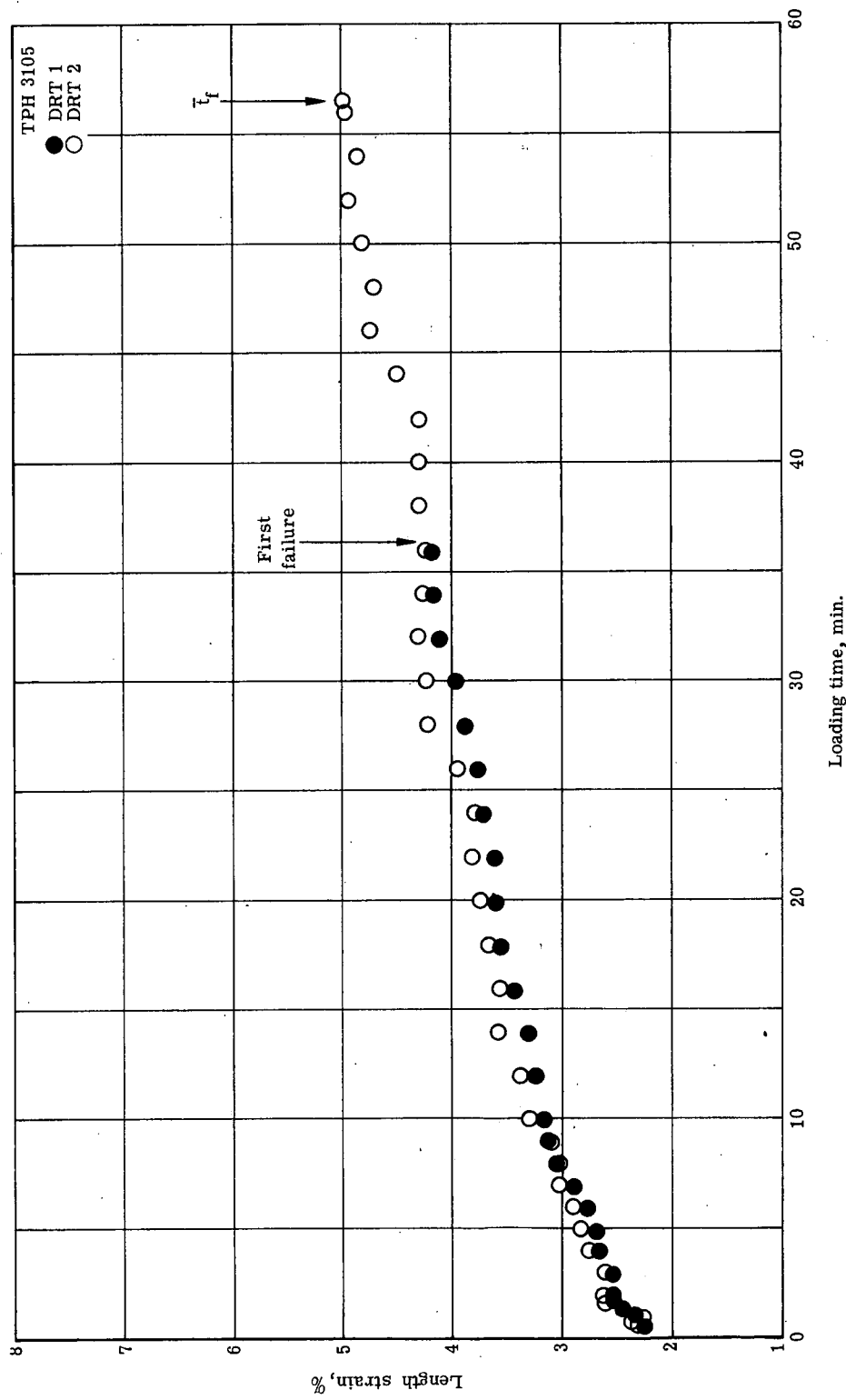


Figure D-12. - Length strain comparison, 61 psi stress, 337 hours vacuum.

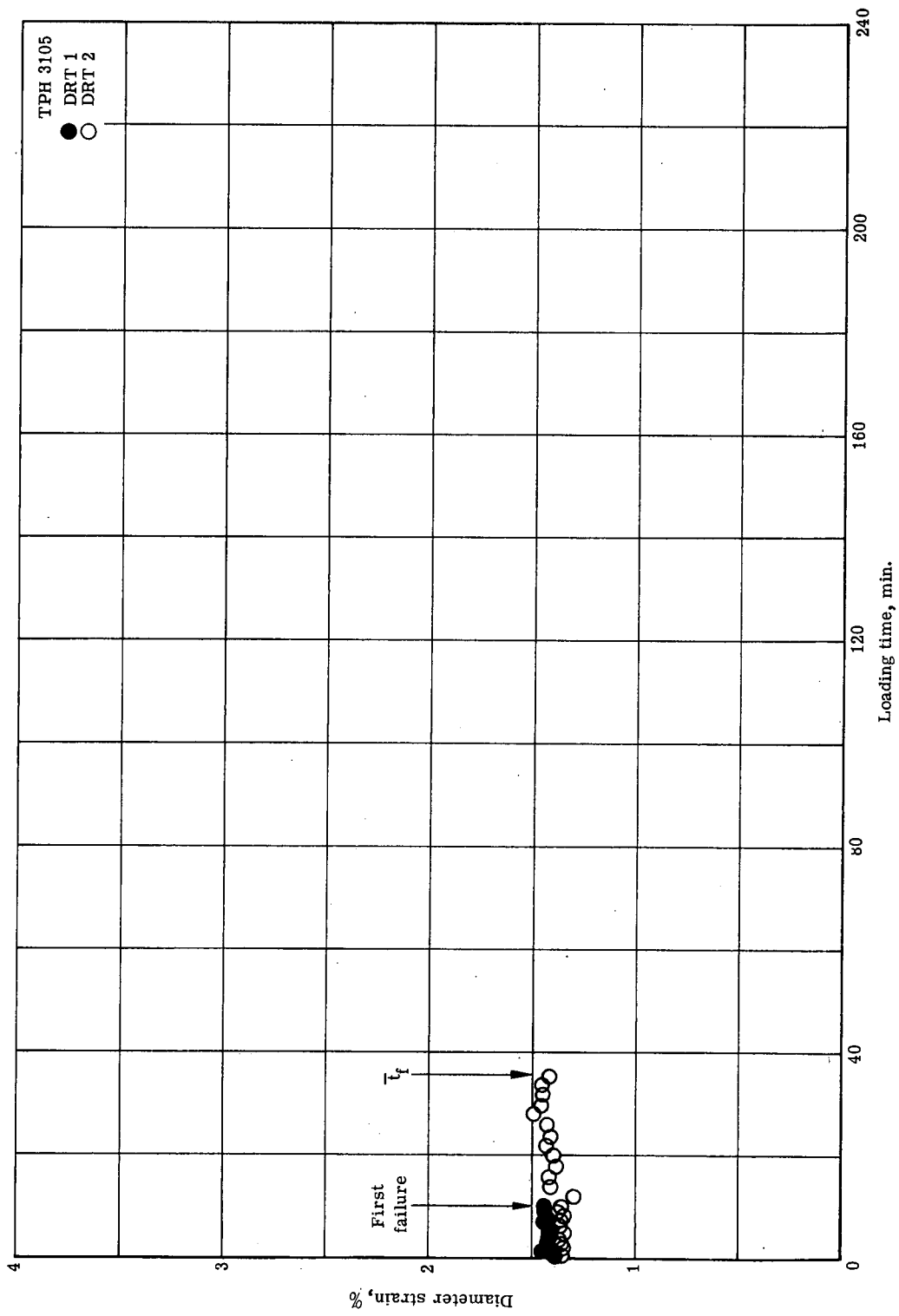


Figure D-13. - Diameter strain comparison, 51 psi stress, 50% r.h. air.

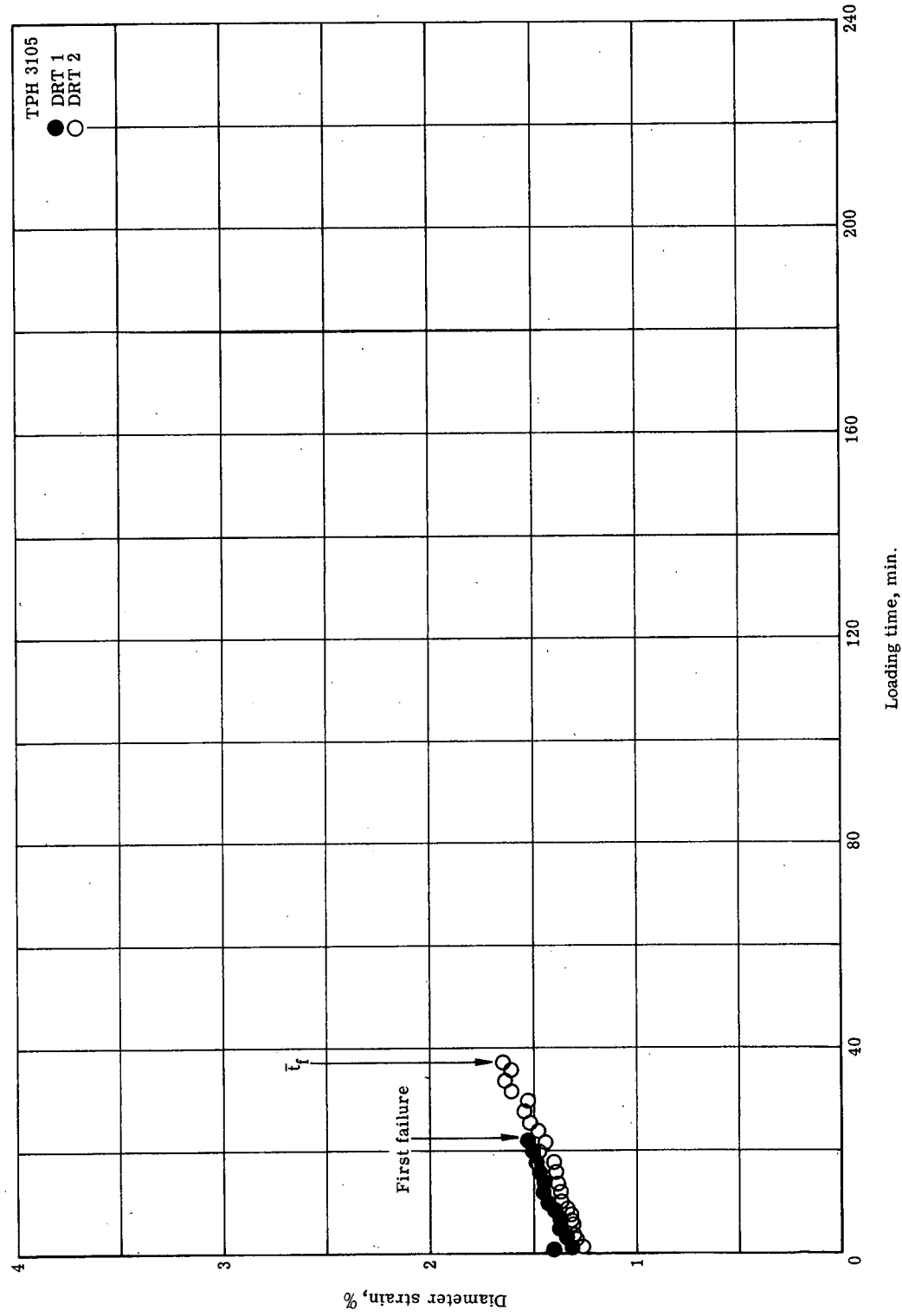


Figure D-14. - Diameter strain comparison, 51 psi stress, 51 hours vacuum.

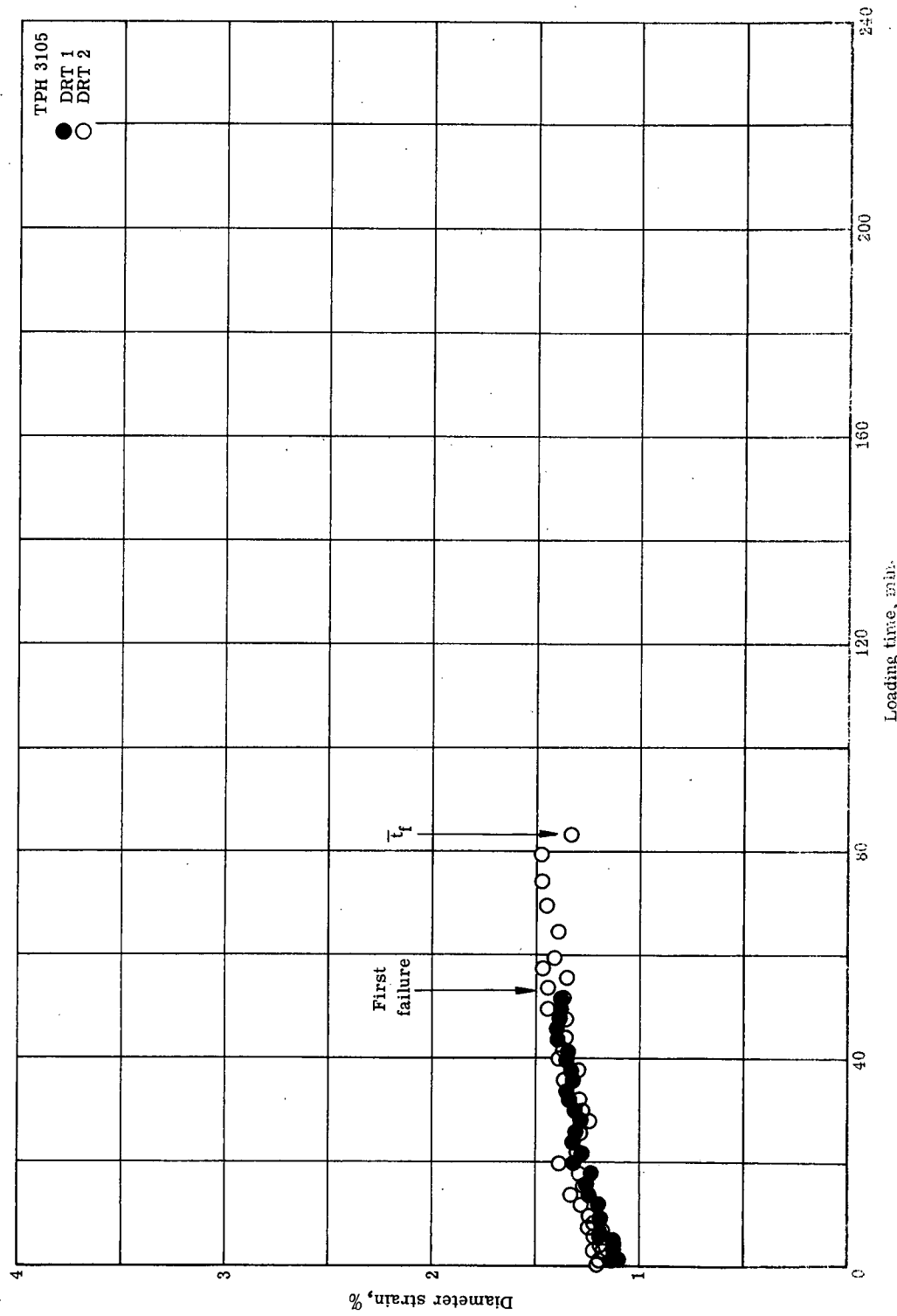


Figure D-15. - Diameter strain comparison, 51 psi stress, 173 hours vacuum.

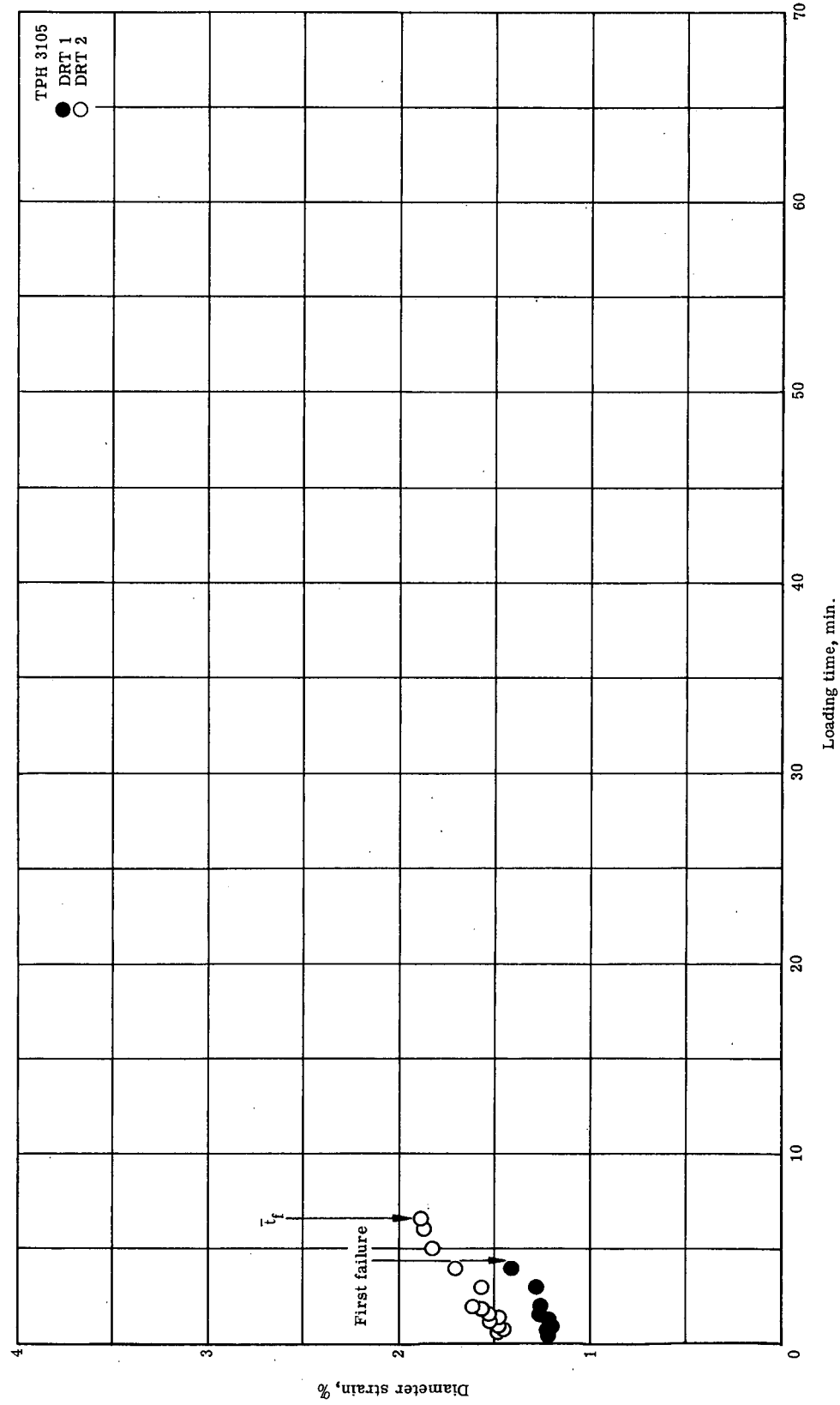


Figure D-16. - Diameter strain comparison, 56 psi stress, 50% r.h. air.

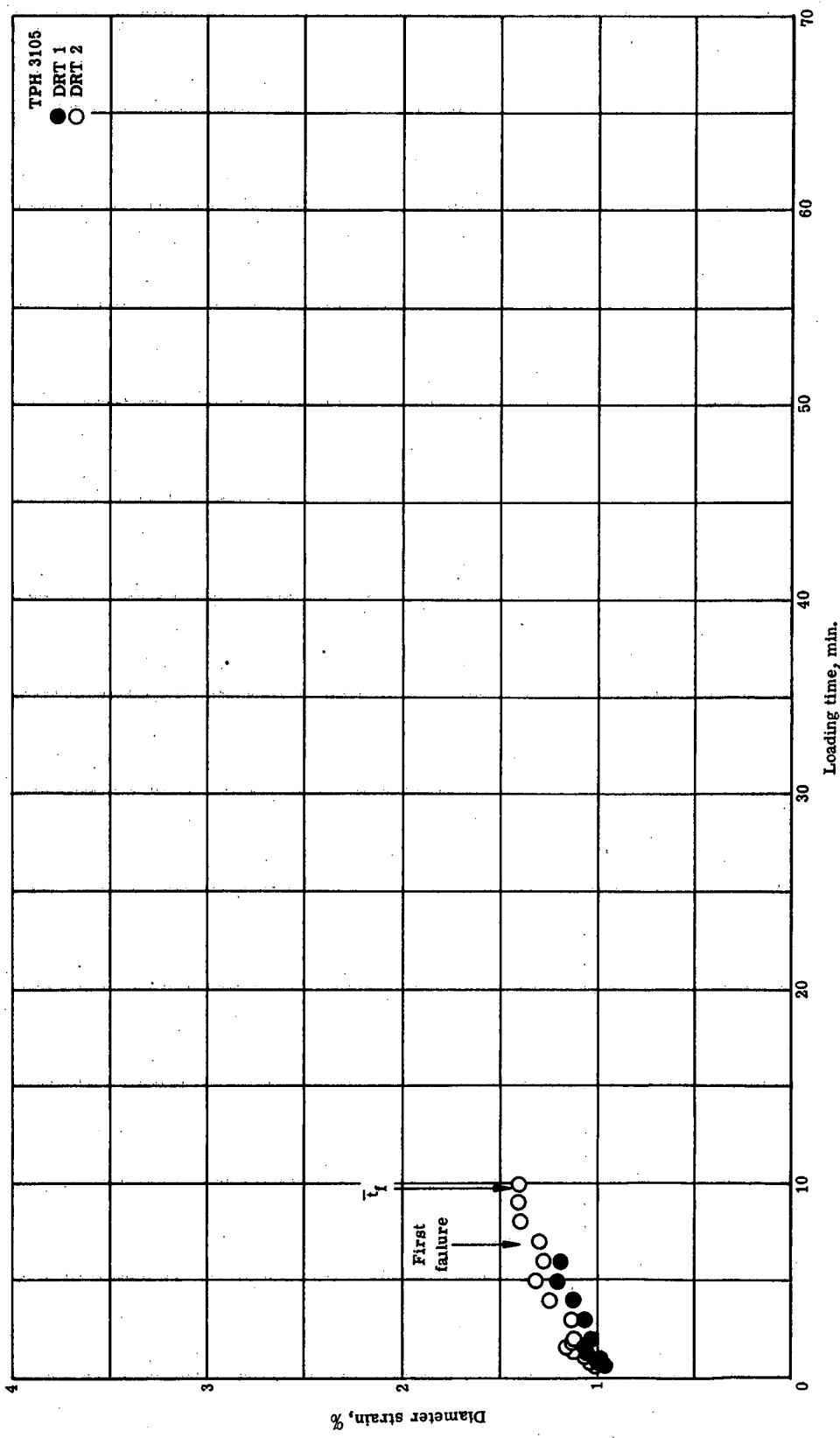


Figure D-17. - Diameter strain comparison, 56 psi stress, 47 hours vacuum.

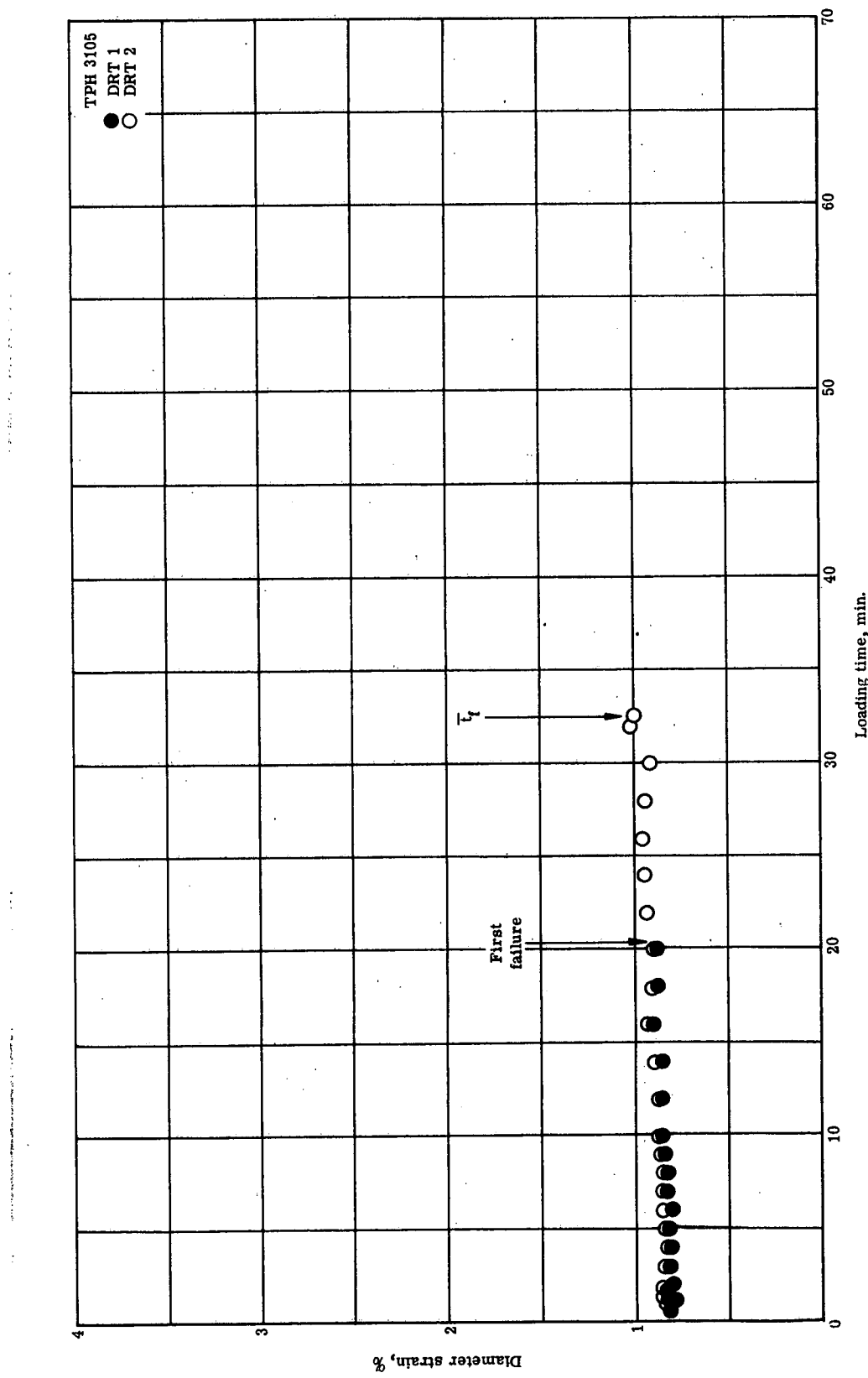


Figure D-18. - Diameter strain comparison, 56 psi stress, 170 hours vacuum.

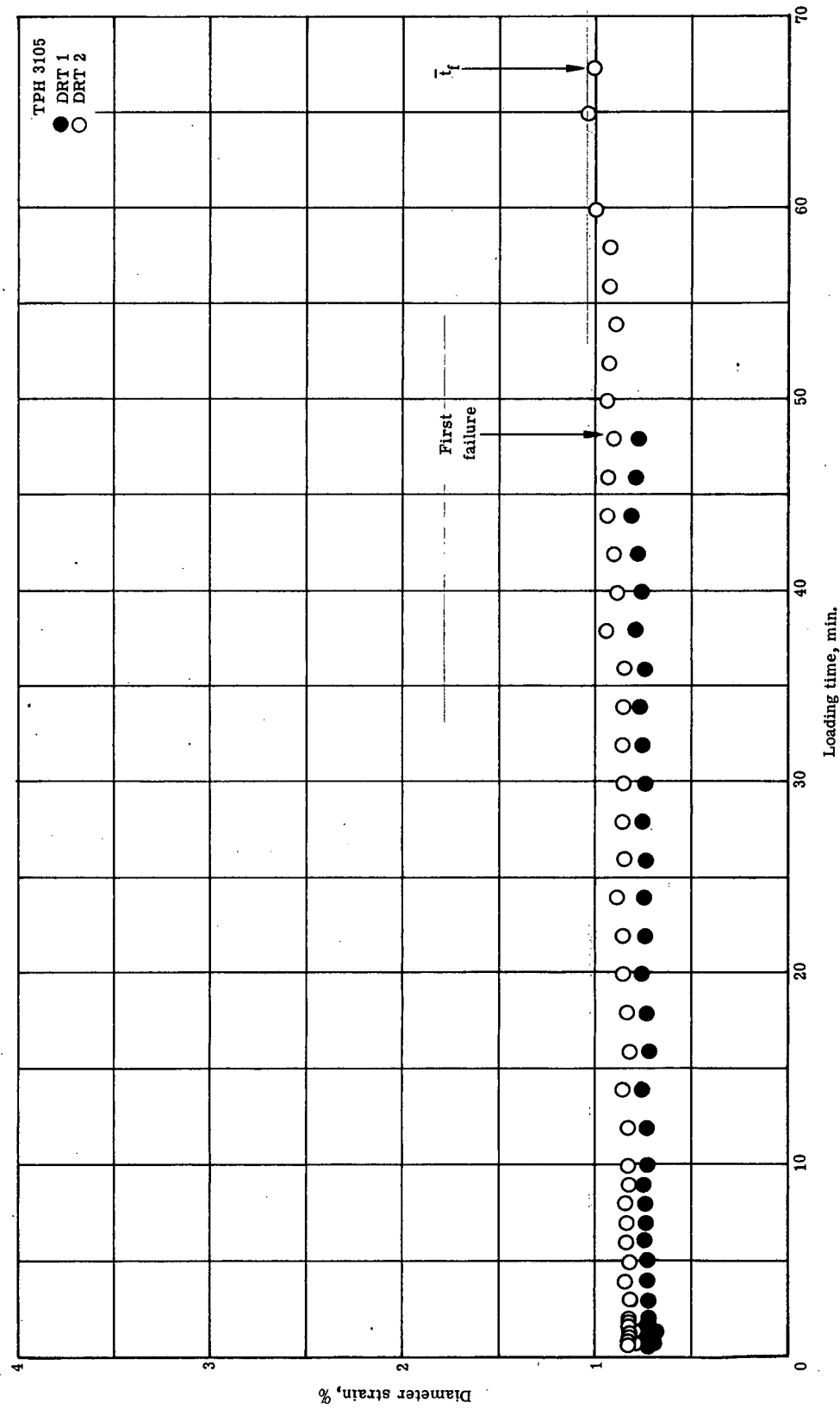


Figure D-19. - Diameter strain comparison, 56 psi stress, 350 hours vacuum.

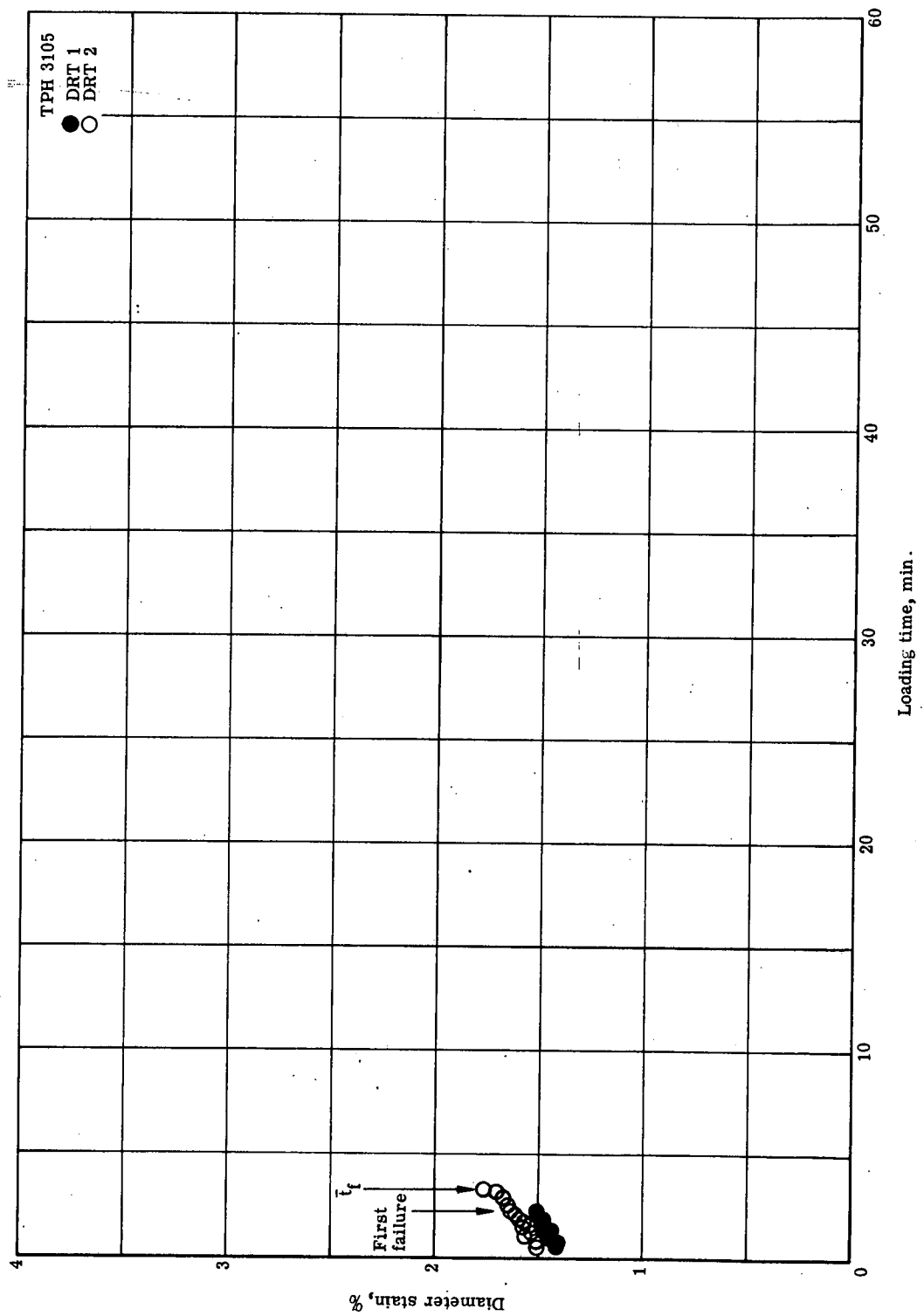


Figure D-20. - Diameter strain comparison, 61 psi stress, 50% r.h. air.

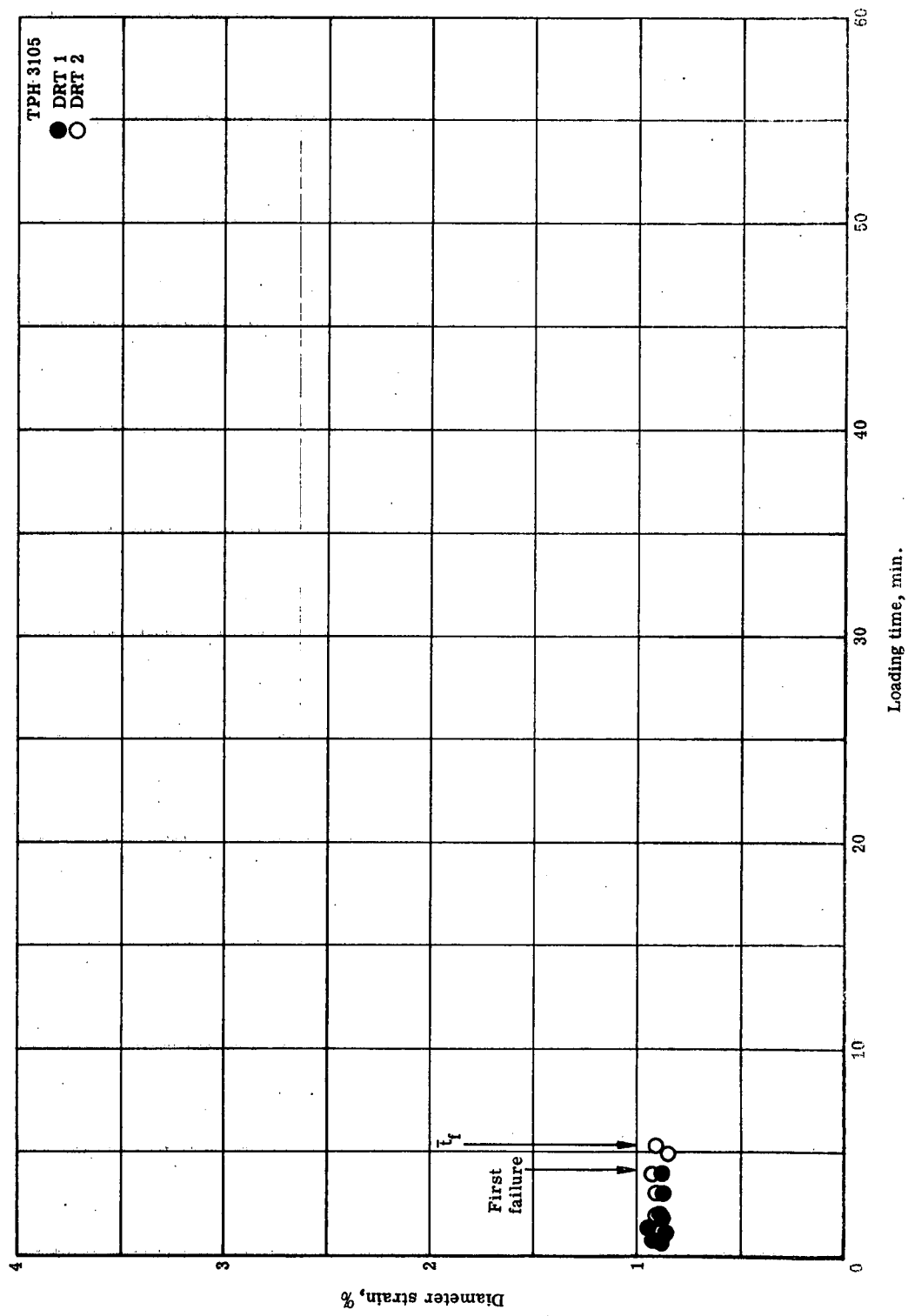


Figure D-21. - Diameter strain comparison, 61 psi stress, 46 hours vacuum.

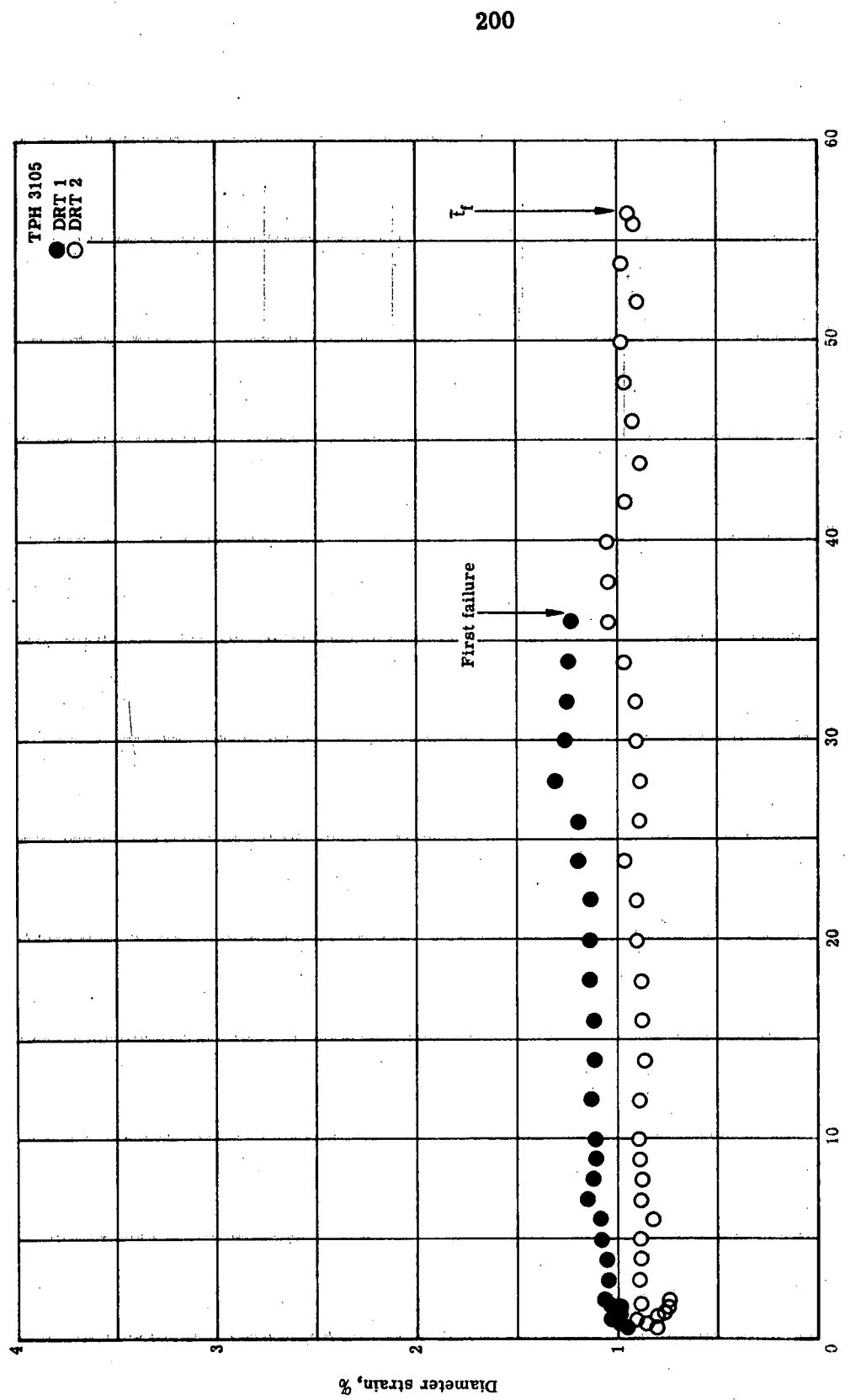


Figure D-22. - Diameter strain comparison, 61 psi stress, 337 hours vacuum.

Appendix E: List of Equipment

1. Vacuum Chamber. Langley Research Center 20-ft.<sup>3</sup> Ultrahigh Vacuum Chamber, designed and constructed by National Research Company, Newton, Massachusetts. The chamber was used for vacuum storage of the test samples.
2. Tensile Creep Apparatus. Designed and constructed at the Langley Research Center. The apparatus was used for in situ storage and testing of the samples.
3. Glove Box. Make unknown. The glove box was used to store samples during preconditioning.
4. Ionization Gage. Veeco Vacuum Corporation, New Hyde Park, Long Island, New York, type RG 75, pyrex tubulation, thoria-coated iridium filament, range  $2 \times 10^{-10}$  to  $10^{-3}$  torr, NASA #X13 and NASA #218C98. The ionization gages were used to measure the pressure in the vacuum chamber.
5. Ionization Gage Controller. Veeco Vacuum Corporation, New Hyde Park, Long Island, New York, type 21X, range  $2 \times 10^{-10}$  to  $10^{-3}$  torr, NASA #125593 and NASA #120105. The ionization gage controllers were used as power supplies for the operation of the ionization gages.

6. Temperature Recorder. Recording potentiometer, two-pen, Honeywell, Industrial Division, Fort Washington, Pa., model Eleckronik 194, NASA #154-372. The recorder was used to record output of the test thermocouples.
7. Temperature Reference Junction. Con-Ohmic Devices, Carle Place, New York, type T. The reference junctions were used in association with the test thermocouples.
8. Mass Spectrometer. Consolidated Electrodynamics Corp., 360 Sierra Madre Villa, Pasadena, California, type 21-614, NASA #138904. The mass spectrometer was used to monitor the water outgassing from the test samples.
9. Electric Motor. Bodine Electric Co., West Bradley Place, Chicago, Illinois, model B 8126E-06A, 300 RPM, 1/1500 hp. The motor was used to provide the motion for loading of the test samples.
10. Rotary Feedthru. Varian Associates, Palo Alto, California, magnetic type, model 954-5026. The feedthru was used to transmit external rotary motion into the vacuum chamber for indexing of the storage table.
11. Synchronizer. Designed and constructed by Mission Environmental Effects Section, Langley Research Center. The synchronizer was designed to activate the camera at a pre-assigned time schedule and to count the number of photographs taken of a given sample.

12. Timer-Alarm. Designed and constructed by Mission Environmental Effects Section, Langley Research Center. The timer-alarm had two functions: (1) measure the sample failure time, (2) sound an audible alarm if sample was improperly loaded.
13. Heater System. Designed and constructed by Mission Environmental Effects Section, Langley Research Center. The heater system provided the necessary controls and heat for temperature control of the vacuum chamber.
14. Camera. Charles A. Hulcher, Co., Inc., Hampton, Virginia, model 102, type 70 mm, NASA #85730. The camera was used to photograph the test samples during the test program.
15. Strobelight. Gilco Corp., Hampton, Virginia, 115V, 60 cy., NASA #88871. The light was used in conjunction with the 70 mm camera.
16. Mini Mite (Potentiometer Pyrometer). Thermo Electric Co., Inc., Saddle Brook, New Jersey, model 80200, range 0-2400°F and -1.6 to 52.0 millivolts. The mini mite was used to read sample temperatures during sample preconditioning.
17. Psychrometer. Princo Company, Southhampton, Pennsylvania, model WA-S-27629-F. The psychrometer was used to measure the relative humidity in the room during installation of samples in vacuum chamber.

18. Refractometer. Bausch and Lomb Optical Co., Rochester, New York, model 33-45-56. The refractometer was used to measure the refractive index of the water-glycerin humidity solutions.
19. Film. Eastman Kodak Company, Eastman, Tennessee, 70 mm, plus X. The film was used in the photographing of the test samples.
20. Temperature Controller. Yellow Springs Instrument Company, Yellow Springs, Ohio, proportional controller model 72. The controller was used to control the test sample temperature during preconditioning.